A CONTINUUM MIXTURE THEORY APPROCH TO SEDIMENT TRANSPORT WITH APPLICATION TO TURBULENT OSCILLATORY BOUNDARY LAYERS

JOHN NIGEL ALDRIDGE

A thesis submitted in partial fulfilment of the requirements of the Council for National Academic Awards for the degree of Doctor of Philosophy

November 1990

Polytechnic South West in collaboration with
Sir William Halcrow and Partners

Dedicated to my Parents

and to

Maddy

Abstract: A continuum mixture theory approach to sediment transport with application to turbulent oscillatory boundary layers.

Author: John Nigel Aldridge

Two aspects of the modelling of suspended sediment transport are investigated. One is the development of a theoretical base for sediment transport models starting from the continuum theory of immiscible mixtures (also know as two-phase flow theories). The other is a comparison with experimental data of numerical predictions from a number of turbulence models for oscillatory, turbulent boundary layer flow containing suspended sediment.

A review is given of previous work that has applied continuum mixture theories to the field of sediment transport. Turbulent averaged forms of the mixture equations are presented and, in the dilute particle concentration limit and neglecting the effects of particle inertia, the equations are shown to reduce to those encountered in traditional approaches to modelling suspended sediment concentrations. Likewise, the equations governing the motion of the fluid phase reduce to standard forms, with the effect of the sediment particles appearing as a buoyancy term in the fluid momentum equation. Particle inertia is taken into account by expanding in terms of a non-dimensional parameter, the ratio of the response time of the particle to a characteristic time of the flow. Terms arising from particle inertia are then reduced to correlations for which models are available in the literature. The assumption of dilute particle concentrations is made throughout the derivation.

An extensive comparison between a number of turbulence models is made by comparing numerical predictions with experimental data, whilst making the conventional assumption of zero particle inertia. The $k-\varepsilon$ model was found to perform well, with simpler models also giving reasonable agreement with experiment. Also investigated is the sensitivity of the solution to a number of factors, including: boundary conditions, empirical turbulence constants, and the stratifying effect of the suspended sediment.

The effect of including terms associated with particle inertia are investigated in turbulent oscillatory boundary layer flows. This is found to lead to an enhancement of the vertical particle volume flux. However, given the uncertainties of specifying the boundary condition for the concentration at the bed, the effect is probably not of significance for small particles (diameter $\sim$ 0.1 mm). Larger particles (diameter $\sim$ 0.25 mm) show more significant effects due to their inertia. The difference in mean horizontal velocity between the fluid and particle phases which results from the inclusion of inertia in the particle momentum equations is calculated. This difference is found to be very small.

Acknowledgements

I would like to thank all those that have helped me during my course of study; in particular the following people.

My supervisory team: Dr. Phil Dyke for encouragment, useful discussion and giving the necessary pep talks when things weren't going too well; Dr. Nicole Rockliff for her particular support, advice, and willingness to find time to read and discuss all aspects of the work; Prof. David Huntley whose suggestions were never less than helpful and were often crucial to making progress.

I should also like to thank Dr. Phil James for giving up time to discuss a number of topics connected with fluid mechanics.

I am grateful to Mr. Jon Warbrick of Polytechnic South West for help and advice in the use of the text processing package LaTeX, with which this thesis was prepared.

Finally, thanks are due to the MAFF Fisheries Laboratory Lowestoft for giving me a months grace in which to write up this thesis, and to the Proudman Oceanographic Laboratory for allowing me the use of facilities in the evening to complete the writing.

Contents

Abstract i

Acknowledgements ii

Contents iii

Notation v

1 Introduction 1

1.1 Review of Theories of Immiscible Mixtures 3

1.2 Derivation of continuum equations for immiscible mixtures 8

1.2.1 Balance laws 8

1.2.2 Constitutive relations 13

1.2.3 Stability and well-posedness for two-phase flow equations . . . 19

2 Application of Two-Phase Flow Theory to Sediment Transport 25

2.1 Sediment dynamics and a review of the two-phase flow approach . . . 25

2.2 Equations for flow of turbulent two-phase mixtures. 30

2.2.1 Favré averaging 30

2.2.2 Particle phase implications 34

2.2.3 Fluid phase implications 37

2.2.4 Comparison between the work of Drew and McTigue 38

2.2.5 Including further fluid-particle interactions 40

2.3 Turbulence modelling 43

2.3.1 Fluid mass and momentum correlations 43

2.3.2 Particle equation: closure I 49

2.3.3 Particle equation: closure II 55

3 Numerical Model for Oscillatory, Turbulent Boundary Layer Flow 58

3.1 The oscillatory boundary layer approximation 58
3.1.1 Boundary conditions 67
3.1.2 Non-dimensional form of equations 72
3.2 Finite difference scheme 76

4 Numerical Calculations without Particle Inertia **85**
4.1 Sensitivity calculations 86
4.1.1 Hydrodynamic results 86
4.1.2 Particle concentration results 99
4.2 Comparison of turbulence models 109
4.2.1 Comparison of hydrodynamic predictions between turbulence models 109
4.2.2 Comparison of sediment predictions between turbulence models 136
4.3 Conclusions 151

5 Numerical Calculations with Particle Inertia Effects **154**
5.1 Vertical particle flux 157
5.2 Horizontal particle velocity 166
5.3 Discussion and Summary 171

6 Conclusions **173**

References **176**

Appendices:

A Proof of the Averaging Theorem for a Simple Case **182**

B Equations for a Mixture Regarded as a Single Continuum **185**

Notation

'Direct' rather than component notation is used throughout. Vectors and tensors appear in bold type (lower case Roman for vectors and upper case Roman, or lower case Greek, for tensors).

If $\boldsymbol{a}$, $\boldsymbol{b}$ are vectors and $\boldsymbol{A}$, $\boldsymbol{B}$ are (second order) tensors the following operations are defined:

Inner product

Symbol '.'

Defined between vectors, vectors and tensors and between tensors:

$$\begin{aligned} \boldsymbol{a}.\boldsymbol{b} &\equiv a_i b_i \\ \boldsymbol{a}.\boldsymbol{B} &\equiv a_i B_{ij} \\ \boldsymbol{A}.\boldsymbol{b} &\equiv A_{ij} b_j \\ \boldsymbol{A}.\boldsymbol{B} &\equiv A_{ik} B_{kj} \end{aligned}$$

'Double' inner product

Symbol ':'

Defined between tensors:

$$\boldsymbol{A} : \boldsymbol{B} \equiv A_{ij} B_{ij}$$

Tensor product

Symbol '$\otimes$'

Defined between vectors:

$$\boldsymbol{a} \otimes \boldsymbol{b} \equiv a_i b_j$$

Generally the operator $\otimes$ will be omitted so that

$$\boldsymbol{a}\boldsymbol{b} \equiv \boldsymbol{a} \otimes \boldsymbol{b}$$

The identity tensor is denoted by the symbol $\boldsymbol{I}$.

Also defined are the following differential operators:

Gradient

Symbol ∇

Defined for scalars and vectors:

$$\begin{aligned} \nabla\phi &\equiv \frac{\partial\phi}{\partial x_i} \\ \nabla v &\equiv \frac{\partial v_j}{\partial x_i} \dagger \end{aligned}$$

†This expression is ambiguous when we come to consider the inner product of this quantity with a vector. The inner product, as defined, is not symmetrical between the tensor subscripts and we have not specified in the gradient definition which of the subscripts i or j comes 'first'. We therefore make the definition that the subscript on the variable with respect to which we are differentiating (i in this case) comes first. Thus:

$$\begin{aligned} v.\nabla f &\equiv v_i \frac{\partial f_j}{\partial x_i}, \\ (\nabla f).v &\equiv v_j \frac{\partial f_j}{\partial x_i}. \end{aligned}$$

This ensures that the conventional notation for the convective derivative

$$\frac{Dv}{Dt} \equiv \frac{\partial v}{\partial t} + v.\nabla v$$

is consistent with the definitions introduced above.

Divergence

Symbol $\nabla.$

Defined for vectors and tensors:

$$\begin{aligned} \nabla.v &\equiv \frac{\partial v_i}{\partial x_i} \\ \nabla.A &\equiv \frac{\partial A_{ij}}{\partial x_j} \end{aligned}$$

'Double' divergence

Symbol $\nabla:$

Defined for tensors:

$$\nabla : \sigma \equiv \frac{\partial^2 \sigma_{ij}}{\partial x_j \partial x_i}$$

The operator ∇^t operating on a vector is defined such that

$$\nabla^t f \equiv (\nabla f)^t.$$

Volume integrals over a set of points $\mathcal{D}$ are shown as

$$\int_{\mathcal{D}} \Phi \, dV,$$

where Φ may be scalar, vector or tensor. Surface integrals over the boundary $\partial\mathcal{D}$ of a set $\mathcal{D}$ are denoted

$$\int_{\partial\mathcal{D}} n.\Phi \, ds.$$

List of main symbols

Scalars

a	Orbital amplitude just outside the boundary layer ($a = V_\infty/\omega$).
a_i, a_i'	($i = 1, 2, 3$) Constants in pressure-concentration correlation model (Section 2.3.2).
b	Volume of spherical particle ($b = \frac{4}{3}\pi r^3$).
b_i	($i = 1, 2$) Turbulence model constant (see Section 2.3.2).
c, c_p	Particle concentration.
c_f	Fluid 'concentration' ($c_f = 1 - c_p$).
c_0	Reference concentration at bed, see (3.41).
C_D	Turbulence model constant.
$C_{1\epsilon}$	Turbulence model constant.
$C_{2\epsilon}$	Turbulence model constant.
$C_{3\epsilon}$	Turbulence model constant.
C_{vm}	Added mass coefficient, see (2.35).
d	Particle diameter.
d_n	For a sample of particles, the diameter such that $n\%$ of the sample has a diameter less than d_n.
f_c	Wall correction function for pressure-concentration correlation model (Section 2.3.2).
g	Acceleration due to gravity ($g = 9.8 m/s^2$).
G	Buoyancy production term for k, see (2.48).
k	Turbulent kinetic energy.
k_N	Nikuradse roughness length.
l	Turbulent length scale.
p_p	Pressure associated with particle phase.
p_f	Pressure associated with fluid phase.
$p_{(i)}$	Interfacial pressure.
p_h	Total fluid pressure including hydrostatic component.
p	Fluid pressure minus hydrostatic component.
P_∞	Value of pressure just outside boundary layer.
P	Shear production term for k, see (2.47).
q	Average excess pressure over particle surface, see (1.39).
r	Particle radius.
R	Constant appearing in turbulence model for concentration variance.
Re	Flow Reynolds number.
R_p	Particle Reynolds number, see (1.35).

R_w	Wave Reynolds number ($R_w = aV_\infty/\nu$).
S	Shields number ($S = \tau_0/g\Delta\rho d$).
S_0	Critical Shields number for initial movement (see Section 3.1.1).
S_1	'Saturation' Shields number (see Section 3.1.1).
t	Time variable.
T	Period of oscillatory boundary layer flow.
u_1	Horizontal component of particle velocity.
u_2	Vertical component of particle velocity.
v_1	Horizontal component of fluid velocity.
v_2	Vertical component of fluid velocity.
v_*	Friction velocity ($v_* = \sqrt{\tau_0/\rho_f}$).
v_{*m}	Maximum friction velocity over wave cycle.
V_∞	Amplitude of velocity at the edge of the boundary layer.
V	Volume of Ω.
w_0	Particle fall velocity, $w_0 = g(\rho_p - \rho_f)/\gamma$.
x	Horizontal distance from origin.
z	Vertical distance from origin.
z_0	Value of z at which fluid velocity is zero in a turbulent boundary layer.
z_1	Value of z at which the bottom boundary conditions are applied.
z_2	Value of z at which the upper boundary conditions are applied.
z_b	Height of the bed-load region (base of region of suspended load).
γ	Drag coefficient ($\gamma = 9\eta/2r^2$ assuming Stokes law).
δ	Boundary layer thickness.
δ_ω	Measure of oscillatory boundary layer thickness ($\delta_\omega = v_{*m}/\omega$).
δ_1	Measure of oscillatory boundary layer thickness, see (4.4).
Δ	Value of z at which turbulent length scale is specified as becoming constant, see (4.1).
$\Delta\rho$	Density difference $\rho_p - \rho_f$.
ε	Dissipation rate of turbulent kinetic energy, see (2.45).
ζ	Transformed vertical distance, see (3.52).
η	Dynamic viscosity of fluid ($\eta = 1.1 \times 10^{-3} Ns/m^2$).
θ	Weighting factor in implicit numerical scheme, see Section 3.2.
κ	von Karman constant ($\kappa = 0.4$).
κ_T	Eddy diffusivity.
ν	Kinematic viscosity of fluid ($\nu = \eta/\rho_f$).
ν_T	Eddy viscosity.

ρ_f	Fluid density.
ρ_p	Particle density.
ρ	Ratio ρ_p/ρ_f.
τ	Turbulent shear stress.
τ_0	Bottom stress, see (3.30).
τ^*	Ratio of particle response time to characteristic flow frequency ($\tau^* = \rho_p\omega/\gamma$).
ω	Oscillation frequency ($\omega = 2\pi/T$).

Vectors and tensors

g	Gravitational acceleration vector $(0, 0, -g)$.
k	Unit vector in vertical direction.
u	Particle velocity.
v	Fluid velocity.
w_0	Particle fall velocity vector $(0, 0, -w_0)$.
x	Position vector.
Π_j	Components of pressure-concentration correlation, $j = 1, 2, 3$, see (2.58).
I	Identity tensor.
σ_f	Fluid stress tensor.
σ_p	Particle stress tensor.
$\sigma_{(i)}$	Interfacial stress tensor.

Sets

Ω	Set of points over which averages are defined.
C_k	Set of points occupied by kth mixture constituent.
$C_k \cap \Omega$	Set of points occupied by the kth mixture constituent in Ω.
$C_f \cap \Omega$	Set of points occupied by the fluid phase in Ω.
$C_p \cap \Omega$	Set of points occupied by the particle phase in Ω:
$\mathcal{D}$	Set of points occupied by the entire mixture, $\mathcal{D} = \bigcup_k C_k$.
$\mathcal{I}$	Interface between mixture constituents within Ω.
$\mathcal{I}_k$	Interface between portion of kth constituent inside Ω and portion outside Ω.
$\mathcal{R}$	The real number line.
$\mathcal{S}$	Collection of closed surfaces in Ω.
$\mathcal{U}$	Collection of open surfaces in Ω.

Subscripts, superscripts and modifying symbols

$< f >$	Turbulent average.
$\bar{f}$	Turbulent averaged quantity.
$\overline{\overline{f}}$	Volume average.
f'	Fluctuating quantity such that $< f' >= 0$.
f''	Fluctuating quantity such that $\overline{\overline{f''}} = 0$.
$\tilde{f}$	Fluctuating quantity such that $< c_p \tilde{f} >= 0$ or $< c_f \tilde{f} >= 0$.
$\hat{f}$	Local instantaneous quantity defined only on region occupied by a given mixture constituent.
f^*	Generally indicates a non-dimensional quantity
Φ^t	Indicates the transpose of the tensor Φ.
f^+	Indicates a typical value or 'scale' for the quantity f.
f_i^n	Finite difference variable at the ith grid point and nth time step.
$f_i^{n,s}$	The sth iterate of f_i^n.

Chapter 1

Introduction

Two aspects of the modelling of suspended sediment transport are investigated. One is the development of a theoretical base for sediment transport models starting from the continuum theory of immiscible mixtures (also known as 'two-phase flow theories'). The other is a comparison with experimental data of numerical predictions from a number of turbulence models for oscillatory, turbulent boundary layer flow containing suspended sediments.

There have been several papers published which apply continuum mixture theories to sediment transport problems. Notable contributions include those by Drew (1975), De Vantier & Larock (1983) , McTigue (1981) and Kobayashi & Seo (1985). However, a review of this work in Section 2.1 indicates that there is still ample scope for further investigation. On the theoretical side several problems need addressing. There is apparent disagreement about what are the dominant terms in the momentum balance. Work is required to take account of the effect of suspended sediment on the turbulence and to incorporate this into a turbulence model; although plausible, the application of models such as $k - \varepsilon$, derived for single-phase fluids, to a fluid-sediment mixture requires some justification. Also, after after taking care to account for the two-phase nature of the flow when formulating the continuity and momentum equations, it seems logical to do the same for the equations comprising the turbulence model. From a practical point of view it must be asked if the undoubtedly more complicated approach of starting from the continuum mixture equations adds anything new.

A large number of studies have been concerned with the modelling of oscillatory boundary layers due to the importance of these flows in a number of areas. In particular, knowledge of the turbulent boundary layer generated by a water wave

at the sea bed is an essential pre-requisite to predicting sediment movement, calculating forces on bodies on the bed, and determining wave attenuation due to energy dissipation at the bed. Turbulence models of varying degrees of sophistication have been used, ranging from the relatively simple, time independent eddy viscosity model of Kajiura (1968), through mixing length and turbulent kinetic energy models e.g. Bakker (1974) , Johns (1977), to $k-\epsilon$ models, Hagatun & Eidsvik (1986) and Justesen (1988), and even second moment closure, Sheng (1982). Although each author generally compares model results with experiment, there does not seem to have been published a detailed inter-comparision of a these models against a common set of experimental measurements. Only then can some assessment of the benefits (or otherwise) of more complicated turbulence modelling be made. This we attempt to do by a comparison of with experiment of predictions for mean velocity profiles, bed stress and suspended sediment concentrations using all the models mentioned above, apart from the second moment closure.

The remainder of Chapter 1 contains a review of the historical development of continuum mixture theories[1], along with a derivation of the fundamental equations using averaging techniques. Constitutive relations suitable for a mixture consisting of solid particles suspended in a Newtonian fluid are prescribed. A number of assumptions are required to yield a closed set of equations. The most simple assumptions lead to a system that is 'ill-posed' and a discussion is given of attempts that have been made by other workers to rectify this deficiency.

Chapter 2 contains a brief introduction to sediment transport concepts and a review of previous work applying continuum mixture theories to the field. Turbulent averaged forms of the mixture equations are then presented and, in the dilute particle concentration limit and neglecting the effects of particle inertia, the equations are shown to reduce to those encountered in traditional approaches to modelling suspended sediment concentrations. Likewise, the equations governing the motion of the fluid phase reduce to standard forms. The effects of particle inertia are taken into account by expanding in terms of a non-dimensional parameter, the ratio of the response time of the particle to a characteristic time of the flow. The assumption of dilute particle concentrations is made throughout the derivation. Terms arising from particle inertia are then reduced to turbulent correlations for which models are available in the literature.

In Chapter 3 the full equations, including terms associated with particle inertia,

[1] A more detailed review may be found in Bedford & Drumheller (1983).

are simplified to a form suitable for application to turbulent oscillatory boundary layer flows. A discussion of suitable boundary conditions for modelling such flows is given, and a numerical scheme for solving the system of partial differential equations (without the presence of 'inertia' terms) is described.

The results of a critical evaluation of a number of turbulence models is made is made in Chapter 4. This takes the form of a comparison of model predictions with experimental data, whilst making the conventional assumption of zero particle inertia to yield standard oscillatory boundary layer equations. Also investigated is the sensitivity of the solution to a number of factors, including boundary conditions, empirical turbulence constants, and the stratifying effect of the suspended sediment.

Chapter 5 shows the results of including particle inertia terms in the equations governing the particle momentum. The required modifications to the numerical scheme are described and results are presented for both vertical and horizontal components of particle momentum.

Finally, a short chapter giving conclusions and suggestions for further work completes the investigations presented herein.

1.1 Review of Theories of Immiscible Mixtures

The central tenet upon which continuum mechanics relies is that material properties can be represented by continuous functions of space and time. Once this representation has been shown to be valid, the powerful techniques of mathematical analysis can be used to formulate problems and obtain solutions.

That this approach has been extraordinarily successful there is no doubt. However when we examine matter closely enough, we find that instead of being a continuum with no intrinsic structure, as the success of continuum mechanics might imply, it is the complete opposite, consisting mostly of empty space with matter concentrated in highly complicated entities which we call atoms and molecules. The resolution of this apparent paradox lies on taking account of the different length scales at which we are considering a material. It is well known from statistical mechanics that although the detailed behaviour of a material is too complex to predict at the molecular or atomic level, the 'average' behaviour *is* predictable. This average behaviour manifests itself at much larger length scales than the molecular and it is this that continuum mechanics attempts to describe and which appears to vary continuously with space and time.

Classical continuum theories generally deal with materials where the microscopic

scales, characterised by inhomogeneities and discontinuities, are well separated from the macroscopic scales of averaged behaviour. More recently theories have been proposed where this wide separation of length scales is not present. The state of the material at the level of its inhomogeneities has a direct effect on the macroscopic behaviour. This class of theories are generally known as theories of materials with microstructure.

Work has also been done on formulating continuum theories for material composed of a number of distinct constituents i.e. a mixture. Such mixture theories retain separate variables and equations for each constituent and allow each constituent to affect others. In common with theories of materials with microstructure, mixture theory attempts to describe material where the microscopic structure has an important effect on the macroscopic behaviour.

The systems that we wish to describe, particulate suspensions, are included in the class of mixtures that Bedford & Drumheller (1983) call immiscible and structured. That is, the constituents remain physically separate on a scale large in comparison with molecular dimensions, and with structure arising from the interface separating the constituents. Theories describing them are related to, but are not identical with, the theories of mixtures and of materials with microstructure mentioned above.

"Classical" Mixture theory

The modern theory of mixtures was initiated by Truesdell (1957). The fundamental concept considered a mixture as a number of superimposed continua, one for each of the components of the mixture. Each point of space is thus apparently occupied by each component simultaneously. Once this underlying idea has been accepted, balance laws based on the principles of mass, momentum and energy conservation can be postulated. These principles should be valid for each constituent in the mixture, so each constituent has its own set of equations expressing the balance of mass, momentum and energy associated with that constituent. In general it is assumed that either the constituents are mixed at the molecular level or are otherwise so well mixed that it is not sensible to consider the relative amounts of each constituent in a given volume. Thus no equivalent of the volume fraction, a key feature of the theories of immiscible mixture theory, emerges in the classical theory.

Theories of Materials with Microstructure

In these theories the usual kinematic variables (i.e. velocities, pressures and densities) are augmented by extra variables, with the aim of being able to describe more complex

materials than classical continuum theories deal with. These additional variables are interpreted as describing the state of the material at the microscopic length scale (i.e. the length scale characterising the material inhomogeneities) and give information about the structure of the material at this level. As in mixture theory and continuum mechanical theories in general, all equations of motion are based on the fundamental principles of mass, momentum and energy conservation.

Early work on theories of this type were largely ignored and it was the developments by Ericksen & Truesdell (1958) that initiated the modern development of this area.

The concept of the microelement, which replaces the point particle of classical continuum mechanics, was introduced by Eringin (1964), and others. Each microelement is considered as being able to undergo deformations independently of the material as a whole. By allowing the microelements to undergo more or less complicated deformations, a hierarchy of theories can be built such that the number of extra variables, and the complexity of the theory, increases with the complexity of deformations that microelements are allowed. For example, if the microelements are assumed to be rigid bodies, their only independent motions are rigid body rotations. Such materials are termed 'micropolar' and micropolar theories contain a vector, the microelement angular momentum, as an extra independent variable (see for example Eringin 1974).

For our purposes, the theories of most interest are the simplest possible that incorporate microstructure – namely those where a single scalar is the only extra variable. Goodman & Cowin (1972), (1976) and Nunziato & Cowin (1979) introduced such a theory to describe granular and porous materials respectively. A single variable, the volume fraction (the volume of solid per unit volume), is included as an independent kinematical variable. Note that these theories are not mixture theories since only a single material is assumed to be present. The simplest theories of structured immiscible mixtures contain the same type of variable representing the volume fraction of each constituent.

Immiscible and Structured Mixtures

Since materials belonging to this class are mixtures and have structure as a consequence of being immiscible, continuum theories describing them have much in common with the theories of mixtures and materials with microstructure described above.

As with mixture theory, each constituent has its own set of equations, representing mass, momentum and energy balance for that constituent. Like mixture theory the equations contain terms representing the exchange of mass, momentum and energy

with other constituents. Unlike mixture theory, but like the simplest theories of materials with microstructure, extra scalar variables are introduced, one for each constituent. These are interpreted as representing the proportion of the total mixture occupied by each constituent at a given point. Such variables can be regarded as giving the 'concentration' of the constituent. It is required that $\sum_k c_k = 1$ where c_k is the concentration of the kth mixture constituent.

Most classical continuum mechanical theories are postulated as continuum theories from the outset and differential equations derived by considerations of mass, momentum and energy balance. Typically this is accomplished via the "control volume" approach found in almost any textbook of fluid dynamics. It is possible to derive some of the simpler theories by considering the microscopic structure of the material and applying averaging procedures. For example the Navier-Stokes equations can be derived on the basis of kinetic theory.

Similarly for immiscible structured mixtures, theories can be postulated with the material represented as a number of superimposed continua at the outset. Alternatively, averaging can be carried out at the microscopic scale, which in the case of immiscible mixture is at the length scale of the inhomogeneities, which is much greater than the molecular level.

Early work based on the postulational approach was done by a number of workers in the early 1960's including Hinze (1962) and Murray (1965). The former proposed constitutive relations for the flow of a fluid-particle mixture in a tube while the latter was interested in modelling fluidized beds and postulated equations for a fluid-particle mixture. He wrote balance equations for the mixture as a whole which were then split into equations satisfied by each constituent. This introduced interaction terms which sum to zero when the individual equations are added - hence recovering the balance equations for the mixture. The interaction terms are constitutive and represent the transfer of mass, momentum and energy from one component to another. The work of Soo (1967) and his co-workers is based on a similar approach.

Much work on the equations of motion for immiscible structured mixtures has been based on averaging procedures. Many authors have put forward such procedures and all have arrived at very similar sets of equations. Again early examples of averaging being used to develop equations for immiscible mixtures were connected with work on fluidized beds. The work of Anderson & Jackson (1967) and Panton (1968) are examples. Drew & Segal (1971) in presenting their own forms for the equations made a comparison with a number of previous derivations (both averaged and postulational) noting differences between them and their own derivations. A large number

of papers have appeared (and continue to appear) in this aspect of immiscible mixture theory. Among these, contributions by Whitaker (1969), Drew & Segal (1971), Ishii (1975), Delhaye (1977), and Nigmatulin (1979) have been influential and the resulting theories have achieved a certain degree of maturity and acceptance.

The averaging procedures can be based on time averaging, space (line, area or volume) averaging, or ensemble averaging. All lead to essentially identical forms for the equations; the differences arise in the interpretation of the variables. Most start from a so-called local instantaneous formulation (which also needs to be derived) where quantities are expressed in unaveraged form, and where the boundaries separating the constituents are explicitly accounted for. Included as part of this formulation are jump conditions giving the allowed relationships between quantities on either side of the boundaries. In general the local instantaneous formulation is impossible to solve directly, even in an approximate form, for anything other than the simplest possible cases. The averaging procedure, by removing unwanted details, yields equations which, potentially at least, are much more amenable to solution.

The averaging procedure itself involves applying formal theorems that allow averages of derivatives to be replaced by derivatives of the product of the averaged quantity with its associated concentration — thereby arriving at equations containing averaged quantities. Also present are:

1. terms representing the transfer of mass, or momentum or energy between constituents (interfacial terms);

2. terms similar to the Reynolds stress terms arising in the theory of turbulence.

To close the equations constitutive relations are required.

We briefly mention two other methods that have been used to derive equations for immiscible mixtures. One is to use a variational principle. Among the first to apply this approach were Bedford & Drumheller (1978), while more recently Geurst (1985) and Capriz & Giovine(1987) have made important contributions using this method. Another approach, e.g. Travis et al. (1976), uses ideas derived from the kinetic theory of gases and is suitable for disperse mixtures where discrete particles of one material (solid, liquid or gas) are distributed within a fluid medium. The role of atoms and molecules in kinetic theory is taken over by the particles of the dispersed constituent.

All the approaches are found give rise to essentially the same basic set of equations, although there may be differences in the exact form of some terms and in the interpretation of the meaning of some quantities.

Finally, we note that in the literature, what we have termed theories of immisci-

ble mixtures are more commonly called *two-phase* (or *multi-phase*) flow theories or occasionally *continuum mixture* theories. The first term arose due to the fact that in the majority of cases immiscibility comes about because the constituents are in different phases, (e.g. solid, liquid or gas). For the remainder of this work the term 'two phase flow' or 'mixture' theory will be used interchangeably. Some workers prefer to use the latter name for theories that derive equations for the total mixture. The approach whereby separate equations for each mixture constituent are used is sometimes known as the 'two-fluid' approach.

1.2 Derivation of continuum equations for immiscible mixtures

1.2.1 Balance laws

The continuum equations are to be derived by the use of a volume average. We have adopted a more direct approach than is usual. Most authors derive, using a control volume argument, so-called local instantaneous equations which, because they are too complicated to solve, are transformed to produce more tractable equations in terms of averaged variables. Since the processes of obtaining the local–instantaneous form and from this the averaged equations are very nearly the reverse of each other, we have gone directly from the control volume statement of the laws of mass and momentum conservation in integral form to the equivalent form in terms of volume averaged quantities. The price of this brevity is that some of the information obtained from the local instantaneous formulation is lost, in particular the jump conditions satisfied by quantities on either side of constituent boundaries. For the relatively simple case we are interested in, that of solid particles suspended in a liquid, the two approaches yield identical equations. In more complicated cases, where mass transfer between constituents occurs (such as in a boiling water-steam mixture), the more complete derivation is to be preferred since terms arising from the mass transfer are automatically accounted for in the momentum equations.

As we are only concerned with mechanical systems no derivation of the energy balance will be given.

We first suppose the region occupied by the mixture, $\mathcal{D} \subset \mathcal{R}^3$, be partitioned into subsets $\mathcal{C}_k$, each associated with a mixture constituent and satisfying $\bigcup \mathcal{C}_k = \mathcal{D}$. Since the mixture, and the individual constituents that comprise it, are assumed to be in motion $\mathcal{C}_k = \mathcal{C}_k(t)$. Let $\Omega = \Omega(x; V)$, $x \in \mathcal{D}$, be a set of fixed shape and fixed

volume V, but with arbitrary position in space (for example a cube of fixed size centred at some point x).

From now on we assume, for simplicity, that there are only *two* constituents. Figure 1.1 shows a typical distribution of mixture constituents within Ω.

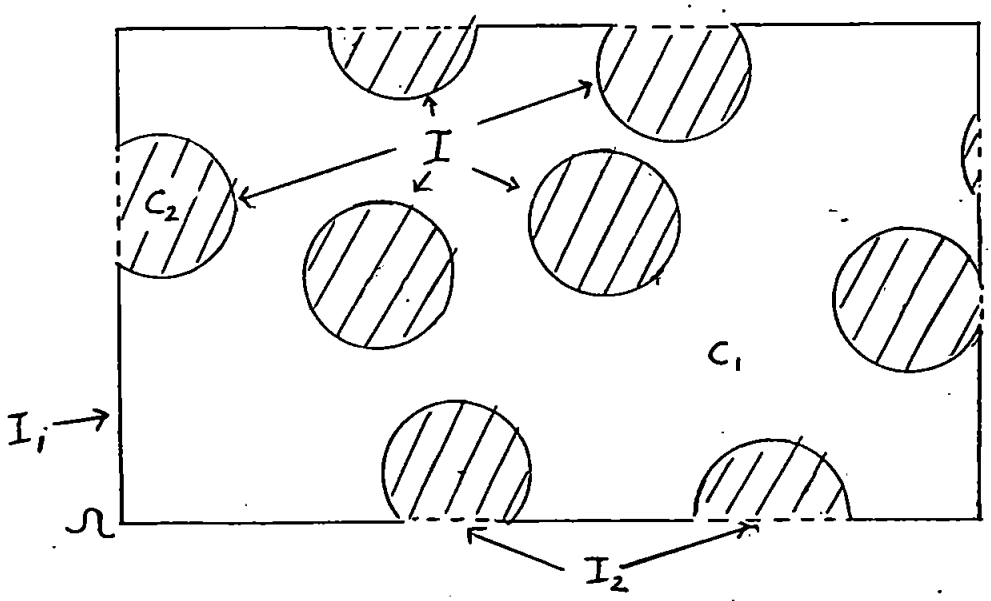

Figure 1.1:

Of crucial importance is the distinction between the boundary, $\mathcal{I}$, that separates the constituents within Ω, and the boundaries $\mathcal{I}_k$, that separate the portion of C_k within Ω from that lying outside. If the kth constituent has associated with it a field variable $\hat{f}(x)$, $x \in C_k$, then the volume average of this quantity, denoted by f, is defined by

$$f \equiv \overline{\overline{\hat{f}}} = \frac{1}{c_k V} \int_{C_k \cap \Omega(x)} \hat{f}\, dV, \tag{1.1}$$

where $c_k(x)$ is the proportion of V occupied by the kth constituent, i.e. the volume fraction, and is defined as

$$c_k(x) = \frac{1}{V} \int_{C_k \cap \Omega(x)} dV. \tag{1.2}$$

Since $\bigcup_k (C_k \cap \Omega) = \Omega$, the volume fractions satisfy the constraint

$$\sum_k c_k = 1. \tag{1.3}$$

It is important to appreciate that the volume averaged quantities are still functions of position, since $C_k \cap \Omega(x)$ is a function of position and therefore in general the value

of $\hat{f}$ within $C_k \cap \Omega(\boldsymbol{x})$ will change as $\boldsymbol{x}$ is varied.

Averaging theorems

Before introducing the main result we quote here the standard divergence theorem to which the averaging theorem is related.

$$\int_{\partial(C_k \cap \Omega)} \hat{\boldsymbol{f}}.\boldsymbol{n}_k \, ds = \int_{C_k \cap \Omega} \nabla.\hat{\boldsymbol{f}} \, dV$$

Here $\boldsymbol{n}_k$ is the unit vector normal to and pointing *away* from the surface bounding the kth constituent. From this we can derive the following result for the tensor Φ, which will be used later in the chapter

$$\int_{\partial(C_k \cap \Omega)} \boldsymbol{n}_k \otimes \hat{\boldsymbol{f}} \, ds = \int_{C_k \cap \Omega} \nabla \hat{\boldsymbol{f}} \, dV \tag{1.4}$$

The key relation needed to derive the balance laws relates the integral around $\mathcal{I}_k$ to the volume integral over $C_k \cap \Omega$ as follows,

$$\int_{\mathcal{I}_k} \hat{\boldsymbol{f}}.\boldsymbol{n}_k \, ds = \nabla. \int_{C_k \cap \Omega} \hat{\boldsymbol{f}} \, dV, \tag{1.5}$$

which holds even for the disconnected regions illustrated in figure 1.1. In appendix A we give a proof of this result for the case of a rectangular region in $\mathcal{R}^2$ — more general proofs are given in Slattery (1967) and Gray & Lee (1977). In terms of the volume average defined by (1.1), the result (1.5) can be written

$$\frac{1}{V} \int_{\mathcal{I}_k} \hat{\boldsymbol{f}}.\boldsymbol{n}_k \, ds = \nabla.(c_k \boldsymbol{f}). \tag{1.6}$$

Analogous results hold for the case of scalar and tensor integrands:

$$\frac{1}{V} \int_{\mathcal{I}_k} \boldsymbol{n}_k.\hat{\Phi} \, ds = \nabla.(c_k \Phi), \tag{1.7}$$

$$\frac{1}{V} \int_{\mathcal{I}_k} \hat{\phi} \boldsymbol{n}_k \, ds = \nabla(c_k \phi), \tag{1.8}$$

$$\frac{1}{V} \int_{\mathcal{I}_k} \boldsymbol{n}_k \otimes \hat{\boldsymbol{f}} \, ds = \nabla(c_k \boldsymbol{f}). \tag{1.9}$$

An important special case of (1.8) is that

$$\frac{1}{V} \int_{\mathcal{I}_k} \boldsymbol{n}_k \, ds = \nabla c_k, \tag{1.10}$$

which, since $\mathcal{I}_k \cup \mathcal{I} = \partial(C_k \cap \Omega)$ is closed implies that

$$\frac{1}{V}\int_{\mathcal{I}} n_k \, ds = -\nabla c_k. \tag{1.11}$$

Mass and momentum balances

Let the kth constituent of the mixture have (constant) density ρ_k and assume for every point in C_k there is defined a velocity $\hat{v}_k$. Then, with reference to Figure 1.1, the conservation of mass implies

$$\frac{\partial}{\partial t}\int_{C_k \cap \Omega} \rho_k \, dV = -\int_{\mathcal{I}_k} \rho_k \hat{v}_k . n_k \, ds,$$

assuming no mass transfer occurs across the interface I. Using (1.5) this is

$$\frac{\partial}{\partial t}\int_{C_k \cap \Omega} \rho_k \, dV + \nabla . \int_{C_k \cap \Omega} \rho_k \hat{v}_k \, dV = 0.$$

Multiplying through by $1/V$ and using the definition of the volume average (1.1) and the definition of c_k, (1.2), yields an equation for the mass balance of the kth constituent

$$\frac{\partial c_k}{\partial t} + \nabla . c_k v_k = 0, \tag{1.12}$$

after dividing through by the density.

When considering the momentum balance it is necessary to introduce stress tensors for each of the constituents. This is a less familiar concept for a solid constituent than for a fluid, but enters the equations in an analogous way to the fluid stress tensor in that it represents the force exerted on the solid within the control volume by the solid outside it. For a particle straddling the control volume boundary (figure 1.2) such a force will arise from the transmission of the fluid stress acting on the surface of the particle which is outside the control volume. Particle collisions may also contribute to the solid stress, although this is likely to be important only at high concentrations. Again referring to figure 1.1 we see that the momentum balance for the kth constituent can be written down in integral form as

$$\begin{aligned}\frac{\partial}{\partial t}\int_{C_k \cap \Omega} \rho_k \hat{v}_k \, dV \;=\; & -\int_{\mathcal{I}_k} \rho_k n_k \hat{v}_k \hat{v}_k \, ds + \int_{C_k \cap \Omega} \rho_k g \, dV \\ & + \int_{\mathcal{I}_k} n_k \hat{\sigma}_k \, ds + \int_{\mathcal{I}} n_k \hat{\sigma}_k \, ds.\end{aligned}$$

Here $\hat{\sigma}_k$ is the stress tensor for the kth constituent and $g = (0, 0, -g)$ is the gravita-

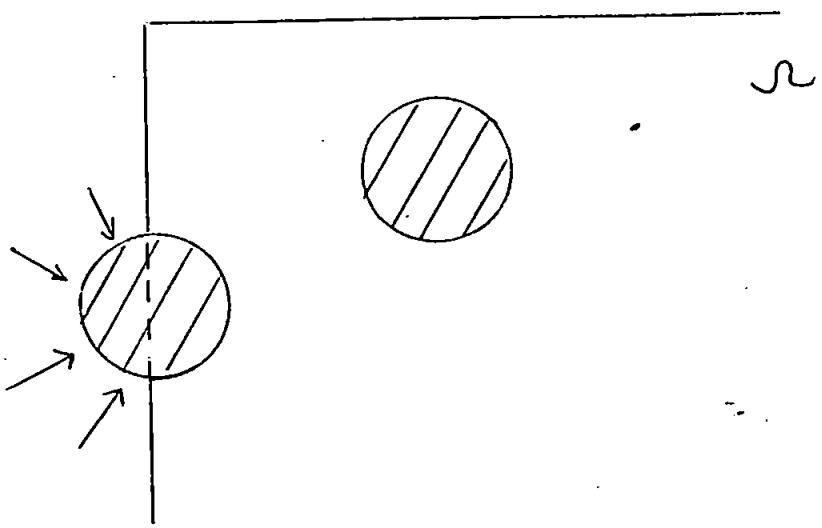

Figure 1.2: Particle stress

tional acceleration vector. Using (1.5) this becomes

$$\frac{\partial}{\partial t}\int_{C_k\cap\Omega}\rho_k\hat{v}_k\,dV+\nabla.\int_{C_k\cap\Omega}\rho_k\hat{v}_k\hat{v}_k\,dV = \int_{C_k\cap\Omega}\rho_k g\,dV + \nabla.\int_{C_k\cap\Omega}\hat{\sigma}_k\,dV+\int_I n_k\hat{\sigma}_k\,ds$$

which, in terms of averaged variables, is

$$\frac{\partial}{\partial t}\rho_k c_k v_k+\nabla.\rho_k c_k\overline{\overline{\hat{v}_k\hat{v}_k}} = c_k\rho_k g+\nabla.c_k\sigma_p+\frac{1}{V}\int_I n_k\hat{\sigma}_k\,ds. \qquad (1.13)$$

This equation is not suitable as a momentum balance because of the occurrence of the quantity $\overline{\overline{\hat{v}_k\hat{v}_k}}$. The problem is similar to that which arises when the Navier-Stokes equations are averaged in turbulence theory and occurs because of the non-linear nature of the laws of motion. A 'fluctuating' velocity field v_k'' is defined such that

$$v_k''(x,x') = \hat{v}_k(x') - v_k(x), \qquad (1.14)$$

where the variable x is associated with the position in space of the averaging volume Ω and x' is the variable with respect to which the averaging integration is carried out. With this definition

$$\overline{\overline{v_k}} = v_k,$$

$$\overline{\overline{v_k''}} = 0,$$

so that substituting for $\hat{v}_k$ in $\overline{\overline{\hat{v}_k\hat{v}_k}}$ yields $\overline{\overline{\hat{v}_k\hat{v}_k}} = v_k v_k + \overline{\overline{v_k''v_k''}}$. Thus (1.13) becomes

$$\frac{\partial}{\partial t}\rho_k c_k v_k + \nabla.\rho_k c_k v_k v_k + \nabla.\rho_k c_k \overline{\overline{v_k''v_k''}} = c_k\rho_k g + \nabla.c_k\sigma_p + \frac{1}{V}\int_I n_k\hat{\sigma}_k\,ds \tag{1.15}$$

It is usual to neglect the term involving v_k'', thereby introducing an unknown error into the momentum balance. Some attempts have been made to account for this term (see Trapp 1986).

Finally, note that use of the mass balance equation, (1.12), enables the acceleration terms to be written in an alternative form, as follows

$$\frac{\partial}{\partial t}\rho_k c_k v_k + \nabla.\rho_k c_k v_k v_k = \rho_k c_k[\frac{\partial v_k}{\partial t} + v_k.\nabla v_k] \equiv \rho_k c_k \frac{Dv_k}{Dt} \tag{1.16}$$

1.2.2 Constitutive relations

In this section we propose forms for the terms involving the stress tensor σ_p occurring in (1.15), assuming the mixture consists of solid particles suspended in a Newtonian fluid. The following notation is introduced: fluid and particle velocities will be denoted by v and u respectively, other quantities associated with the fluid or particle phases will be given an appropriate subscript f or p.

The mass balance equations for the two constituents are

$$\frac{\partial c_p}{\partial t} + \nabla.c_p u = 0, \tag{1.17}$$

$$\frac{\partial c_f}{\partial t} + \nabla.c_f v = 0. \tag{1.18}$$

On account of (1.3) we have $c_f = 1 - c_p$ so that the sum of (1.17) and (1.18) yields

$$\nabla.(c_p u + c_f v) = 0,$$

which we use in place of (1.18).

Turning to the momentum balance (1.15), it is clear that the integral of the stress tensor around the interface I gives the force acting between the two phases which, from Newton's third law, satisfies

$$\int_I n_p\hat{\sigma}_p\,ds = -\int_I n_f\hat{\sigma}_f = \int_I n_p\hat{\sigma}_f.$$

The momentum balances for the two phases can thus be written:

$$\frac{\partial}{\partial t}\rho_p c_p \boldsymbol{u} + \nabla.\rho_f c_k \boldsymbol{u}\boldsymbol{u} = c_p\rho_p \boldsymbol{g} + \nabla.c_p\boldsymbol{\sigma}_p + \frac{1}{V}\int_{\mathcal{I}} \boldsymbol{n}_p\hat{\boldsymbol{\sigma}}_f\, ds, \tag{1.19}$$

$$\frac{\partial}{\partial t}\rho_f c_f \boldsymbol{v} + \nabla.\rho_f c_k \boldsymbol{v}\boldsymbol{v} = c_f\rho_f \boldsymbol{g} + \nabla.c_f\boldsymbol{\sigma}_f - \frac{1}{V}\int_{\mathcal{I}} \boldsymbol{n}_p\hat{\boldsymbol{\sigma}}_f\, ds. \tag{1.20}$$

Interfacial terms

To proceed further we consider in detail the bounding surface $\mathcal{I}$. Figure 1.3 shows that it can be split into a collection of surfaces S, associated with particles lying entirely within the averaging volume, and a collection of open surfaces $\mathcal{U}$, associated with particles straddling the boundary. The reason for making the distinction lies in

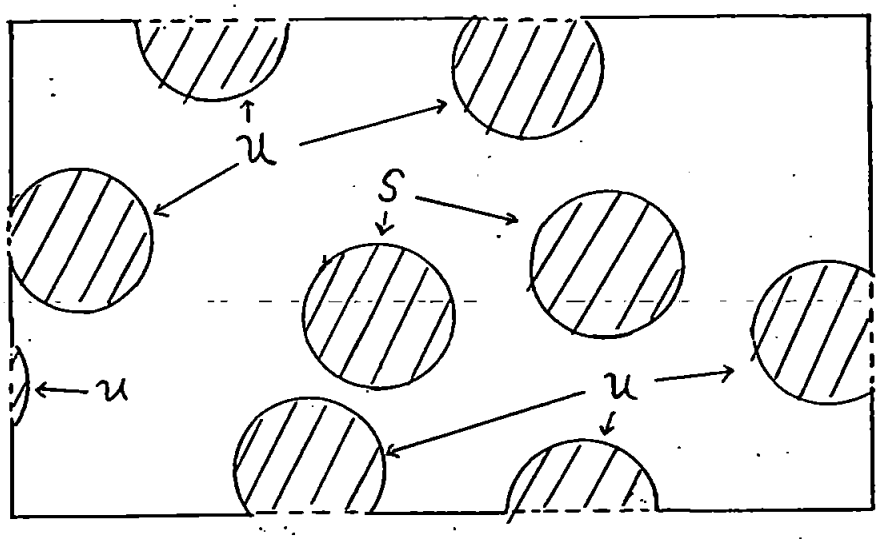

Figure 1.3: Open and closed surfaces comprising $\mathcal{I}$.

the following results. Since S consists of closed surfaces

$$\int_S \boldsymbol{n}_p\, ds = 0.$$

Now $\mathcal{I} = S \cup \mathcal{U}$, thus we can write (1.11) as

$$\frac{1}{V}\int_{\mathcal{I}} \boldsymbol{n}_p\, ds = \frac{1}{V}\int_{\mathcal{U}} \boldsymbol{n}_p\, ds = -\nabla c_p. \tag{1.21}$$

This result means it is not possible to ignore the contribution from the particles lying on the boundary on the reasoning that the ratio of the number of these particles to those within Ω is of $O(1/L)$, where L is the length scale associated with the averaging

volume. If we estimate the contribution from the integral around $\mathcal{U}$ by replacing $\hat{\sigma}_p$ by its average value σ_p then

$$\frac{1}{V}\int_{\mathcal{U}} n_p.\sigma_p\, ds = \frac{1}{V}(\int_{\mathcal{U}} n_p\, ds).\sigma_p = -(\nabla c_p).\sigma_p,$$

which is of the same form as the mean stress term that appears in the particle momentum equation (1.19) and so cannot be discarded.

To proceed from here, a number of authors, e.g. Ishii 1975, have proposed defining an average interfacial stress $\sigma_{(i)}$ (not necessarily equal to the volume averaged stress) and to write

$$\hat{\sigma}_f(x') = \sigma_{(i)}(x) + \sigma'''_f(x, x'). \tag{1.22}$$

where x, x' have the same interpretation as in (1.14). The point of this is to estimate the contribution from the integral around $\mathcal{U}$ using $\sigma_{(i)}$ so that only the stress around complete particles (associated with the closed surfaces S) needs subsequently to be considered. If the following formal definition of $\sigma_{(i)}$ is made

$$(\int_{\mathcal{U}} n_p\, ds).\sigma_{(i)} = -(\nabla c_p).\sigma_{(i)} \equiv \int_{\mathcal{U}} n_p\hat{\sigma}_f\, ds, \tag{1.23}$$

where we have used (1.11), then the integral around $\mathcal{U}$ is accounted for exactly. If (1.22) is substituted into the momentum equations (1.19) and (1.20) we obtain

$$\frac{\partial}{\partial t}\rho_p c_p u + \nabla.\rho_f c_k uu = c_p\rho_p g + c_p\nabla.\sigma_p + (\nabla c_p).[\sigma_p - \sigma_{(i)}] + \frac{1}{V}\int_{\mathcal{I}} n_p\sigma'''_f\, ds, \tag{1.24}$$

$$\frac{\partial}{\partial t}\rho_f c_f v + \nabla.\rho_f c_k vv = c_f\rho_f g + c_f\nabla.\sigma_f - (\nabla c_p).[\sigma_f - \sigma_{(i)}] - \frac{1}{V}\int_{\mathcal{I}} n_p\sigma'''_f\, ds. \tag{1.25}$$

Note that the concentrations in the second term on the right hand side (RHS) of both equations now appear outside the divergence operator. A number of earlier derivations, e.g. Soo (1978), retain the concentrations inside the operator. However the analysis above indicates that this is almost certainly incorrect, and arises from not considering carefully enough the integral around $\mathcal{I}$. The controversy is now generally resolved in favour of the form presented here.

The definition of the interfacial stress via the formal relation (1.23) is criticised by Prosperetti & Jones (1984) since it breaks down if $\nabla c_p = 0$. After undertaking

their own analysis, these authors arrive at a different form for the interfacial stress[2] terms. However, although avoiding the problem associated with the definition of the interfacial stress via (1.23), the equations seem deficient in other respects, as discussed briefly in Section 1.2.3.

Surface integral forces

The integral of σ_f around $\mathcal{I}$ is comprised of two parts; the part associated with the collection of open surfaces, $\mathcal{U}$, has been dealt with by introducing the average interfacial stress, $\sigma_{(i)}$. This leaves the contribution from the collection of closed surfaces, $\mathcal{S}$, to consider. For the integral around a closed surface it is only the variation of stress around the surface that is important; the removal of the constant (for each averaging volume) interfacial stress, $\sigma_{(i)}$, has no effect on the result. Thus the result of integrating σ_f''' around $\mathcal{S}$ is the same as that of integrating σ_f around $\mathcal{S}$. We have also that

$$\frac{1}{V}\int_{\mathcal{S}} n_p \sigma_f''' \, ds = \frac{1}{V}\int_{\mathcal{S}} n_p \sigma_f \, ds = \frac{1}{V}\sum_j \int_{s_j} n_p \sigma_f \, ds,$$

where $\int_{s_j}$ is the integral around the jth particle.

If we can carry out the the calculation for some representative particle s_1 then, supposing there are N particles in the averaging volume, it is plausible to put

$$\frac{1}{V}\sum_j \int_{s_j} n_p \sigma_f \, ds = \frac{N}{V}\int_{s_1} n_p \sigma_f \, ds.$$

The value of N can be determined from the particle concentration c_{p_1} via

$$N \approx \frac{c_p V}{b},$$

assuming all the particles have equal volume b. Therefore

$$\frac{1}{V}\sum_j \int_{s_j} n_p \sigma_f \, ds \approx \frac{c_p}{a}\int_{s_1} n_p \sigma_f \, ds \equiv m. \tag{1.26}$$

The complicated integral is thus reduced to the consideration of forces acting on single particles. Well-known solutions derived for simple cases reveal that a number of forces such as drag, added mass and lift can arise. The dominant force is often the

[2]The analysis is complicated and is carried out using the pressure component of the stress only. Extension of the result to deal with the viscous stress is indicated.

steady drag force, and if we assume the particles are spheres and small enough for Stokes' law to be valid, then it is reasonable to put

$$\boldsymbol{m} = \frac{c_p}{b}[6\pi r\mu(\boldsymbol{v}-\boldsymbol{u})] = c_p\frac{9}{2}\frac{\mu}{r^2}(\boldsymbol{v}-\boldsymbol{u}) \equiv c_p\gamma_0(\boldsymbol{v}-\boldsymbol{u}), \tag{1.27}$$

where the volume averaged velocity difference is clearly appropriate as a 'typical' value of the velocity difference around different particles.[3] It should be borne in mind that Stokes' law is derived for the situation of an isolated particle settling through a quiescent liquid and this is likely to be far from the case in a fluid-particle mixture undergoing motion. However the analytical difficulties involved in deriving results for anything but the most simple cases means that simple forms such as that presented above are the only practicable choice. As a first approximation in accounting for the effect of the presence of other particles the Einstein correction (see e.g. Landau & Lifshitz 1987, p 73) to the fluid viscosity μ in terms of the particle volume fraction can be used so that

$$\mu(c_p) = \mu(1+\frac{5}{2}c_p).$$

For higher concentrations empirical dependencies of μ on c_p exist.

Attempts to incorporate other forces into the continuum theory have met with varying degrees of success. The added mass force in particular has received a lot of attention (Voinov & Petrov 1977, Geurst 1985, Drew & Lahey 1987 and others) but no generally accepted expression for this term has emerged.

Mean stress terms

For a Newtonian fluid the stress tensor is

$$\hat{\sigma}_f = -\hat{p}_f\boldsymbol{I} + \mu[\nabla\hat{\boldsymbol{v}} + \nabla^t\hat{\boldsymbol{v}}], \tag{1.28}$$

where $\hat{p}_f$ is the fluid pressure. The volume average of this appears in the fluid momentum equation (1.25). Averaging the pressure component yields simply the volume averaged pressure p_f; the viscous stress is less straight forward. Using (1.4) the volume averaged viscous stress term can be written

$$\frac{1}{V}\int_{C_f\cap\Omega}[\nabla\hat{\boldsymbol{v}} + \nabla^t\hat{\boldsymbol{v}}]\,dV \;=\; \frac{1}{V}\int_{\partial(C_f\cap\Omega)}[\boldsymbol{n}_f\hat{\boldsymbol{v}} + \hat{\boldsymbol{v}}\boldsymbol{n}_f]\,ds$$

[3] This is the case because the Stokes' drag is linear in the velocity difference.

$$= \frac{1}{V}\int_{\mathcal{I}_f}[n_f\hat{v}+\hat{v}n_f]\,ds + \frac{1}{V}\int_{\mathcal{I}}[n_f\hat{v}+\hat{v}n_f]\,ds$$
$$= \nabla c_f v + \nabla^t c_f v + \frac{1}{V}\int_{\mathcal{I}}[n_f\hat{v}+\hat{v}n_f]\,ds,$$

where (1.9) has been used to convert the integral over $\mathcal{I}_f$ to a term involving volume averaged quantities. To proceed further we approximate the integral around $\mathcal{I}$ as follows: around the surface of each particle $\hat{v}$ must be constant and equal to the particle velocity, assuming the particle to be rigid. Thus approximating the individual particle velocities with the volume averaged velocity we use (1.11) to obtain

$$\frac{1}{V}\int_{\mathcal{I}}[n_f\hat{v}+\hat{v}n_f]\,ds \approx -(\nabla c_f)u - u\nabla c_f.$$

Using (1.3) the averaged stress tensor can be modelled as

$$\sigma_f = -p_f I + \sigma_\mu, \tag{1.29}$$

where

$$\sigma_\mu = \mu c_f(\nabla v + \nabla^t v) - \mu[(v-u)\nabla c_p - (\nabla c_p)(v-u)]. \tag{1.30}$$

When we come to consider the case where the particle concentrations are small and $c \to 0$, the exact form of (1.30) is not important as the term reduces to the that for a single-phase incompressible flow.

For the particle phase we assume the simplest possible constitutive relation, $\hat{\sigma}_p = \hat{p}_p I$, leading to the volume averaged expression $\sigma_p = p_p I$. The only alternative that has appeared in the literature is to assume a Newtonian relation similar to (1.28) — see for example Anderson & Jackson (1967), Needham & Merkin (1983), both of whom considered fluidized beds. However, the physical basis of the the deviatoric stress and the associated viscosity is unclear and at present it seems preferable to consider an isotropic stress only.

With the constitutive assumptions made so far, the equations describing the fluid-solid mixture can be written

$$\frac{\partial c_p}{\partial t} + \nabla.c_p u = 0, \tag{1.31}$$
$$\nabla.(c_p u + c_f v) = 0, \tag{1.32}$$
$$\frac{\partial}{\partial t}\rho_p c_p u + \nabla.\rho_f c_p uu = c_p\rho_p g + c_p\nabla p_p + (\nabla c_p).(p_p I - \sigma_{(i)}) + m, \tag{1.33}$$
$$\frac{\partial}{\partial t}\rho_f c_f v + \nabla.\rho_f c_f vv = c_f\rho_f g + c_f\nabla p_f - (\nabla c_p).(\sigma_f - \sigma_{(i)}) - m + c_f\nabla.\sigma_\mu, \tag{1.34}$$

where σ_f is given by (1.29), m by (1.26) and where $c_f = 1 - c_p$. These are four (vector) equations for six unknowns c_p, u, v, p_f, p_p and $\sigma_{(i)}$. To close the equations some further relation between these quantities is needed. A discussion of forms proposed for these relations, and the connection with the nature and stability of the resulting set of equations, is the subject of the next section.

1.2.3 Stability and well-posedness for two-phase flow equations

In this section we discuss work that has been done to obtain a closed set of equations based on (1.31) to (1.34). All authors have agreed that it is relations between the fluid, particle and interfacial stress terms that are required. In addition nearly all have assumed $\sigma_{(i)} = p_{(i)}I$, both for simplicity and because they have been concerned with flows where the particle Reynolds number,

$$Re_p = \frac{2r|\hat{v} - \hat{u}|}{\nu}, \tag{1.35}$$

is high enough for the viscous stress acting over the surface of a particle to be negligible[4]. At this point it is important to distinguish between the particle Reynolds number, which determines the nature of the interfacial stress, and what might be termed the 'bulk', or flow Reynolds number which is the usual quantity scaling the viscous terms in the non-dimensionalised fluid momentum equation. In general these two numbers are independent of each other. Thus it is quite consistent to use, for example, Stokes law to represent the particle drag, on the assumption that the particles are small and the stress around the particles is dominated by viscous forces, while at the same time neglecting the effect of viscosity on the fluid motion as a whole. Essentially the length scale in the particle Reynolds number is the particle diameter which is clearly independent of the external dimensions of the flow which is used to define the flow Reynolds number.

For the purpose of the following discussion we assume all stresses, including the interfacial stress, can be represented by pressures. This simplifies the argument and is consistent with the presentations of the original authors.

If we assume all stresses can be represented as pressures, the momentum balances

[4]Much work has been motivated by applications in the nuclear power industry where bubbly flows consisting of gas or vapour 'particles' dispersed within a liquid are of interest.The size of the particles is then usually great enough for the pressure to be the primary stress acting on the surface.

become

$$\rho_p c_p \frac{Du}{Dt} = c_p \rho_p g - c_p \nabla p_p - (p_p - p_{(i)}) \nabla c_p + m, \quad (1.36)$$

$$\rho_f c_f \frac{Dv}{Dt} = c_f \rho_f g - c_f \nabla p_f + (p_f - p_{(i)}) \nabla c_p - m, \quad (1.37)$$

where (1.16) has been used to re-write the left hand side (LHS). Note that it is *not* consistent now to use the Stokes law result (1.27) for m, since we are assuming the interfacial stress arises solely from pressure forces. For this case, which implies a large particle Reynolds number, a drag law depending on the square of the velocity difference would be more appropriate.

The simplest possible assumption is that

$$p_p = p_{(i)} = p_f. \quad (1.38)$$

This leads to a closed set of four equations (assuming m has been specified), with four dependant variables c, u, v and p_f, which are identical to those obtained by many early workers in the field. After attempts to solve them numerically gave rise to highly unstable solutions it was discovered that, although having the appearance of a set of hyperbolic (or parabolic) equations, the non-zero characteristics are complex valued, indicating that the equations are *elliptic* in nature[5]. Ramshaw & Trap (1978) give a clear account of the connection between complex characteristics, unstable solutions and the ill-posed nature of the equations. In summary they show that the occurrence of complex characteristics not only implies that solutions are unstable, but that the growth rate of the instability tends to infinity as the wavelength of the perturbation causing the instability tends to zero. Thus starting from some initial condition at $t = 0$, solutions can become arbitrarily large in any given interval of time and the equations are regarded as being 'ill-posed' when solved as an initial value problem. It needs to be emphasized that the occurrence of instability can be legitimate since the equations may possess solutions corresponding to flows that are physically unstable. It is the potentially *unbounded* growth rate of the instabilities that results in the equations being considered mathematically ill-posed.

Since the instabilities are manifest primarily at short wave lengths, Arai (1980) investigated the effect of adding second order viscous terms to the momentum equations. It is well known that terms of this form have the effect of damping high

[5]This has not dissuaded the development of large computer codes based on this set of equations. The instabilities can often be controlled using "artificial viscosity" e.g. Travis et al. (1976).

wavenumber fluctuations. Although yielding well-posed equations, the solutions are still found to be unstable if the constituents are incompressible[6]. This is a special case of a result of Prosperetti & Jones (1985) who look at a very general form of the momentum equations for multi-phase flow and, assuming incompressible constituents, show that if a set of first order equations possesses unstable solutions this cannot be cured by the addition of higher order terms. Real characteristics and stable solutions can however be obtained by including terms of the form $\kappa \nabla c_p$ — as shown in Hill & Bedford (1979). Although the authors include such terms to represent the diffusive effect of Brownian motion, it is evident from an examination of (1.36) and (1.37) that the terms involving the interfacial pressure are of the required form.

The first consideration of the interfacial pressure was given in Stuhmiller (1977) and his assumption is equivalent to putting $p_f = p_p$ and $p_{(i)} = p_f + q$, where q is the surface average of the excess fluid pressure over a particle. For an inviscid flow over an isolated sphere this can be calculated to be

$$q = \alpha \rho_f (v - u)^2, \tag{1.39}$$

where $\alpha = -1/4$. For one-dimensional flows at least, the resulting equation set is found to have real characteristics provided the particle concentration is not too large. Figure 1.4 gives the 'critical' value of q required to ensure real characteristics as a function of concentration.

In Givler (1987) the (reasonable) suggestion is made that the pressure appearing in the solid phase should be the equal to the average pressure around the particle i.e. $p_p = p_f + q$. However, the author neglects to consider the average interfacial pressure and effectively assumes that $p_{(i)} = p_f$. Also, q is determined from a solution valid for $Re_p < 1$, where a major contribution to the interfacial stress must arise from the viscous stress. The resulting expression is of the same form as (1.39) (as it must be on dimensional grounds) except that $\alpha = 9/32$. As the author points out the resulting concentration gradient term is diffusive i.e. it causes a force that tends to move the particles away from regions of high concentration to ones of lower concentration. If α is determined from an inviscid solution, as is surely more correct if the viscous stress is to be ignored, then the sign of α is such that the term is *anti*-diffusive, which is unphysical. Despite this the resulting set of equations possesses real characteristics.

A more satisfactory formulation would appear to be to assume the particle pres-

[6] In the compressible case, stable solutions were found to be possible.

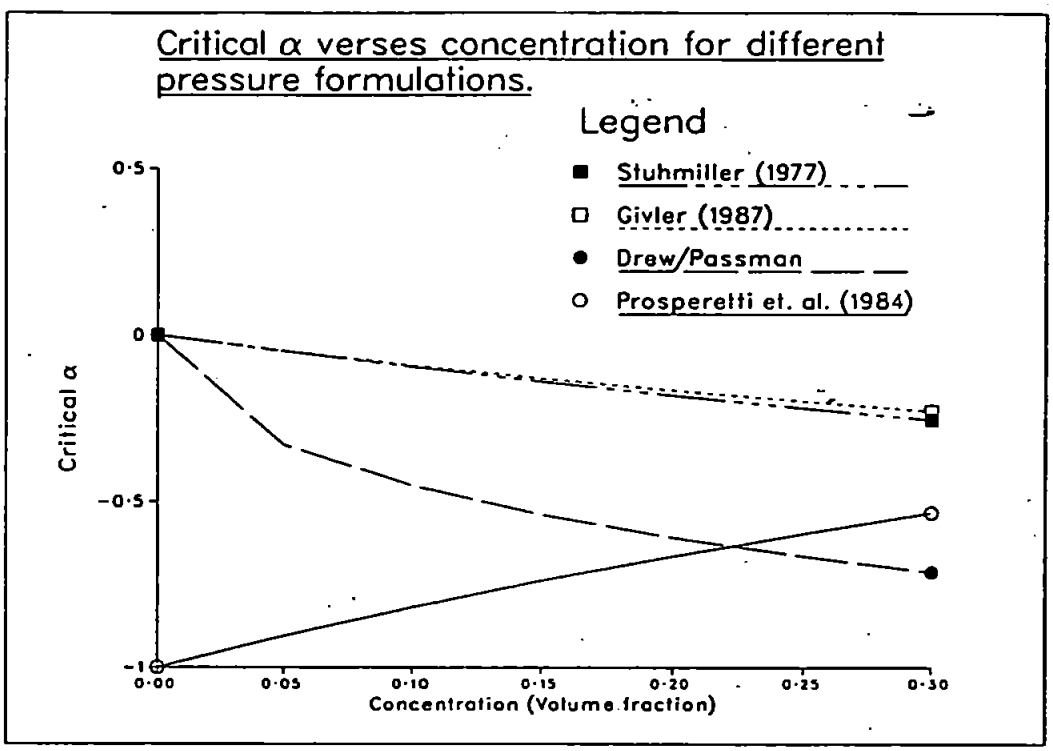

Figure 1.4:

sure is given by the average interfacial pressure $p_p = p_{(i)}$ and to put $p_{(i)} = p_f + q$, where q is the surface average of the excess pressure calculated from (1.39). Again this leads to real characteristics providing the value of α is made large enough for a given concentration (see figure 1.4). This formulation does not appear be mentioned explicitly in the open literature, but Turner (1987) states that a model which essentially the same was communicated to him by Drew. In addition, the multi-phase theory of Passman et al. (1984) includes a relation between the pressures which is of this form.

The equations of Prosperetti & Jones (1985) are derived by pursuing an elaborate analysis based on similar ideas to those presented in deriving the form of the interfacial terms in Section 1.2.2, but allowing the value of $p_{(i)}$ to be different for each particle. The momentum equations the authors obtain, although similar to (1.36) and (1.37) cannot be put exactly into the form of these latter equations. These authors obtain a quantity equivalent to q and they also suggest calculating it from (1.39). An examination of figure 1.4 which shows the value α required to ensure real characteristics, reveals some peculiar behaviour with respect to the Prosperetti model.

Apart from α decreasing as c_p increases, in contrast with all the others, we can see that in the limit $c \rightarrow 0$, which corresponds to a single isolated particle, the value of α required to give real characteristics appears unrealistically large. This does not necessarily invalidate the reasoning behind the derivation but may merely indicate that other effects also need to be accounted for.

A number of workers have proposed equation sets that include extra equations rather than postulating explicit relations between p_f, p_p and $p_{(i)}$. A number of such equation sets are derived by Stewart & Wendroff (1984) and further examples are reviewed in Turner (1987). Baer et al. (1986) look at the detonation of an explosive and, although the equations are considerably more complex than the ones we have considered, they effectively assume $p_{(i)} = p_f$ and derive a further equation relating p_f and p_p to the particle concentration. Holm & Kupershmidt (1986) use techniques based on the Hamiltonian theory of dynamical systems to examine the stability of the multi-phase flow equations with the equal pressure assumption (1.38). They come to the conclusion that it is the equal pressure assumption that leads to problems. The equation set is then extended, using the Hamiltonian formalism, to include equations describing the evolution of interfacial quantities. This extended system is shown to possess real characteristics and stable solutions.

It should be mentioned that a number of the equations sets described above do *not* conserve kinetic energy and can even "create" kinetic energy due to the presence of the interfacial terms (ironically the otherwise unsatisfactory single pressure model does conserve kinetic energy). This can be explained by the fact that the approximations involving relations between the various pressures do not necessarily account correctly for the energy associated with the interfacial forces.

Finally, the work of Geurst (1985) employs a derivation based on a variational principle which includes the added mass effect known from studies of the hydrodynamics of single particles. The resulting equations possess real characteristics. Pressure in the two phases are related by $p_p = p_f + q$, where q is given by an expression similar to (1.39). Unlike the theories discussed above, which derive q from a consideration of average values of pressure around a particle, the pressure difference in Geurst's theory arise from added mass forces and α is found to be a function of c_p. Kinetic energy is conserved by the equations and this, together with the mathematical elegance of the method by which the equations are derived, indicate that this work may constitute a promising starting point for further development (see for example Geurst 1985, 1988).

There seems to be no reason in principle why some of the ideas discussed below

could not be extended to include a consideration of the total fluid stress, which is more appropriate for small particles, rather than just the pressure component. However, for the application to turbulent flows presented in Chapter 2 it is not necessary to consider any of the modifications suggested above and the simple equal pressure assumption is made. The process of taking a turbulent average generates additional terms which, when modelled, circumvent the problem of complex characteristics.

Chapter 2

Application of Two-Phase Flow Theory to Sediment Transport

In this chapter we first give an overview of the field of sediment transport and review work that has been done in applying two-phase flow equations to sediment transport problems. We then develop the necessary theory, based on the work of McTigue (1981), to begin our own investigations which attempt to use the equations two-phase flow theory to account for the effects of particle inertia. This chapter thus presents the main theoretical results of the thesis.

2.1 Sediment dynamics and a review of the two-phase flow approach

The literature connected with the problems of sediment dynamics and sediment transport is extensive, significant contributions having come from a range of disciplines including earth sciences, engineering and physics. A brief overview only will be presented of the major topics before moving on to the main object of this section, which is a discussion the work that has been done applying continuum mixture theories to the field.

The field of sediment transport is concerned with the lifting up, transport, and deposition of solid particles (sediment) by a fluid, usually in the context of the natural environment. From a practical viewpoint the ultimate goal is to be able to predict,

given a set of parameters describing the fluid flow and the sediment properties, where the material is picked up, how much is transported and where it re-settles. From a scientific viewpoint, it is further required that an understanding of the physical processes that occur during sediment transport is achieved.

The two fundamental components of any sediment transport theory are the properties of the sediment and the nature of the flow that interacts with it. There are a number of properties of the sediment are of importance.

Size Sediment is broadly classified into cohesive and non-cohesive types; cohesive sediments are those whose constituent particles are small enough to be affected by forces arising from electrical charges on their surface. Typically cohesive sediment diameters would be less than 0.06mm. Particles with larger diameters are generally non-cohesive and are subject to hydrodynamic and direct collisional forces only.

Shape Although many attempts have been made, particle shape is difficult to quantify. Naturally occuring sediments are often irregular in shape. For simplicity, most theoretical work treats sediment particles as spherical since mathematical expressions, or well documented experimental data, are available for quantities such as drag and added mass coefficients.

Density Typically sediments have relative densities of between 2.0 and 3.0.

Fall velocity This is likely to be a key parameter in any theory of sediment movement since it measures how quickly sediment will fall out of suspension. It will in general depend on all three of the factors mentioned above. Experimental work has also indicated a dependence on the concentration of particles within the fluid, although this is likely to be significant only near the bed where concentrations are high.

When beds of sediment are considered, aspects that become important are the nature of the packing of the particles and the distribution of particle size, shape and density within the bed. Additionally, in a marine environment, the bed is rarely flat but is often rippled, and this can have a major effect on the fluid flow and hence on the transport of sediment.

It is found that the flows associated with significant amounts of sediment movement are almost invariably turbulent. The most extensively studied flows are either steady unidirectional or oscillatory boundary layer flows. The latter are of importance when considering marine sediment transport since, in shallow water, such boundary

layers will be generated by waves.

At the heart of (non-cohesive) sediment transport is the complex interaction between a turbulent fluid and a collection of solid particles, some of which lie settled in the bed and some of which are being carried along by the fluid. A number of aspects of this combined fluid-particle system have been studied.

Threshold conditions: The condition required for the motion of sediment was one of the first aspects of sediment dynamics to be considered (Shields 1924). Despite subsequent work, the empirical relationship discovered by Shields for the shear stress at the bed required to begin to move a particle of given weight can still be recommended (Sleath 1984, pp 260), both for steady and oscillatory flows.[1]

Transport: When particles are transported, a distinction is generally made between two regimes.

1. Moving sediment in the region immediately above the bed is considered to be in the bedload region where, in addition to hydrodynamic and gravity forces, direct contact between particles and between particles and the bed is supposed significant. The classic work for steady flows was done by Bagnold in the 1950s and is described by Raudkivi (1967, pp 58–77). The processes taking place in this region are still poorly understood however.
2. Away from the bed is the region of suspended load where it is supposed that particle concentrations are low and particle collisions negligible. Forces acting on the particles are gravitational and hydrodynamic only. This region is far more amenable to experimental measurement than the bed load region and consequently the properties, for steady unidirectional flows at least, somewhat better known (Raudkivi 1967).

Bedforms The formation of bedforms is a dynamic process that requires consideration of the interaction between a changing bed profile (due to sediment erosion and deposition) and the flow above the bed. Again the classic work on this problem is described in Raudkivi (1967, Chapter 12). The details of the mechanisms involved in this interaction are still far from being understood.

[1] A related, but more difficult, topic is to determine, if possible, some relation between the bed shear stress and the concentration of the sediment immediately above the bed. This so-called reference concentration is needed as a boundary condition for nearly all theories that have been developed for predicting sediment concentration profiles and will be discussed further in Sections 3.1.1 and 4.1.2.

A number of researchers have considered sediment transport problems starting from continuum equations such as those presented in Chapter 1. Since there have been only a few papers it is feasible to review each of them here.

The earliest example of this approach, remarkably, pre-dates all the developments in theories of continua reviewed in Section 1.1. Barenblatt, whose work is described in Bogardi (1974, pp 140–144), put forward a theory, based on a continuum representation of particle dynamics, for turbulent flow of a fluid-particle mixture which he applied to sediment transport in rivers. Unfortunately the complexity of the equations was such that little practical advance could be made at a time when there was no ready access to computers.

More recently Drew (1975) considered the steady unidirectional flow of sediment starting from the same equations as we do (see Section 2.2.1). His approach thereafter is different, and to some extent at odds with ours, as he neglects the term which we, following McTigue (1981), identify as the dominant flux that balances the downward gravitational force. In Drews' theory a different term emerges as the corresponding balance.

The work of McTigue (1981) deals with the same situation as Drew but comes to a different conclusion concerning the dominant terms. We will discuss this disagreement further in Section 2.2.4.

More recently still, De Vantier & Larock (1983) start from a volume averaged formulation, similar to the one we use. The authors combine the equations for each constituent to obtain equations for the total fluid-particle mixture. This approach is likely to be valid if the velocity of the mixture constituents are not too dissimilar. For many types of sediment under field conditions this is reasonable. The standard assumption is made that the sediment velocity equals the fluid velocity minus the fall velocity. The authors also take into account the dependence of the fall velocity on the local concentration. This leaves three equations representing respectively the mixture incompressibility, the balance of momentum for the mixture, and the conservation of particle mass. As noted by the authors, these are very similar to those attributed to Barrenblatt in Bogardi (1974, pp 140–144). The flow is then assumed to be turbulent, the equations averaged, and a $k - \varepsilon$ turbulence closure is used to account for the turbulent correlations. The resulting set of equations are solved numerically for the case of steady uni-directional channel flow. Comparison with experiment is generally satisfactory, although discrepancies are apparent close to the bed. In particular, the horizontal velocity is significantly under-predicted in this region and the authors speculate that this may be due either to stratification

or to the neglect of particle collision forces in the model. The former explanation appears unlikely since the effects of stratification on the turbulence should have been accounted for in the buoyancy terms of the $k - \varepsilon$ model.

The case of sediment transport in steady uni-directional flow is also considered by Kobayashi & Seo (1985). Here a treatment of the bed load as well as the suspended load region is given. In contrast to De Vantier & Larock (1983), the author retains momentum equations for each constituent, rather than combining them to obtain equations for the mixture. Use is made of 'conventional' rather than a concentration-weighted turbulent average (see Section 2.2.1). In the region of suspended load a relatively simple form of turbulence closure is used with eddy viscosity and eddy diffusivity given explicitly as increasing linearly with the distance from the bed. The effects of stratification due to suspended sediment are taken account of by incorporating a Richardson number modification to the mixing length. In the bed load region, the effect of particle collisions is based on the work of Bagnold (1966). Solutions for the fluid velocity, particle velocity, and concentration are found numerically once the boundary conditions at the top of the bed load region are specified. These are obtained by solving the bed load model, from which the authors obtain analytic expressions. The comparison with experimental data is unfortunately limited to regions away from the bed, whereas the effects of fluid-sediment interaction are predicted by the model to be greatest very near the bed.

The paper by Hagatun & Eidsvik (1986) looks at an oscillatory turbulent boundary layer with suspended sediment. Although the authors state that their model derives from two-phase flow equations they give no derivation in the paper. An indication of the simplifying approximations based on scaling arguments is given. The equations presented for mean horizontal fluid velocity and concentration profiles are standard boundary layer equations. Advection terms are omitted in the momentum equation so that only the depth variation of quantities is accounted for. As in De Vantier & Larock (1983), a $k - \varepsilon$ model is used with the effect of stratification due to suspended sediment accounted for by buoyancy terms dependent on concentration. No model of the bed load region is proposed, so that the effect of the bottom flow must be accounted for by the lower boundary conditions. Given the lack of knowledge of the flow in this region this is a difficult task and the authors use well-accepted boundary conditions for velocity and dissipation rate equations while specifying $\partial k/\partial z = 0$ for the turbulent kinetic energy equation. The bottom boundary condition for the concentration, which plays a crucial role in determining the concentration field, assumes the concentration just above the bed to be proportional

to the instantaneous Shields number. Solutions to the equations are found numerically and model predictions for velocity profiles, turbulent stress, and variation of sediment concentration over a wave cycle were found to agree well with experimental data.

2.2 Equations for flow of turbulent two-phase mixtures.

Turbulence averaging of the two-phase flow equations is accomplished in an identical manner to the procedure used in averaging the Navier-Stokes equations of single-phase flow. The field variables are written as the sum of mean and fluctuating components, substituted into the equations of motion and an averaging operation applied. However since the variables appearing in the mixture theory equations already represent averaged quantities the necessity of further averaging might be questioned. Justification for the approach adopted here is two-fold.

1. From a conceptual viewpoint we regard the equations derived in Chapter 2 as being the two-phase equivalent of the continuity and Navier-Stokes equations of single-phase fluid dynamics, and therefore valid in both both turbulent and non-turbulent flows. When the flow becomes turbulent, instantaneous values of the flow variables are not usually of interest, only their time or ensemble averages, thus the equations are further averaged to obtain the equation governing the mean flow.

2. The further averaging of the equations along the lines used for turbulent single-phase flows is particularly revealing, giving rise to terms that can be identified with a number of physical processes that affect the interaction between the turbulent fluid and particle phases.

2.2.1 Favré averaging

The approach here will be based on ideas presented by McTigue (1981). The form of the two-phase flow equations, even for incompressible constituents, has in common with the equations of compressible single-phase flow, that the velocities always appear weighted by a density-like variable, namely the partial densities $\rho_p c$ and $\rho_f(1-c)$. As in the case of the turbulent averaging of single-phase compressible flows, we can define average velocities directly, as in 'Reynolds' averaging, or using density weighted (so-called Favré) averaging. The latter approach has generally been preferred in

work done on turbulent compressible flow and also in the few papers dealing with turbulent two-phase flow flow[2]. An advantage in using the weighted average is that correlations involving concentration fluctuations are generally avoided, leading to equations that are closer to the more familiar Reynolds averaged single-phase case. A further advantage is that a number of properties of the Reynolds average carry over to the two-phase case if concentration-weighted averages are used. This is particularly important when the turbulent kinetic energy is discussed in Section 2.3.

As the starting point the following equation set will be used:

$$\frac{\partial c}{\partial t} + \nabla.(c\boldsymbol{u}) = 0, \tag{2.1}$$

$$\nabla.[c\boldsymbol{u} + (1-c)\boldsymbol{v}] = 0, \tag{2.2}$$

$$\frac{\partial}{\partial t}(\rho_p c\boldsymbol{u}) + \nabla.(\rho_p c\boldsymbol{u}\boldsymbol{u}) = \rho_p c\boldsymbol{g} - c\nabla p_h + c\gamma(\boldsymbol{v}-\boldsymbol{u}), \tag{2.3}$$

$$\frac{\partial}{\partial t}[\rho_f(1-c)\boldsymbol{v}] + \nabla.[\rho_f(1-c)\boldsymbol{v}\boldsymbol{v}] = \rho_f(1-c)\boldsymbol{g} - (1-c)\nabla p_h - c\gamma(\boldsymbol{v}-\boldsymbol{u}) + (1-c)\nabla.\boldsymbol{\sigma}_\mu. \tag{2.4}$$

The above are derived from equations (1.31) to (1.34) by the neglect of interfacial stress terms which multiply the concentration gradient in (1.33) and (1.34). More specifically, we have put $\boldsymbol{\sigma}_{(i)} = \boldsymbol{\sigma}_f$, $p_p = p_f$, and discarded the residual viscous terms that will arise from $p_p\boldsymbol{I} - \boldsymbol{\sigma}_{(i)}$ in equation (1.33). The neglect of terms involving viscosity is justified in the application to high Reynolds number flows, as discussed when the turbulent averaged equations are presented below.

The notation and definition of most quantities are as given in Section 1.2. The symbol for the pressure is written with the subscript 'h' to emphasise that it contains the hydrostatic component $\rho_f g z$. Here z measures the distance in the vertical direction. Also we have written $c_p = c$ and put $c_f = 1 - c$ using (1.3). The quantity γ is initially taken to be the constant, γ_0, defined in (1.27). A more general form dependent on the particle Reynolds number, and thus giving rise to a non-linear drag law, is considered later. The pressure appearing in the equations is the same for both phases. That this leads to the difficulties discussed in Section 1.2.3 need not concern us. As discussed briefly at the end of Section 1.2.3, the terms introduced to remove these difficulties are relevant to obtaining well-posed equations in non-turbulent flow only. Although crucial for this case, the terms are in general very small numerically. Our aim here is to retain only the main terms, and determine the form these take

[2] An exception is Pourahmadi et al. (1983).However they ignore correlations involving concentration fluctuations and the equations they eventually obtain are similar to those we obtain using the Favré average.

after applying a turbulent average.

The Favré averaged velocities are defined via

$$\begin{aligned} \bar{c}\tilde{u} &\equiv < cu >, \\ (1-\bar{c})\tilde{v} &\equiv < (1-c)v > \end{aligned}$$

with

$$\begin{aligned} \bar{c} &\equiv < c >, \\ \bar{p} &\equiv < p > \end{aligned}$$

We then write

$$\begin{aligned} c = \bar{c} + c' \quad , \quad p = \bar{p} + p', \\ u = \tilde{u} + \tilde{u} \quad , \quad v = \tilde{v} + \tilde{v}, \end{aligned}$$

where primed quantities refer to fluctuations defined by direct averaging, whilst quantities with a tilde are fluctuations defined by concentration weighted averaging. Note that

$$< c' >=< p' >= 0$$

but that

$$< \tilde{u} >, < \tilde{v} > \neq 0.$$

The equivalent property of the concentration-weighted average is that

$$< c\tilde{u} >=< c(u-\tilde{u}) >=< cu > - < c\tilde{u} >= \bar{c}\tilde{u} - \bar{c}\tilde{u} = 0,$$

with the fluid phase concentration-weighted average satisfying similarly the relation $< (1-c)v >= 0$. We have therefore

$$< c\tilde{u} >=< (1-c)\tilde{v}) >= 0. \tag{2.5}$$

Since the averaged momentum densities for the particle and fluid phases are respectively $\rho_p < cu >$ and $\rho_f < (1-c)v >$, the property of the standard single-phase average, that there is no contribution to the average momentum arising from the fluctuating motion, is preserved. Further, when we come to consider the kinetic en-

ergy associated with the fluctuating motion in a two-phase flow, the concentration-weighted average is more satisfactory than the use of direct averaging for the following reason. Using the concentration-weighted average the mean kinetic energy density for each phase is partitioned into a component associated with the mean flow and a component associated with the fluctuations. Thus

$$< cu^2 > = \tilde{c}\tilde{u}^2 + < c\tilde{u}^2 >, \tag{2.6}$$

$$< (1-c)v^2 > = (1-\tilde{c})\tilde{v}^2 + < (1-c)\tilde{v}^2 > . \tag{2.7}$$

where, for clarity, we have divided through by the constant mass densities. The turbulent kinetic energy densities are therefore naturally given by $\rho_p < c\tilde{u}^2 >$ and $\rho_f < (1-c)\tilde{v}^2 >$. If direct averaging is used instead, the following expressions arise for the kinetic energy:

$$\begin{aligned} < cu^2 > &= \bar{c}\bar{u}^2 + \bar{c} < (u')^2 > + 2\bar{u} < c'u' > + < c'(u')^2 >, \\ < (1-c)v^2 > &= (1-\bar{c})\bar{v}^2 + (1-\bar{c}) < (v')^2 > - 2\bar{v} < c'v' > \\ &\quad - < c'(v')^2 > . \end{aligned}$$

No obvious partition into mean and fluctuating components of kinetic energy is apparent.

Carrying out a concentration-weighted average of the two-phase flow equations yields:

$$\frac{\partial \bar{c}}{\partial t} + \nabla.(\bar{c}\bar{u}) = 0, \tag{2.8}$$

$$\nabla.[\bar{c}\bar{u} + (1-\bar{c})\bar{v}] = 0, \tag{2.9}$$

$$\begin{aligned} \frac{\partial}{\partial t}(\rho_p \bar{c}\bar{u}) + \nabla.(\rho_p \bar{c}\bar{u}\bar{u}) &= \rho_p \bar{c} g - \bar{c}\nabla\bar{p}_h - < c'\nabla p' > + \bar{c}\gamma(\bar{v}-\bar{u}) \\ &\quad + \gamma < c\tilde{v} > - \nabla. < \rho_p c\tilde{u}\tilde{u} >, \end{aligned} \tag{2.10}$$

$$\begin{aligned} \frac{\partial}{\partial t}[\rho_f(1-\bar{c})\bar{v}] + \nabla.[\rho_f(1-\bar{c})\bar{v}\bar{v}] &= \rho_f(1-\bar{c})g - (1-\bar{c})\nabla\bar{p}_h + < c'\nabla p' > \\ &\quad - \nabla. < \rho_f(1-c)\tilde{v}\tilde{v} > \\ &\quad - \bar{c}\gamma(\bar{v}-\bar{u}) - \gamma < c\tilde{v} > . \end{aligned} \tag{2.11}$$

As expected the averaging procedure has given rise to extra terms involving correlations between fluctuating quantities. We have suppressed the viscous contribution in (2.11) on the assumption that the (flow) Reynolds number is large. As discussed in Section 1.2.3 there is no inconsistency between using Stokes law for the particle drag,

a quantity dependant on the *particle* Reynolds number, and the neglect of viscosity in the equations for the motion as a whole.

2.2.2 Particle phase implications

We compare the approach followed above with the conventional one for modelling the suspended sediment concentrations in turbulent flow (see Wang & Liang 1975 for example). In the conventional approach direct, rather than concentration-weighted, averaging is applied to (2.1), yielding

$$\frac{\partial \bar{c}}{\partial t} + \nabla.(\bar{c}\bar{u} + < c'u' >) = 0.$$

The assumption is then made that the particle velocity can be replaced by the fluid velocity minus the still water settling velocity of the particle, leading to

$$\frac{\partial \bar{c}}{\partial t} + \nabla.[\bar{c}(\bar{v} + w_0) + < c'v' >] = 0 \tag{2.12}$$

where $\mathbf{w_b} = (0, 0, -w_0)$. The steady particle fall velocity, w_0, is determined by the balance between, gravity, buoyancy and particle drag forces and in our notation is given by

$$w_0 = g(\rho_p - \rho_f)/\gamma. \tag{2.13}$$

Using concentration-weighted averaging (2.1) has exactly the same form (2.8) before and after averaging. The averaged particle momentum equation (2.10) becomes essentially an equation for the particle volume flux, $\bar{c}\bar{u}$, that appears in (2.8). We show that in the limit of zero particle inertia and assuming the concentrations are small that (2.12) can be derived from the two-phase flow equations. It is possible to start from either the averaged equations (2.8) to (2.11), or the pre-averaged set (2.1) to (2.4). We use the latter, as this gives an additional relation that will be of use subsequently to relate quantities involving particle velocities to ones involving fluid velocities.

We first separate out the hydrostatic component of pressure, putting

$$\nabla p_h = \rho_f g + \nabla p.$$

Introducing now velocity and time scales v^+, $1/\omega$ (anticipating the application to oscillatory flows the time scale is defined via a frequency ω), and defining length and pressure scales v^+/ω and $\rho_f(v^+)^2$ respectively, we find that (2.3) can be written in

non-dimensional form as

$$c(v^* - u^*) + cw_0^* = \tau^* c \left(\frac{Du^*}{Dt^*} + \frac{1}{\rho} \nabla p^* \right). \tag{2.14}$$

Here

$$\tau^* = \frac{\rho_p \omega}{\gamma}, \tag{2.15}$$

$$\rho = \frac{\rho_p}{\rho_f}, \tag{2.16}$$

$$w_0^* = w_0/v^+, \tag{2.17}$$

Although crude, the scaling analysis is sufficient for the purpose of revealing the key non-dimensional parameters. The quantity τ^* is the ratio of the particle response time ρ_p/γ, to the characteristic time scale of the flow. The terms in (2.14), and in its turbulent averaged form, that are scaled by τ^* we will call the "inertia terms". Note that in addition to the particle acceleration terms proper, this definition includes the pressure term. Neglect of particle inertia is equivalent to setting $\tau^* = 0$. If this "zero particle inertia" approximation is made in (2.14) we obtain

$$c(v^* - u^*) + w_0^* c = 0,$$

correct to zeroth order in τ^*. In dimensional form this is

$$c(v - u) + w_0 c = 0. \tag{2.18}$$

Dividing (2.18) through by c gives the standard approximation, that the fluid and particle velocities differ only by the fall velocity

$$u = v + w_0. \tag{2.19}$$

Averaging (2.18) yields

$$\bar{c}\bar{u} = \bar{c}w_0 + \bar{c}\bar{v} + < c\tilde{v} > . \tag{2.20}$$

The averaged particle volume flux, $\bar{c}\bar{u}$, is seen to consist of three components, due to gravity, the mean fluid velocity, and the fluid velocity fluctuations. If (2.20) is substituted into (2.8) we have

$$\frac{\partial \bar{c}}{\partial t} + \nabla . [\bar{c}(\bar{v} + w_0) + < c\tilde{v} >] = 0, \tag{2.21}$$

which is identical to (2.12), apart from the form of the concentration-velocity correlation. This essentially is the result of McTigue (1981), extended to the case of general flows.

We now derive a relation between the concentration-velocity correlations that appear in (2.12) and (2.21), showing that they become equal in the limit of $\bar{c} \to 0$. From basic definitions

$$\begin{aligned} v' &= v - < v >, \\ \tilde{v} &= v - \frac{< (1-c)v >}{1-\bar{c}}, \end{aligned}$$

so that

$$\tilde{v} = v' - \frac{< (1-c)v > -(1-\bar{c}) < v >}{1-\bar{c}}.$$

Putting $v = < v > + v'$ we obtain, since $< v' > = 0$, the relation

$$\tilde{v} = v' + \frac{< c'v' >}{1-\bar{c}}. \tag{2.22}$$

Multiplying through by c and averaging leads to the result

$$< c\tilde{v} > = \frac{1}{1-\bar{c}} < c'v' > . \tag{2.23}$$

Another useful result is obtained from (2.22) by taking the tensor product of (2.22) with $\tilde{v}$, then using (2.22) again, to substitute for $\tilde{v}$ on the RHS of the expression, and finally averaging to obtain

$$\begin{aligned} < \tilde{v}\tilde{v} > &= < v'v' > + \frac{< c'v' >< c'v' >}{(1-\bar{c})^2} \\ &= < v'v' > + O(c^2). \end{aligned} \tag{2.24}$$

Similarly we find that

$$< c\tilde{v}\tilde{v} > = < cv'v' > + O(c^3). \tag{2.25}$$

To conclude this section we list two advantages that we consider the mixture theory approach has over the conventional one.

1. Although reducing to standard expressions when the particles are taken to be inertia-less and the concentrations small, mixture theory offers, in principle at least, a way of accounting for more complex interactions between the particle and fluid fields by retaining additional terms in the particle momentum balance.

2. Mixture theory provides a sound theoretical framework in which to investigate turbulent two-phase flows. It can lead to insight into the dynamics of the flow, for example the identification of the important term $< c\tilde{v} >$ as arising from the interaction between the fluid velocity fluctuations and the particle drag.

2.2.3 Fluid phase implications

An examination of the implications of the mixture theory equations for the fluid phase is now made for the case when particle inertia is assumed small ($\tau^* \ll 1$) and the concentration is low. As in Section 2.2.2 it is possible to use either the averaged or pre-averaged sets of equations and again we use the pre-averaged set. If $c \ll 1$ in equations (2.2) and (2.4) then we obtain, after separating out the hydrostatic component of pressure,

$$\begin{aligned} \nabla.v &= 0, \\ \rho_f[\frac{\partial v}{\partial t} + \nabla.(vv)] &= -\nabla p - c\gamma(v-u) + \mu\nabla^2 v. \end{aligned} \tag{2.26}$$

The drag terms are retained because small particle inertia implies that γ will be large, even if formally the term is of $O(c)$. Applying the same scaling analysis as in Section 2.2.2 leads to

$$\frac{\partial v^*}{\partial t^*} + \nabla.(v^*v^*) = -\nabla p^* - \rho\frac{c}{\tau^*}(v^*-u^*) + \frac{1}{Re}\nabla^2 v^*$$

where $Re = (v^+)^2/\omega\nu$. Note the drag term scales as c/τ^*, the ratio of two small quantities, justifying its retention in the equation. Substituting for the velocity difference in the drag term and using the assumption of zero particle inertia in the form (2.19) yields

$$\frac{\partial v^*}{\partial t^*} + \nabla.(v^*v^*) = -\nabla p^* + \rho\frac{c}{\tau^*}w_0^* + \frac{1}{Re}\nabla^2 v^*,$$

which, in terms of dimensional variables, is

$$\frac{\partial v}{\partial t} + \nabla.(vv) = \frac{\Delta\rho}{\rho_f}cg - \frac{1}{\rho_f}\nabla p + \nu\nabla^2 v, \tag{2.27}$$

where $\Delta\rho = \rho_p - \rho_f$. Defining the mixture density $\rho_m = \rho_p c + \rho_f(1-c)$ enables (2.27) to be written in the form

$$\frac{\partial v}{\partial t} + \nabla.(vv) = \frac{\rho_m - \rho_f}{\rho_f}g - \frac{1}{\rho_f}\nabla p + \nu\nabla^2 v.$$

This is precisely equivalent to the Boussinesq approximation, except that the density changes arise from the presence of the sediment. Averaging (2.27) then gives

$$\frac{\partial \bar{v}}{\partial t} + \nabla.(\bar{v}\bar{v}) = \frac{\Delta\rho}{\rho_f}\bar{c}\bar{g} - \frac{1}{\rho_f}\nabla\bar{p} - \nabla < v'v' >, \tag{2.28}$$

where we have again suppressed the viscous term on the assumption that the Reynolds number is large.

The importance of this result is that we can now use standard turbulence models to close (2.28). The effect of the particles on the fluid motion is, to this level of approximation, to give rise to buoyancy terms which can be accounted for in the turbulence closures which are the subject of Section 2.3.

2.2.4 Comparison between the work of Drew and McTigue

In this section the main concern will be to simplify the full turbulent averaged equation set and look at sediment transport in a steady uni-directional flow with the aim of clarifying the difference in the approaches of McTigue (1981) and Drew (1975). The assumptions made are:

1. only vertical gradients are non-zero (i.e. no horizontal and no time dependence);

2. vertical fluxes are zero ($\bar{u}_2 = \bar{v}_2 \equiv 0$);

3. the particle concentrations are low ($c \ll 1$).

It is easy to show that for the non-turbulent flow of a mixture, the first two conditions imply the trivial solution $\rho_f = \rho_p$, $c = 1$ or $c = 0$, and a hydrostatic pressure. The reason for this is the absence any of force supporting the heavier constituent of the mixture against gravity. If a non-trivial solution is to exist in the turbulent case, the force acting to support a distribution of particles must be associated with terms that arise due to the turbulence. In Section 2.2.2 the term $< c\bar{v} >$, resulting from the drag term in the particle momentum equation, was identified with the turbulent flux that arises in the conventional sediment transport approach, and provides a mechanism for supporting the sediment load against gravity. However Drew (1975), in his analysis of steady unidirectional flow, decides that a different term, essentially the particle equivalent of the Reynolds stress, provides the requisite balance.

For steady uni-directional flow the mass conservation equations are satisfied identically. The vertical momentum balances are:

$$\rho_p \frac{d}{dz} < c\tilde{u}_2^2 > = -\rho_p \bar{c} g - \bar{c}\frac{d\bar{p}}{dz} + \gamma < c\tilde{v}_2 > - < c' \frac{dp'}{dz} >, \tag{2.29}$$

$$\rho_f \frac{d}{dz} < (1-c)\tilde{v}_2^2 > = -\rho_f (1-\bar{c}) g - (1-\bar{c})\frac{d\bar{p}}{dz} - \gamma < c\tilde{v}_2 > + < c' \frac{dp'}{dz} > . \tag{2.30}$$

The vertical fluid momentum balance for low concentrations becomes, using (2.23) and (2.24),

$$-\rho_f g - \frac{d\bar{p}}{dz} - \rho_f \frac{d}{dz} < v_2'^2 > + \gamma < c' v_2' >= 0,$$

where all $O(c)$ terms, apart from those associated with drag, have been neglected. Rearranging this to give an expression for the mean pressure gradient and substituting into (2.29) yields,

$$\rho_p \frac{d}{dz} < c\tilde{u}_2^2 > -\bar{c}\rho_f \frac{d}{dz} < v_2'^2 > -\gamma < c' v_2' > + < c' \frac{dp'}{dz} >= -\bar{c} g (\rho_p - \rho_f), \tag{2.31}$$

after neglecting the $O(c^2)$ term, $\gamma \bar{c} < c' v_2' >$. Drew retains only the RHS and the first two terms on the LHS , having eliminated the remaining two terms near the beginning of his analysis on scaling arguments. In particular $< c' v_2' >$ is neglected after comparing it with the mean drag $\bar{c}(\bar{v}_2 - \bar{u}_2)$. This cannot be valid; the mean vertical component of drag is identically zero and so clearly cannot overwhelm the corresponding component of the 'fluctuating' drag term. The argument used for eliminating the pressure fluctuation term also seems questionable.

Carrying out our own scaling analysis, the assumption is made that both fluid and particle velocity fluctuations can be assigned a typical scale v'^+ and that this is suitable for both horizontal and vertical components. Pressure fluctuations are scaled with $\rho_f (v'^+)^2$ (see for example Hinze 1959, pp 454). If l_z is a typical vertical length over which the quantities vary we can write (2.31) in terms of scaled variables as

$$S[\rho \frac{d}{dz} < c\tilde{u}_2^2 > -\bar{c}\frac{d}{dz} < v_2'^2 > + < c' \frac{dp'}{dz} >] - < c' v_2' >= -\bar{c} w_0^*, \tag{2.32}$$

where $\rho = \rho_p / \rho_f$, $S = \rho_f v'^+ / \gamma l_z$ and $w_0^* = w_0 / v'^+$, with w_0 given by (2.13).

To determine typical values for these quantities the experimental parameters reported by Drew in comparing his theory with experiment will be used. For a run using particles of mean diameter 0.25 mm and density 2670 kg/m^3, the friction veloc-

ity, which will be equated with v'^{+}, was determined to be 0.064 m/s. This gives the following values for the parameters appearing in (2.32): $\rho = 2.67$, $S = 2.0 \times 10^{-4}/l_z$ and $w_0^* = 0.8$. It would therefore seem that terms of order S can only be significant if $l_z < 1$ mm. This is not implausible near the bed where concentrations and velocities change rapidly. Drew in comparing his theoretical curves with experiment apparently obtains good agreement with quite reasonable values for the two empirical constants of his theory[3]. However, our analysis clearly shows that the term $< c'v_2' >$ is of the same order as the buoyant weight and cannot, on scaling arguments, be excluded from any consideration of vertical momentum balance. Indeed, apart from regions where large vertical gradients are present, the analysis suggests that this term, together with the gravity term, dominate the balance. This is in agreement with McTigue (1981) who carries out a similar analysis to the one just presented. The importance of the terms of order S near the bed can only be determined by proposing models for these terms and comparing the solutions of the resulting equations with experiment. This will be done for the case of oscillatory flow in Chapter 5.

For completeness, the horizontal momentum balances for the steady flow considered in this section are given:

$$\rho_p \frac{d}{dz} < c\tilde{u}_1\tilde{u}_2 > = -\bar{c}\frac{d\bar{p}}{dx} + \gamma\bar{c}(\bar{v}_1 - \bar{u}_1) + \gamma < cv_1' >, \tag{2.33}$$

$$\rho_f \frac{d}{dz} < (1-c)v_1'v_2' > = -(1-\bar{c})\frac{d\bar{p}}{dx} - \gamma\bar{c}(\bar{v}_1 - \bar{u}_1) - \gamma < cv_1' > . \tag{2.34}$$

Using (2.20) and assuming low sediment concentrations (2.34) becomes

$$\rho_f \frac{d}{dz} < v_1'v_2' > = -\frac{d\bar{p}}{dx},$$

the standard result for the fluid phase momentum balance in steady unidirectional turbulent flow. If the turbulent stress is assumed constant (i.e. the pressure gradient is zero) dimensional reasoning leads to the prediction of the well-known logarithmic velocity profile.

2.2.5 Including further fluid-particle interactions

In the interests of simplicity we have so far considered momentum transfer between the fluid and solid resulting from pressure and linear (Stokes) drag forces only. It is

[3]It is interesting that the particle fall velocity does not enter as a parameter into his theory at all.

well known that a variety of other forces act on a particle moving through a fluid, — the added mass force, Basset force, and lift forces for example. In addition the linear relation between the relative velocity $v - u$ and the drag force will become increasingly inaccurate as the particle Reynolds number (1.35) becomes of order one, or greater.

The correct specification of the added mass force within the continuum theory is at present an open one, although the work of Geurst (1985) appears to go a long way toward resolving it, and the form we adopt here is one among a number that have been proposed. Further, no attempt, so far as this author is aware, has been made to incorporate the Bassett force into a mixture theory[4]. The derivation of an expression for this force is considered outside the scope of the work presented here and hence no attempt is made to include it. No attempt is made either to include lift forces, although the form of added mass force used does contain a term that can be identified as a lift force.

Inclusion of added mass

We use the form derived by Drew & Lahey (1987) for the added mass terms in a non-turbulent flow,

$$\begin{aligned} A &= c\rho_f C_{vm}\left[\left(\frac{\partial v}{\partial t} - \frac{\partial u}{\partial t} + v.\nabla v - u.\nabla u\right) - (v-u).\left(\nabla v - \nabla^t v\right)\right] \\ &\equiv c\rho_f C_{vm}\left[\left(\frac{Dv}{Dt} - \frac{Du}{Dt}\right) - (v-u).\left(\nabla v - \nabla^t v\right)\right]. \end{aligned} \tag{2.35}$$

Here C_{vm} is taken to be constant. Interestingly, solutions derived for single spheres in unbounded fluids assuming either potential or Stokes flow both give $C_{vm} = \frac{1}{2}$ and this is the value adopted here. In general we might expect C_{vm} to be a function of Re_p and c, however for simplicity we will neglect such considerations. The form of (2.35) satisfies the principle of 'material frame indifference' (see Drew & Lahey 1987) and is also consistent with the force obtained for a single sphere in an unbounded, *inviscid* fluid. It is seen to consist of two parts, a relative acceleration, which is the added mass force proper, and a 'lift' force proportional to the relative velocity. This lift force is that experienced by a particle moving relative to a rotating fluid first considered by Proudman (1916). It might be questioned whether a form derived from a consideration of inviscid fluids is suitable for the situation we are interested in, where viscous forces are predominant around the surface of the particle. In defence,

[4] Experimental studies, e.g. Carley & Al-Taweel (1971), have indicated the Basset force to be at least as significant as the added mass force.

it can be said that the added mass force, for a single particle at least, is same in both potential and Stokes flow.

If we substitute for the convective derivative of the fluid velocity in (2.35) using (2.27), and add the resulting expression to the RHS of (2.3) we obtain, after separating out the hydrostatic pressure component,

$$(\rho_p + \rho_f C_{vm})\left[\frac{\partial}{\partial t}cu + \nabla.cuu\right] = c(1+cC_{vm})\Delta\rho g - c(1+C_{vm})\nabla p + c\gamma(v-u) + C_{vm}c\mu\nabla^2 v - c\rho_f C_{vm}(v-u).(\nabla v - \nabla^t v).$$

Apart from the viscous term and the lift term, this equation can be averaged in exactly the same manner as equation (2.3). The averaging of the lift term is considered in Section 2.3.2, while averaging the term involving viscosity yields

$$\bar{c}\nabla^2 v + \nabla^2 < c'v' > + < (\nabla c').(\nabla v') > .$$

When scaled, the first two terms can be neglected, assuming the Reynolds number is large, and the last term is identically zero if the turbulence is assumed to be locally isotropic (Rodi 1980).

Inclusion of non-linear drag

We include the effect of non-linear drag in the term

$$D = \gamma c(v-u)$$

by modifying γ to be a function of the particle Reynolds number Re_p. In the linear regime $\gamma = \gamma_0$, where γ_0 is given by Stokes law as

$$\gamma_0 = \frac{9}{2}\eta/r^2. \tag{2.36}$$

Empirically derived formula are necessary when Re_p becomes large enough for (2.36) to become inadequate. Clifte et al. (1978) list a number of such formulae and, for the approximate range $0 < Re_p < 10^3$, these give the Re_p dependence of γ in the form

$$\gamma = \gamma_0(1 + \alpha Re_p^{\beta}), \tag{2.37}$$

where α, β are chosen to fit experiment.

The Favré averaged particle momentum equation, with allowance made for a non-

linear drag and with added mass included, is then given by

$$\begin{aligned}\rho_{vm}\left(\frac{\partial}{\partial t}\bar{c}\bar{u}+\nabla.\bar{c}\bar{u}\bar{u}\right) &= \left[\bar{c}+C_{vm}(\bar{c}+<c'^2>)\right]\Delta\rho g+<c\gamma(|v-u|)(v-u)> \\ &\quad -\rho_{vm}(\bar{c}\nabla\bar{p}+<c'\nabla p'>)-\rho_{vm}\nabla.<c\tilde{u}\tilde{u}> \\ &\quad -\rho_f C_{vm}<c(v-u).(\nabla v-\nabla^t v)>, \qquad (2.38)\end{aligned}$$

where $\rho_{vm}=(\rho_p+\rho_f C_{vm})$. In the next section the closure of the turbulent averaged equations is considered.

2.3 Turbulence modelling

All practical methods for predicting turbulent flow solve averaged forms of the equations such as those presented in Section 2.2.1. This is only a preliminary and essentially formal step as the resulting equations contain correlations that arise due to the non-linear form of the original expressions. It is possible to derive formal equations for these correlations but these are found themselves to contain further and more complicated correlations. In fact the sequence of deriving equations for successively more complicated correlations will never produce a closed system. At some point we have to stop and model the unknown terms using quantities for which we are solving. This closure problem is at the heart of turbulence theory. At the present time, and despite a research effort that goes back at least to G. I. Taylor in the 1920s, there is no consistent , quantitative theory of turbulence, even for the simplest practical single-phase, incompressible flow. The construction of such a theory is one of the outstanding unsolved problems of classical physics.

Despite the lack of a satisfactory fundamental theory, the need to predict turbulent flows has been such that a number of methods based on a phenomenological approach have been developed. That is, no attempt is made to describe the underlying mechanisms of turbulence but only its effects. In spite of the difficulties, these methods have achieved a fair degree of success in predicting the effects of turbulence in transporting mass,momentum and energy.

2.3.1 Fluid mass and momentum correlations

Central to most phenomenological approaches to turbulence modelling is the simulation of the effects of turbulence by gradient diffusion. This comes about by an analogy with the effect of random molecular motions which, among other things, give rise to viscous effects in fluids.

Gradient diffusion

Consider a uniform density shear flow with steady, mean horizontal velocity $\bar{v}_1(z)$ and zero mean velocities in the other directions. Although there is no mean vertical velocity component, the velocity will fluctuate about this zero value. Suppose that a 'typical' vertical velocity fluctuation v_2' brings in material from a 'typical' distance l and that the mean horizontal velocity per unit volume at a distance l can be approximated by

$$\bar{v}_1(z_1 + l) = \bar{v}_1(z_1) + l\left(\frac{\partial \bar{v}_1}{\partial z}\right)_{z_1}. \tag{2.39}$$

The fluid drawn in by the vertical velocity fluctuation therefore gives rise to a corresponding fluctuation in the horizontal velocity

$$v_1' = l\left(\frac{\partial \bar{v}_1}{\partial z}\right)_{z_1}.$$

Since v_2' and l were taken to be typical, or average, values we assume that we are justified in writing

$$< v_1' v_2' >= l v_2' \frac{\partial \bar{v}_1}{\partial z}. \tag{2.40}$$

Note that lv_2' is essentially negative since if v_2' is positive then the fluid transported by the fluctuation comes from below z_1 so that $l < 0$ and vice versa. For turbulent flow the quantity $-|lv_2'|$ is called the 'eddy viscosity' and given the symbol ν_T. The name comes from the conceptual picture of velocity fluctuations being caused by the movement of eddies or organised packets of fluid that interact with the mean flow. Unlike the molecular viscosity the eddy viscosity is not a property of the fluid but is a function of the flow itself.

This is the physical basis of gradient diffusion of momentum. If the fluctuations are due to turbulence then the length scale l is interpreted as being a representative size for the eddies that are responsible for the majority of momentum transport. Often l is of the same order as the distance over which the mean values vary significantly and the use of (2.39) cannot be justified *a-priori*. However for many simple types of flow, including boundary layer flows that we will be concerned with, models based on gradient diffusion of momentum often produce good agreement with experiment, thus justifying their use in practice.

The generalisation of gradient diffusion of momentum to three dimensions leads, by analogy to the equivalent expression for the viscous stress, to

$$< \boldsymbol{v}'\boldsymbol{v}' >= -\nu_T[\nabla \boldsymbol{v} + \nabla^t \boldsymbol{v}] + \lambda_T I \tag{2.41}$$

where I is the unit tensor. If the trace of both sides is taken then, assuming the fluid is incompressible, for consistency we must have $\lambda_T \equiv (1/3) < v'^2 >$.

Transport of momentum by turbulent velocity fluctuations occurs by the actual transfer of fluid. Thus a transfer of mass as well as momentum takes place. If the fluid has suspended within it solid particles (say) whose concentration field is non-uniform, then a net flux of particle mass may occur. An exactly analogous argument to that presented above, but in terms of the particle concentration instead of the horizontal fluid velocity, yields the equivalent of (2.40), that

$$< v_2' c' >= l v_2' \frac{\partial \bar{c}}{\partial z}.$$

The generalisation of gradient diffusion to three dimensions is simpler than for the case of momentum and leads to

$$< c' v' >= \kappa_T \nabla \bar{c} \tag{2.42}$$

where κ_T is the 'eddy diffusivity'. It has dimension length $\times$ velocity.

Quantification of the length and velocity scales that appear in the gradient diffusion laws are the subject of the next section.

Velocity scale determination

The simplest possible case is a velocity scale that is constant. For steady boundary layer flows this can be a reasonable approximation. Consider a turbulent shear flow as envisaged in the previous section and suppose that there is a solid boundary at $z = 0$. If τ, the mean turbulent stress, is constant then following Landau & Lifshitz (1987, pp 173) the mean velocity gradient must on dimensional grounds satisfy

$$\frac{d\bar{v}_1}{dz} = \frac{1}{\kappa z}\sqrt{\frac{\tau}{\rho_f}},$$

where κ is a constant of proportionality. Multiplication by $v_* = \sqrt{\tau/\rho_f}$ yields

$$\tau = \kappa z v_* \frac{d\bar{v}_1}{dz}. \tag{2.43}$$

Since $\tau =< v_1' v_2' >$, comparison of (2.43) with (2.40) shows that the constant v_*, which has the dimensions of velocity, is the required scale (assuming that κ is combined with z to make the length scale). Relation (2.43) gives the well-known logarithmic velocity profile. This approach, using a constant velocity and linearly varying

length scale has been extended to oscillatory turbulent boundary layers, and will be considered further in Chapter 4.

More sophisticated turbulence models define the velocity scale via the turbulent kinetic energy density of the fluctuating velocity field, a quantity for which a transport equation can be derived starting from the equations of motion.

With reference to the result (2.7), we define the quantity

$$k_f = (1/2) < (1-c)\tilde{v}^2 >$$

to be the turbulent kinetic energy for the fluid phase. This is not strictly correct since the dimensions of k_f are velocity squared and not that of energy, however it has become standard to refer to the equivalent quantity in single phase flow, namely $k = (1/2) < v'^2 >$, as the 'turbulent kinetic energy' and we follow this convention. The full equation for the fluid turbulent kinetic energy based on concentration weighted averages will be given, before any approximations, such as dilute particle concentrations, are made. The mean flow kinetic energy equation is obtained by taking the scalar product of (2.11) with the average fluid velocity. The scalar product of the pre-averaged momentum equation (2.4) with the exact fluid velocity gives an equation for the total (mean plus fluctuating) kinetic energy density. Writing the velocities that appear in this last equation as mean plus a fluctuation, taking the average (concentration weighted), and subtracting the mean flow kinetic energy equation yields the turbulent energy balance

$$\begin{aligned}\frac{\partial}{\partial t}(\rho_f k_f) + \nabla.(\rho_f \bar{v} k_f) &= -\nabla. < \tilde{v}[\rho_f k_f + (1-c)p' + \sigma'_\mu] > \\ &\quad - \rho_f < (1-c)\tilde{v}\tilde{v} > : \nabla v \\ &\quad + < p'\nabla.[\tilde{v}(1-c)] > - \gamma < c\tilde{v}.(\tilde{v}-\tilde{u}) > \\ &\quad - \gamma(\bar{v}-\bar{u}).< c\tilde{v} > - \varepsilon_f . \end{aligned} \tag{2.44}$$

Here both σ'_μ and ε_f are derived from the viscous stress tensor (1.30); their exact form is complicated and is not given here.

As $c \to 0$,

$$\begin{aligned}\bar{v} &\to v', \\ k_f &\to k, \\ \varepsilon_f &\to \varepsilon, \\ < p'\nabla.\tilde{v}(1-c) > &\to < p'\nabla v' > \equiv 0\end{aligned}$$

and (2.44) becomes the usual single-phase turbulent kinetic energy equation, apart from the presence of the terms arising from the fluid drag. Standard modelling assumptions (Launder & Spalding 1972, p 76) for the fluid turbulent kinetic energy equation, which we assume to be valid for (2.44) as $c \to 0$, are:

1. eddies responsible for viscous dissipation are isotropic so that

$$\varepsilon = \nu < (\frac{\partial v_i'}{\partial x_j})^2 >, \tag{2.45}$$

   see e.g. Bradshaw et al. (1981), pp 28;

2. the viscous contribution $\sigma_\mu' \tilde{v}$ in the first term on the right hand side is neglected, assuming high Reynolds number;

3. the triple correlation $< \tilde{v} k_f >$ and the pressure correlation $< \tilde{v} p' >$, appearing in the first term on the RHS and both unknown, re-distribute turbulent kinetic energy without producing or dissipating it. This re-distribution is taken to be diffusive in nature so that

$$< \tilde{v} k_f > + < \tilde{v} p' > = -\frac{\nu_T}{\sigma_k} \nabla k_f,$$

   where σ_k, the turbulent kinetic energy Schmidt number, is supposed constant.

If the zero particle inertia approximation (2.18) is made in the drag derived terms, then the modelled form of (2.44) becomes

$$\frac{\partial k}{\partial t} + \nabla.(\tilde{v} k) = \nabla.(\frac{\nu_T}{\sigma_k} \nabla k) + P + G - \varepsilon. \tag{2.46}$$

Here

$$P = - < v' v' > : \nabla v, \tag{2.47}$$

$$G = \Delta\rho g. < c' v' > / \rho_f \tag{2.48}$$

are production terms for turbulent kinetic energy, and arise from the mean velocity shear and buoyancy effects respectively. The same equation can be derived starting from the fluid momentum equation (2.27). Essentially we have made the same approximations in both cases, the only difference is the stage at which they are made.

If it is assumed that ε can be expressed in terms of k, l and ρ_f, then dimensional considerations imply

$$\varepsilon = \frac{C_D^{3/4} k^{3/2}}{l}, \tag{2.49}$$

where C_D is an experimentally determined coefficient, constant at high Reynolds number. The eddy viscosity is given by

$$\nu_T = C_D^{1/4} k^{1/2} l,$$

where $k^{1/2}$ is now the turbulent velocity scale[5].

Length scale determination

When discussing the turbulent velocity scale it was found that dimensional reasoning, in the case of a wall bounded shear flow with constant turbulent stress, led to (2.43). This expression contains a constant velocity scale (v_*) but a turbulent length scale that *increases linearly* with distance from the solid boundary. Such a specification of length scale, with modifications away from the solid boundary where the assumption of constant turbulent stress is not valid, has been widely used for both steady and oscillatory boundary layers. For flows where an empirical specification of l is difficult, or where improved agreement with experiment is sought, an attempt to determine l from some additional relation involving the flow variables can be made.

Von Karman proposed obtaining a length scale by taking the ratio of first and second derivatives of the velocity profile

$$l = \kappa \left| \frac{\partial \bar{v}_1}{\partial z} \right| \Big/ \left| \frac{\partial^2 \bar{v}_1}{\partial z^2} \right|,$$

and this idea can be extended for use with the turbulent kinetic energy equation by putting

$$l = \kappa \Psi \Big/ \frac{\partial \Psi}{\partial z}, \tag{2.50}$$

where $\Psi \equiv k^{1/2}/l$ has the dimensions of a velocity gradient. This approach has been used recently by Soulsby & Eidsvik (1988) for a combined steady/oscillatory turbulent boundary layer flow.

A more sophisticated approach is to determine l, like the velocity scale, from a transport equation. Most workers have chosen to solve an equation for the dissipation rate ε and derive l, if needed, from (2.49). In Section 2.2.3 it was shown that for low particle concentrations, and assuming zero particle inertia, the fluid momentum equation (2.27) is identical to the Navier-Stokes Stokes equations for single phase

[5]The way in which C_D enters into the relations for ν_T and ε is arranged so that Prandtl's mixing length formulation is recovered in boundary layer flows when all terms other than P and ε are neglected in (2.46); see Section 3.1.

flow, with the addition of terms associated with buoyancy. The transport equation for ε that is derived from this equation of motion is of standard form. Quoting here the equation for ε, with buoyancy effects included (see Rodi 1980)

$$\frac{\partial \varepsilon}{\partial t} + \tilde{v}.\nabla\varepsilon = \nabla.(\frac{\mu_T}{\sigma_\varepsilon}\nabla\varepsilon) + C_{1\varepsilon}\frac{\varepsilon}{k}(P+G)(1+C_{3\varepsilon}R_f) - C_{2\varepsilon}\frac{\varepsilon^2}{k}, \qquad (2.51)$$

we note that a considerable number of modelling assumptions, many of them unverified by comparison with experiment (Bradshaw et al. 1981) are required to derive it from the exact equation. Here P and G are the stress and buoyancy production terms from the turbulent kinetic energy equation (2.46). R_f is the flux Richardson number

$$R_f = -G/P.$$

$C_{1\varepsilon}, C_{2\varepsilon}$ and $C_{3\varepsilon}$ are constants, assumed universal and determined experimentally.

2.3.2 Particle equation: closure I

The particle momentum equation (2.38) will be considered 'closed' if we can relate all the correlations which appear in it to correlations for which a model has been proposed in the literature. This generally entails expressing terms containing particle velocity fluctuations in terms of correlations involving fluid velocity fluctuations. Since we have shown, to a first approximation, that the presence of the particles affects the fluid velocities only via buoyancy affects, it is valid to use turbulence models for fluid velocity correlations that have been developed for buoyancy-affected single-phase flows. In outline, the technique used is to obtain equations correct to first order in the parameter τ^*. Since the problematical terms generally appear in the equations at first order anyway, it is sufficient to approximate the correlations themselves to *zeroth* order in τ^*.

Non-linear drag

Averaging (2.38) with the drag coefficient, γ, given by (2.37) leads to correlations of the form $< c|v-u|^\beta(v-u) >$. Note that the occurrence of the modulus means that all components of particle velocity contribute to the drag force for any given component. We do not attempt to model this correlation directly, but approximate $|v-u|$ using (2.19)[6]. With this approximation γ is now a constant and hence no complica-

[6] It is easy to see that form of (2.19) is unchanged if the drag law is non-linear. The only difference is the value of the fall velocity is now determined from the non-linear drag law.

tions arise when averaging the drag term. Unfortunately, the approximation has also entailed neglecting terms of $O(\tau^*)$ since the drag term appears at zeroth order and we are then using a zeroth order approximation for it. This is perhaps mitigated by the knowledge that we have, for example, already neglected the Bassett term whose contribution would also be of $O(\tau^*)$. Given the current state of knowledge regarding the forces acting on particles suspended in a fluid undergoing complicated motion, it would perhaps be unrealistic to expect to be able to account for all the possible forces.

Figure 2.1 gives the fall velocity as a function of the particle diameter for particles with a relative density $\rho = 2.65$ using the drag law (2.37) with $\alpha = 0.15$ and $\beta = 0.687$. Also shown is the corresponding result assuming Stokes drag; as can be seen the two diverge for $d > 0.1$mm.

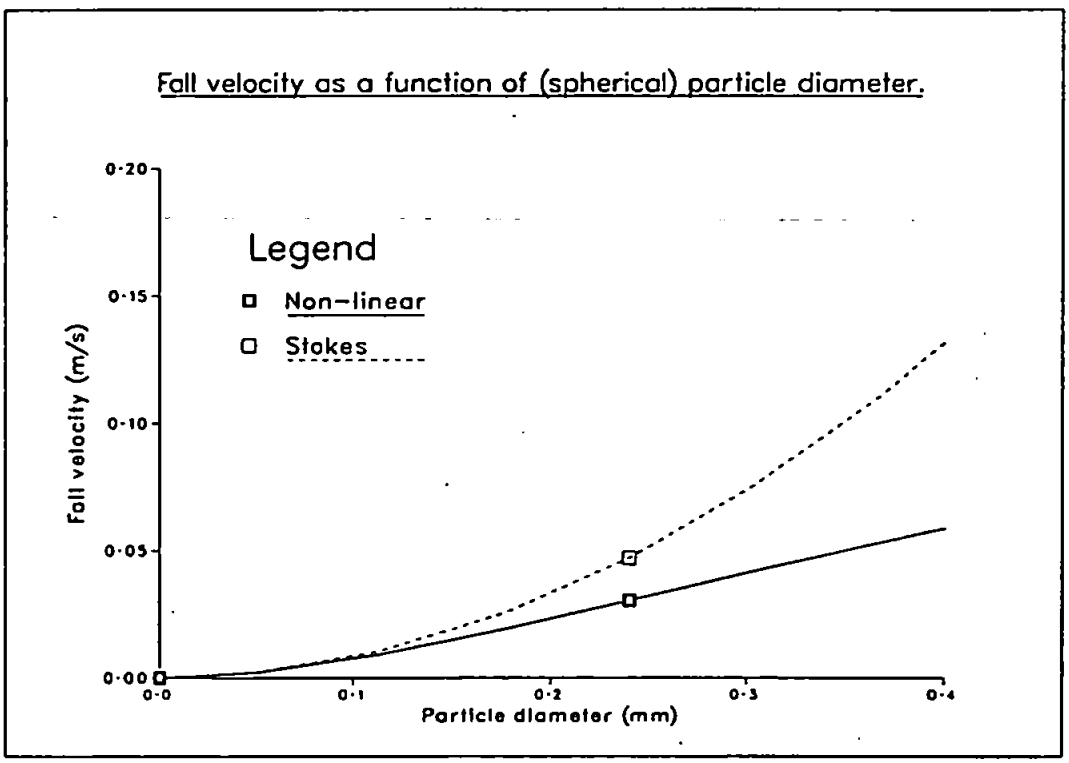

Figure 2.1: Particle fall velocity against particle diameter

Lift force

The term representing the lift force in (2.35) appears at first order in τ^* and is modelled by first using (2.19) to approximate $v - u$. Averaging the resulting expression

yields

$$\rho_f C_{vm} w_0 .[\bar{c}\nabla\bar{v} - \bar{c}\nabla^t\bar{v} + < c'\nabla v' > - < c'\nabla^t v' >].$$

The terms involving fluctuating quantities can be re-written as

$$\nabla < c'v' > -\nabla^t < c'v' > + < v'\nabla c' > - < v'\nabla^t c' >,$$

so that the only new correlation introduced is $< v'\nabla c' >$. Lottey et al. (1983) derive a model for this correlation in their investigation of the "crossing trajectory effect" — see Lottey et al. (1983) , Shih & Lumley (1986) and the discussion in Section 5.3. They put

$$< v'\nabla c' > = < c'v' > \otimes \left(f_1 \nabla < c'^2 > + f_2 w_0\right)$$

where

$$\begin{aligned} f_1 &= \frac{1}{2} < c'^2 >^{-1}, \\ f_2 &= F_D \left[b_1 + b_2 \frac{(w_0 . < c'v' >)^2}{w_0^2 < c'v' >^2} \right], \\ F_D &= \frac{9\varepsilon}{4k^2} \sqrt{1 - \frac{< c'v' >^2}{< c'^2 > 2k}}, \\ b_1 &= 0.7778,\ b_2 = -0.725. \end{aligned}$$

These complicated expressions simplify considerably for the case we eventually consider. On the basis of an algebraic flux model derived from a transport equation for $< c'^2 >$, Rodi (1980) suggests

$$< c'^2 > = -2R\frac{k}{\varepsilon} < c'v' > .\nabla\bar{c} \tag{2.52}$$

where R is a constant.

Specification of the triple scalar correlation

The averaged particle momentum equation, with the non-linear drag and lift force approximated as described above, can be written in non-dimensional form as

$$\begin{aligned} \tau^*(1 + \frac{C_{vm}}{\rho}) \left[\frac{\partial}{\partial t^*}\bar{c}\bar{u}^* + \nabla .\bar{c}\bar{u}^*\bar{u}^* \right] = \\ (\bar{c} + C_{vm})(\bar{c}^2 + < c'^2 >) w_0^* + \bar{c}(v^* - u^*) + < c'v' > \\ - \tau^* \left[\frac{1}{\rho}(1 + C_{vm}) (\bar{c}\nabla\bar{p}^* + < c'\nabla p' >^*) + (1 + \frac{C_{vm}}{\rho})\nabla . < c\tilde{u}\tilde{u} >^* - h^* \right], \end{aligned} \tag{2.53}$$

where

$$h^* = -\frac{C_{vm}}{\rho} w_0^* \cdot (\bar{c}\nabla\bar{v}^* - \bar{c}\nabla^t\bar{v}^* + < c'\nabla v^{*\prime} > - < c'\nabla v^{*\prime} >^T),$$
$$\gamma = \gamma(|w_0|).$$

with non-dimensional quantities as defined in Section 2.2.2. Equation (2.53) contains the triple correlation $\stackrel{\sim}{<} c\tilde{u}\tilde{u} >^*$, which can be regarded as the particle equivalent of the Reynolds stress. Since it appears in the equation at $O(\tau^*)$ we require it to be approximated to zeroth order only. Such an approximation can be found by pre-multiplying (2.18) by $\tilde{u}$, averaging to obtain

$$< c\tilde{u}\tilde{u} >^* = < c\tilde{u}\tilde{v} >^* + O(\tau^*),$$

then post-multiplying (2.18) by v' and averaging to give

$$\begin{aligned} < c\tilde{u}\tilde{v} >^* &= < c\tilde{v}\tilde{v} >^* + (\bar{v}^* - \bar{u}^* + w_0^*) < c\tilde{v} >^* + O(\tau^*), \\ &= < c\tilde{v}\tilde{v} >^* - \frac{1}{\bar{c}}(< c\tilde{v} >^*)^2 + O(\tau^*). \end{aligned}$$

Use of (2.23) and (2.24) yields

$$< c\tilde{u}\tilde{v} > = < cv'v' > - \frac{1}{\bar{c}}(< c'v' >^*)^2 + O(\tau^*, c^2). \qquad (2.54)$$

The modelling of the particle correlation $< c\tilde{u}\tilde{u} >^*$ has thus been reduced to modelling correlations between fluid velocities and concentration. Since

$$< cv'v' > = \bar{c} < v'v' > + < c'v'v' >$$

the only new correlation in fact introduced is $< c'v'v' >$. A term of this form arises in the equation for the scalar flux (see Rodi 1980) and in modelling this equation, a number of authors have suggested using a gradient diffusion representation for $< c'v'v' >$. Gibson & Launder (1978) for example use

$$< c'v'v' > = C_s \frac{k}{\varepsilon} [< v'v' > .\nabla < c'v' > + (\nabla^t < c'v' >). < v'v' >] \qquad (2.55)$$

which in free shear flows gives reasonable agreement with experiment — as shown by Dekeyser & Launder(1983). However, the recent work of Nagano & Tagawa (1988) suggests that for wall boundary layers the main contributions to the triple scalar correlation $< c'v'v' >$ arise from turbulent bursting phenomena, for which none of

the gradient diffusion laws tried gave an adequate representation. Fortunately, it is possible to derive an alternative formulation of the averaged particle equation which avoids the occurrence of $< c\tilde{u}\tilde{u} >$; this is presented in Section 2.3.3.

Fluctuating pressure-concentration correlation

The correlation $< c'\nabla p' >$ represents a transfer of momentum between fluid and particle phases via pressure fluctuations and appears with opposite signs in the fluid and particle momentum equations. The same term arises in the transport equations derived for the scalar flux $< c'v' >$ and we model it as described in Rodi (1980). That is, writing

$$< c'\nabla p' >= \nabla < c'p' > - < p'\nabla c' > \tag{2.56}$$

the first term is neglected. Because of the result of Section 2.2.3, that the presence of the particles affects the fluid motion primarily through buoyancy, we can derive a standard expression for $< p'\nabla c' >$. Starting from (2.27) we write all variables as mean plus a fluctuation and subtract (2.28); the resulting expression can be written as

$$-\nabla p' = \rho_f(\frac{\partial v'}{\partial t} + b), \tag{2.57}$$

where the exact form of b is not important at present. To zeroth order in the particle concentration we have $\nabla.v' = 0$ so that taking the divergence of (2.57) we can neglect, assuming $c \ll 1$, the contribution from $\nabla.v'$. This gives a Poisson equation for p'

$$\frac{1}{\rho_f}\nabla^2 p' = \nabla.b \equiv R$$

where

$$R = \nabla^2 : (< v'v' > - v'v') - 2\nabla\bar{v} : \nabla v' + \frac{\Delta\rho}{\rho_f} g.\nabla c'$$

Inverting the Laplacian by the use of the Green's function

$$G = -\frac{1}{4\pi|x-y|}$$

yields

$$p'(x)/\rho_f = \int_{\mathcal{D}} G(x,y)\, R\, dy + S$$

where S is the contribution from a surface integral around the boundary of the flow domain $\mathcal{D}$. Multiplying this expression for p' through by $\nabla c'$ and averaging leads to

$$\frac{1}{\rho_f} < p'\nabla c' >= \Pi_1 + \Pi_2 + \Pi_3 + s,$$

where

$$\begin{aligned} s &= < S\nabla c' >, \\ \Pi_1 &= -\int_{\mathcal{D}} < (\nabla^2 : v'v')^* \nabla c' > G\, dy, \\ \Pi_2 &= -2\int_{\mathcal{D}} < (\nabla \bar{v} : \nabla v')^* \nabla c' > G\, dy, \end{aligned}$$

and

$$\Pi_3 = \frac{\Delta\rho}{\rho_f}\int_{\mathcal{D}} < (g.\nabla c')^* \nabla c' > G\, dy,$$

Starred quantities are subject to integration with respect to dy. The following models have been proposed for these expressions (see Rodi 1980):

$$\begin{aligned} \Pi_1 &= -a_1\frac{\varepsilon}{k} < c'v' >, \\ \Pi_2 &= a_2 < c'v' > .\nabla \bar{v}, \\ \Pi_3 &= -a_3\frac{\Delta\rho}{\rho_f} g < c'^2 >, \end{aligned}$$

where a_1, a_2 and a_3 are experimentally determined coefficients. The correlation $< c'^2 >$ is modelled using (2.52). All these models must represent gross simplifications in that local values are used to approximate the integrals on the LHS of the above expression.

Near the boundary the contribution from the surface integral S cannot be neglected. For the case we are interested in, of a single horizontal boundary in the $x-y$ plane at $z = 0$, the effect of the surface integral can be represented by modifications to the terms Π_1, Π_2 and Π_3 (see Gibson & Launder 1978). The z component of each Π_i is multiplied by $1 + f_c$, where $f_c = f(l/z)$ is an empirical function of the turbulent length scale. A simple linear form, $f_{ci} = a_i' k^{3/2}/(z\varepsilon)$, where the a_i' are a set of experimental constants, has been found by Gibson & Launder (1978) to be adequate.

The final form for the pressure-concentration correlation, including the wall cor-

rection, can be written

$$< p'\nabla c' >= -\rho_f < c'v' > .a_1 \frac{\varepsilon}{k} + \rho_f(< c'v' > .\nabla v).a_2 - \Delta\rho < c'^2 > g.a_3 \quad (2.58)$$

where

$$a_i = a_i I + a_i' f_c kk$$

The final ('closed') form of the particle momentum equation is given by (2.53) with the triple correlation given by (2.54) and the pressure-concentration correlation modelled using (2.56) and then (2.58).

2.3.3 Particle equation: closure II

In Section 2.3.2 we have provided models for the turbulent correlations in the particle momentum equation correct to $O(\tau^*)$, apart from the non-linear drag. For the situation we are interested in, that of wall bounded shear flows, the apparent inadequacy of current models for the triple scalar correlation $< c'v'v' >$ (Nagano & Tagawa , 1988) presents a severe problem. We here derive an alternative formulation which avoids the occurrence of this correlation. Although it is possible to start from (2.10) it is easier to use the pre-averaged equation (2.3). The procedure followed is similar to that of Shih & Lumley (1985) except we use as an expansion parameter the non-dimensional quantity τ^* rather than the dimensional parameter γ/ρ_p. This leads to differences in the zeroth and first order approximations. For example Shih & Lumley obtain $u = v$ as the zeroth order solution instead of (2.19).

Essentially, the equations are expanded about the zero inertia solution to obtain a first order correction for the particle inertia. The result (2.19) implies that correct to $O(\tau^*)$

$$\begin{aligned} \frac{Du^*}{Dt} &= \frac{Dv^*}{Dt} + w_0^*.\nabla v^* \\ &= -\nabla p^* + \frac{\rho}{\tau^*} c w_0^* + \frac{1}{Re}\nabla^2 v^* + w_0^*.\nabla v^*, \end{aligned} \quad (2.59)$$

which we then ~~then~~ use to substitute for the convective derivative in (2.14) leading to

$$c(v^* - u^*) + c w_0^* = \rho w_0^* c^2 + \tau^* \left[-(1 - \frac{1}{\rho}) c\nabla p^* + c w_0^*.\nabla v^* + \frac{1}{Re}\nabla^2 v^* \right].$$

Using (2.59) the added mass term (2.35) becomes simply

$$-c\rho_f C_{vm} w_0 . \nabla^t v,$$

so the pre-averaged particle momentum equation takes the form

$$\begin{aligned} c(v^* - u^*) + cw_0^* &= \rho w_0^* c^2 \\ &+ \tau^* \left[-(1 - \frac{1}{\rho}) c\nabla p^* + \frac{1}{Re} c\nabla^2 v^* + cw_0^* . (\nabla v^* + \frac{C_{vm}}{\rho} \nabla^t v^*) \right], \end{aligned} \tag{2.60}$$

which in terms of dimensional variables is

$$c(v - u) + cw_0 = \rho w_0 c^2 + \frac{1}{\gamma} \left[-(\rho - 1) c\nabla p + \rho\mu c\nabla^2 v + cw_0 . (\rho_p \nabla v + \rho_f C_{vm} \nabla^t v) \right].$$

Re-arranging and averaging this expression, approximating the non-linear drag law as described at the beginning of Section 2.3.2, yields

$$\bar{c}\bar{u} = \bar{c}\bar{v} + \bar{c}w_0 + < c'v' > -\rho w_0 (\bar{c}^2 + < c'^2 >) + \frac{1}{\gamma} \left[(\rho - 1)(\bar{c}\nabla\bar{p} - < p'\nabla c' >) + q \right], \tag{2.61}$$

where

$$\begin{aligned} q &= -w_0 . \left[\bar{c} \left(\rho_p \nabla\bar{v} + \rho_f C_{vm} \nabla^t \bar{v} \right) + \left(\rho_p < c'\nabla v' > + \rho_f C_{vm} < c'\nabla^t v > \right) \right] \\ \gamma &= \gamma(|w_0|). \end{aligned}$$

In (2.61) we have also written $< c'\nabla p' >= \nabla < c'p' > - < p'\nabla c' >$ and then neglected the first term on the RHS. The pressure-concentration correlation is modelled using (2.58). As usual the viscous terms are neglected by assuming high Reynolds number and local isotropy.

Although the formulation (2.53) presented in Section 2.3.2 has the advantage of keeping more terms in an exact form, the approach described above is preferred because:

1. the triple scalar correlation $< c\tilde{u}\tilde{u} >$ and hence $< c'v'v' >$ no longer appears;
2. no derivatives of u appear in (2.61), thus it is no longer a differential equation but gives u explicitly in terms of correlations involving c and v.

Apart from making the calculation of inertia effects more straight forward, the second point has the important consequence that no boundary conditions on u have to be

specified.

Chapter 3

Numerical Model for Oscillatory, Turbulent Boundary Layer Flow

In this chapter simplified forms of the averaged equations derived in Section 2.3 are presented for the case of the suspended load region of a turbulent oscillatory boundary layer. Boundary conditions required for the solution of the equations describing such flows are discussed, and a detailed description is given of a numerical model used to obtain these solutions.

3.1 The oscillatory boundary layer approximation

The physical situation corresponds to that sketched in Figure 3.1 and consists of a solid horizontal boundary over which a flow is imposed such that far from the boundary the horizontal fluid velocity is given by

$$V = V_\infty \cos(mx - \omega t) \tag{3.1}$$

If we define a 'wave Reynolds number' by

$$R_w = V_\infty a/\nu$$

where $a = V_\infty/\omega$, then for sufficiently large values of R_w, the flow is turbulent. Sleath (1984, p 58), summarizes the results of a number of experimental investigations

of this critical Reynolds number for oscillatory flows. We assume that the value of R_w is large enough for the assumption of a fully developed turbulent flow to be valid. In addition the mean flow is assumed to be purely two dimensional (no variation normal to the direction of propagation of the wave).

Quantities occuring in equations (2.8), (2.9), (2.28) and (2.61) are scaled to determine which terms, if any, can be neglected. The scale for a variable will be denoted by the symbol for that variable with a cross (+) superscript. Thus if the symbol '$\sim$' means 'scales as' we have

$$\bar{c} \sim \bar{c}^+, \bar{u}_1 \sim \bar{u}_1^+ \text{ etc.}$$

Horizontal and vertical velocity components will be indicated by subscripts 1 and 2 respectively.

At the edge of the boundary layer the horizontal fluid velocity is given by (3.1), with V_∞, m, ω given. This leads naturally to the following choices for scales:

$$\begin{aligned} t^+ &= 1/\omega, \\ x^+ &= \lambda \equiv 2\pi/m, \\ \bar{v}_1^+, \bar{u}_1^+ &= V_\infty. \end{aligned}$$

The boundary layer is taken to have a typical thickness δ which is used to scale z. For the fluctuating quantities we assume

$$\begin{aligned} v_1', v_2', \bar{u}_1, \bar{u}_2 &\sim v'^+, \\ p' &\sim \rho_f (v'^+)^2, \\ c' &\sim \bar{c}^+. \end{aligned}$$

The assumptions, made in Chapter 2 of dilute particle concentrations and short particle response times, imply:

$$\bar{c}^+ \ll 1, \tag{3.2}$$

$$\frac{\rho_p \omega}{\gamma} \equiv \tau^* \ll 1. \tag{3.3}$$

In addition, the application to oscillatory boundary layers enables the following additional approximations to be made.

Boundary layer approximation

$$\frac{\delta}{\lambda} \ll 1. \tag{3.4}$$

This allows the assumption of a constant horizontal pressure gradient through the boundary layer and also the neglect of all spatial derivatives other than those normal to the boundary.

Small oscillatory amplitude approximation

$$\frac{V_\infty}{\omega\lambda} \ll 1. \tag{3.5}$$

If the amplitude of the oscillations ($a \equiv V_\infty/\omega$) are small compared to the wavelength λ, it is permissible to neglect the advective acceleration terms in comparison with the temporal acceleration term in the fluid momentum equations. This approximation is consistent with the assumption of a linear water wave (for which the surface slope a/λ, is vanishingly small) driving the flow.

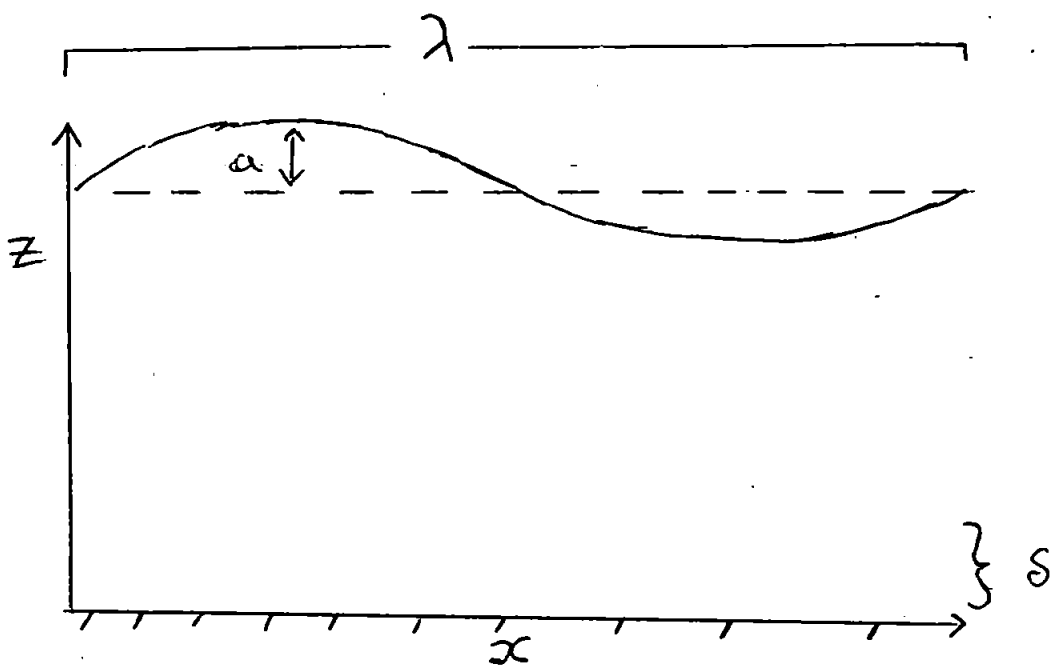

Figure 3.1: Definition sketch of oscillatory boundary layer

Fluid phase

The dilute concentration assumption reduces the fluid-phase mass and momentum equations to the standard Reynolds averaged equations of single-phase turbulent flow — apart from the addition of the buoyancy term in the momentum equation. Scaling

arguments based on (3.4) and (3.5) are then standard; Batchelor (1967, pp 315–318) for example deals with the laminar case. The turbulent case is almost identical and most authors simply quote the result. However it is advantageous to go through the scaling arguments in preparation for the non-standard, and more involved, particle mass and momentum balances.

In the limit of dilute particle concentrations (2.9) reverts to the continuity equation $\nabla.\bar{v} = 0$, leading to the following relation between scales

$$\frac{\bar{v}_1^+}{\lambda} \sim \frac{\bar{v}_2^+}{\delta}. \tag{3.6}$$

Using this relation between velocities, the scaled horizontal momentum equation for the fluid can be written

$$\frac{\partial \bar{v}_1}{\partial t} + \frac{V_\infty}{\omega\lambda}\left[\frac{\partial}{\partial x}\bar{v}_1^2 + \frac{\partial}{\partial z}\bar{v}_1\bar{v}_2\right] = - \frac{\bar{p}^+}{\rho_f \omega \lambda V_\infty}\frac{\partial \bar{p}}{\partial x} - \frac{(v'^+)^2}{\omega\delta V_\infty}\left[\left(\frac{\delta}{\lambda}\right)\frac{\partial}{\partial x} < v_1'^2 > + \frac{\partial}{\partial z} < v_1' v_2' >\right]$$

From (3.5), the advection terms can be neglected in comparison to the time derivative and, from (3.4), the first Reynolds stress term can neglected in comparison to the second such term. In addition, if the effects of turbulence are to be significant in the situation considered here, the remaining Reynolds stress term must be of the same order as the acceleration. The simplified momentum equation in dimensional form therefore becomes

$$\rho_f \frac{\partial \bar{v}_1}{\partial t} = -\frac{\partial \bar{p}}{\partial x} - \rho_f \frac{\partial}{\partial z} < v_1' v_2' > . \tag{3.7}$$

In addition the following relationship between mean and fluctuating velocity scales is assumed to hold

$$\omega V_\infty \sim \frac{(v'^+)^2}{\delta}, \tag{3.8}$$

so that the gradient of the Reynolds stress is assumed to be of comparable magnitude to the acceleration in (3.7).

Consider now the vertical momentum balance. Arguments used for the horizontal momentum balance can be applied to the acceleration and Reynolds stress terms in the vertical case, leading to the simplified equation

$$\rho_f \frac{\partial \bar{v}_2}{\partial t} = -\Delta\rho\bar{c}g - \frac{\partial \bar{p}}{\partial z} - \rho_f \frac{\partial}{\partial z} < v_2'^2 > .$$

By (3.6) and (3.4) the vertical velocity is negligible compared to the horizontal ve-

locity and so by (3.8) the acceleration term in the vertical momentum balance can be discarded to leave simply

$$0 = -\Delta\rho\bar{c}g - \frac{\partial\bar{p}}{\partial z} - \rho_f \frac{\partial}{\partial z} < v_2'^2 > . \tag{3.9}$$

Thus, to maintain a negligible mean vertical fluid velocity the pressure gradient must balance the mean vertical turbulent stress and the buoyancy force due to the particle flux. If (3.9) is integrated from some point z in the boundary layer to the top of the layer at $z = z_2$ we obtain, assuming the Reynolds stress vanishes at z_2,

$$\bar{p}(x,z,t) = P_\infty(x,t) - \rho_f < v_2'^2 > + \Delta\rho g \int_z^{z_2} \bar{c}\, dz. \tag{3.10}$$

Here P_∞ is the pressure at the edge of the boundary layer which is determined by the flow outside. Let V_1 and V_2 be the horizontal and vertical velocity components of the flow outside the boundary layer. Assuming this flow to be irrotational we have that

$$\frac{\partial V_1}{\partial t} + \frac{\partial}{\partial x} V_1^2 + \frac{\partial}{\partial z} V_1 V_2 = -\frac{\partial P_\infty}{\partial x}.$$

By (3.5) and (3.6) the advection terms are negligible so

$$\rho_f \frac{\partial V}{\partial t} = -\frac{\partial P_\infty}{\partial x}.$$

Therefore

$$(\frac{\partial p}{\partial x})^+ \sim \rho_f \omega V_\infty. \tag{3.11}$$

If (3.10) is differentiated with respect to x then (3.11), together with (3.8), show that the Reynolds stress term can be neglected compared to the resulting horizontal pressure gradient. The ratio of the term involving the integral of the concentration to the pressure gradient is of the order

$$\frac{g}{\omega V_\infty} c^+ \frac{\delta}{\lambda}.$$

The magnitude of this cannot be directly ascertained using the proposed scaling relations and therefore we are forced to substitute in typical values for the quantities that appear based on the the application we have in mind. With $V_\infty = 1$ m/s, $\omega = 0.5$ rad/s and $c^+ = 0.01$, the ratio becomes approximately δ/λ which, by (3.4),

is therefore negligible. Thus we can put

$$\frac{\partial \bar{p}}{\partial x} = \frac{\partial P_\infty}{\partial x}, \tag{3.12}$$

and the horizontal momentum balance for the fluid becomes

$$\frac{\partial \bar{v}_1}{\partial t} = -\frac{1}{\rho_f}\frac{\partial P_\infty}{\partial x} - \frac{\partial}{\partial z} < v_1' v_2' > .$$

The forms taken by the turbulent kinetic energy and dissipation rate equations, (2.46) and (2.51), in the oscillatory boundary layer are likewise determined using the scaling relations (3.4) and (3.5).

Particle Phase

Following the procedure used in scaling the terms in the fluid-phase equations the particle mass balance is examined first. The scaled mass balance equation is

$$\frac{\partial \bar{c}}{\partial t} + \left(\frac{V_\infty}{\omega\lambda}\right)\frac{\partial}{\partial x}\bar{c}\bar{u}_1 + \left(\frac{\bar{u}_2^+}{\omega\delta}\right)\frac{\partial}{\partial z}\bar{c}\bar{u}_2 = 0.$$

By (3.5) the x-derivative can be neglected compared to the time derivative so that

$$\frac{\partial \bar{c}}{\partial t} + \frac{\partial}{\partial z}\bar{c}\bar{u}_2 = 0,$$

implying the following relation between scales

$$\omega \sim \frac{\bar{u}_2^+}{\delta}. \tag{3.13}$$

Combining (3.13) with (3.6) leads to the relation

$$\frac{\bar{v}_2^+}{\bar{u}_2^+} \sim \frac{V_\infty T}{\lambda} \ll 1. \tag{3.14}$$

The particle momentum equations (2.61) presented in Section 2.3.3 can be simplified using similar arguments to those used for the equations of the fluid phase. Effectively these arguments amount to neglecting all terms multiplied either by derivatives with respect to x or by the vertical fluid velocity, $\bar{v}_2$. Because of the complexity of the original equation, only the final result is given. In the following expressions, $\Pi_{i,j}$ is the jth component of the Π_i that comprise (2.58) ($j = 1$ and $j = 2$ are the horizontal and vertical components respectively).

The horizontal balance for the oscillatory boundary layer is

$$\bar{c}\bar{u}_1 = \bar{c}\bar{v}_1 + \frac{1}{\gamma}\left[\bar{c}(\rho-1)\frac{\partial P_\infty}{\partial x} + \bar{c}w_0\frac{\partial \bar{v}_1}{\partial z} - (1+a_1'f_c/a_1)\Pi_{2,1}\right].$$

Using the definition of $\Pi_{2,1}$ yields

$$\bar{c}\bar{u}_1 = \bar{c}\bar{v}_1 + \frac{1}{\gamma}\left\{\bar{c}(\rho-1)\frac{\partial P_\infty}{\partial x} + [\bar{c}w_0 - (a_2+a_2'f_c)\Delta\rho < c'v_2' >]\frac{\partial \bar{v}_1}{\partial z}\right\}. \qquad (3.15)$$

By contrast the assumption of zero particle inertia, (2.20), gives $\bar{c}\bar{u}_1 = \bar{c}\bar{v}_1$.

The oscillatory boundary layer approximation to the vertical component of (2.61) can be shown (after much algebra) to be

$$\begin{aligned}\bar{c}\bar{u}_2 &= -\bar{c}w_0 + < c'v_2' > + \rho w_0(\bar{c}^2 + < c'^2 >) \\ &\quad + \frac{1}{\gamma}\left[-(\rho-1)\bar{c}\frac{\partial \bar{p}}{\partial z} - \Delta\rho(\alpha_1'\Pi_{1,2} + \alpha_3'\Pi_{3,2}) + q\right], \qquad (3.16)\end{aligned}$$

where

$$\begin{aligned}\alpha_i' &= 1 + \frac{a_i'}{a_i}f_c, \\ \Pi_{1,2} &= -a_1\frac{\varepsilon}{k} < c'v_2' >, \\ \Pi_{3,2} &= a_3\frac{\Delta\rho}{\rho_f}g < c'^2 >, \\ q &= -(\rho_p + \rho_f C_{vm})\left[\left(f_1\frac{\partial}{\partial z} < c'^2 > - f_2 w_0\right) < c'v_2' > - \frac{\partial}{\partial z} < c'v_2' >\right] w_0, \\ f_1 &= \frac{1}{2} < c'^2 >^{-1}, \\ f_2 &= \frac{9}{4}\frac{\varepsilon}{k}(b_1+b_2)\sqrt{1 - \frac{C_D^2}{4R}}.\end{aligned}$$

Note that in (3.16) we have neglected the contribution from $\bar{c}\bar{v}_2$ to the vertical particle volume flux on account of (3.14). Substituting for the mean pressure gradient using (3.9) yields

$$\begin{aligned}\bar{c}\bar{u}_2 &= -\bar{c}(1-\bar{c})w_0 + < c'v_2' > + \rho w_0 < c'^2 > \\ &\quad - \frac{1}{\gamma}\left[\Delta\rho\left(\bar{c}\frac{\partial}{\partial z} < v_2'^2 > + \alpha_1'\Pi_{1,2} + \alpha_3'\Pi_{3,2}\right) - Q\right].\end{aligned}$$

Finally, substituting for $\Pi_{1,2}$ and $\Pi_{3,2}$, we obtain the following expression for the vertical particle volume flux

$$\bar{c}\bar{u}_2 = -\bar{c}(1-\bar{c})w_0 + < c'v_2' > + [\rho - (\rho-1)\alpha_3]w_0 < c'^2 >$$

$$+\frac{1}{\gamma}\left[\Delta\rho\left(-\bar{c}\frac{\partial}{\partial z}<v_2'^2>+\alpha_1\frac{\varepsilon}{k}<c'v_2'>\right)+q\right], \qquad (3.17)$$

where

$$\alpha_i = a_i + a_i' f_c$$

By contrast, the assumption (2.20), of zero particle inertia, gives in the boundary layer

$$\bar{c}\bar{u}_2 = -\bar{c}w_0 + <c'v_2'> . \qquad (3.18)$$

Turbulent correlations are modelled using (2.52), (2.41) and (2.42). For a boundary layer these give:

$$\begin{aligned} <c'^2> &= -2R\frac{k}{\varepsilon}<c'v_2'>\frac{\partial\bar{c}}{\partial z}, \\ <c'v_2'> &= -\kappa_T\frac{\partial\bar{c}}{\partial z}, \\ <v_1'v_2'> &= -\nu_T\frac{\partial\bar{v}_1}{\partial z}, \end{aligned}$$

and

$$<v_2'^2> = \frac{2}{3}k.$$

It is assumed that $\kappa_T = \nu_T/\sigma_c$, where σ_c, the turbulent Schmidt number for the concentration, is a non-dimensional constant. In general σ_c may be a function of the flow parameters (see Rodi 1980) but, for simplicity, we take $\sigma_c = 1.0$.

Oscillatory boundary layer equations

We present now the complete set of equations for the oscillatory turbulent boundary layer, neglecting for the moment all terms associated with particle inertia. The modifications necessary to include these terms into the formulation given below are discussed in Chapter 5 when the significance of the particle inertia terms is examined. Without particle inertia, a standard set of equations is obtained for the oscillatory turbulent boundary layer (see for example Hagatun & Eidsvik , 1986).

$$\frac{\partial\bar{c}}{\partial t} = -\frac{\partial}{\partial z}\bar{c}\bar{u}_2, \qquad (3.19)$$

$$\frac{\partial\bar{v}_1}{\partial t} = -\frac{1}{\rho_f}\frac{\partial P_\infty}{\partial x}+\frac{\partial}{\partial z}\left(\nu_T\frac{\partial\bar{v}_1}{\partial z}\right), \qquad (3.20)$$

$$\frac{\partial k}{\partial t} = \frac{\partial}{\partial z}\left(\frac{\nu_T}{\sigma_k}\frac{\partial k}{\partial z}\right)+P+G-\varepsilon, \qquad (3.21)$$

$$\frac{\partial\varepsilon}{\partial t} = \frac{\partial}{\partial z}\left(\frac{\nu_T}{\sigma_\varepsilon}\frac{\partial\varepsilon}{\partial z}\right)+C_{1\varepsilon}\frac{\varepsilon}{k}(P+G)(1+C_{3\varepsilon}R_f)-C_{2\varepsilon}\frac{\varepsilon^2}{k}, \qquad (3.22)$$

where

$$\bar{c}\bar{u}_2 = -w_0\bar{c} - \kappa_T \frac{\partial \bar{c}}{\partial z}, \tag{3.23}$$

$$P = \nu_T \left(\frac{\partial \bar{v}_1}{\partial z}\right)^2, \tag{3.24}$$

$$G = \frac{\Delta\rho}{\rho_f} g \kappa_T \frac{\partial \bar{c}}{\partial z}, \tag{3.25}$$

$$R_f = -G/P.$$

Here $C_{1\epsilon}, C_{2\epsilon}$ and $C_{3\epsilon}$ and the Schmidt numbers $\sigma_k, \sigma_\epsilon$ are experimentally determined constants.

If the eddy viscosity velocity scale is derived from the turbulent kinetic energy then

$$\nu_T = C_D^{1/4} k^{1/2} l. \tag{3.26}$$

The dissipation rate ϵ and length scale l are assumed to be related by

$$\epsilon = \frac{C_D^{3/4} k^{3/2}}{l}. \tag{3.27}$$

If the transport and buoyant production terms are neglected in (3.21) leaving a balance between shear production and dissipation (so-called "local equilibrium") then

$$k^{1/2} = C_D^{-1/4} l \left|\frac{\partial \bar{v}_1}{\partial z}\right|. \tag{3.28}$$

Substituting this into (3.26) gives

$$\nu_T = l^2 \left|\frac{\partial \bar{v}_1}{\partial z}\right|$$

which is precisely the form given for ν_T by Prandtl's mixing length hypothesis.

In Chapter 4 the effect that the form of the turbulent length scale has on the mean velocities and particle concentrations is investigated. Three approaches are compared:

1. an empirical specification of l based on results from steady boundary layers;

2. determining l from the turbulent kinetic energy by re-arranging (2.50) to yield

$$l = \kappa k^{1/2} \int_{z_1}^{z_2} k^{-1/2}\, dz + l_1, \tag{3.29}$$

where l_1 is the value of l at the bottom boundary $z = z_1$ (effectively l_1 is a

boundary condition for l), and κ is the von Karman constant;

3. using the $k-\varepsilon$ model, and calculating the l in terms of k and ε via (3.27).

The stress exerted on the bottom boundary by the turbulent transfer of momentum is denoted by τ_0. This quantity, which is important in sediment transport problems, is calculated from the Reynolds stress evaluated at the bottom boundary z_1. In terms of the gradient diffusion model, τ_0 is therefore given by the following evaluated at z_0

$$|\tau_0| = \rho_f \nu_T \left| \frac{\partial \bar{v}_1}{\partial z} \right|. \tag{3.30}$$

3.1.1 Boundary conditions

Equations (3.19) to (3.22) will be solved on a bounded domain, $z_1 \leq z \leq z_2$, and boundary conditions near the bed $z = z_1$, and at some point above at the edge of the boundary layer $z = z_2$, are required.

Bottom boundary

At the bed, the boundary conditions on the velocity for oscillatory flow are based on ideas originally developed for steady flows and involves setting the velocity to zero not at $z = 0$ [1], but at some point z_0 above this level. This is because the assumptions used to derive the turbulence model, which neglect viscosity and the nature of the bed, are no longer valid in the vicinity of the bottom boundary. The determination of z_0 is essentially empirical and has been investigated thoroughly for the case of steady shear flows above a solid boundary where the mean velocity profile takes a logarithmic form. In general z_0 depends on the flow itself (via the friction velocity v_*), the laminar viscosity ν, and the Nikuradse roughness height k_N (a measure of the height of elements making up the bed). For a *rough* turbulent boundary layer the roughness height is sufficiently large, compared to the viscous boundary layer thickness, for the viscous sub-layer to have no effect on the turbulent flow further from the bed; for this case z_0 is given by

$$z_0 = \frac{1}{30} k_N.$$

For flat beds of sand a number of formulae relating the sand diameter d and the Nikuradse roughness length have been suggested. Generally these have taken the

[1] For flat uniform sand covered beds, the theoretical level of the bed is usually taken $\frac{1}{3}d$ below the top of the sand grains.

form

$$k_N = mD_n, \tag{3.31}$$

where D_n is defined such that $n\%$ by weight of the sample has a diameter less than D_n. Sleath (1984, p. 35) presents a selection of such relationships and suggests using $k_N = 2D_{65}$, as given by Engelund & Hansen (1967). The boundary condition for the velocity is thus taken as

$$\bar{v}_1 = 0 \quad \text{at } z_1 = z_0 = \frac{1}{30}k_N. \tag{3.32}$$

An alternative way of formulating the velocity boundary condition near the bed (e.g. Johns 1977), is to assume explicitly that a logarithmic velocity profile of the form

$$\bar{v}_1(z,t) = \frac{v_*(t)}{\kappa} \ln \frac{z}{z_0}, \tag{3.33}$$

exists below z_1, where $z_1 > z_0$. The instantaneous friction velocity $v_*(t)$ is related to the bed stress by

$$v_*(t) = \sqrt{\frac{\tau_0(t)}{\rho_f}}. \tag{3.34}$$

Differentiating (3.33) with respect to z and substituting from (3.33) for v_* yields the following (Robins) boundary condition for the velocity at $z = z_1$:

$$z \ln\left(\frac{z}{z_0}\right) \frac{\partial \bar{v}_1}{\partial z} - v = 0. \tag{3.35}$$

The approach has the advantage of saving the computational points that would otherwise have been used below z_1, but requires the extra assumption of the logarithmic velocity profile (3.33). Note that z_0 is still required. In Section 4.1.1 numerical solutions using (3.32) applied at z_0 and using (3.35) at $z = z_1 > z_0$ are compared.

It should be mentioned that some authors, e.g. Smith (1977), have suggested that in conditions where sediment transport is occuring, the bed load will have an effect on the value of z_0. VanRijn (1981) is reported in Sleath (1984, p. 39) to have found no evidence for this after reviewing the available data. Contrary to this however, the recent paper by Wilson (1984) indicates that z_0 should be proportional to the thickness of the bed load layer under sheet flow conditions. Although this is the regime with which we will be most concerned, we have decided not to introduce the added complexity of such a dependence of z_0.

Two choices have been reported in the literature for the bottom boundary condition for the turbulent kinetic energy equation in oscillatory boundary layer flow.

Justesen (1988) assumes the local equilibrium form (3.28) to hold at $z_1 = z_0$. This allows k to be written in terms of the instantaneous bed stress by substituting for the velocity gradient in (3.28) from (3.30) and then using (3.26) to obtain

$$k = \rho_f^{-1} C_D^{-1/2} |\tau_0|. \tag{3.36}$$

In practice this relation needs to be satisfied using an iterative procedure since τ_0 is itself determined from the solution. Alternatively, Hagatun & Eidsvik (1986) and King et al. (1985) put

$$\frac{\partial k}{\partial z} = 0 \tag{3.37}$$

at $z_1 = z_0$.

If the assumption of a logarithmic velocity profile (3.33) is made, then (3.36) represents a reasonable boundary condition for k, providing that τ_0 is replaced with the turbulent shear stress at z_1. The assumption is that the turbulence is in local equilibrium at z_1. If it is assumed that the region below z_1 is one of constant turbulent shear stress then τ_0 and the shear stress evaluated at z_1 should be equal anyway. This leads to an alternative boundary condition (Johns 1977) in which the assumption of a constant stress region, together with (3.36), implies

$$\frac{\partial k}{\partial z} = 0. \tag{3.38}$$

at $z = z_1$.

When the turbulent length scale l is not specified empirically, some boundary condition at the bed is required. Based on ideas from steady wall-bounded shear flows, the assumption is made that l is proportional to the distance from the wall. Since the constant of proportionality can be changed arbitrarily by the way C_D enters into the equations, we choose the constant to be von Karman's constant, as for steady flows. Thus we have at the bottom boundary

$$l = \kappa z_1$$

By (3.27) this implies the bottom boundary condition for ε should be

$$\varepsilon = \frac{C_D^{3/4} k^{3/2}}{\kappa z_1}. \tag{3.39}$$

Even for steady unidirectional flows the bottom boundary condition for the concentration equation (3.19) is problematic. The quantities required are the level above

the bed at which the concentration should be given — the reference level, and the value of the concentration at that level — the reference concentration. The two values are not expected to be independent however, since clearly the value of the reference concentration will vary depending on the choice of reference level. Two obvious choices for the reference level are:

1. at the top of the bed load layer;

2. where the velocity boundary condition is applied at z_0.

Apart from a dependence on the reference level, the reference concentration will, more importantly, also depend upon the nature of the flow and the properties of the sediment. The Shields parameter,

$$S = \frac{\tau_0}{g(\rho_p - \rho_f)d}, \tag{3.40}$$

the ratio of the weight per unit area of the sediment and the force per unit area exerted by the flow, appears in a number of empirical formulae that have been suggested the bottom boundary concentration. For the calculations presented in Chapter 4, we use a relatively simple expression adapted for use in oscillatory flow by Hagatun & Eidsvik (1986) from an expression derived originally for steady flows by Engelund & Fredsœ(1976). This is applied at $z = z_0$ and is given by

$$\bar{c}(z_0, t; S) = \begin{cases} 0, & S < S_0, \\ c_0(S - S_0)/(S_1 - S_0), & S_0 < S < S_1, \\ c_0, & S > S_1. \end{cases} \tag{3.41}$$

Here c_0 is adjusted to fit experiment while S_0 and S_1 are the critical and what we term the 'saturation' values of the Shields parameter. The critical value is the value of S below which no sediment movement is supposed to occur. The saturation value represents an upper bound on the sediment concentration in the bed load region, the name implying that at this point the bed load cannot take up further quantities of sediment. We follow Hagatun & Eidsvik and assign $S_0 = 0.05$ and $S_1 = 0.75$.

Since z_0 will be well below the top of the bed load region, we cannot expect the the concentrations that are predicted near the bed to be correct since the equations are not valid there. In Chapter 5 we take into account particle inertia and pressure effects and will wish to avoid the bed load region entirely because spurious effects predicted in this region, where the model is not valid, will influence the solution in the suspended load region above. The approach adopted, and explained in more

detail in Chapter 5, is to solve the model without inertia terms using (3.41) at z_0 and so obtain a value of $\bar{c}$ at the top of the bed load which is then used as the bottom boundary condition for the model with inertia terms.

Rather than specify the concentration at the lower boundary, a number of workers (e.g. Nielson 1979) have preferred to specify the lower boundary condition using a 'flux' boundary condition involving the concentration gradient. In general it is supposed that this is most appropriate for flows of a dynamic nature, where the bed load concentration has no time to reach an equilibrium value. No consensus appears to exist concerning the merits if this type of boundary condition, as opposed to the more traditional approach of supplying a reference concentration. For our purposes the latter is assumed to be adequate.

Upper boundary conditions

Fortunately, conditions to be imposed at the upper boundary, $z = z_2$, are more straightforward than those at the bed. For the velocity two reasonable choices are either to put $\bar{v}_1$ equal to the free stream velocity

$$\bar{v}_1(z_2, t) = V_\infty \sin \omega t, \tag{3.42}$$

or to require

$$\frac{\partial \bar{v}_1}{\partial z} = 0. \tag{3.43}$$

The upper boundary conditions for the turbulent kinetic energy k and turbulent kinetic energy dissipation rate ε are

$$\frac{\partial k}{\partial z} = \frac{\partial \varepsilon}{\partial z} = 0.$$

For the concentration reasonable boundary conditions might be

$$\bar{c} = 0, \tag{3.44}$$

or

$$\frac{\partial \bar{c}}{\partial z} = 0. \tag{3.45}$$

Results obtained using all the suggested boundary conditions are compared in Chapter 4.

3.1.2 Non-dimensional form of equations

By scaling the equations using the dimensional parameters that enter into the problem, it is possible to identify the non-dimensional groups which characterise the flow. It is also often advantageous numerically to solve the equations in non-dimensional form.

Quantities used to non-dimensionalise the equations are in this instance chosen for convenience rather than to obtain realistic magnitudes for all terms. The free stream velocity V_∞ and the frequency ω define obvious velocity and time scales and, via (3.11), the pressure scale. Introducing these and δ (as yet unspecified) to scale the vertical coordinate z, the following non-dimensional momentum equation is obtained from (3.20)

$$\frac{\partial \bar{v}_1^*}{\partial t^*} = -\frac{\partial P_\infty^*}{\partial x^*} + \frac{1}{\omega\delta}\frac{\partial}{\partial z^*}\left(\frac{\nu_T}{\delta}\frac{\partial \bar{v}_1^*}{\partial z^*}\right).$$

If the length scale is now defined as the ratio

$$\delta = \frac{v^+}{\omega},$$

with v^+ some velocity scale, we obtain

$$\frac{\partial \bar{v}_1^*}{\partial t^*} = -\frac{\partial P_\infty^*}{\partial x^*} + \frac{\partial}{\partial z^*}\left(\nu_T^*\frac{\partial \bar{v}_1^*}{\partial z^*}\right),$$

where

$$\nu_T^* = \nu_T/(v^+\delta). \tag{3.46}$$

A natural choice for v^+ is the maximum friction velocity over a wave period T,

$$v_{*m} = \max_{0\le t\le T} v_*(t), \tag{3.47}$$

because:

1. for oscillatory boundary layers the typical boundary layer thickness is often taken to be $\delta_\omega = v_*/\omega$ (see for example Smith 1977, pp 546–547) and thus δ would be representative of the boundary layer thickness;
2. the velocity scale appearing in the definition of the non-dimensional eddy viscosity (3.46) should be representative of the velocity fluctuations, which v_{*m} is.

Previous workers, (Johns 1977, King et al. 1985) have used V_∞ to define the value of δ. Whilst v_{*m} would have to be estimated from some additional theory, V_∞ is one

of the given parameters and therefore we follow previous work and put

$$\delta = \frac{V_\infty}{\omega} \equiv a,$$

so that δ becomes the amplitude of the oscillatory motion at the edge of the boundary layer. Adopting this definition of δ the boundary conditions are applied at $z_2^* = z_2/a$ and, assuming a rough boundary layer, at $z_0^* = \frac{1}{30}k_N/a$. Two non-dimensional parameters, z_2^* and a/k_N, are seen to characterise the flow [2]. Most studies have not been concerned with z_2^*, specifying it to be large so that effectively the problem being approximated is the one with $z_2^* \to \infty$, Physically, this corresponds to a boundary layer that is completely contained within the external flow which is the assumption made in Section 3.1 when the boundary layer equations were derived. We therefore take z_2^* to be large and concentrate attention on a/k_N, the ratio of the amplitude of oscillation to the roughness height, which is then the single parameter that characterises the hydrodynamic aspects of the flow.

It should be mentioned that the concept of roughness height is likely to be valid only for $k_N \ll a$. As the bed features become nearer to the scale of the flow itself, the shape of the bed must be expected to influence the near bed flow (for example by the shedding of eddies from individual surface elements) and these effects cannot accounted for by the idea of a simple roughness value. Justesen (1988) suggests that $a/k_N > 30$.

With $v^+ = V_\infty$ we should, for consistency with (3.46) given that $\nu_T \propto k^{1/2}$, use V_∞^2 to non-dimensionalise k. This in turn implies, upon rearranging (3.27) and scaling l with δ, that ε is to be non-dimensionalised with the quantity ωV_∞^2.

For the vertical particle flux $\bar{u}_2$ there are two velocity scales that could be used to obtain a non-dimensional quantity; the free stream velocity V_∞ and the fall velocity w_0. Although w_0 is characteristic of the magnitude of $\bar{u}_2$, it is more convenient to use V_∞ as the terms in the resulting non-dimensional equation are closer to those appearing in the momentum equation. This makes the implementation of the numerical scheme slightly easier. The concentration is scaled on the reference concentration c_0, introduced in the boundary condition (3.41). The non-dimensional form of (3.19) is then found to be

$$\frac{\partial \bar{c}^*}{\partial t^*} + \frac{\partial}{\partial z^*}\bar{c}^*\bar{u}_2^* = 0, \tag{3.48}$$

[2] The fact that both enter through the boundary conditions is due only to the definition of δ. If, for a rough boundary layer, we had put $\delta = k_N$ then the non-dimensional number a/k_N would have appeared in the momentum equation rather than in the boundary conditions.

where

$$\bar{c}^*\bar{u}_2^* = -w_0^*\bar{c}^* - \kappa_T^*\frac{\partial \bar{c}^*}{\partial z}, \tag{3.49}$$

$$w_0^* = w_0/V_\infty, \tag{3.50}$$

$$\kappa_T^* = \kappa_T/(V_\infty \delta). \tag{3.51}$$

Thus a third non-dimensional parameter w_0^* emerges. It is expected that the quantity of sediment in suspension will depend inversely on the value of w_0^*. For $w_0^* < 1$ the turbulent fluctuations, scaling on V_∞, are large relative to the fall velocity tending to keep sediment in suspension whilst, for $w_0^* > 1$, the fall velocity dominates the velocity fluctuations and the quantity of sediment in suspension will decrease.

Coordinate transformation

A characteristic of the turbulent oscillatory boundary layer is the occurrence of large velocity (and concentration) gradients near the bed. It is usual to introduce a transformation to the vertical coordinate to avoid the use of extremely fine grids that would otherwise be required to resolve the near-bed flow. Therefore we define a new independent variable

$$\zeta(z^*) = [\ln\frac{z^*}{z_0^*} + \frac{(z^* - z_0^*)}{h}]/\zeta_N, \tag{3.52}$$

where h is a pre-set weighting factor and where

$$\zeta_N = \ln\frac{z_2^*}{z_0^*} + \frac{(z_2^* - z_0^*)}{h}.$$

Since

$$\frac{\partial}{\partial z^*} = \frac{d\zeta}{dz}\frac{\partial}{\partial \zeta} \equiv \dot{\zeta}\frac{\partial}{\partial \zeta},$$

we can re-write the non-dimensional form of the equations in terms of ζ.

$$\frac{\partial \bar{c}^*}{\partial t^*} = -\dot{\zeta}\frac{\partial}{\partial \zeta}\bar{c}^*\bar{u}_2^*, \tag{3.53}$$

$$\frac{\partial \bar{v}_1^*}{\partial t^*} = -\frac{\partial P_\infty^*}{\partial x} + \dot{\zeta}\frac{\partial}{\partial \zeta}\left(\nu_T^{**}\frac{\partial \bar{v}_1^*}{\partial \zeta}\right), \tag{3.54}$$

$$\frac{\partial k^*}{\partial t^*} = \dot{\zeta}\frac{\partial}{\partial \zeta}\left(\frac{\nu_T^{**}}{\sigma_k}\frac{\partial k^*}{\partial \zeta}\right) + P^* + G^* - \varepsilon^*, \tag{3.55}$$

$$\frac{\partial \varepsilon^*}{\partial t^*} = \dot{\zeta}\frac{\partial}{\partial \zeta}\left(\frac{\nu_T^{**}}{\sigma_\varepsilon}\frac{\partial \varepsilon^*}{\partial \zeta}\right) + C_{1\varepsilon}\frac{\varepsilon^*}{k^*}(P^* + G^*)(1 + C_{3\varepsilon}R_f) - C_{2\varepsilon}\frac{(\varepsilon^*)^2}{k^*}, \tag{3.56}$$

where

$$\begin{aligned}
\bar{c}^{\bullet}\bar{u}_2 &= w_0^{\bullet}\bar{c}^{\bullet} - \kappa_T^{\bullet\bullet}\frac{\partial \bar{c}^{\bullet}}{\partial \zeta}, \\
P^{\bullet} &= \zeta \nu_T^{\bullet\bullet}\left(\frac{\partial \bar{v}_1^{\bullet}}{\partial \zeta}\right)^2, \\
G^{\bullet} &= c_0 \frac{\Delta\rho}{\rho_f} g \kappa_T^{\bullet\bullet}\frac{\partial \bar{c}^{\bullet}}{\partial \zeta}, \\
\nu_T^{\bullet\bullet} &= \zeta \frac{\nu_T}{V_\infty \delta}, \\
\kappa_T^{\bullet\bullet} &= \nu_T^{\bullet\bullet}.
\end{aligned}$$

The local equilibrium expression for k (3.28) becomes

$$(k^{\bullet})^{1/2} = C_D^{-1/4}\zeta l^{\bullet}\left|\frac{\partial \bar{v}_1^{\bullet}}{\partial \zeta}\right|. \tag{3.57}$$

The non-dimensional length scale l/δ is calculated either from k and ε using

$$l^{\bullet} = \frac{C_D^{3/4}(k^{\bullet})^{3/2}}{\varepsilon^{\bullet}},$$

or from k only via

$$l^{\bullet}(\zeta) = \kappa(k^{\bullet})^{1/2}\int_{\zeta_1}^{\zeta}(k^{\bullet})^{-1/2}\frac{d\zeta}{\zeta} + l_1^{\bullet}.$$

Summarising, the boundary conditions are:

Velocity At the lower boundary

1. $\bar{v}_1^{\bullet} = 0$ at $z_1^{\bullet} = z_0^{\bullet}$;
2. $z_1^{\bullet}\ln\left(\frac{z_1^{\bullet}}{z_0^{\bullet}}\right)\zeta\frac{\partial \bar{v}_1^{\bullet}}{\partial \zeta} - \bar{v}_1^{\bullet} = 0 \qquad$ at $z_1^{\bullet} > z_0^{\bullet}$.

At the upper boundary

1. $\bar{v}_1^{\bullet} = \sin t$;
2. $\frac{\partial \bar{v}_1^{\bullet}}{\partial \zeta} = 0$.

Turbulent kinetic energy At the lower boundary

1. $k^{\bullet} = \rho_f^{-1}C_D^{1/2}|\tau|/V_\infty^2$ at $z_1^{\bullet} \geq z_0^{\bullet}$;
2. $\frac{\partial k^{\bullet}}{\partial \zeta} = 0$ at $z_1^{\bullet} \geq z_0^{\bullet}$.

At the upper boundary

$$\frac{\partial k}{\partial \zeta} = 0.$$

Length scale At the lower boundary

$$l^* = \kappa z^*.$$

Dissipation rate At the lower boundary

$$\varepsilon^* = \frac{C_D^{3/4}(k^*)^{3/2}}{\kappa z_1^*}.$$

At the upper boundary

$$\frac{\partial \varepsilon^*}{\partial \zeta} = 0.$$

Concentration At the bottom boundary, $z_1^* = z_0^*$

$$\bar{c}^*(z_0, t; S) = \begin{cases} 0, & S < S_0 \\ (S - S_0)/(S_1 - S_0), & S_0 < S < S_1 \\ 1, & S > S_1 \end{cases}.$$

At the upper boundary,

1. $\bar{c}^* = 0$;
2. $\dfrac{\partial \bar{c}^*}{\partial \zeta} = 0.$

3.2 Finite difference scheme

The equations whose numerical solution is sought can all be broadly classified as being advection-diffusion equations and parabolic in type. Numerical solutions can be effected relatively easily by standard finite difference techniques. We adopt an implicit scheme based on the classic Crank-Nicolson method (Smith 1978). This method is similar to that used by King et al. (1985) for an oscillating boundary layer.

In an implicit scheme the solution at the $(n+1)$th time step for a specific finite difference node is given in terms of the solution at the surrounding nodes at the $(n+1)$th time step and the solution at the nth time step. This gives rise to a system of algebraic equations whose solution yields the values of the dependent variables at the next step. Typically such methods entail more computation per time step than an explicit method, which gives the solution at $(n+1)$ using only the solution at n. However they enjoy superior stability properties enabling larger time steps to be used and hence an overall saving in computational cost. For a *linear* diffusion equation an explicit scheme has a time step that is constrained by the square of the space step whilst the Crank-Nicolson, and related methods, can be shown to be stable for

any time step. This property of the Crank-Nicolson scheme does not necessarily carry over to the complicated, non-linear system given by (3.19) to (3.22); however in practice the scheme has been found to be stable for all the cases tried.

Each of the equations (3.53) to (3.56) can be cast in the general form

$$\frac{\partial \phi}{\partial t} = \zeta \frac{\partial}{\partial \zeta}(K \frac{\partial \phi}{\partial \zeta}) + A\zeta \frac{\partial \phi}{\partial \zeta} + B\phi + C, \tag{3.58}$$

where A, B, C and K will generally be functions of ϕ if the system is non-linear. Let the function ϕ_i^n be defined on a discreet set of points $\{\zeta_i\}$ and at times $\{t_n\}$, where $1 \leq i \leq M$, $0 \leq n$. Let

$$\begin{aligned} \zeta_i &= \zeta_1 + (i-1)\Delta\zeta, \\ t_n &= n\Delta t, \\ \Delta\zeta &= (\zeta_M - \zeta_1)/(M-1). \end{aligned}$$

At intermediate times define $\phi_i^{n+\theta}$, $0 \leq \theta \leq 1$ by

$$\phi_i^{n+\theta} = \theta\phi_i^{n+1} + (1-\theta)\phi_i^n. \tag{3.59}$$

Let

$$\begin{aligned} D_+\phi_i^n &\equiv \phi_{i+1}^n - \phi_i^n, \\ D_0\phi_i^n &\equiv \phi_{i+1}^n - \phi_{i-1}^n. \end{aligned}$$

The derivatives of ϕ in (3.58) are replaced by finite difference equivalents involving ϕ_i^n thus

$$\begin{aligned} \frac{\phi_i^{n+1} - \phi_i^n}{\Delta t} &= \frac{\zeta_i}{\Delta\zeta^2}[K_{i+1/2}^{n+\theta} D_+\phi_i^{n+\theta} - K_{i-1/2}^{n+\theta} D_+\phi_{i-1}^{n+\theta}] \\ &\quad + A_i^{n+\theta} D_0\phi_i^{n+\theta}/(2\Delta\zeta) + B_i^{n+\theta}\phi_i^{n+\theta} + C_i^{n+\theta}. \end{aligned} \tag{3.60}$$

It is easy to show that this finite difference expression is consistent with the original partial differential equation (3.58). That is, writing the finite difference expression as $F(\phi_i^n; \Delta\zeta, \Delta t) = 0$ and substituting in ϕ satisfying (3.58), then $F(\phi; \Delta\zeta, \Delta t) \to 0$ as $\Delta\zeta, \Delta t \to 0$.

Using (3.59), the finite difference expression (3.60) can be written

$$-d_i\phi_{i-1}^{n+1} + e_i\phi_i^{n+1} - f_i\phi_{i+1}^{n+1} = r_i \tag{3.61}$$

where

$$
\begin{aligned}
d_i &= \theta(-\lambda_2 A_i^{n+\theta} + \lambda_1 K_{i-1/2}^{n+\theta}),\\
e_i &= 1 + \theta[\lambda_1(K_{i+1/2}^{n+\theta} + K_{i-1/2}^{n+\theta}) - \Delta t B_i^{n+\theta}],\\
f_i &= \theta(\lambda_2 A_i^{n+\theta} + \lambda_1 K_{i+1/2}^{n+\theta}),\\
r_i &= \phi_i^n + \Delta t C_i^{n+\theta}\\
&\quad + (1-\theta)[\lambda_1(K_{i+1/2}^{n+\theta} D_+ \phi_i^{n+\theta} K_{i-1/2}^{n+\theta} D_+ \phi_{i-1}^{n+th}) + \lambda_2 A_i^{n+\theta} D_0 \phi_i^{n+\theta} + \Delta t B_i^{n+\theta} \phi_i^{n+\theta}],\\
\lambda_1 &= \frac{\Delta t}{\Delta \zeta^2}, \qquad \lambda_2 = \frac{\Delta t}{2\Delta \zeta}.
\end{aligned}
$$

If, for the moment, we assume that (3.58) is linear, i.e. that A, B, C and K are *not* functions of ϕ, then (3.61) is a tri-diagonal linear algebraic system which can be written in matrix form as

$$\Lambda \phi^{n+1} = b, \tag{3.62}$$

where

$$\phi^{n+1} \equiv (\phi_1^{n+1}, \phi_2^{n+1}, \ldots, \phi_M^{n+1}).$$

The solution of such systems, with the only non-zero elements occuring along the leading diagonal and the two diagonals on either side, can be obtained efficiently using Gaussian elimination. The elimination algorithm is stable without requiring pivoting if the following are satisfied:

$$
\begin{aligned}
d_i &> 0, \quad e_i > 0, \quad f_i > 0,\\
e_i &> d_i + f_i.
\end{aligned}
$$

Adding d_i to f_i shows that the last condition is also satisfied automatically for $K > 0$.

Boundary conditions are implemented as follows.

Dirichlet If $\phi = \alpha$ is specified at ζ_1 then (3.61) at $i = 2$ is written

$$e_2 \phi_2^{n+1} - f_2 \phi_3^{n+1} = r_2 + d_2 \alpha.$$

The solution is then obtained for $i \geq 2$. An exactly analogous procedure is employed at $M - 1$ if ϕ is specified at M.

Neumann If the derivative $\partial\phi/\partial\zeta = \alpha$ is specified at ζ_1 then an extra variable ϕ_0^{n+1}

is introduced and the finite difference equivalent of the boundary condition

$$\frac{\phi_2^{n+1} - \phi_0^{n+1}}{\Delta\zeta} = \alpha,$$

is substituted into (3.61) at $i = 1$ to yield

$$e_1\phi_1^{n+1} - (d_1 + f_1)\phi_2^{n+1} = r_1 + d_1\alpha\Delta\zeta.$$

The solution is then obtained for $i \geq 1$. Again a similar procedure, introducing an extra variable ϕ_{M+1}^{n+1}, is applied at $i = M$ if a derivative is specified at the top boundary.

Robin If $\partial\phi/\partial\zeta = \alpha\phi$ is specified at ζ_1 then an extra variable ϕ_0^{n+1} is introduced and the finite difference equivalent of the boundary condition

$$\frac{\phi_2^{n+1} - \phi_0^{n+1}}{\Delta\zeta} = \alpha\phi_1^{n+1}$$

is substituted into (3.61) at $i = 1$ to yield

$$-(d_1\alpha\Delta\zeta + e_1)\phi_1^{n+1} - (d_1 + f_1)\phi_2^{n+1} = r_1.$$

The solution is then obtained for $i \geq 1$.

When the dependence of A, B, C and K on ϕ is taken into account, the finite difference equations are of the same form as (3.62) except that A and b are now functions of ϕ^{n+1}. The solution can still be accomplished using the efficient algorithm for a linear system by using a standard iterative technique. Define, for given n, a sequence of iterates $\phi^{n+1,s}$ by

$$\begin{aligned} \phi^{n+1,0} &= \phi^n, \\ A(\phi^{n+1,s})\phi^{n+1,s+1} &= b(\phi^{n+1,s}), \end{aligned}$$

then $\phi^{n+1,s+1}$ can be calculated at each iteration using the algorithm for a tri-diagonal linear system. Assuming the sequence converges then

$$\phi^{n+1,s+1} - \phi^{n+1,s} \to 0$$

as $s \to \infty$. If $\phi^{n+1} = \phi^{n+1,\infty}$, then ϕ^{n+1} satisfies the non-linear form of (3.62) exactly. Of course in practice it is necessary to stop after a finite number of iterations

so that the resulting value of ϕ^{n+1} satisfies the non-linear system only approximately.

The finite difference formulae for equations (3.53) to (3.56) are:

$$\frac{c_i^{n+1,s+1}-c_i^n}{\Delta t} = \frac{1}{2\Delta\zeta}D_0(w_0^* c_i^{n+\theta,s+1}) + \frac{\dot{\zeta}_i}{(\Delta\zeta)^2}D_+\left[(\nu_T^{**})_{i-1/2}^{n+\theta,s}D_+ c_{i-1}^{n+\theta,s+1}\right] \tag{3.63}$$

$$\frac{v_i^{n+1,s+1}-v_i^n}{\Delta t} = -\left(\frac{\partial P^*}{\partial x^*}\right)^{n+\theta} + \frac{\dot{\zeta}_i}{(\Delta\zeta)^2}D_+\left[(\nu_T^{**})_{i-1/2}^{n+\theta,s}D_+ v_{i-1}^{n+\theta,s+1}\right] \tag{3.64}$$

$$\begin{aligned}\frac{k_i^{n+1,s+1}-k_i^n}{\Delta t} &= \frac{\dot{\zeta}_i}{(\Delta\zeta)^2}D_+[(\nu_T^{**})_{i-1/2}^{n+\theta,s}D_+ k_{i-1}^{n+\theta,s+1}] + P_i^{n+\theta,s+1} + G_i^{n+\theta,s+1} \\ &\quad - C_D^{3/4}\left(\frac{k_i^{n+\theta,s}}{l_i^{n+\theta,s}}\right)^{1/2} k_i^{n+1,s+1},\end{aligned} \tag{3.65}$$

$$\begin{aligned}\frac{\varepsilon_i^{n+1,s+1}-\varepsilon_i^n}{\Delta t} &= \frac{\dot{\zeta}_i}{(\Delta\zeta)^2}D_+[(\nu_T^{**})_{i-1/2}^{n+\theta,s}D_+ \varepsilon_{i-1}^{n+\theta,s+1}] \\ &\quad + C_{1\varepsilon}\frac{\varepsilon_i^{n+\theta,s}}{k_i^{n+\theta,s+1}}\left(P_i^{n+\theta,s+1}+G_i^{n+\theta,s+1}\right)\left(1+C_{3\varepsilon}(R_f)_i^{n+\theta,s+1}\right) \\ &\quad - C_{2\varepsilon}\left(\frac{\varepsilon_i^{n+\theta,s}}{k_i^{n+\theta,s+1}}\right)\varepsilon_i^{n+1,s+1},\end{aligned} \tag{3.66}$$

where

$$\begin{aligned}P_i^{n+\theta,s+1} &= \dot{\zeta}_i(\nu_T)_i^{n+\theta,s}\left(\frac{D_0 v_i^{n+h,s+1}}{2\Delta\zeta}\right)^2, \\ G_i^{n+\theta,s+1} &= (\kappa_T)_i^{n+\theta,s}\frac{D_0 c_i^{n+\theta,s+1}}{2\Delta\zeta}, \\ (\nu_T)_i^{n+\theta,s} &= C_D^{1/4}\dot{\zeta}_i i_i^{n+\theta},(k_i^{n+\theta,s})^{1/2}, \\ (\nu_T)_{i-1/2}^{n+\theta,s} &= \frac{1}{2}C_D^{1/4}\left[\dot{\zeta}_i l_i^{n+\theta,s}(k_i^{n+\theta,s})^{1/2} + \dot{\zeta}_{i-1}l_i^{n+\theta,s}(k_{i-1}^{n+\theta,s})^{1/2}\right], \\ (R_f)_i^{n+\theta,s+1} &= -G_i^{n+\theta,s+1}/P_i^{n+\theta,s+1}.\end{aligned} \tag{3.67}$$

For any variable, the value at $n+\theta$ is defined via (3.59).

If the mixing length model is being used, then k is given explicitly by the finite difference expression corresponding to (3.57)

$$k_i^{n+1,s+1} = C_D^{-1/4}\dot{\zeta}_i l_i^{n+1,s}\left|\frac{D_0 v_i^{n+1,s+1}}{2\Delta\zeta}\right| \tag{3.68}$$

The discrete length scale is given, depending on the turbulence model, by either

$$l_i^{n+1,s+1} = \frac{C_D^{3/4}(k_i^{n+1,s+1})^{3/2}}{\varepsilon_i^{n+1,s+1}}, \tag{3.69}$$

or

$$l_i^{n+1,s+1} = \kappa(k_i^{n+1,s+1})^{1/2} \int_{\zeta_1}^{\zeta_i} (k_i^{n+th,s+1})^{-1/2} \frac{d\zeta}{\zeta} + l_1 \tag{3.70}$$

where $l_1 = \kappa z_1^*$. The trapezium rule is used to evaluate the integral for $i > 1$.

At boundaries, one-sided finite difference formula are used if necessary. For example, if a derivative boundary condition on k is specified at the bottom then, as written, the finite difference form of the k-equation would need $v_i^{n+1,s+1}$ at $i = 0$ which is not defined. Therefore the central difference is replaced with the second order accurate finite difference approximation

$$\left(\frac{\partial v}{\partial z}\right)_1^{n+\theta,s+1} = (4v_2^{n+\theta,s+1} - 3v_1^{n+\theta,s+1} - v_3^{n+\theta,s+1})/(2\Delta\zeta) + O((\Delta\zeta)^2).$$

The same expression is used to calculate the velocity gradient appearing in the bottom stress, the finite difference form of which is

$$(\tau_0^*)^{n+\theta,s+1} = C_D^{1/4}\zeta_1(k_1^{n+\theta,s})^{1/2} l_1^{n+\theta,s} \left(\frac{\partial v}{\partial z}\right)_{i=1}^{n+\theta,s+1} \tag{3.71}$$

At the top the equivalent one-sided difference is

$$\left(\frac{\partial v}{\partial z}\right)_{M}^{n+\theta,s+1} = (3v_M^{n+\theta,s+1} - 4v_{M-1}^{n+\theta,s+1} - v_{M-2}^{n+\theta,s+1})/(2\Delta\zeta) + O((\Delta\zeta)^2).$$

Solution procedure outline

In outline the solution is obtained at a given time step by the following sequence:

Solve for the horizontal fluid momentum using (3.64) with the value of the eddy viscosity from the previous time step.

Calculate the bottom stress using (3.71).

Solve for the particle concentration using (3.63) with the value of the eddy viscosity from the previous time step.

loop

Calculate the turbulent kinetic energy from (3.65) or (3.68) depending on the turbulence model.

Calculate the turbulent length scale either from (3.66) and (3.69), or from (3.70), depending on the turbulence model.

If converged exit loop.

Re-calculate the eddy viscosity (3.67) using the latest iterates.

$s := s + 1$

Solve for the horizontal fluid momentum using (3.64) with the current value of the eddy viscosity.

Calculate the bottom stress using (3.71).

Solve for the particle concentration using (3.63) with the new value of the eddy viscosity.

end loop

It was found necessary to switch, at some distance above the bed, from centred to "upwind" differences to prevent the occurrence of oscillations when evaluating the advection term in the concentration equation. Such oscillations are commonly encountered in the numerical solution of advection-diffusion equations when the advection term becomes dominant, hence the occurrence of this problem in the upper part of the boundary layer where turbulent diffusion is decreasing. The use of first order differences removes the oscillations by introducing numerical diffusion into the solution, and so must be used with caution. Figure 3.2 illustrates the effect of indiscriminate use of upwind differencing, with an almost two-fold increase in the predicted concentrations compared to the central difference solution. Fortunately, the oscillations were found to occur above the region of primary interest, which was within 4cms of the bed. Therefore we were able to use central differencing in this region before switching to upwind differences at a point further from the bed. The point was determined by trial and error and was taken as far from the bed as possible while still preventing wiggles. For the $k-\varepsilon$ model and with the parameters used for all the runs presented, this was found to be at about 4.5 cms. As can be seen from figure 3.2, this leads to identical predictions to that obtained using central differencing in the

region shown.

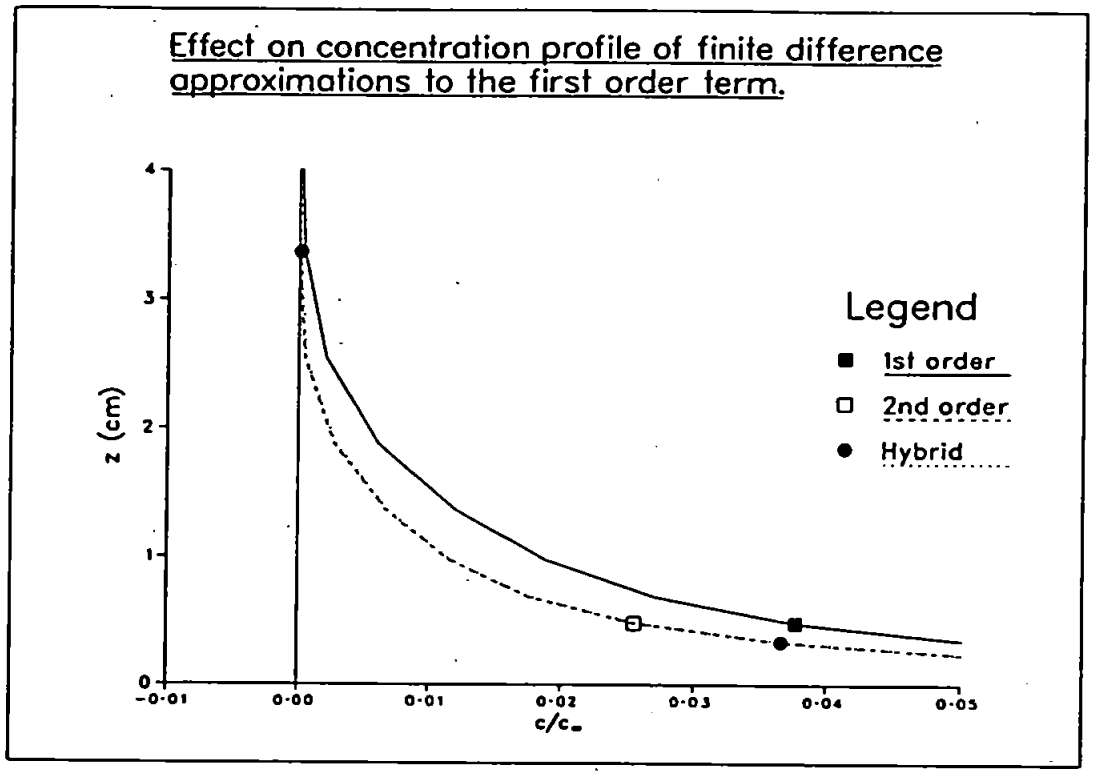

Figure 3.2: Effect of upwind differencing on concentration profiles.

The value of θ has not as yet been fixed, other than requiring it to be between zero and one. Putting $\theta = 0$ yields an explicit scheme; for $\theta > 0$ the scheme is implicit. The choice of $\theta = 1/2$ is particularly interesting as the resulting method is second order in time and space while for other values of θ the method is second order in space but first order in time. Unfortunately it was not possible to run all the models with this value of θ for reasons described below.

General behaviour of the numerical scheme

In general the model proves very stable, taking typically 6 to 8 iterations at any given time step (see table 4.12), and produces smoothly varying solutions in time and space. Problems are encountered at the bottom boundary just before the flow reverses when the bed stress goes through zero. This is particularly severe when the mixing length expression (3.28) is used to determine k and in fact leads to non-convergence. The problem is associated with the vanishing of the eddy viscosity, leading ~~presumably~~ to a singularity in the solution. Adding a small constant viscosity to the eddy viscosity improves the situation but does not cure the problem entirely, even when a very large value (of the order of ten times the laminar viscosity) is used. In addition, it is found

that the kinetic energy profiles can be significantly altered by the addition of this large constant viscosity. Putting $\theta = 1$ to give a fully implicit scheme was found not to improve the behaviour substantially for the mixing length model.

By contrast, the use of the full equation turbulent kinetic energy equation, either with an empirical length scale distribution or with l given by (3.29), proves to be robust, even with $\theta = 1/2$. However, problems are again encountered when the bed stress vanishes if the ϵ equation, (3.22), is included in the system. For $\theta = 1/2$, negative turbulent kinetic energy values are produced leading to a breakdown in the solution. The derivative bottom boundary condition (3.37) is found to be less sensitive, although the solution can still break down depending on the exact value of the flow parameters. Putting $\theta = 1$ leads to satisfactory behaviour with both boundary conditions at the expense of first order accurate solutions only in time. All models, other than the simplest where the length and velocity scale are specified explicitly, are found to require substantially more iterations than normal as the bottom stress goes through zero.

A problem also arises with the $k - \epsilon$ model far away from the bed. Because the transformation from z to ζ concentrates points near the bed the finite difference points near the top boundary are widely separated and so the solution may not be so accurate here. It is found that the length scale calculated from the ratio (3.27) was not smooth in this region and could occasionally become zero leading to obvious problems when dividing by this quantity. Because the eddy viscosity is small far away from the bottom it is considered unlikely that the behaviour of the length scale will have any effect on the solution in the region of interest near the bed.

Chapter 4

Numerical Calculations without Particle Inertia

The chapter is divided into two Sections, both of which deal with purely oscillatory turbulent boundary layer flows. The first deals with the sensitivity of the numerical solution to variations in model parameters and boundary conditions. The second compares the predictions of a number of different turbulence models with experimental data. Results are presented in this chapter with the following aims:

1. verification of the numerical model;
2. indicating the sensitivity of the solutions to the constants contained in the turbulence models, and to the choice of different boundary conditions;
3. determining whether relatively sophisticated turbulence modelling is required to obtain agreement with the experimental results, and to highlight inaccuracies that may result from using simple models.

Hydrodynamic variables, i.e. mean fluid velocities and quantities associated with the turbulence, are generally treated separately to the quantities associated with suspended sediment, and the model was run with different parameter values, corresponding to two different experimental situations, for the two cases.

Turbulence model constants are assigned standard values (Rodi 1980) as shown in table 4.1.

In the numerical scheme the weighting parameter θ was set equal to one for all calculations presented in this chapter. At each time step, convergence was deemed to have occurred when the relative difference between successive iterates of velocity,

κ	C_D	$C_{1\varepsilon}$	$C_{2\varepsilon}$	σ_k	σ_ε
0.4	0.08	1.44	1.92	1.0	1.3

Table 4.1: Values of turbulence constants.

turbulent kinetic energy, turbulent length scale, and concentration were less than 0.5×10^{-4}. A maximum of thirty iterations was allowed before moving onto the next time step.

4.1 Sensitivity calculations

4.1.1 Hydrodynamic results

The following sections present results on the sensitivity of the solution to:

1. the number of time steps and the mesh size;
2. the boundary conditions;
3. the turbulence constants;
4. the parameter a/k_N.

Unless stated otherwise, the flow parameters correspond to those quoted in the experimental work of Sumer et al. — see table 4.3, page 109. The boundary conditions used at the upper boundary were

$$\frac{\partial \bar{v}_1}{\partial z} = \frac{\partial k}{\partial z} = \frac{\partial \varepsilon}{\partial z} = 0,$$

and at the lower boundary

$$\begin{aligned} \bar{v}_1 &= 0, \\ k &= \rho_f^{-1} C_D^{-1/2} \tau_0, \\ \varepsilon &= \frac{C_D^{3/4} k^{3/2}}{\kappa z_1}. \end{aligned}$$

The free stream velocity was specified as

$$V(t) = V_\infty \sin \omega t.$$

For brevity, results are usually presented for the mean velocity profiles and friction velocity only. Mean-velocity profiles are shown at three points during the portion of

the wave cycle when the free-stream velocity goes from zero to its maximum positive value. We term this the accelerating phase, and profiles are shown for $t^* = n\pi/6$, $n = 0 \ldots 2$. The portion during which the the free stream velocity returns to zero is termed the decelerating phase. After this the flow direction will reverse. Once a periodic solution has been obtained the reverse flow will be identical, apart from the sign change, to the flow in the previous half-cycle.

The value of z_0 is taken from the steady shear flow relationship $z_0 = k_N/30$, where k_N was determined from the experimental points by Sumer et al. assuming a logarithmic velocity profile. The Nikuradse roughness k_N and the actual height d of the roughness elements were found by Sumer et al. to be related by $k_N = 2.5d$.

Each figure has a legend giving information about the plot and, to keep these brief, the following abbreviations are used:

E	indicates experimental points,
L	indicates the "linear" turbulence model,
ML	indicates the "mixing length" turbulence model,
k	indicates the "k" turbulence model,
$k-l$	indicates the "$k-l$" turbulence model,
$k-\varepsilon$	indicates the "$k-\varepsilon$" turbulence model.

Section 4.2.1 gives details of each of these models. In general the complexity of the model increases as we go down the list.

Sensitivity to initial conditions

Since a solution is sought that is periodic in time, it is important that the numerical calculation is run long enough for the initial conditions to be "forgotten"; the resulting solution will then depend only upon the periodic forcing in the system. The relative difference between the value of a quantity at a given mesh point, i, at the nth and $(n-1)$th wave cycle is defined as $(\phi_i^n - \phi_i^{n-1})/\phi_i^n$. In figures 4.1 and 4.2 this quantity is plotted for values of the mean velocity at a specified point, and for the maximum bed stress at successive wave cycles for each of the turbulence models. Although not shown, the turbulent kinetic energy and length scale were also sampled, and showed similar behaviour to the mean velocity. The point where the mean velocity is examined is taken (arbitrarily) at about one centimetre above the bed and sampled at the end of the cycle. A second point, further from the bed, yielded a slightly smaller difference at a given cycle than the one shown, for all quantities.

When drawing conclusions from the results, we need to take into account that the

initial conditions, based on an analytic solution to the linear model for the velocity, and a local equilibrium assumption for the kinetic energy, would be expected to favour a more rapid relaxation to an oscillatory state for some models compared to others. From an examination of the turbulent kinetic energy and length scale results (not shown), as well as of figures 4.1 and 4.2, we conclude that:

1. all the models show approximately the same rate of decay of transient effects with time, apart from the linear model which converges very rapidly —probably due to the initial conditions used;

2. no relation can be discerned between the complexity of the model and the time required for the effect of the initial conditions to die out;

3. all the models have settled into a periodic state, reproducing the values of the previous cycle to within 0.2%, by ten wave cycles;

4. the velocity takes the longest time to become periodic, followed by the turbulent kinetic energy, the bed stress and then the length scale.

Results in all subsequent sections were obtained by running the model for six wave cycles —figures 4.1 and 4.2 indicating that the solution is acceptably periodic after this number of cycles.

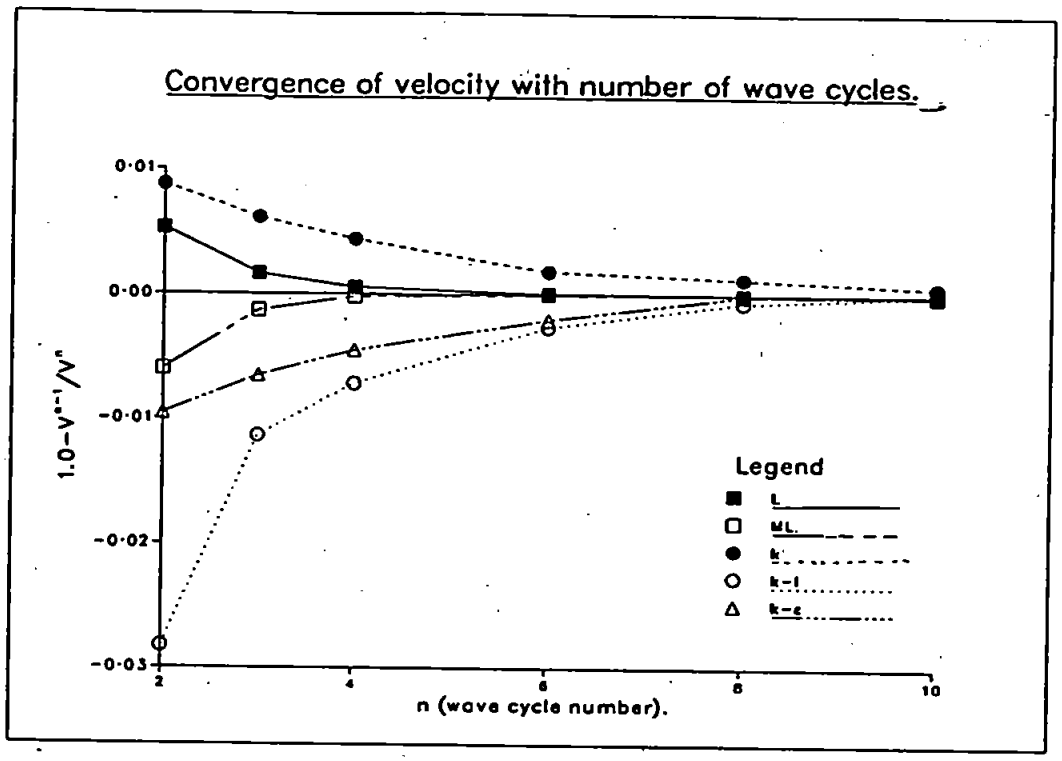

Figure 4.1:

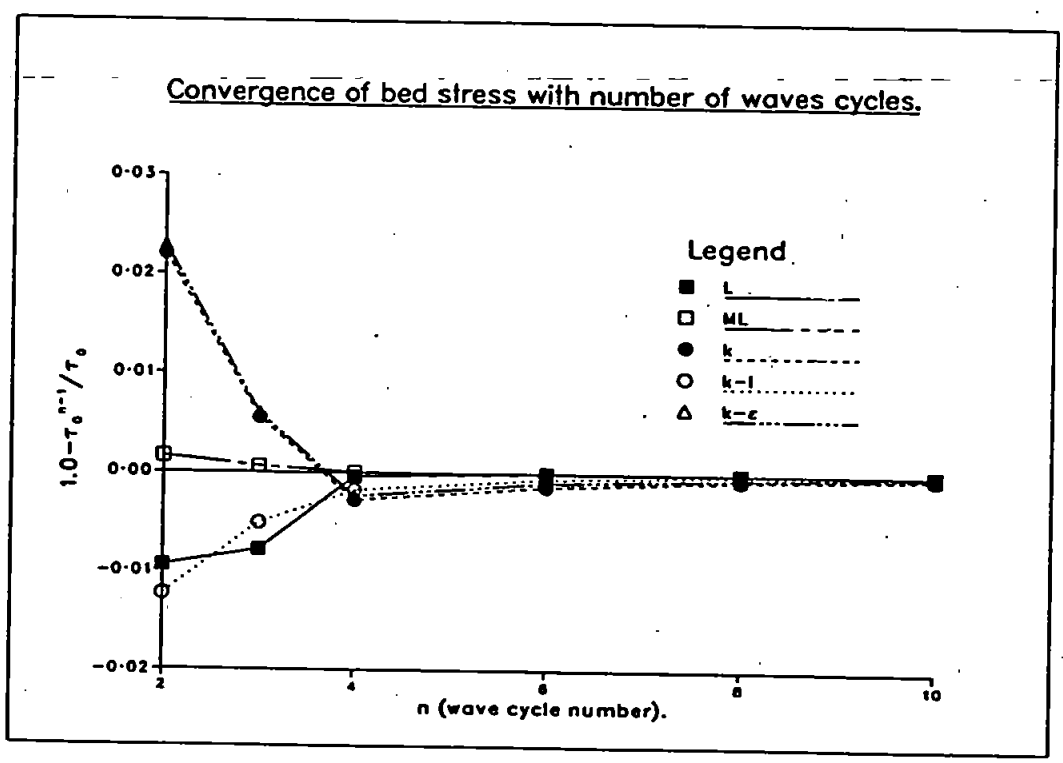

Figure 4.2:

Sensitivity to time and space step.

In figures 4.3 and 4.4 we plot the velocity profiles and friction velocity obtained from calculations with a differing number of mesh points (M), and number of time steps per wave cycle (N). Comparing the curves obtained with $N = 240, M = 48$ to those calculated with half the number of grid points, or half the number of time steps per cycle, shows only a very small effect. We conclude that, for the purpose of graphical comparison, the solutions obtained with $N = 240, M = 48$ are sufficient to obtain solutions unaffected by discretisation errors.

Sensitivity to boundary conditions

A comparison is now made between solutions obtained using the two choices of upper boundary condition for $\bar{v}_1$ given by (3.42) and (3.43), and the two possible bottom boundary conditions on k given by (3.36) and (3.37). It is found that, for the value of z_2 used in this comparison, both the boundary conditions for $\bar{v}_1$ gave rise to identical solutions for all quantities. The two boundary conditions on k also give rise to virtually identical solutions, with only the turbulent kinetic energy profiles (figure 4.5) showing a tiny difference at the bottom boundary. As regards the number of iterations required at each time step to converge the solution, it is found that the stress boundary condition (3.36) is superior to the derivative boundary condition (3.37) (cf table 4.12) and, unless otherwise stated, this boundary condition is used in subsequent calculations.

If the bottom boundary is taken above z_0, then the Robin boundary condition for the velocity, (3.35), is applied at z_1. A logarithmic velocity profile (3.33) is then assumed to hold for $z_0 < z < z_1$. The value of ϵ at z_1 is determined from (3.39); an implicit assumption is therefore made that $l = \kappa z$ for $z_0 < z < z_1$. When using the 'stress' boundary condition for k, (3.36), the velocity gradient in the definition of the stress at z_1 is evaluated from the numerical solution and not from the assumed logarithmic profile via (3.35).

If the numerical model calculations with $z_1 = z_0$ give rise to a constant stress region near the bed then, provided the logarithmic velocity law is correct, the friction velocity calculated at some point within this region using (3.30) should be the same as that evaluated at z_0. Clearly an exactly constant stress region is unlikely to exist because the flow is unsteady, but comparing the solutions calculated with with $z_1 = z_0$ and with $z_1 > z_0$ should indicate how good an assumption constant stress is. There is no reason to suppose *a-priori* that extending the calculation down to z_0 is

more correct, although it has the theoretical advantage of not requiring the explicit assumption of a logarithmic velocity profile.

The friction velocity is plotted for two values of $z_1 > z_0$, and for the two possible choices of boundary condition on k. Figures 4.6 and 4.7 correspond to the use of the stress boundary condition and the derivative boundary condition respectively. These show that the friction velocity calculated using the stress boundary condition is generally less close to the $z_1 = z_0$ result than that calculated with the derivative boundary condition, especially at the beginning of the wave cycle. Interestingly, the agreement between all the curves improve as the wave cycle proceeds, possibly indicating that a constant stress region is forming near the bed by the end of the half-cycle. An examination of the turbulent kinetic energy profiles in figure 4.8a reveals that, for the accelerating phase, this quantity continues to increase below the level of z_1. This will also be true for the stress which, in the local equilibrium approximation, is proportional to $k^{1/2}$. This leads to the under-prediction of the friction velocity when the stress is evaluated at z_1. During the decelerating phase the kinetic energy profiles do become more nearly constant below z_1, as shown in figure 4.8b. This is consistent with the improved agreement between the predictions of friction velocity noted above.

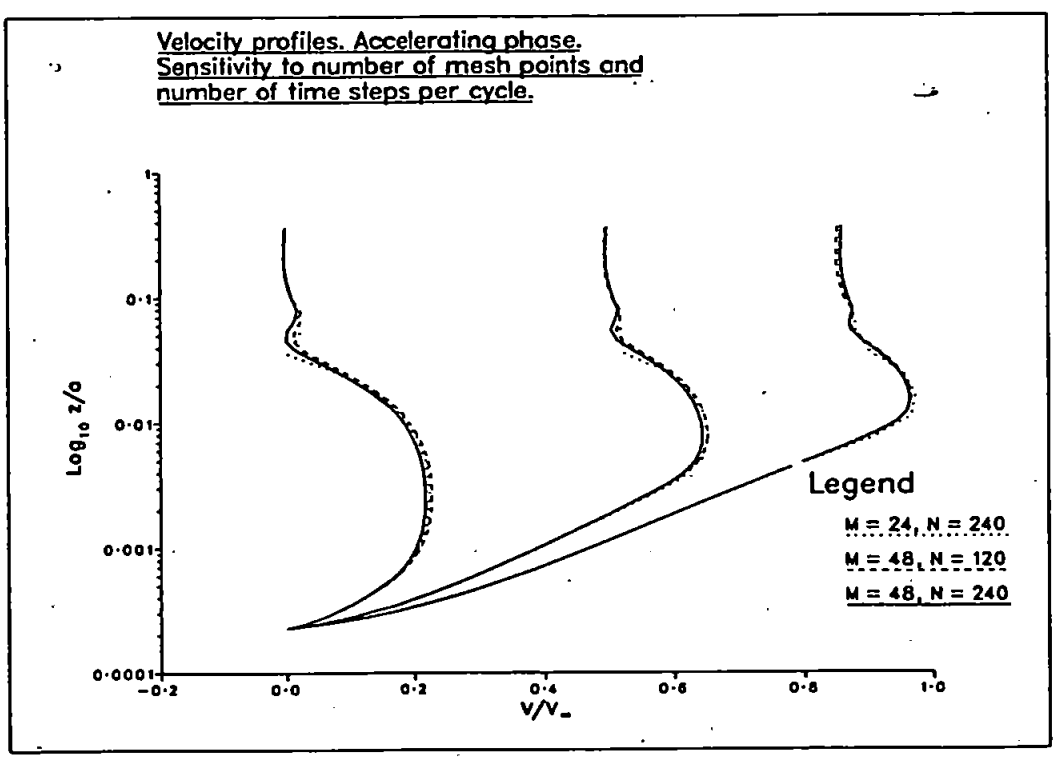

Figure 4.3:

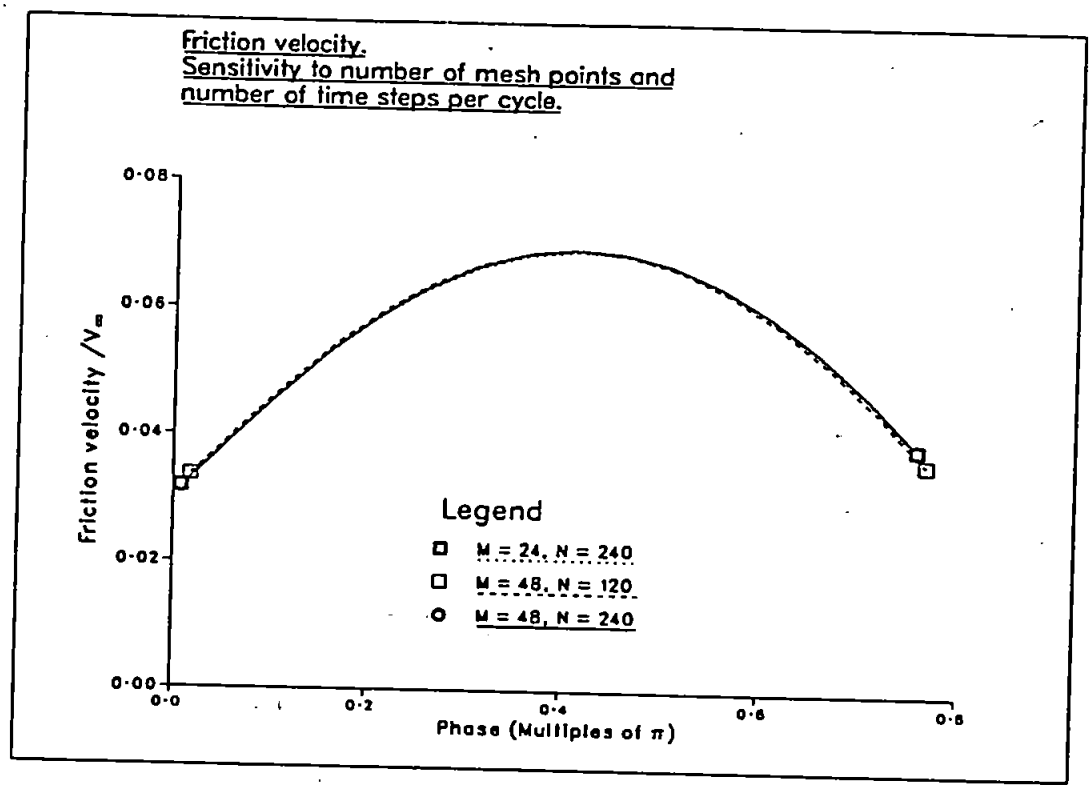

Figure 4.4:

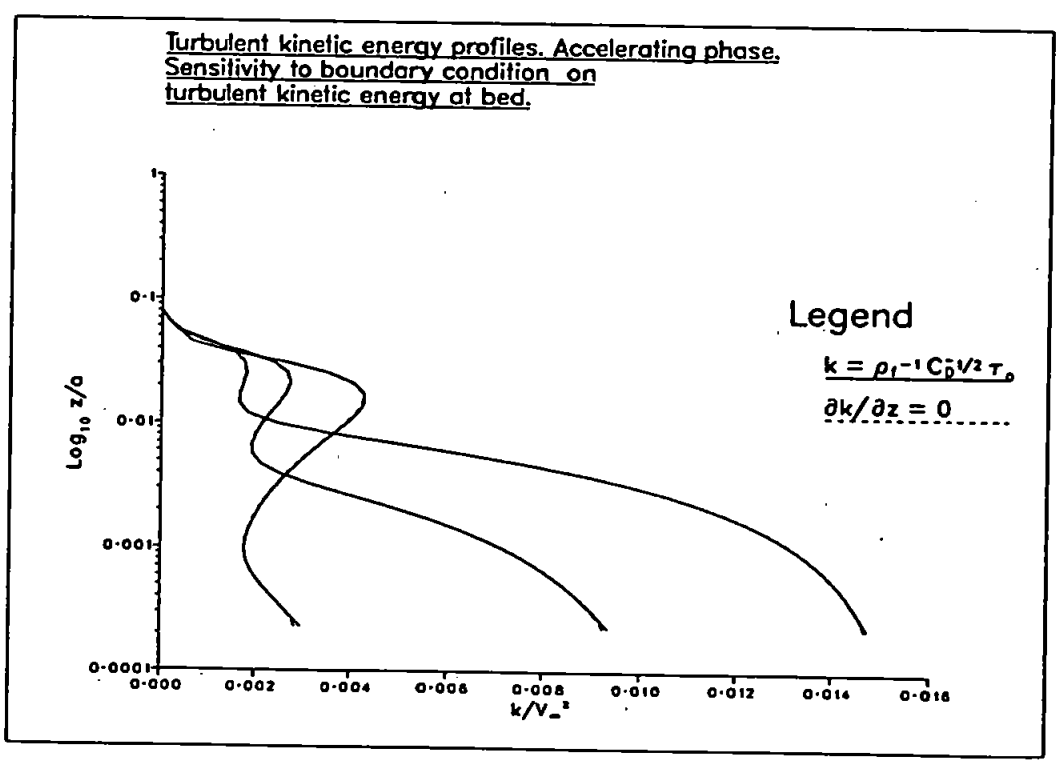

Figure 4.5:

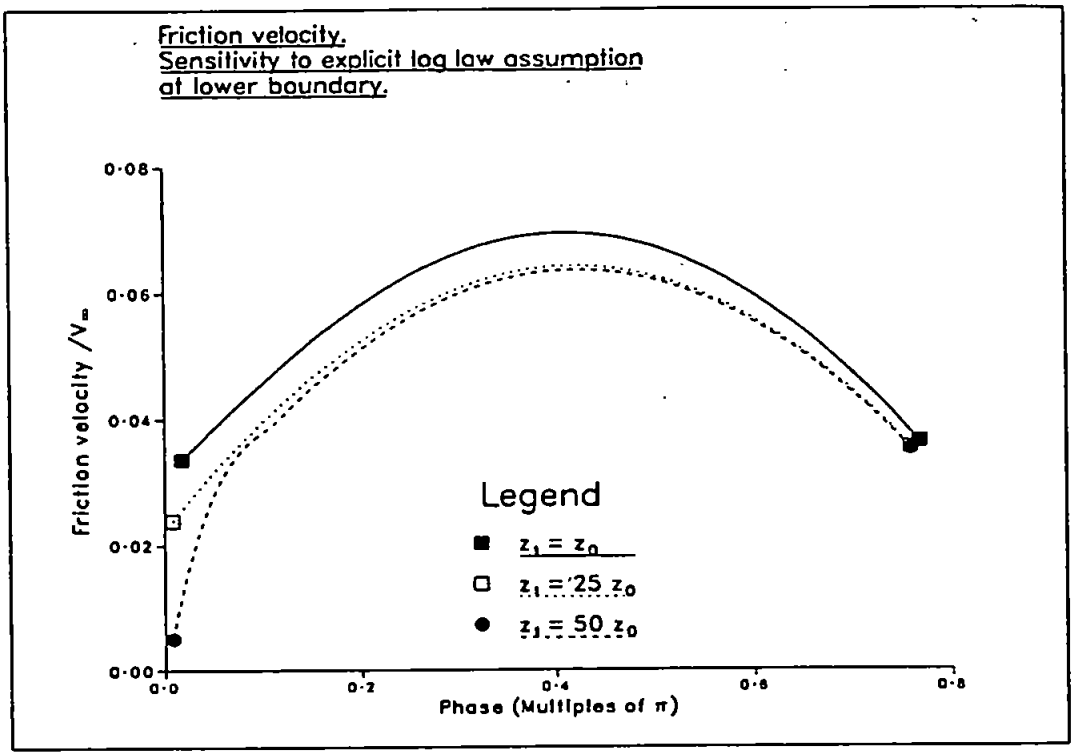

Figure 4.6:

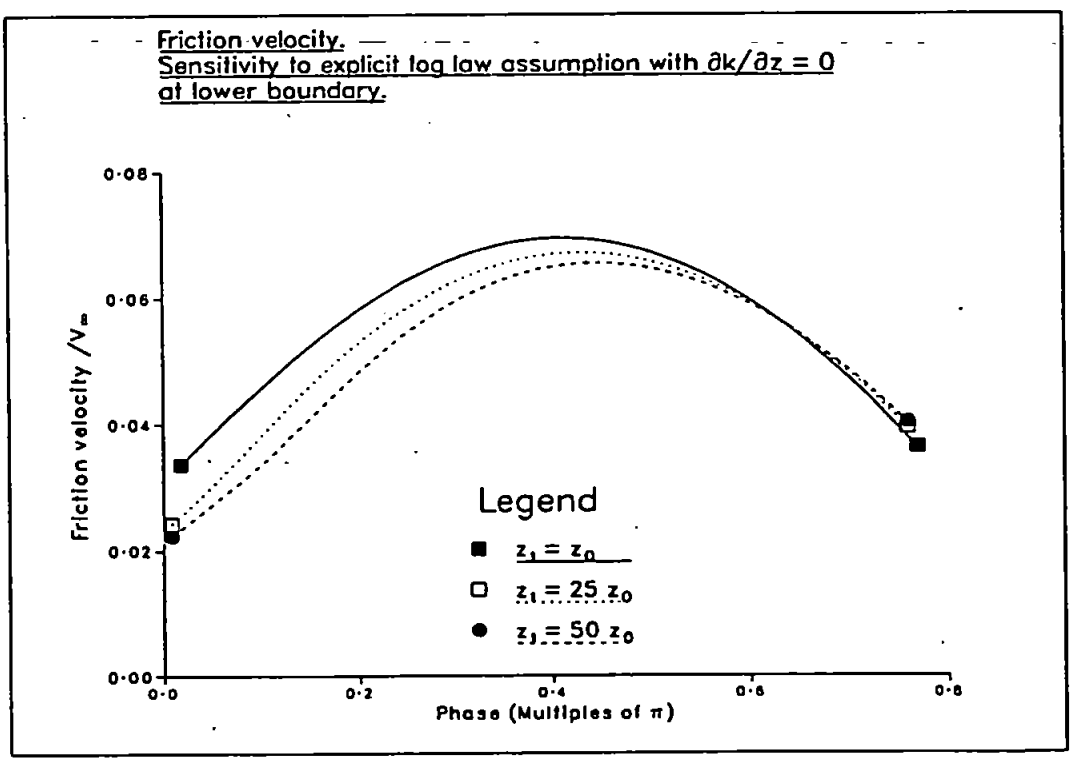

Figure 4.7:

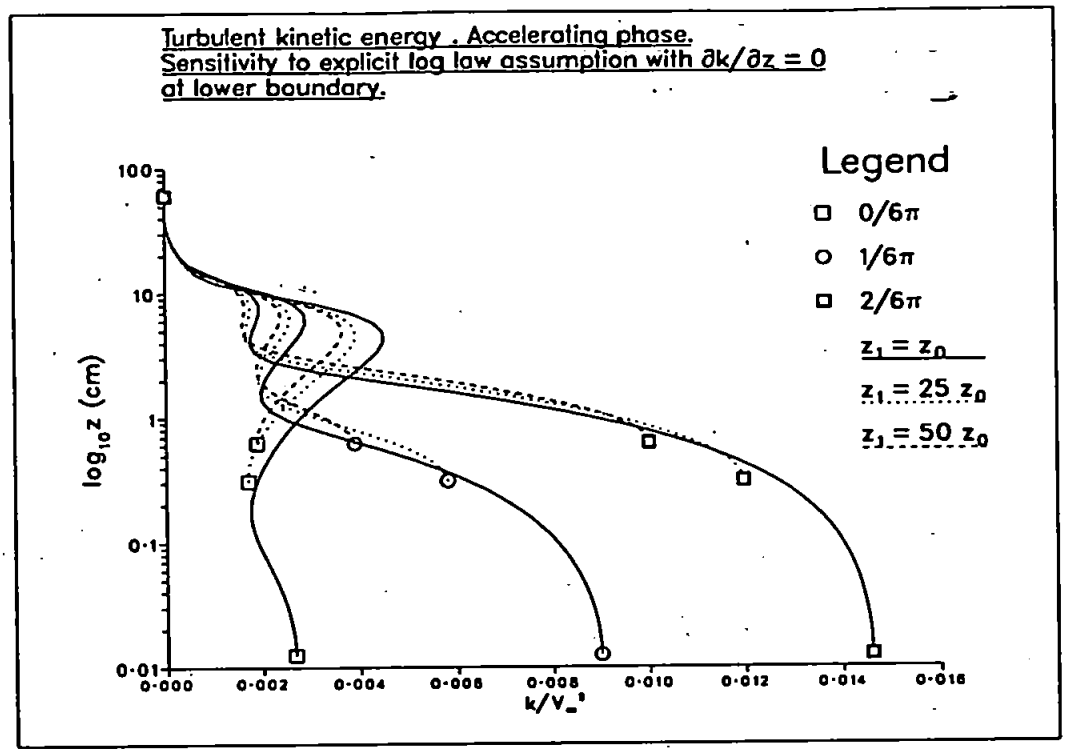

Figure 4.8a:

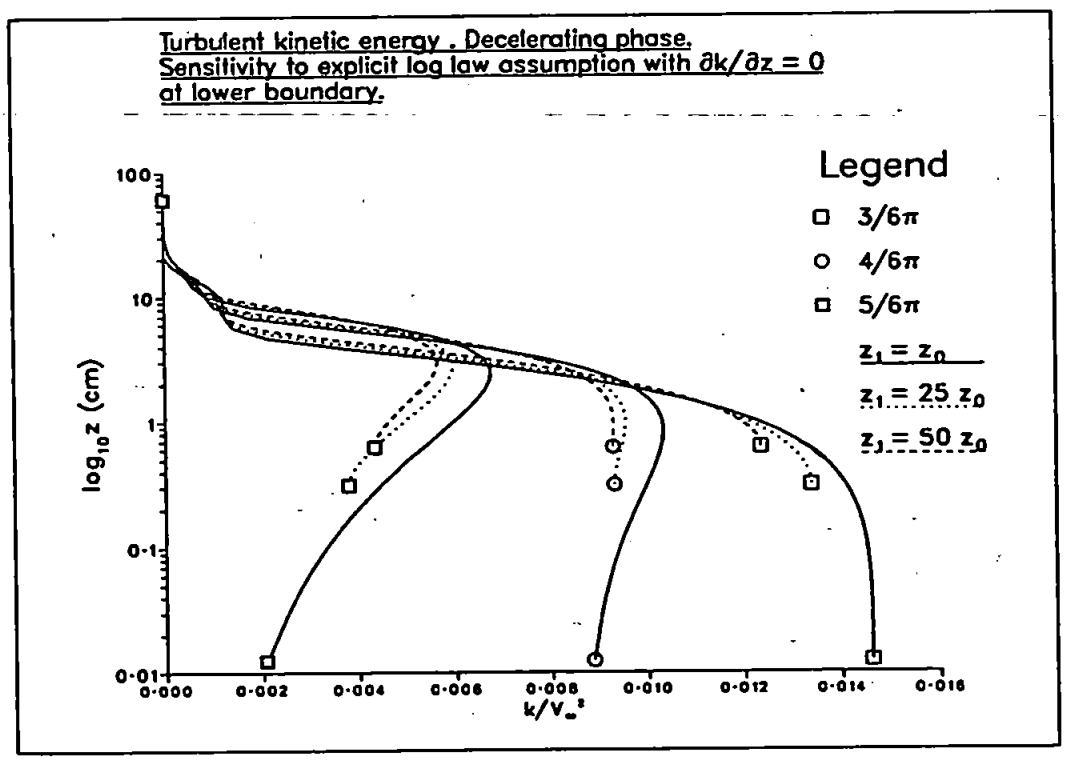

Figure 4.8b:

Sensitivity to turbulence constants

The standard values of the constants are shown in table 4.1. The effects of a 50% change in $\kappa, C_D, \sigma_k, \sigma_\epsilon$, and a 20%[1] change in $C_{1\epsilon}, C_{2\epsilon}$ are briefly summarized in table 4.2. The amount by which these parameters are varied does not reflect their degree of uncertainty, the standard values taken by these constants being generally well accepted.

Constant	Effect on $\bar{v}_1$	Effect on v_*
κ	Moderate	Strong
C_D	Moderate	Strong
$C_{1\epsilon}$	Strong	Strong
$C_{2\epsilon}$	Strong	Strong
σ_k	Weak	Weak
σ_ϵ	Strong	Strong

Table 4.2: Sensitivity to variations in turbulence constants.

From our investigations two conclusions can be drawn.

1. The solution is particularly sensitive to the constants appearing in the equation for the dissipation rate, ϵ; writing the constants in order of decreasing effect gives $C_{2\epsilon}, C_{1\epsilon}, \sigma_\epsilon, \kappa, C_D, \sigma_k$.

2. Compared to the mean fluid velocity, the friction velocity is considerably more sensitive to changes in values of the turbulence constants. From an examination of friction velocity plots (not shown) it appears that it is the magnitude of the friction velocity that is affected; very little change in phase is apparent.

Dependence on a/k_N.

Finally, in this section, the effect on the solution of the key parameter a/k_N is investigated. Figures 4.9a to 4.10b show the velocity profiles calculated using the $k-\epsilon$ model. The curves are plotted with both linear and logarithmic vertical scales to emphasise the profiles in the upper and near bed regions respectively.

When plotted with a logarithmic scale, a region extending up from the bed is observed where the profiles are approximately linear. This indicates that the velocity here follows some sort of logarithmic law, as found in steady turbulent boundary layers. It should be noted that, although emphasized in the logarithmic plots, this region lies very close to the bed and at the beginning of the wave cycle it may be only

[1] Changing $C_{1\epsilon}$ and $C_{2\epsilon}$ by 50% caused the calculation to diverge.

of the order of the roughness height. The top of the logarithmic region is marked by an extreme value where the velocity gradient vanishes, followed as we move further from the bed by a decrease in velocity until the free stream value is reached. The point at which the velocity gradient vanishes has been used by a number of authors as a convenient measure of the boundary layer thickness, and can clearly be seen to increase as the wave cycle proceeds. By contrast, the region above the maximum, where the boundary layer merges into the free stream flow, decreases in extent as the flow develops.

A notable increase in the boundary layer height relative to k_N can also be observed with increasing a/k_N. This is consistent with the non-dimensional friction velocity curves shown in figure 4.11, which *decrease* in magnitude as a/k_N increases and the velocity gradient at the bed becomes more gentle. Also plotted in figure 4.11 is the non-dimensional free-stream velocity. Clearly the maximum friction velocity (and hence bed stress) is closely tied to the maximum free stream velocity. Just discernible is a decrease in the phase difference between the free stream velocity and bed stress as a/k_N increases.

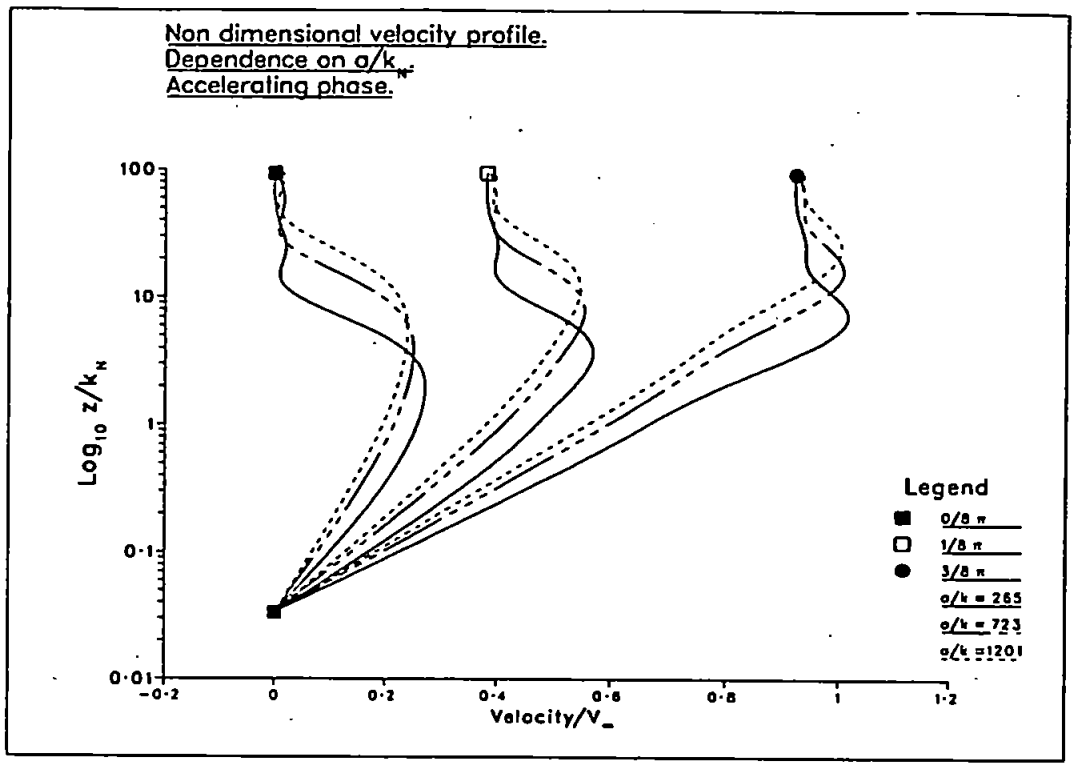

Figure 4.9a:

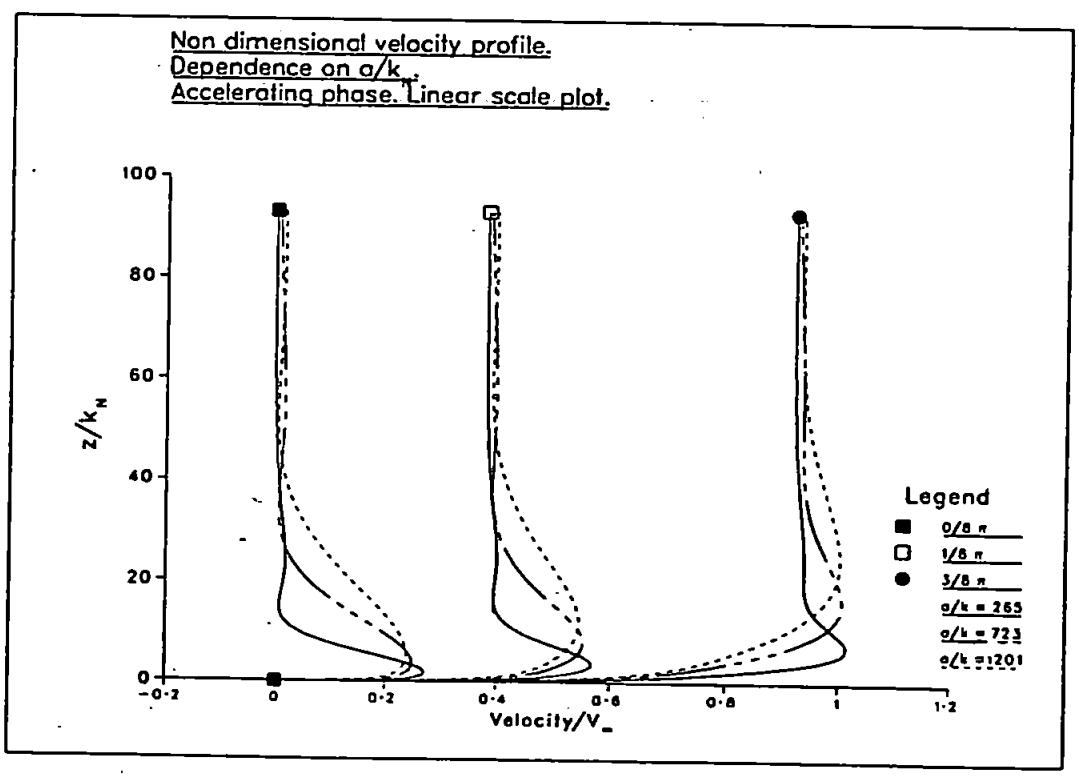

Figure 4.9b:

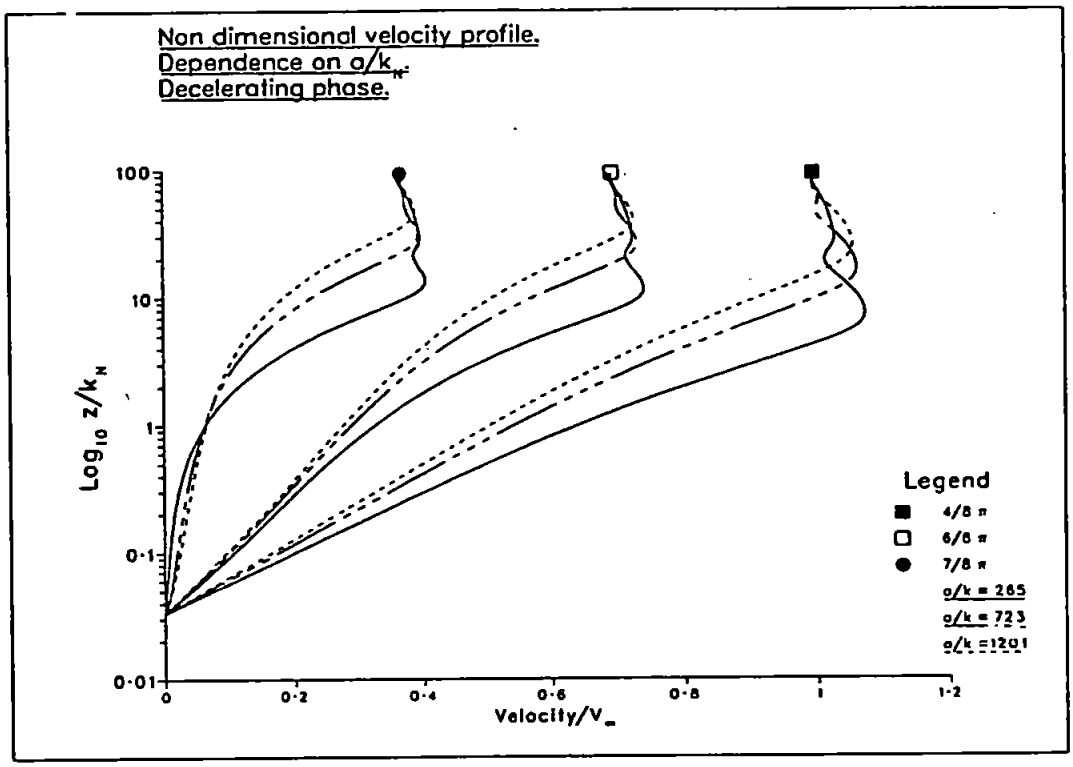

Figure 4.10a:

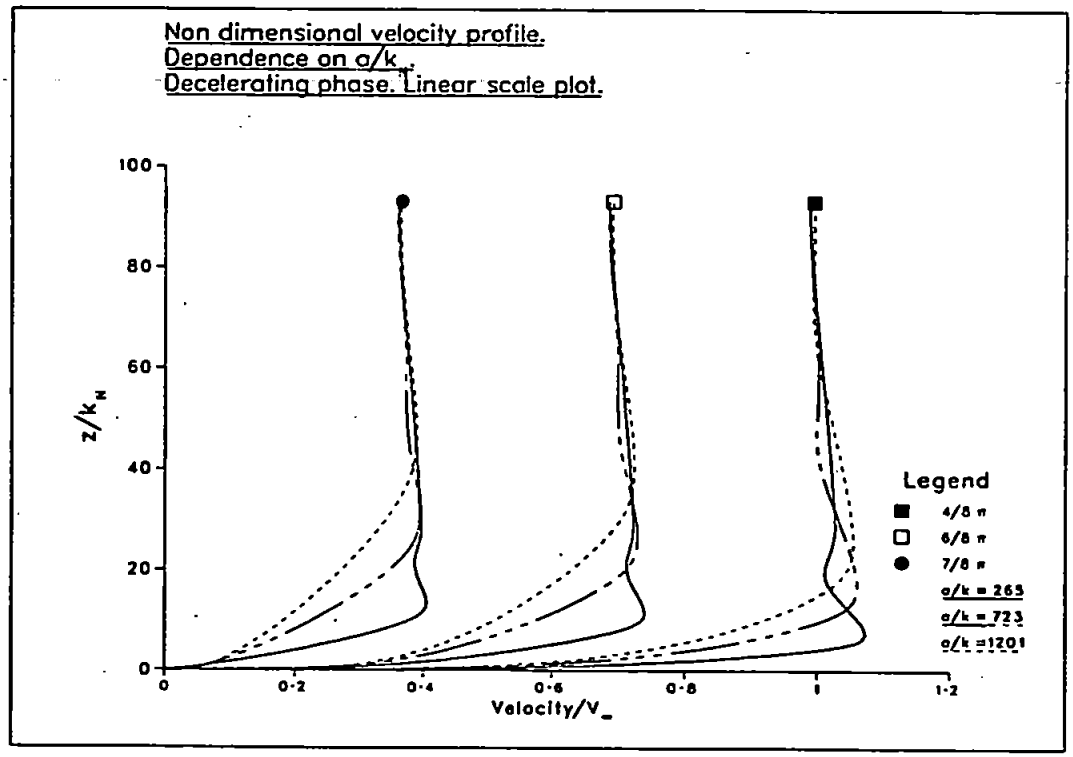

Figure 4.10b:

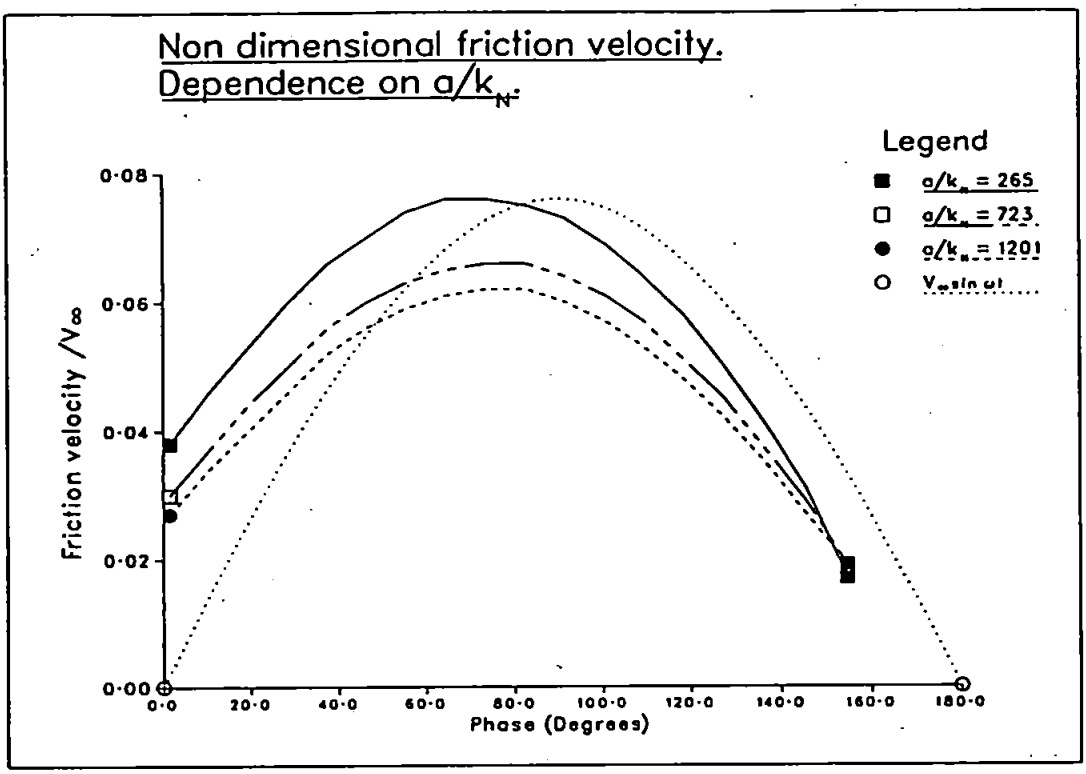

Figure 4.11:

4.1.2 Particle concentration results

All the results to be presented were calculated using the $k - \varepsilon$ model, with the flow and sediment parameters set to those reported by Staub et al. (1983) and shown in table 4.3, page 109. These are also the results that Hagatun & Eidsvik (1986) use to verify their model. We differ from these authors in the value we use for two key parameters.

The value taken for the sediment diameter by Hagatun & Eidsvik is that quoted by Staub et al. as being the median diameter *in the bed*, $d_{50} = 0.19$ mm. However the median diameter of the sand in *suspension*, as measured at 1.8 cm above the bed, was $d_{50} = 0.12$ mm — a 40% difference. We use the value measured for the sand in suspension, since we will be presenting comparisons with experimental data in the height range of about 1.0 to 3.0 cm. Therefore the median value measured near the centre of this range seems appropriate. It is likely that as the particle diameters are measured at successively greater heights above the bed the value of d_{50} will decrease. Thus it is very difficult, if not impossible, to define a single value of d for use in the numerical calculation when simulating an experiment where a range of particle sizes

are present. It is appropriate to note here that the solution was found to be very sensitive to the particle size (in the Stokes regime the fall velocity is proportional to the *square* of the radius). Typically a change of a factor of two in the particle radius caused the concentrations to change by an order of magnitude at 1.8cm above the bed. For all calculations the non-linear drag law (2.37) was used with $\alpha = 0.15$ and $\beta = 0.687$ as given in Clifte et al. (1978) . The water and sand density was taken as 1000 kg/m^3 and 2650 kg/m^3 respectively. The value of the kinematic viscosity used was $1.1 \times 10^{-6} m^2/s$. With $d = 0.12$ mm these parameters yield a value for w_0 of 0.010 m/s.

We differ also from Hagatun & Eidsvik in the value of z_0 that we use. This we calculate from the Nikuradse roughness length curve, with the bed roughness k_N, given as twice the d_{65} value for the grain sizes in the bed as discussed in Section 3.1.1. Since Staub et al. quote only d_{50} (the median grain size) we used twice this value for k_N yielding a value for z_0 of 0.9×10^{-5} m[2]. To take account that we used d_{50} rather than d_{65} the value of z_0 was increased (arbitrarily) to 1.0×10^{-5} m. Given the widely varying relationships between average grain size and the Nikuradse roughness length shown in expression (3.31), this was considered justifiable. What is important is to then assess the sensitivity of the solution to changes in the (essentially uncertain) parameter z_0. This we do latter in this section. Hagatun & Eidsvik use a value for z_0 of 1.6×10^{-5} m which they obtain from a formula given in Madsen & Grant (1977). We note that our parameters enable us to obtain satisfactory agreement with experiment (see Section 4.2.2) without introducing, as do Hagatun & Eidsvik , a non-physical "laminar" viscosity into the advection-diffusion equation for the concentration to enhance particle diffusivity at the bed.

The numerical predictions of the concentration field are conveniently represented in terms of the variation of three quantities with height:

1. the average concentration over a wave cycle

$$C = \frac{1}{T} \int_0^T \bar{c}(z,t)\, dt;$$

2. the "concentration amplitude" $c_a(z) = c_{max} - c_{min}$, where c_{max} and c_{min} are the determined over a complete wave cycle for a given height;

3. the "concentration phase" $\phi(z)$, defined at a given height, as the phase at which

[2]The flow was found to be transitional so that a graphical relationship (e.g. Sleath 1984, figure 1.12) relating z_0 to $v_{*m} k_N/\nu$ is required.

the maximum concentration first occurs. The concentration peaks twice during a complete 2π wave cycle, hence the need to specify the first peak.

Note that if the time series of concentration at a given height were a perfect sinusoid then

$$\bar{c}(z,t) = C(z) + \frac{1}{2}c_a(z)\sin[\omega t - \phi(z)],$$

so c_a and ϕ, together with the average concentration over a cycle, characterise the concentration field completely. In practice this is not the case since the bottom boundary condition does not yield a sinusoidal forcing of the system. In addition, any non-linearity in the turbulence model will tend to preclude the occurrence of a single sinusoidal component. Nevertheless, the three quantities yield the main characteristics of the concentration field. Results in this section will generally be normalised with the reference concentration c_0; see (3.41).

The concentration field was started off from an initial condition of zero at all heights above the bed. A periodic solution was obtained within six wave cycles.

Sensitivity to boundary conditions

The top boundary was found to be sufficiently far removed at 60 cms, for the solution to be independent of the choice of (3.44) or (3.45) in the region of interest close to the bed.

For the bottom boundary condition we did not try any alternative to (3.41). Although this might seem to be an interesting comparison to attempt it would be unlikely, for the flow conditions considered here, to be very illuminating for reasons that are explained presently. Apart from c_0, two additional parameters, S_0 and S_1, occur in the boundary condition. The former is the critical Shields number below which no sediment is lifted from the bed, while the latter gives the value of the Shields number at which saturation occurs i.e. above this value no more sediment can enter the bed load region, however high the applied shear stress. This boundary condition is to account for all the (unknown) mechanics of the bed load region. It was found that altering S_0 from a value of 0.05 to 0.0 or to 0.25 had a negligible effect on the concentration profiles. The concentration was also remarkably insensitive to S_1, as illustrated by figure 4.12. Putting $S_1 = 0$, so that the bottom boundary condition is fixed at the 'saturation' concentration c_0 throughout the wave cycle, yields a solution that is almost identical to the one obtained with the original values of S_0 and S_1. Only when S_1 is increased so that saturation occurs over a much smaller portion of the wave cycle does a significant change in the sediment concentration

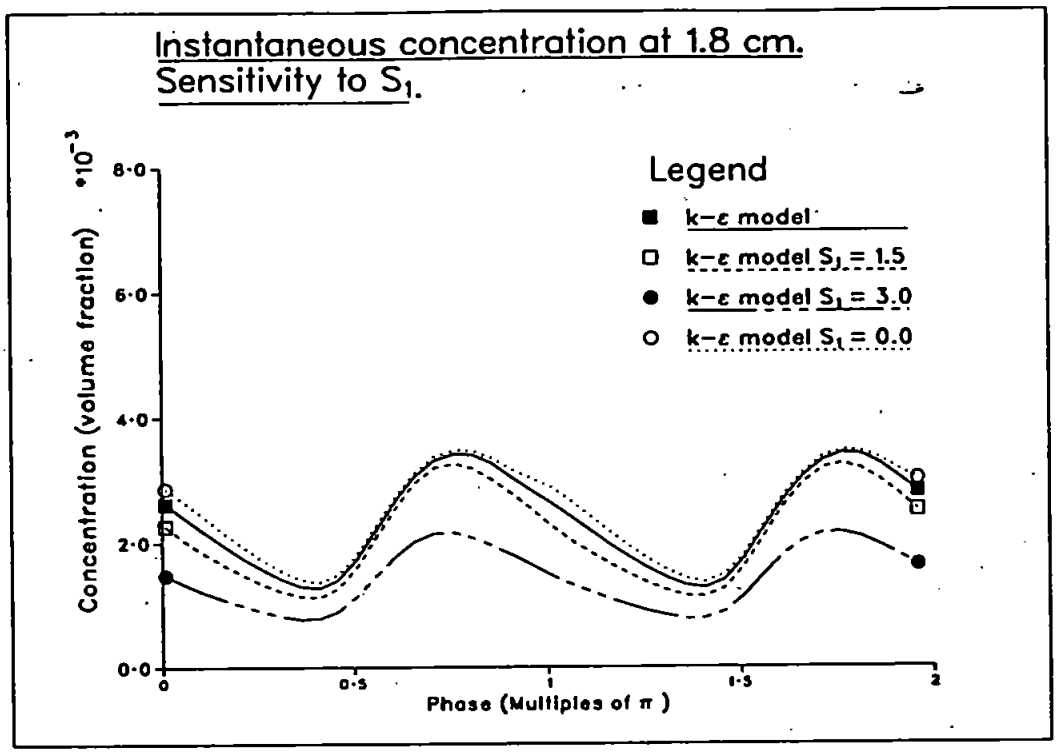

Figure 4.12:

occur. For the flow parameters used here, S reached a peak value of about two[3]. In situations where the bed stress and sediment properties are such that the bed load region is saturated for most of the wave cycle, it appears that the reference concentration c_0 only is important. It is interesting to note however, that for the linear model (see Section 4.2.2) the change in bottom concentration over the wave cycle is crucial because this model has a diffusion coefficient that is a function of z only. Therefore any time dependence in the concentration field must enter through the bottom boundary condition.

The discussion above is likely to be relevant only for flat beds and high Shields numbers. For flow over sand ripples the bottom boundary condition should mimic the injection of sediment into suspension as the flow reverses if realistic time dependant concentration fields are to be obtained, an idea that is discussed in Nielson (1979, Chapter 7).

[3] $S = 0.83$, is the limiting value above which Nielson (1979) suggests bed forms disappear and the bed becomes flat. Hence the assumption of a flat bed in this case appears well justified.

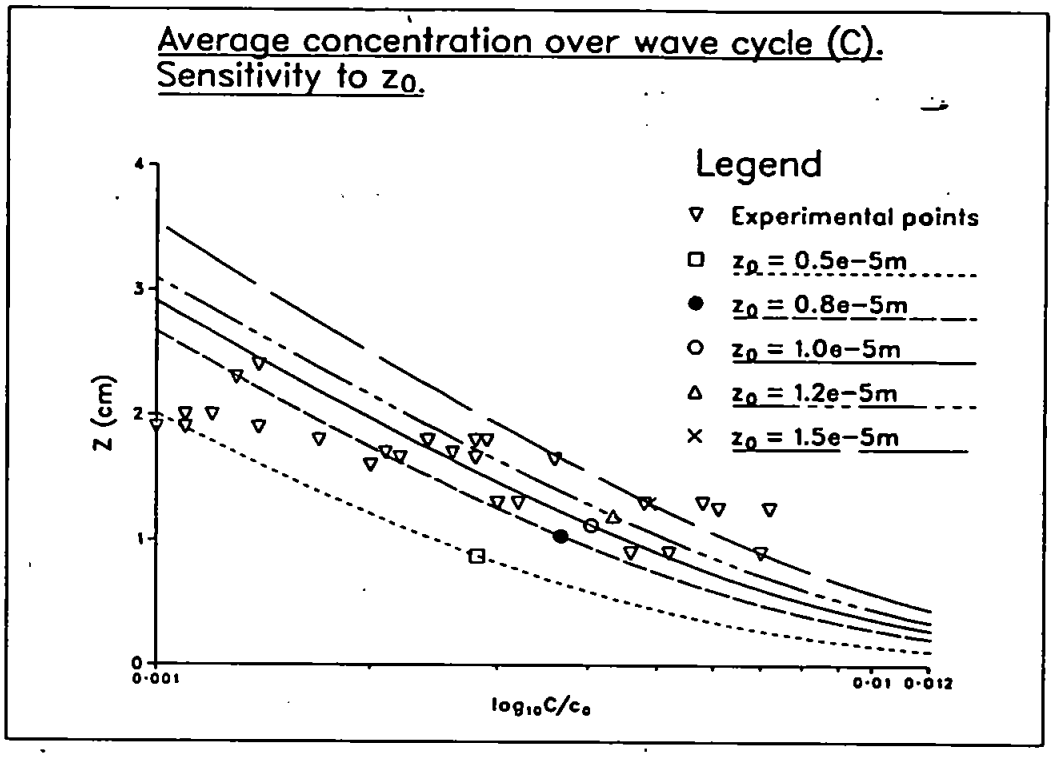

Figure 4.13:

Sensitivity to z_0

Although we have calculated z_0 using ideas derived from steady flows with fixed beds, there is no guarantee that this is the appropriate value for this quantity in the unsteady flow considered here. In addition, a wide range of relationships have been proposed relating the grain size to the equivalent Nikuradse roughness length. Therefore it is important to test the sensitivity of the concentration profiles to this essentially uncertain parameter. Figure 4.13 shows the effect of 20% and 50% variations in z_0 on the concentration as averaged over a wave cycle. A fairly large variation in the concentration is seen to result. Also shown are experimental measurements made by Staub et al. (1983). These indicate that while increasing z_0 improves the agreement with the experimental data nearer the bed, the agreement higher up becomes worse.

Sensitivity to turbulence model constants

As for the velocity profiles and friction velocity, we examine the effect of varying the constants in the $k-\varepsilon$ model equations. In this instance we have altered all quantities by 10%. The outcome is shown in in figures 4.14, 4.15. These results are consistent

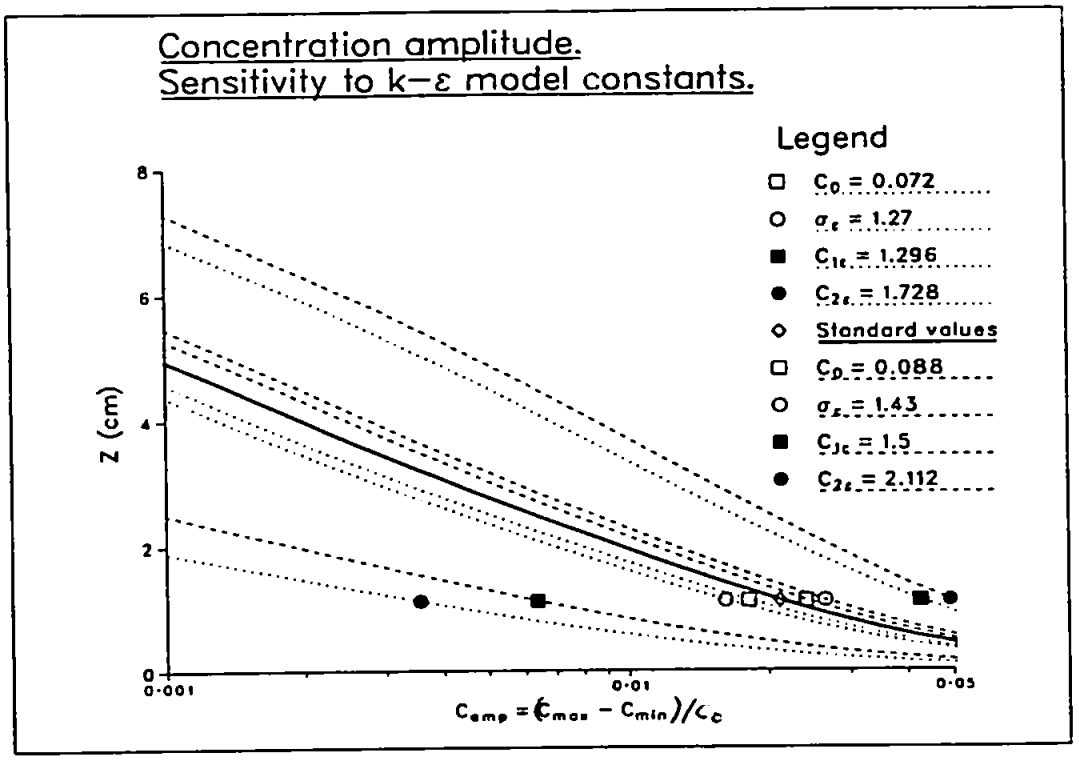

Figure 4.14:

with those obtained for the mean velocity and friction velocity in that variations in $C_{1\epsilon}$ and $C_{2\epsilon}$ are particularly important.

Buoyancy effects

The effect of buoyancy will be to decrease the effective eddy viscosity/diffusivity if the turbulent motion has to do work against a stable stratification. For the case of sediment in suspension, the flow is stably stratified when the more dense fluid-particle mixture, containing a greater concentration of sediment, lies below a less dense mixture. Since the particle concentration is usually found to decrease away from the bed, sediment-laden flows are generally stably stratified.

In the $k-\epsilon$ model, terms arising from buoyancy effects enter into both the k and ϵ equations. Figure 4.16 shows the effect on c_a of including all the buoyancy terms, no buoyancy terms, buoyancy terms in the k equation only and buoyancy terms in the ϵ equation only. From this we see that, for the case of stable stratification, the buoyancy term in the ϵ equation acts to *increase* the sediment concentration and it is the buoyancy term in the k equation that gives rise to an overall decrease. This decrease is quite significant for the flow parameters and sediment size used in this calculation. These results are consistent with an examination of how the terms enter into the turbulence equations (3.21) and (3.22). The contribution that the buoyant

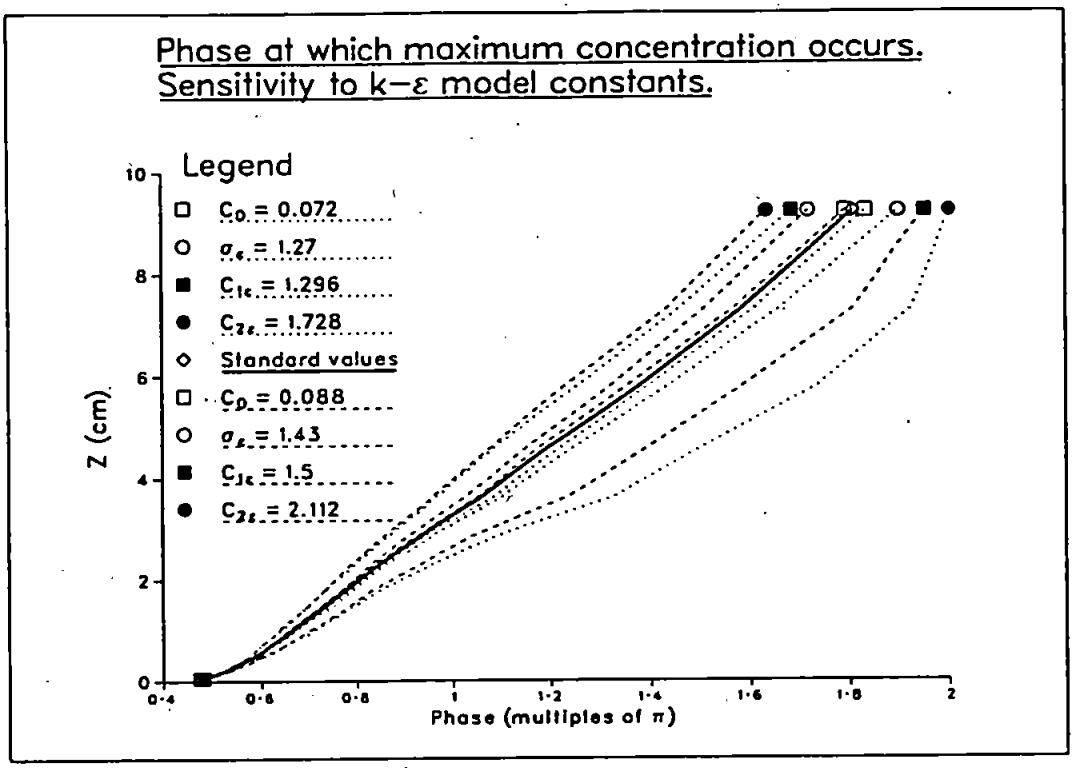

Figure 4.15:

production term G makes to the ϵ equation is controlled by the value of $C_{3\epsilon}$. If $C_{3\epsilon} = 1$, then buoyancy effects only enter into the equations at $O(c^2)$ —which is negligible, while $C_{3\epsilon} = 0$ would give a contribution that was weighted equally with the shear stress production P. The effect of the factor involving the flux Richardson number R_f is thus to decrease the effect of buoyancy in the ϵ equation. A value $C_{3\epsilon} = 0.8$ is used in the calculation, so that the effect of the buoyant production in the ϵ equation would be expected to be small.[4]

A buoyancy effect on ϕ, the concentration phase, is also found to occur, as shown in figure 4.17, where the result is to inhibited slightly the rate of change of ϕ with height.

Shown in 4.18 is the effect, on c_a, of neglecting the buoyancy term in the turbulent kinetic energy equation for the k model. Surprisingly this has virtually no effect, even though exactly the same term was mainly responsible for the much greater buoyancy effects encountered in the $k - \epsilon$ model.

Finally, the effect on the mean velocity profiles of the decrease in eddy viscosity due to the stable stratification is shown in figures 4.19a and 4.19b. Only a minor

[4]This value of $C_{3\epsilon}$ is standard for horizontal boundary layers, although modifications to the definition of the Richardson number are necessary for vertical flows (Rodi 1980).

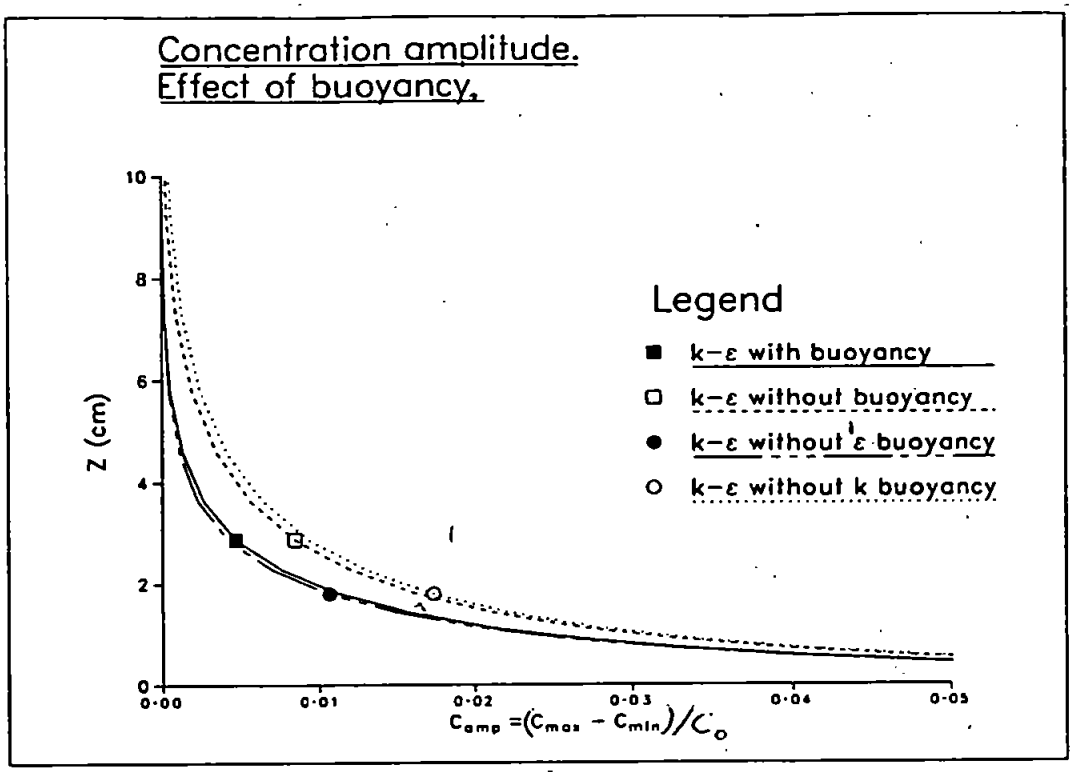

Figure 4.16:

difference in the profiles is apparent.

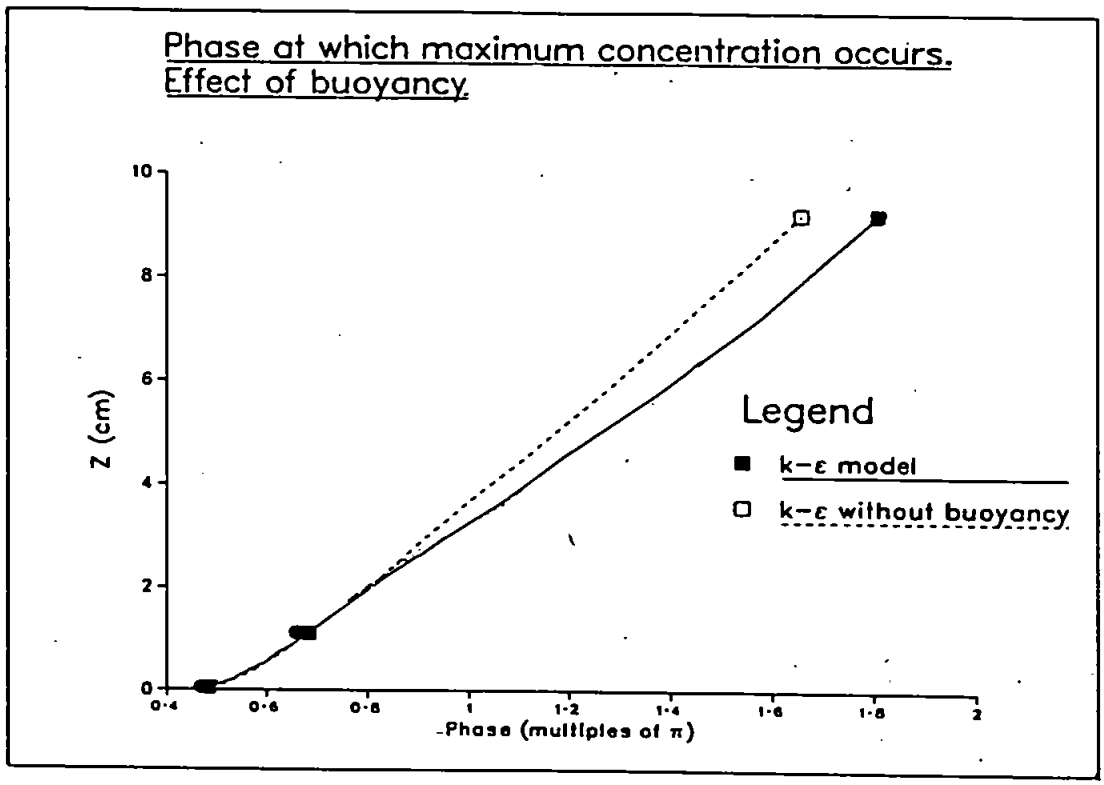

Figure 4.17:

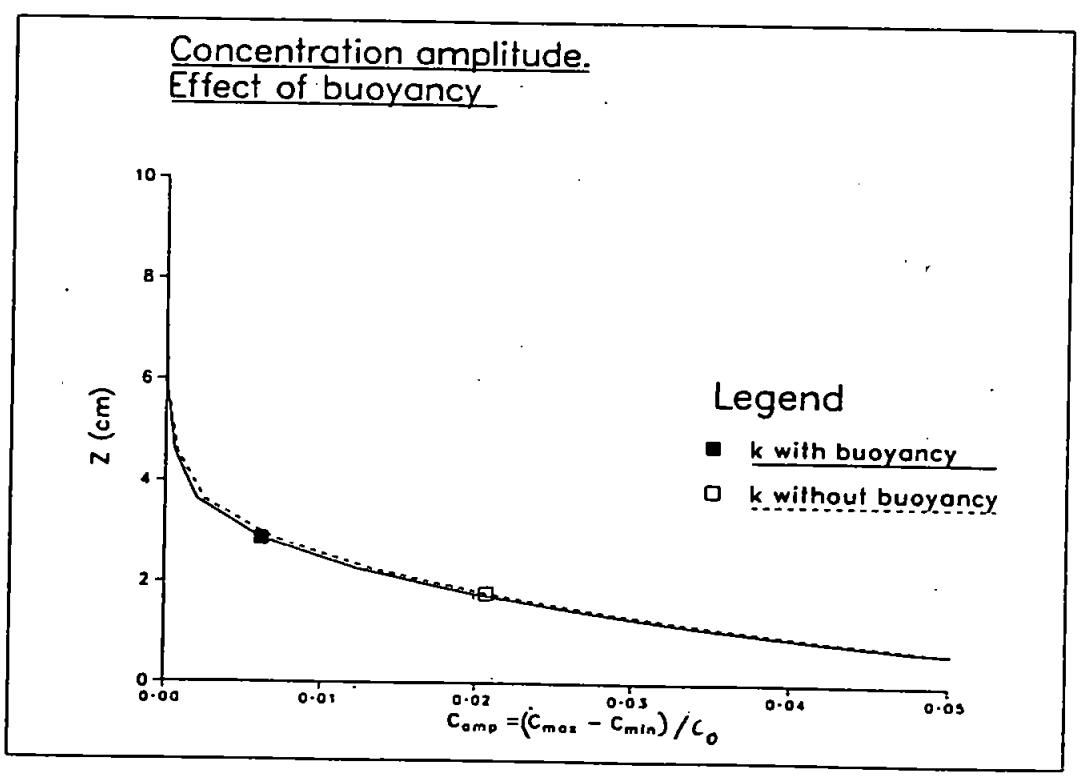

Figure 4.18:

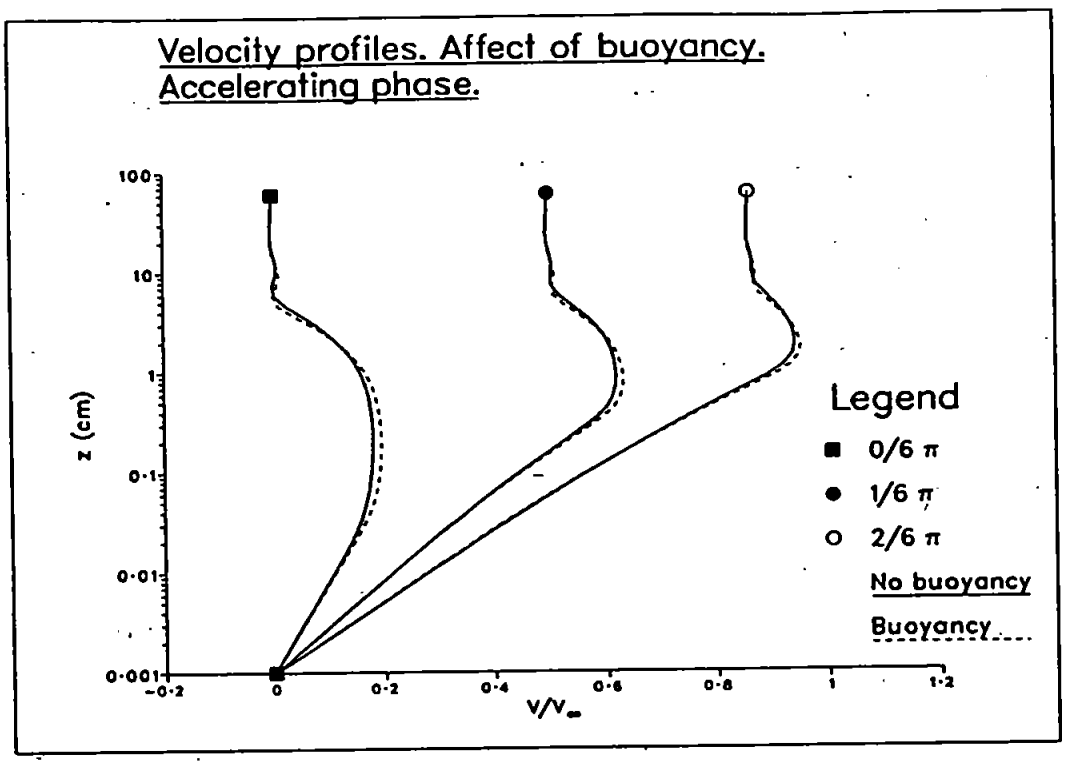

Figure 4.19a:

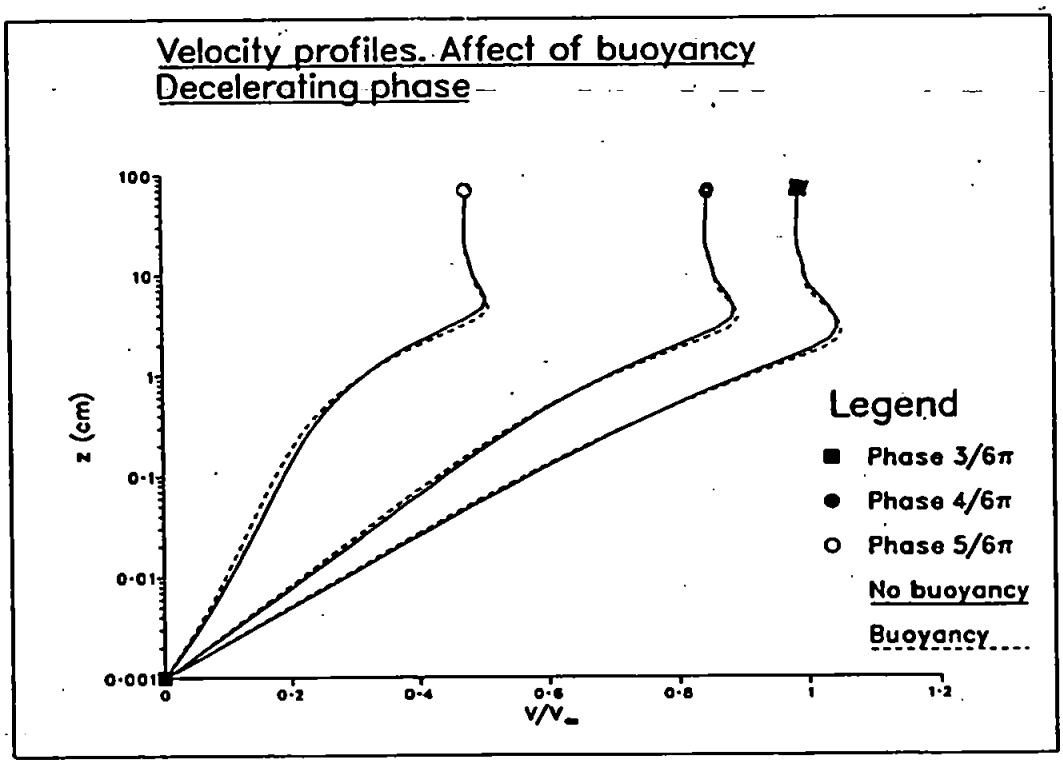

Figure 4.19b:

4.2 Comparison of turbulence models

The numerical predictions for the hydrodynamic variables are now compared with the experimental data of Sumer et al. (1987), while suspended sediment profiles are compared to the experimental data of Staub et al. (1983). Table 4.3 summarises the relevant experimental parameters.

	V_∞ (m/s)	ω (rad/s)	D (mm)	k_N (mm)	a m	a/k_N
Sumer et al.	2.1	0.774	1.5	3.75	2.7	723
Staub et al.	1.2	0.690	0.19	0.475	1.9	3658

Table 4.3: Experimental parameters.

4.2.1 Comparison of hydrodynamic predictions between turbulence models

In comparing the different turbulence models we will concentrate primarily on predictions of mean velocity profiles and the friction velocity. Mean velocity profiles are shown, together with corresponding experimental data, at six points ($t^* = n\pi/6$, $n = 1 \ldots 6$) during a complete half-cycle. The half cycle consists of an accelerating phase, during which the velocity at the edge of the boundary layer increases to a maximum, and a decelerating phase when it then decreases to zero. The accelerating and decelerating phases are shown on separate graphs for clarity. Occasionally we present profiles of turbulent kinetic energy and the turbulent length scale.

As well as presenting the results graphically, the root mean square (RMS) error between the model calculations and the experimental values are calculated for both mean velocity profiles and the friction velocity. Linear interpolation is used to determine the value of the numerical solution at the experimental points, which do not correspond to points on the finite difference grid.

The linear model.

For *steady* shear layers near a flat bed, a constant velocity scale, the friction velocity v_*, and a length scale increasing linearly with height often suffice to reproduce the velocity profile. It is natural to attempt to extend this relatively simple approach to oscillatory flow. For the purposes of this document we will term such models 'linear'

since the resulting partial differential equations for the fluid velocity and sediment concentration are linear.

The first to develop such a model was Kajiura (1968) who considered the flow to be composed of three regions. Subsequently Brevik (1981) presented a simplified form in which the flow is divided into two regions. In the lower region the length scale is taken to increase linearly with distance from the bed, while in the upper region the length scale is constant i.e.

$$l = \begin{cases} \kappa z & z_0 \leq z \leq \Delta, \\ \kappa\Delta & z > \Delta. \end{cases} \tag{4.1}$$

Here Δ is the height at which the layers join and κ is the von Karman constant. In both regions the velocity scale is put equal to the maximum friction velocity over the wave cycle v_{*m}. Two ways of determining Δ are suggested: Kajiura puts

$$\Delta = \delta_\omega/20, \tag{4.2}$$

where $\delta_\omega = v_{*m}/\omega$, whilst Brevik uses

$$\Delta = \delta_1/2, \tag{4.3}$$

where δ_1 is the boundary layer thickness defined by Jonsson (1980). Given a/k_N and k_N, δ_1 can be determined from the relation

$$30\frac{\delta_1}{k_N}\log(30\frac{\delta_1}{k_N}) = 1.2\frac{a}{k_N}. \tag{4.4}$$

An inconvenience of solving the linear model numerically is that v_{*m} is needed before the solution can be effected, but is itself determined by the solution. An iterative approach is therefore needed in which v_{*m} is initially estimated and subsequently corrected by running the computer code repeatedly until (3.47) is satisfied.

In figure 4.20 the values of Δ/k_N, as given by (4.2) and (4.3), are plotted against a/k_N. Also plotted are the values of Δ/k_N given by

$$\Delta = \delta_\omega/10. \tag{4.5}$$

As can be seen, this last expression leads to values that are very close to those obtained from (4.3). For practical purposes it seems that the values of Δ calculated from (4.3) and (4.5) are essentially equivalent. Thus, in using the parameters corre-

sponding to the experimental work of Sumer et al. (1987), the value of Δ obtained from the two expressions differed only by a millimetre, giving rise to velocity profiles that are virtually indistinguishable.

It is possible to solve the momentum equation analytically if the velocity and length scale are specified as above (see Brevik 1981 or Smith 1977). From the analytic solution v_{*m} can be determined directly from a/k_N as, for example, shown in Smith(1977). For the case $\Delta = \infty$, the analytic solution is somewhat simplified (although still involving Kelvin functions) and is used to verify our numerical solution to the momentum equation. With $\theta = 1/2$, $M = 48$,and $N = 240$ the analytic results were reproduced to four significant figures by the computer code. The analytic solution was also used as an initial value for the velocity field.

Figures 4.21a and 4.21b show a comparison between the velocity profiles obtained with the linear model for three choices of Δ, namely $\Delta = \infty$, and the values of Δ calculated from (4.2) and (4.5). These three values of Δ yielded values for v_{*m} of 0.152, 0.155, and 0.150 respectively. Also shown on the same plot are the experimental velocity measurements obtained by Sumer et al. (1987) The effect of decreasing Δ appears to advance the phase and to emphasize the maxima that occurs where the velocity gradient vanishes.

Table 4.4 shows the results of calculating the root mean square error between the theoretical curves and the experimental data. The best overall fit is given with $\Delta = \delta_\omega/20$, the curves with $\Delta = \infty$ being inferior at all stages of the wave cycle. Visual inspection of the velocity profiles indicates that where the free stream velocity is not near the peak value $\Delta = \delta_\omega/10$ gives a good fit.

The predicted friction velocities are plotted, together with experimental values, for the three choices of Δ in figure 4.22. Note the error bars about the experimental points; these correspond to an estimated experimental error of about 1 cm/sec. Although the magnitude of the peak value given by the model is in reasonably agreement with the data, the values of $v_*(t)$ seem to be poorly predicted for all three values of Δ. Table 4.5 indicates that the best fit is given with $\Delta = \delta_\omega/20$ and the worst with $\Delta = \delta_\omega/10$.

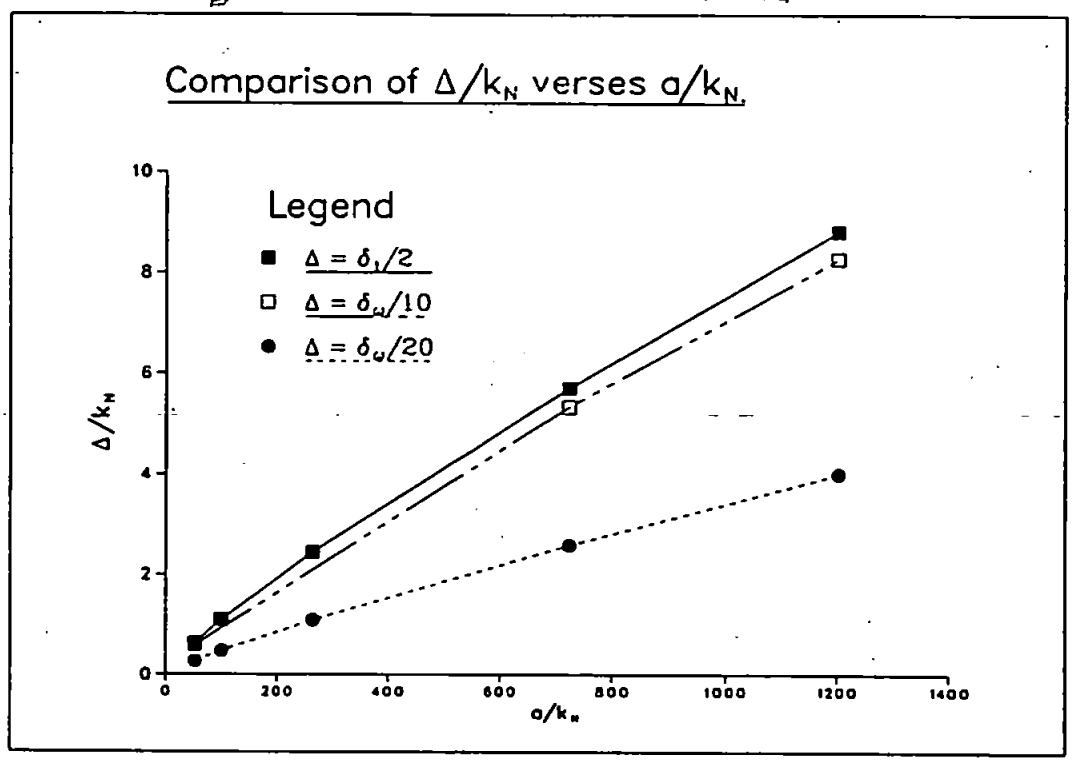

Figure 4.20: Δ/k_N verses a/k_N

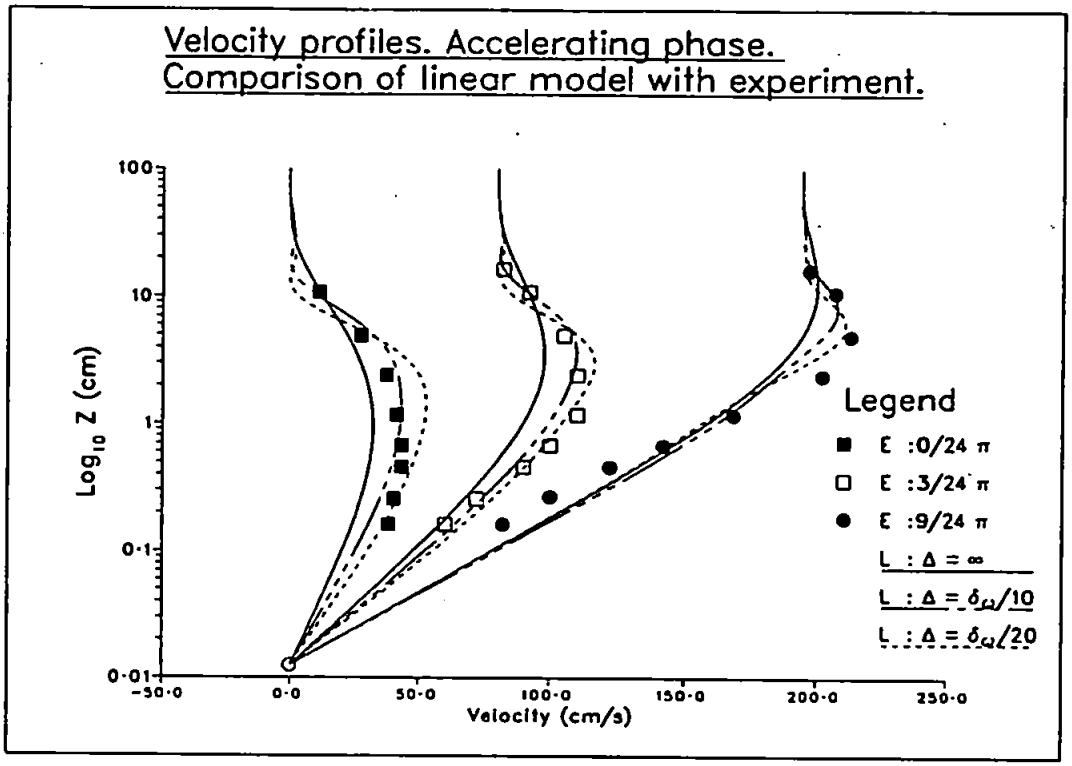

Figure 4.21a:

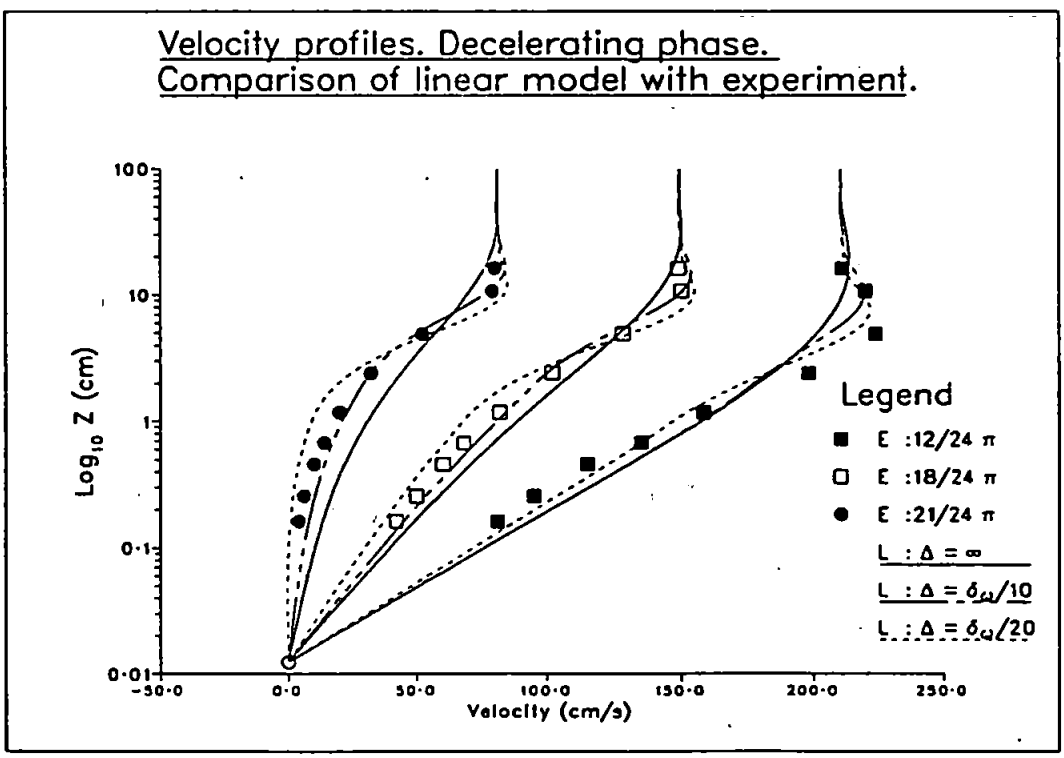

Figure 4.21b:

t^*	RMS error (cm/s) $\Delta = \infty$	$\Delta = \delta_\omega/10$	$\Delta = \delta_\omega/20$
$0\pi/8$	10.1	4.5	7.6
$1\pi/8$	10.6	4.4	5.0
$2\pi/8$	10.3	8.4	8.0
$3\pi/8$	12.3	11.4	9.2
Average	10.9	7.8	7.6
$4\pi/6$	13.0	12.0	8.1
$5\pi/8$	10.6	8.7	6.2
$6\pi/6$	8.3	3.6	6.4
$7\pi/6$	10.1	3.3	5.9
Average	10.6	7.2	6.7
Combined Average	10.8	7.5	7.2

Table 4.4: Root mean square error for linear model velocity profiles.

Δ	RMS error (cms/sec) Accelerating	Decelerating	Combined average
$\Delta = \infty$	1.3	1.3	1.3
$\Delta = \delta_\omega/10$	1.7	1.3	1.5
$\Delta = \delta_\omega/20$	1.5	0.68	1.2

Table 4.5: Root mean square error for linear model friction velocity.

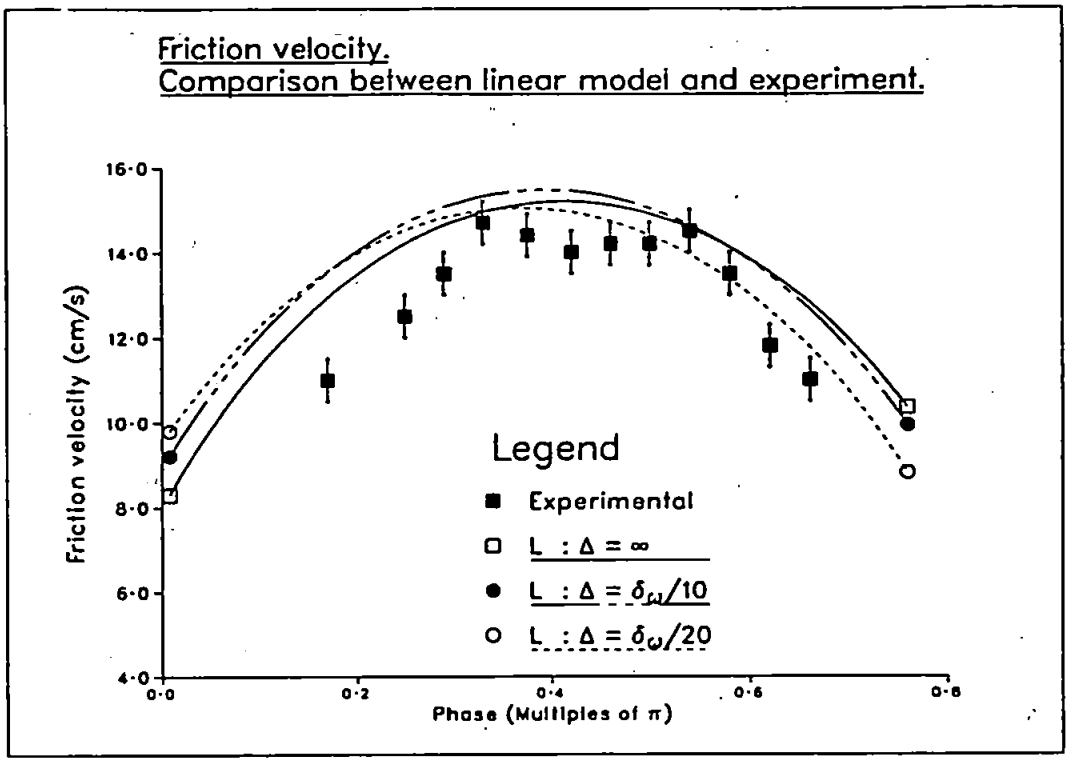

Figure 4.22:

Mixing length model.

Prandtl's mixing length theory can be derived from the turbulent kinetic energy equation (3.21), by assuming the turbulence is in local equilibrium. The length scale is still specified empirically. So that a direct comparison with the linear model is possible, we will use the same length scale distribution, (4.1), and the same values of Δ.

No value of Δ emerges as clearly superior when the velocity profiles are inspected visually in figures 4.23a, 4.23b. A good fit in one portion of the wave cycle is offset by a poor one elsewhere. Table 4.6 gives the root mean square error between the theoretical and experimental points and shows overall $\Delta = \delta_\omega/10$ being best — although it gives the best value for neither the accelerating or decelerating phases individually. Near the beginning of the cycle, the best fit is found with $\Delta = \infty$, while toward the end $\Delta = \delta_\omega/20$ is closer to the experimental points. The intermediate value, $\Delta = \delta_\omega/10$, yields a reasonable fit throughout the half-cycle.

A comparison between mixing length and linear models —figures 4.24a, 4.24b 4.25a, 4.25b and tables 4.4, 4.6 — leads to the conclusion that neither is clearly superior over the other. During the accelerating phase the models differ significantly in their predictions of the mean velocity profiles. For the mixing length model,

$\Delta = \infty$ gives the best agreement with experiment and $\Delta = \delta_\omega/20$ the worst, while for the linear model exactly the opposite is true. During the decelerating phase the agreement between the two models is much closer with both yielding the least error with $\Delta = \delta_\omega/20$. Overall the *linear* model with $\Delta = \delta_\omega/20$ gives the smallest root mean square error of the two models.

When the friction velocity is considered in figure 4.26 and in table 4.7, it is found ~~that~~ that the $\Delta = \infty$ curve gives the smallest root mean square error with respect to the experimental data. It is also apparent, comparing figure 4.26 with 4.22, that the mixing length model predictions are somewhat closer to the experimental values than the linear model predictions and this is confirmed by an examination of tables 4.5 and 4.7. Note also that different values of Δ for the two models give rise to the best fit with the data. Visually the agreement with the experimental points seems poor for both models.

	RMS error (cm/s)		
t^*	$\Delta = \infty$	$\Delta = \delta_\omega/10$	$\Delta = \delta_\omega/20$
$0\pi/8$	3.7	8.0	14.4
$1\pi/8$	4.1	7.2	10.7
$2\pi/8$	7.5	9.5	9.7
$3\pi/8$	10.0	10.4	7.8
Average	6.9	8.9	10.8
$4\pi/6$	11.3	10.2	6.3
$5\pi/8$	10.0	7.4	4.0
$6\pi/6$	9.5	4.6	6.5
$7\pi/6$	10.0	3.9	8.7
Average	10.2	7.0	6.6
Combined average	8.7	8.0	8.9

Table 4.6: Root mean square error for mixing length model velocity profiles.

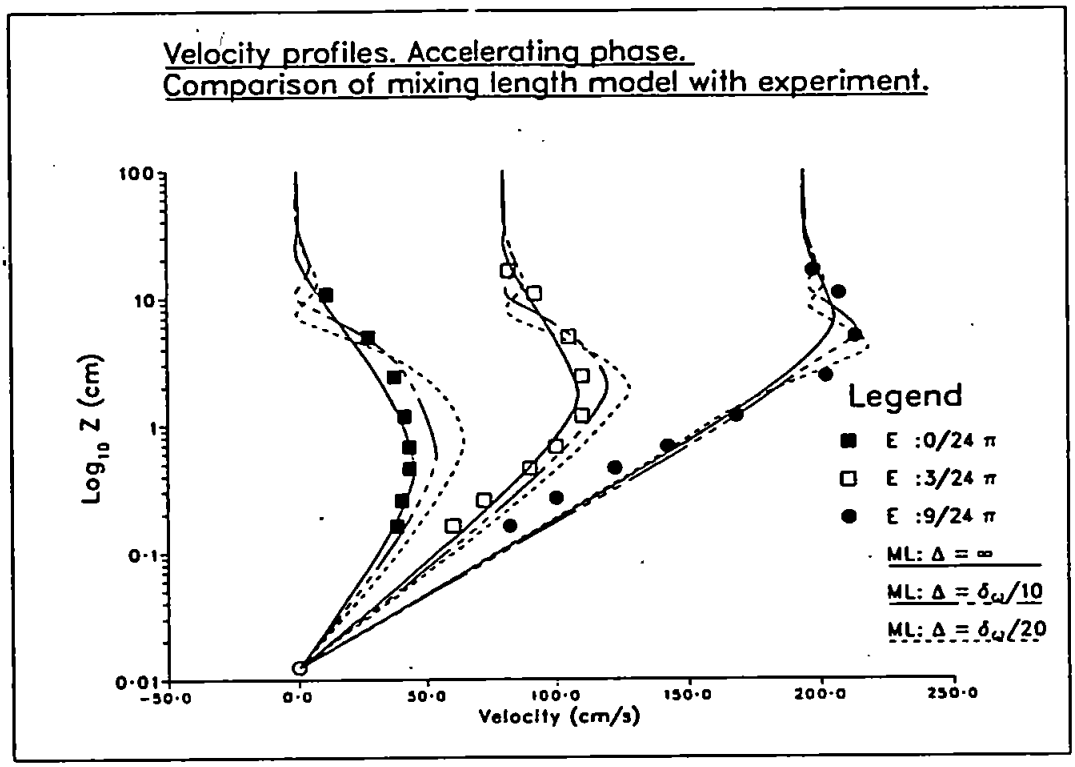

Figure 4.23a:

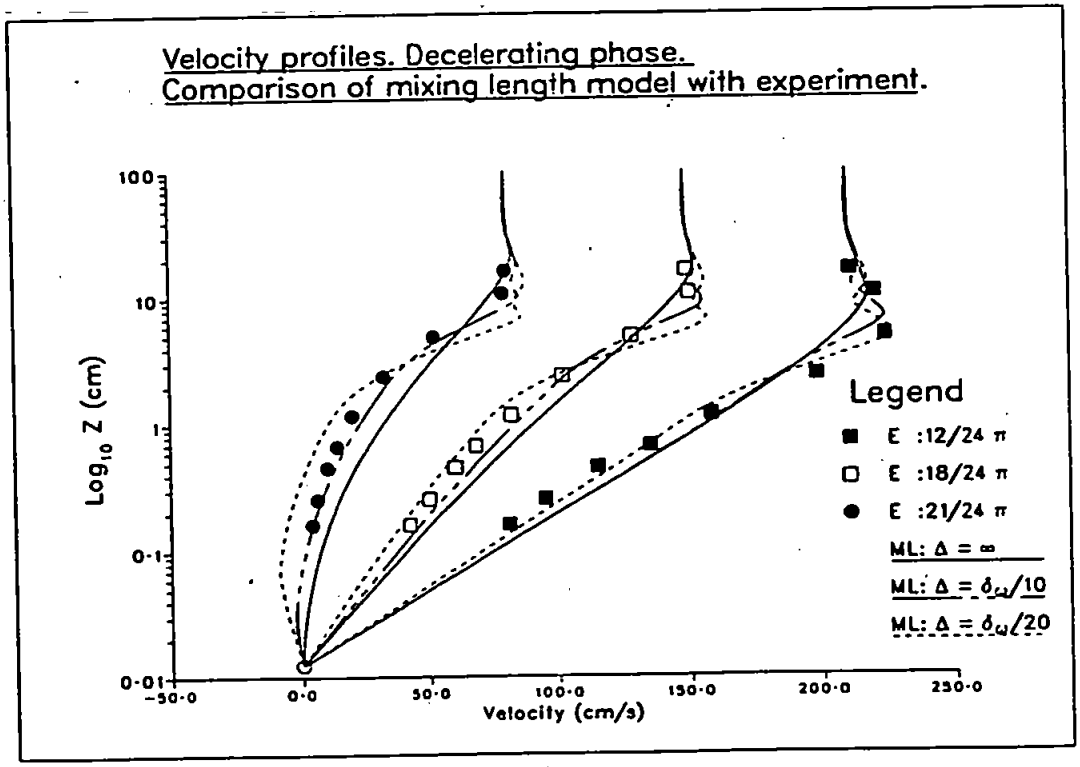

Figure 4.23b:

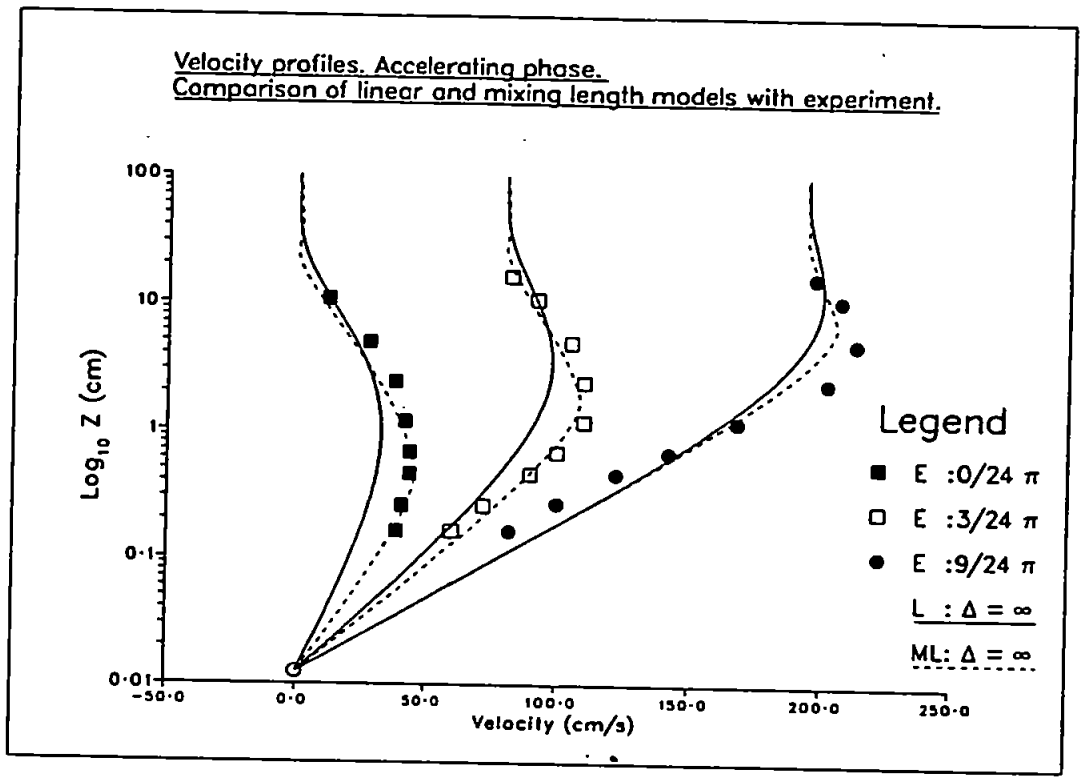

Figure 4.24a:

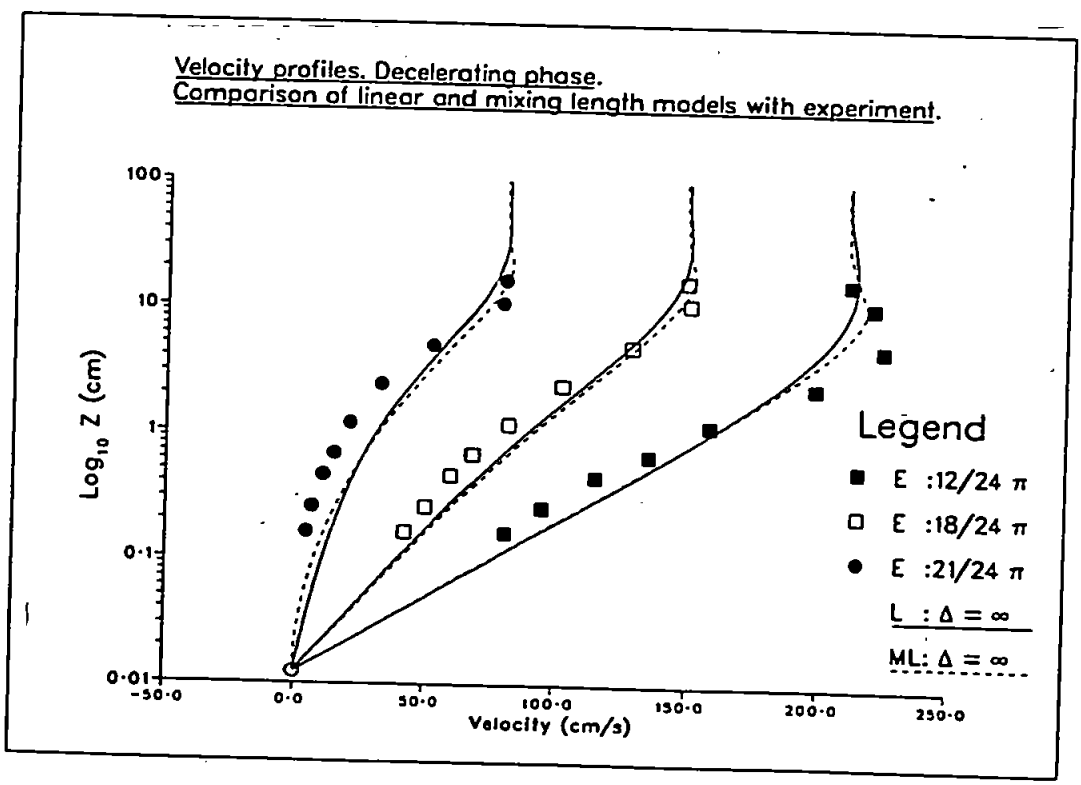

Figure 4.24b:

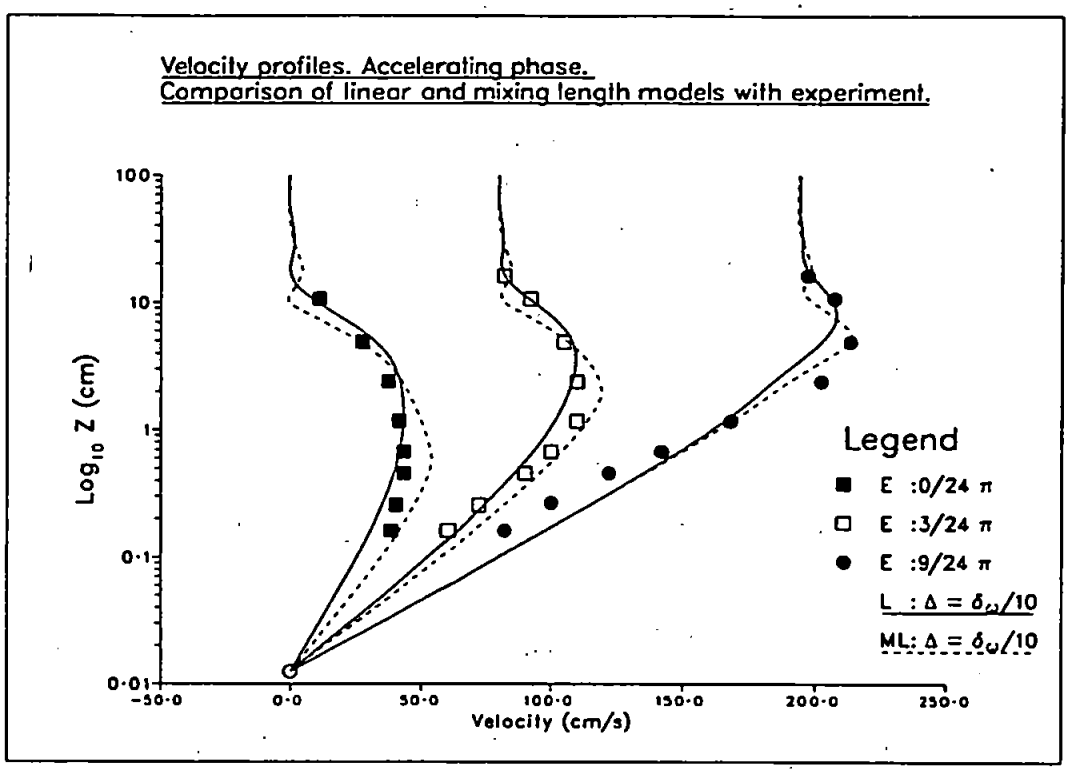

Figure 4.25a:

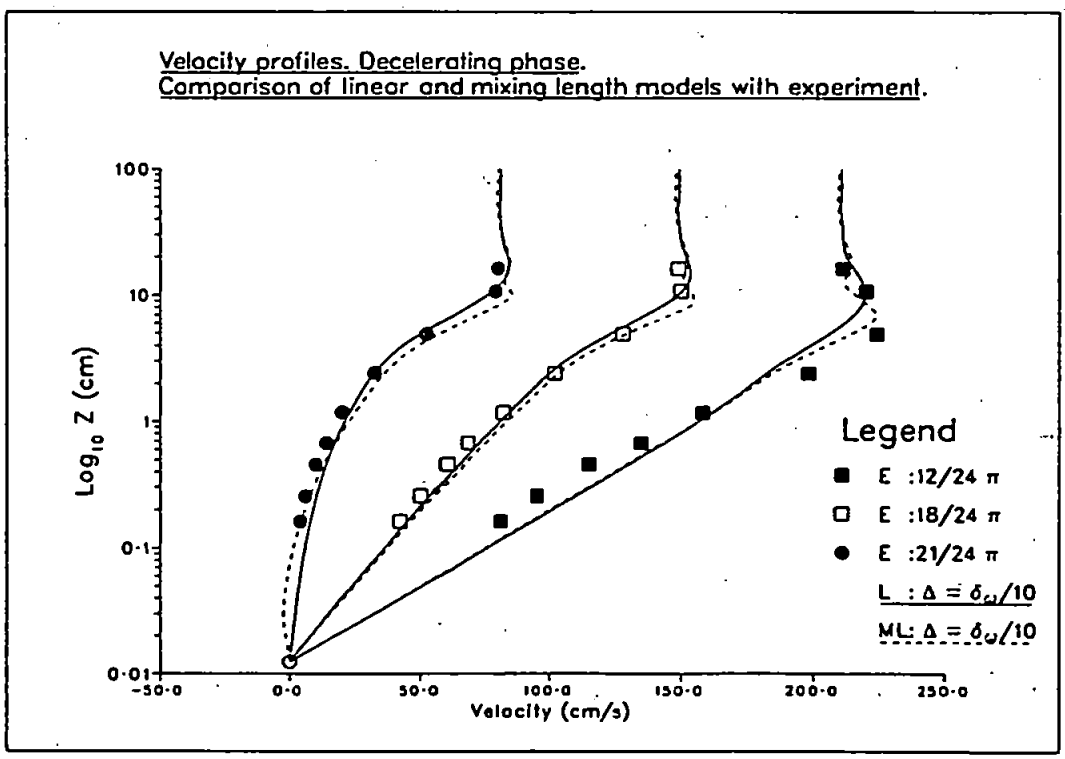

Figure 4.25b:

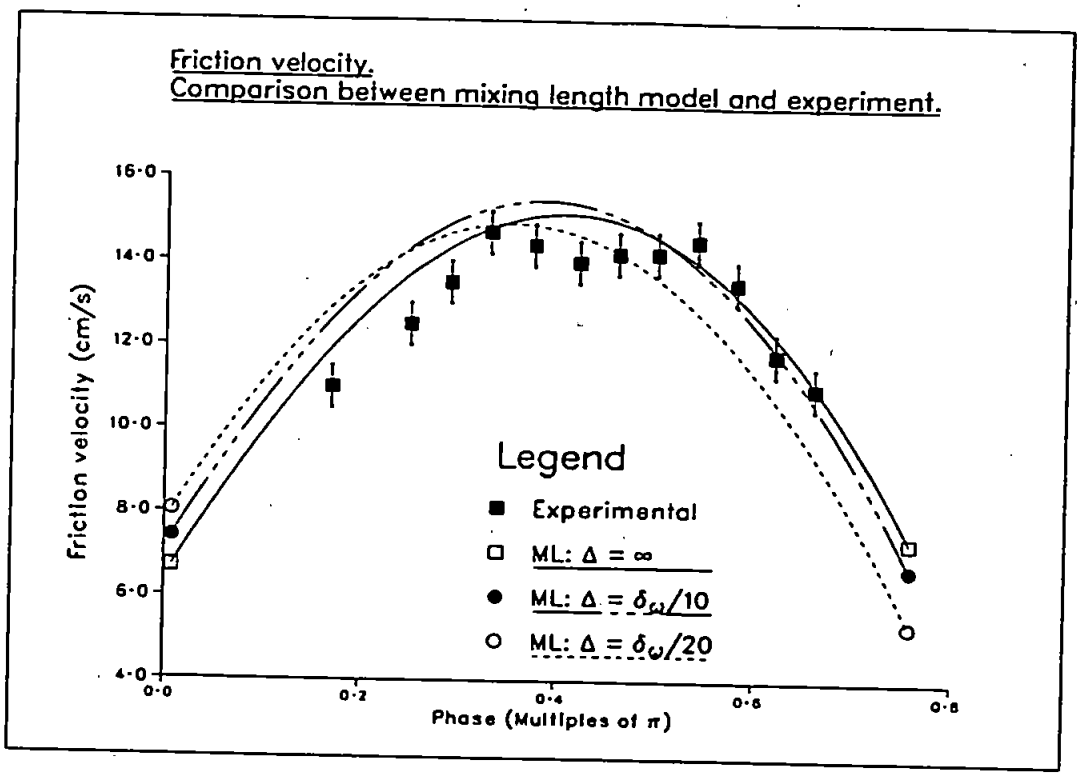

Figure 4.26:

Δ	RMS error (cms/sec) Accelerating	Decelerating	Combined average
$\Delta = \infty$	0.86	0.49	0.7
$\Delta = \delta_\omega/10$	1.3	0.49	1.0
$\Delta = \delta_\omega/20$	1.2	1.1	1.2

Table 4.7: Root mean square error for mixing length model friction velocity.

The k and $k-l$ models.

The velocity scale in the eddy viscosity is now determined from the turbulent kinetic energy equation (3.21), whilst still specifying the length scale empirically via (4.1). We will refer to this turbulence model as the 'k' model. Johns (1977) appears to be amongst the first workers to use a model of this type for oscillatory boundary layers.

Instead of comparing the effect of changing Δ we compare, in figures 4.27a and 4.27b, the velocity profiles obtained using the k model with those obtained from the mixing length model, using the same length scale expression (4.1), with $\Delta = \delta_\omega/10$, for both models. The two sets of curves are almost identical, a result that is repeated if we put $\Delta = \infty$, as shown in figures 4.28a and 4.28b.

In the last two figures we have in addition plotted the profiles obtained using (3.29)

to determine the length scale in conjunction with the turbulent kinetic energy equation. For the purpose of this document, we have termed this the '$k-l$' model.

From an inspection of the figures, together with a comparison of tables 4.6 and 4.8, we conclude that:

1. for the velocity profiles, the mixing length and k models give effectively identical results;

2. no significant improvement in predicting the velocity profiles is gained by calculating the length scale from (3.29) rather than putting $l = \kappa z$.

A consideration of the friction velocity will be given later when all the model predictions for this quantity are plotted in figure 4.35.

Shown in figures 4.29a,4.29b are turbulent kinetic energy profiles for the mixing length and k models. Most noticeable are the points where, for the mixing length model, the profiles touch zero as the velocity gradient vanishes. This leads to a general decrease in the turbulent kinetic energy compared to the k model. Note the profiles are shown at phases that are different to those at which the velocity profiles are presented. Figures 4.30a and 4.30b show turbulent kinetic energy profiles for the k (with $\Delta = \infty$) and $k-l$ models. Profiles calculated from the two models are very similar.

t^*	RMS error (cm/s)			
	$k : \Delta = \infty$	$k : \Delta = \delta_\omega/10$	$k : \Delta = \delta_\omega/20$	$k-l$
$0\pi/8$	3.8	7.0	14.1	4.5
$1\pi/8$	4.2	6.8	10.9	3.8
$2\pi/8$	7.2	9.0	10.0	6.0
$3\pi/8$	9.6 9	10.1	7.9	8.2
Average	6.7	8.4	10.8	5.9
$4\pi/6$	10.9	10.0	6.2	9.5
$5\pi/8$	9.6	7.4	3.8	8.6
$6\pi/6$	9.3	5.2	6.2	8.9
$7\pi/6$	10.2	4.4	8.1	11.0
Average	10.0	7.1	6.3	9.6
Overall Average	8.5	7.8	8.8	8.0

Table 4.8: Root mean square error for k, $k-l$ model velocity profiles.

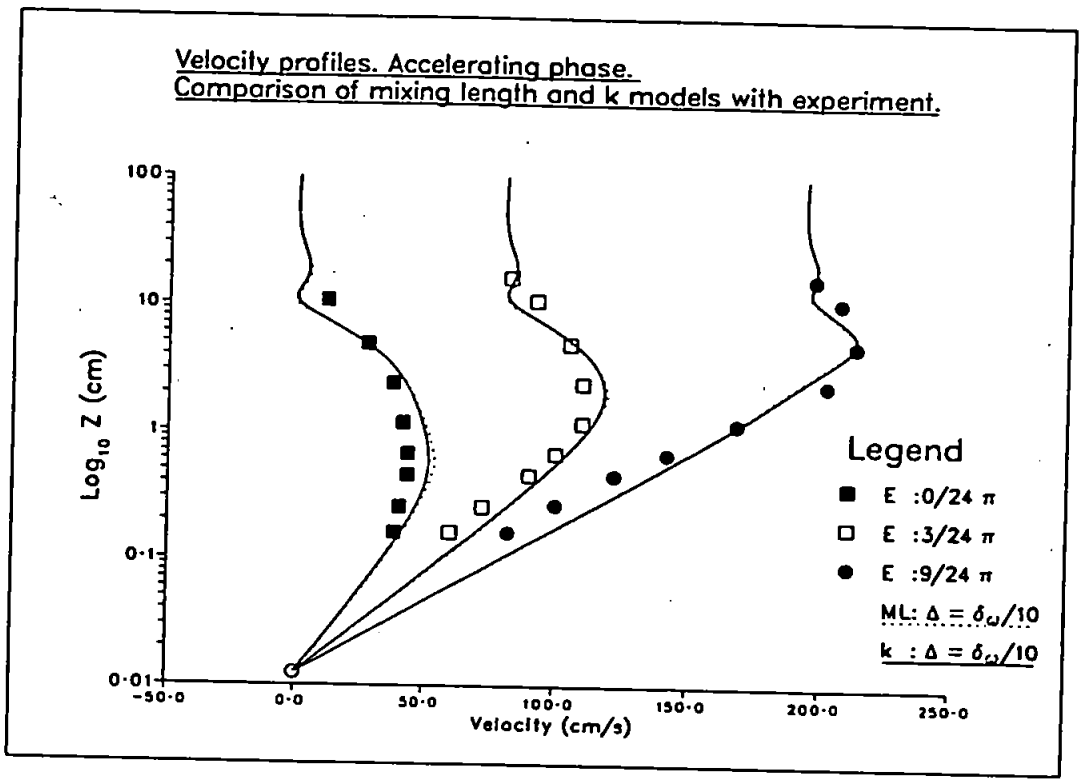

Figure 4.27a:

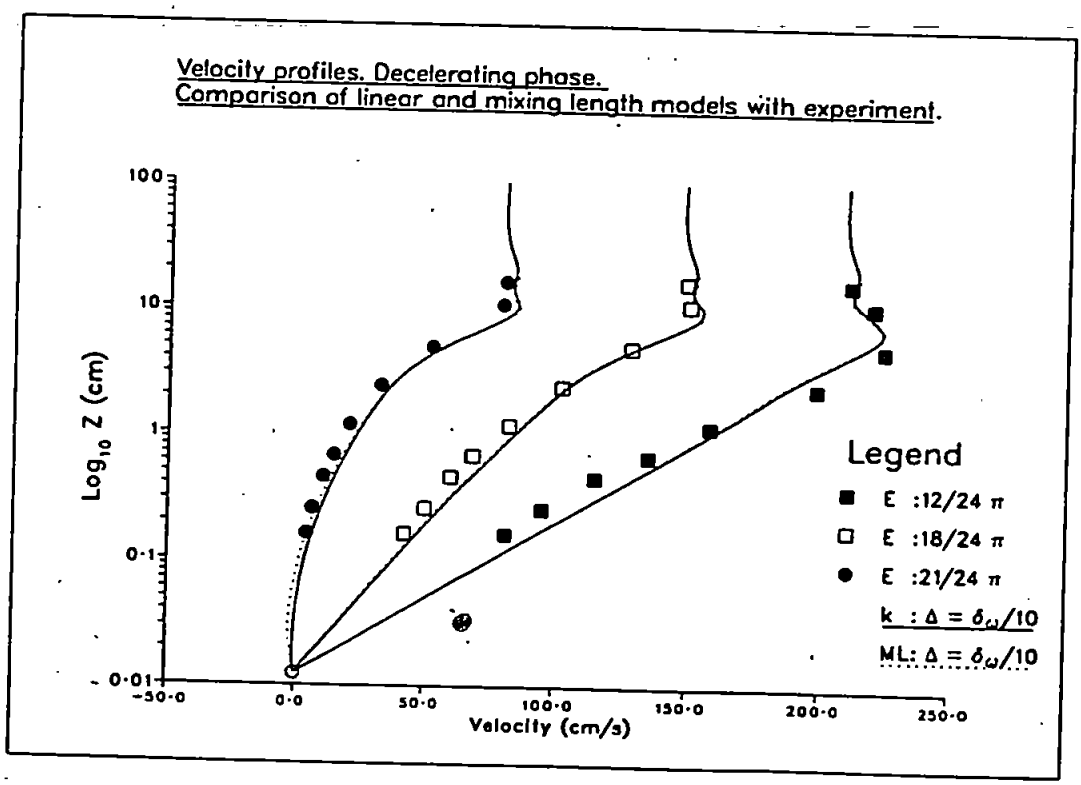

Figure 4.27b:

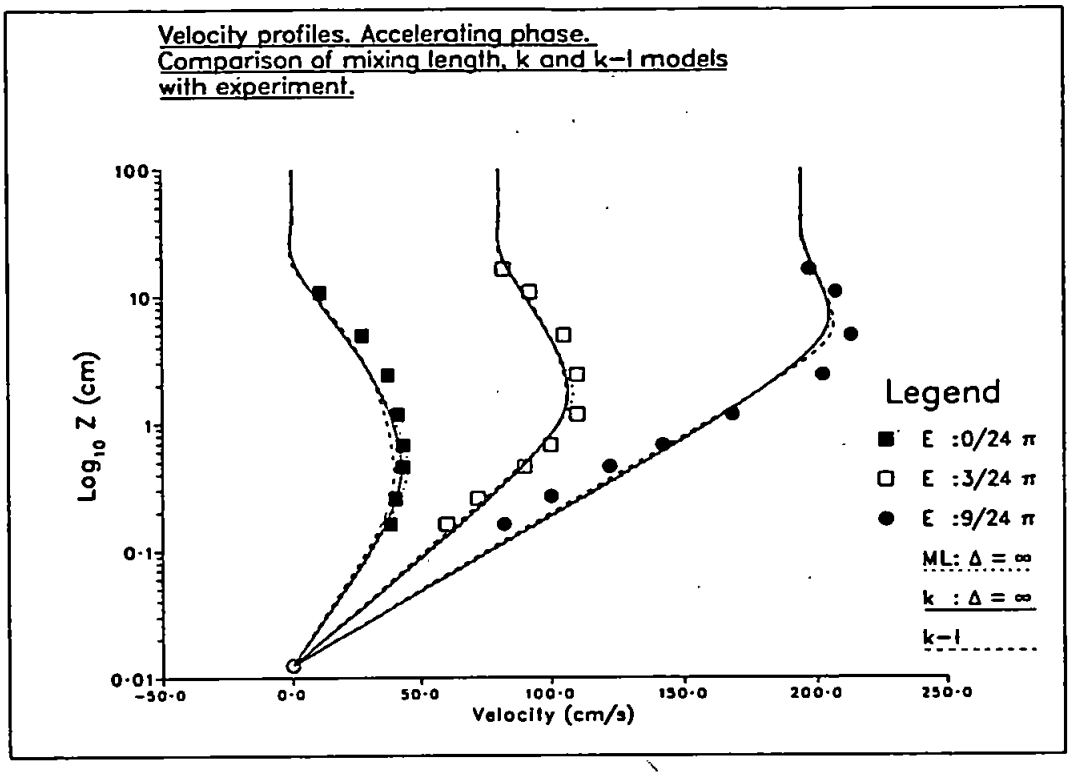

Figure 4.28a:

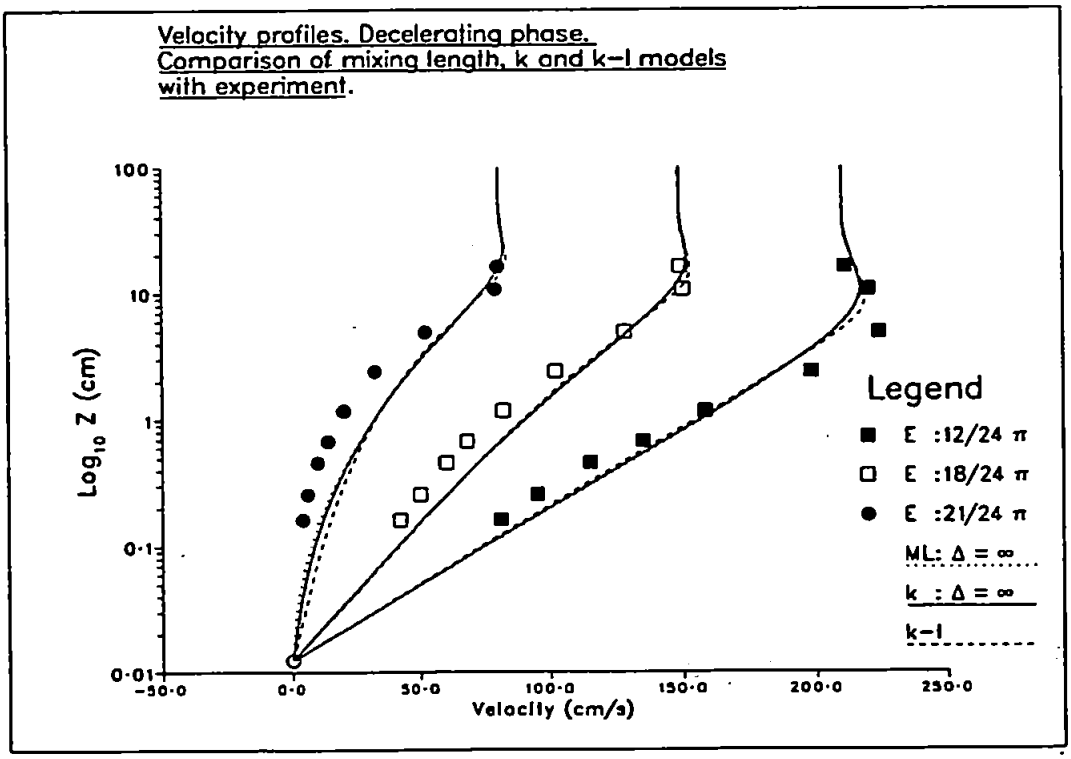

Figure 4.28b:

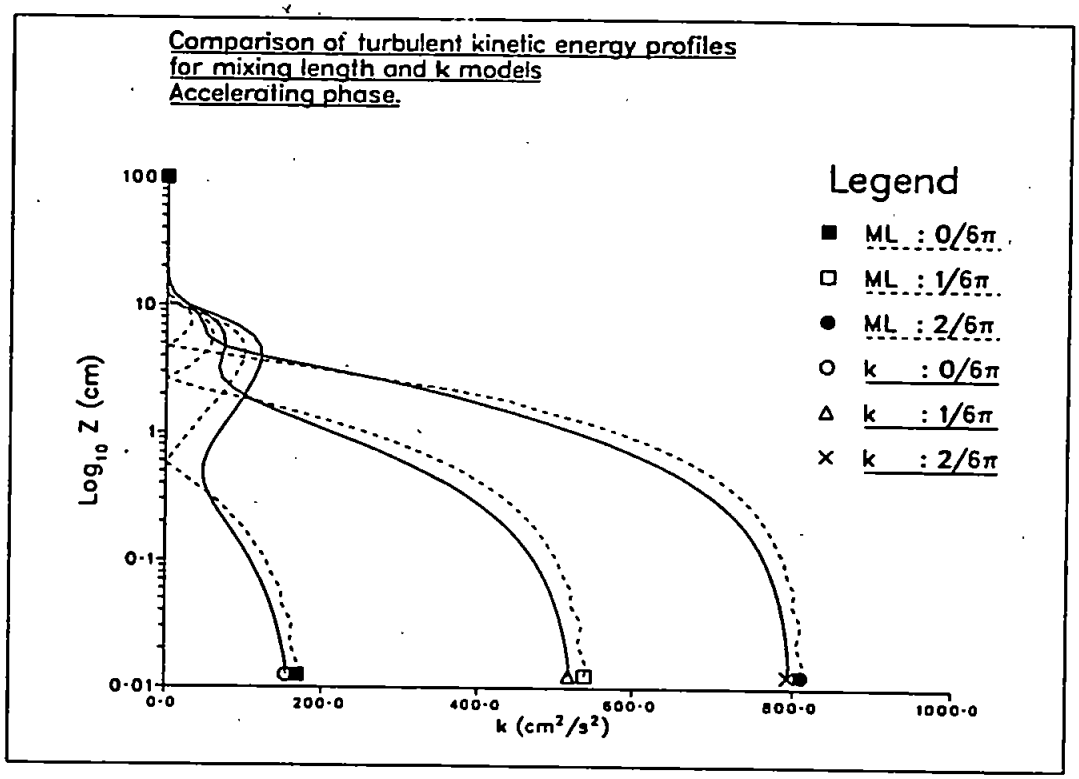

Figure 4.29a:

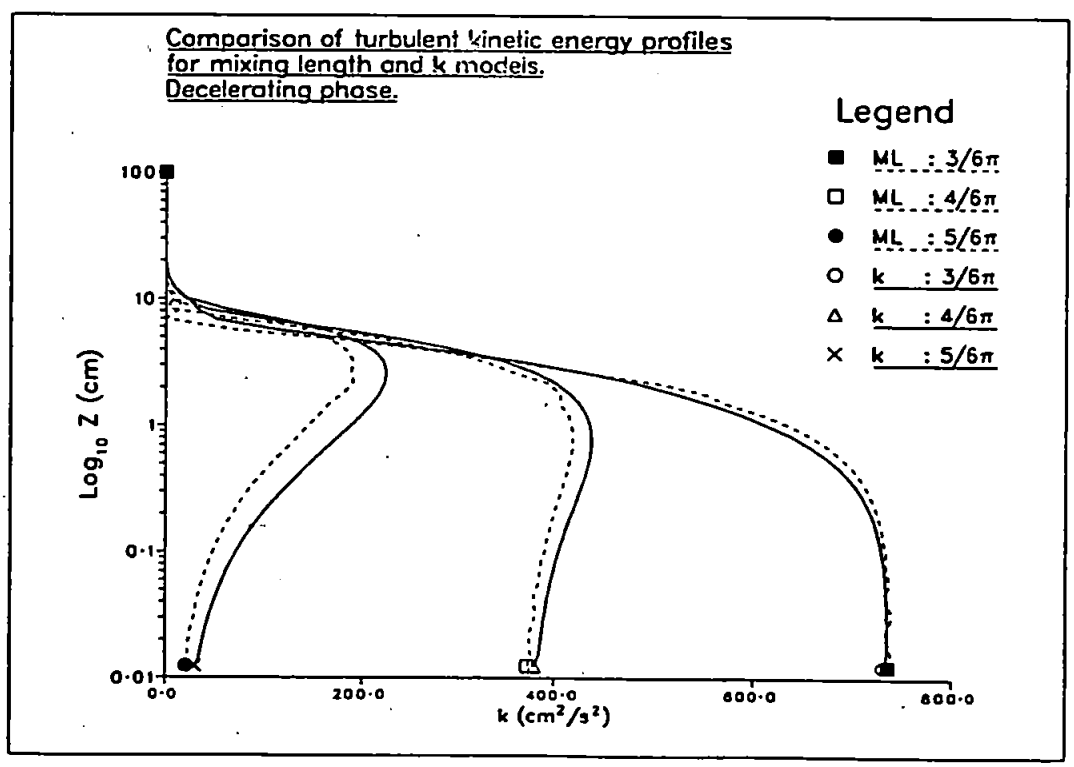

Figure 4.29b:

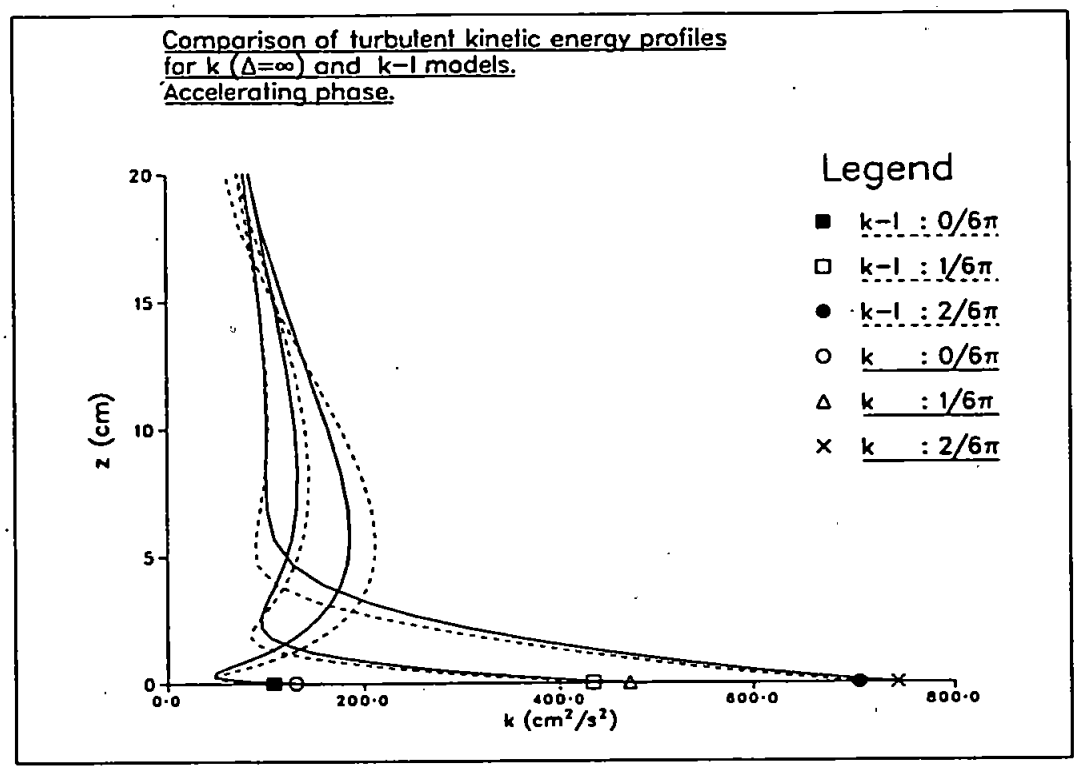

Figure 4.30a:

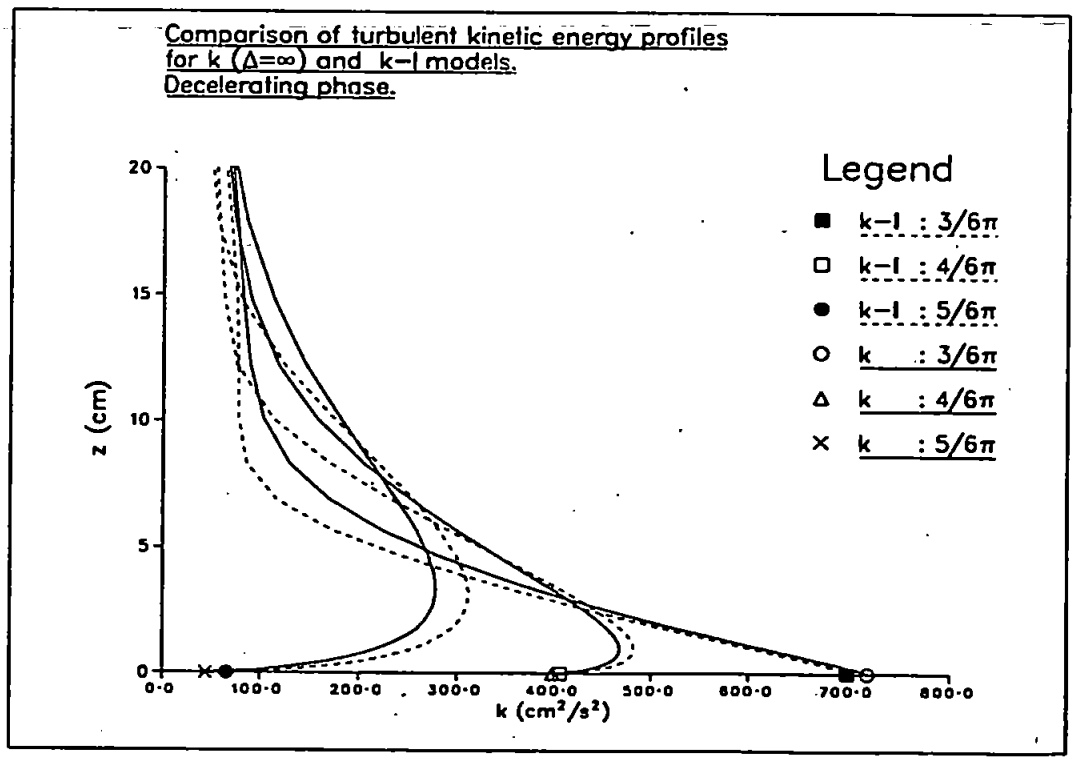

Figure 4.30b:

$k-\epsilon$ model.

Figures 4.31a and 4.31b show the predicted velocity profiles calculated using the $k-\epsilon$ model. The performance of the model is impressive, particularly when it is borne in mind that the model constants are standard values derived from independent experiments. The extreme value where the velocity gradient vanishes is well predicted at all phases of the wave cycle, as is the logarithmic region lower down. None of the previous models were able to give good predictions for both these features simultaneously. Note also the prediction of the slightly concave shape in the logarithmic region, seen also in the experimental data, as the free stream velocity nears its maximum. Again, none of the previous models were able to reproduce this behaviour.

Plotted with the $k-\epsilon$ values are those obtained from the k model with length scale given by (4.1) and $\Delta = \delta_\omega/10$, this model being chosen as it gives reasonable predictions during both the accelerating and decelerating phases of the wave cycle. Although the difference between the two curves is not dramatic, at every point where they do differ it is the $k-\epsilon$ results that lie closer to the experimental points. The only exceptions are data points near the bed at phase $21/24\pi$, where the k model is marginally superior. Table 4.9 shows the root mean square error for the $k-\epsilon$ model and for a selection of other models that give either good overall fit, or a good fit for either the accelerating or decelerating phases.

	RMS error (cm/s)			
t^*	$L:\Delta=\delta_\omega/10$	$k:\Delta=\delta_\omega/10$	$L:\Delta=\delta_\omega/20$	$k-\epsilon$
$0\pi/8$	4.5	7.0	7.6	3.9
$1\pi/8$	4.4	6.8	5.0	4.9
$2\pi/8$	8.4	9.0	8.0	4.9
$3\pi/8$	11.4	10.1	9.2	4.3
Average	7.8	8.4	7.6	4.5
$4\pi/6$	12.0	10.0	8.1	4.5
$5\pi/8$	8.7	7.4	6.2	3.6
$6\pi/6$	3.6	5.2	6.4	3.0
$7\pi/6$	3.3	4.4	5.9	3.8
Average	7.2	7.1	6.7	3.8
Combined Average	7.5	7.8	7.2	4.2

Table 4.9: Root mean square error for $k-\epsilon$ model velocity profiles.

The turbulent kinetic energy profiles for the $k-\epsilon$ model and the k model with $\Delta = \delta_\omega/10$, are plotted in figures 4.32a and 4.32b. The figures indicate a large difference between the models with regard to the predictions for this quantity. For example, the turbulent kinetic energy near the bed is predicted to be larger by the the k model than the $k-\epsilon$ model during the accelerating phase, and the reverse

toward the end of the decelerating phase. Also, the $k-\varepsilon$ model predicts larger values of the turbulent kinetic energy away from the bed during the accelerating phase and less, in comparison to the k model, during the decelerating phase. The implications of these differences for the eddy diffusivity and hence for the predictions the two models make for concentration profiles, are discussed further in Section 4.2.

Of significance is the comparison between the $k-\varepsilon$ prediction of the turbulent kinetic energy and the experimental values of this quantity[5] shown in figures 4.33a and 4.33b. The poor fit, especially near the bed, is discussed by Justesen (1988) who presented essentially the same plots for his $k-\varepsilon$ model and the experimental data of Sumer et al. (1987). The poor predictions near the bed during the accelerating phase are then responsible for the poor predictions away from the bed in the decelerating phase. Interestingly, the near bed predictions improve considerably during the decelerating phase. The turbulent kinetic energy is an important quantity terms accounting for particle inertia presented in Section 2.3 so the discrepancy between the theoretical predictions and experiment has implications for the accuracy of our calculations. This will be discussed further in Chapter 5.

Finally, the turbulent length scale profiles are considered. In figures 4.34a and 4.34b we plot this quantity as given by the empirical expression (4.1) with $\Delta = \delta_\omega/10$, the $k-l$ model, and the $k-\varepsilon$ model. The behaviour of the $k-\varepsilon$ curves follow roughly the empirical curve, showing a definite transition from a linearly increasing regime, to one where the value is more nearly constant with height. By contrast, the $k-l$ curves increase in an approximately linear fashion throughout the boundary layer. This explains the similarity of the velocity profiles between the $k-l$ model and the k model with $\Delta = \infty$ shown in figures 4.28a and 4.28b.

[5]Sumer et.al (1987) did not measure this quantity directly, but presented curves for $< v_1'^2 >, < v_2'^2 >$ from which k can be estimated, assuming a relation for $< v_3'^2 >$. The details are given in Justesen (1988), and it is the values derived by this author that we compare with the curves from our $k-\varepsilon$ model.

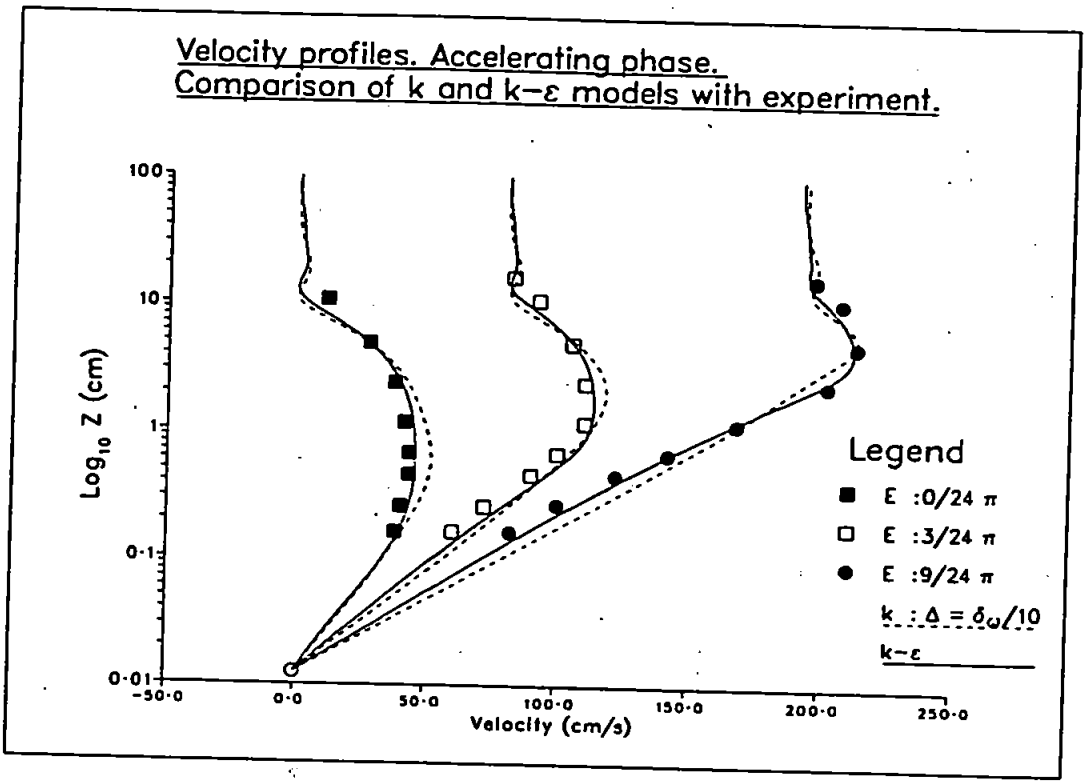

Figure 4.31a:

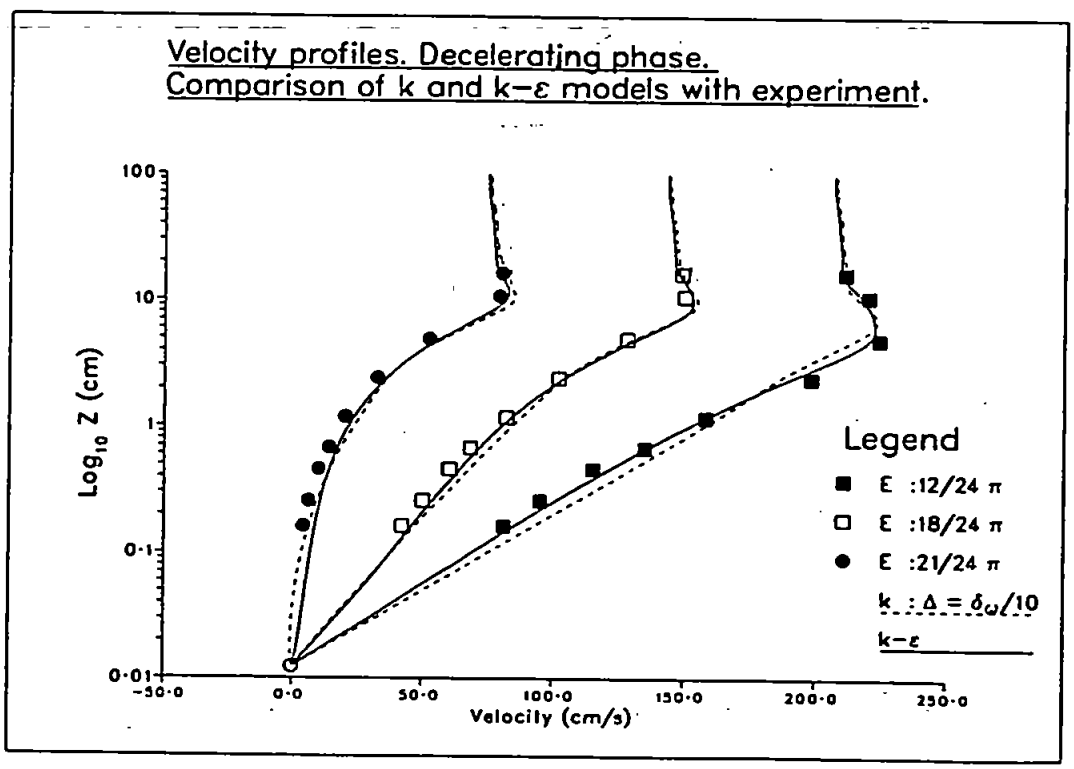

Figure 4.31b:

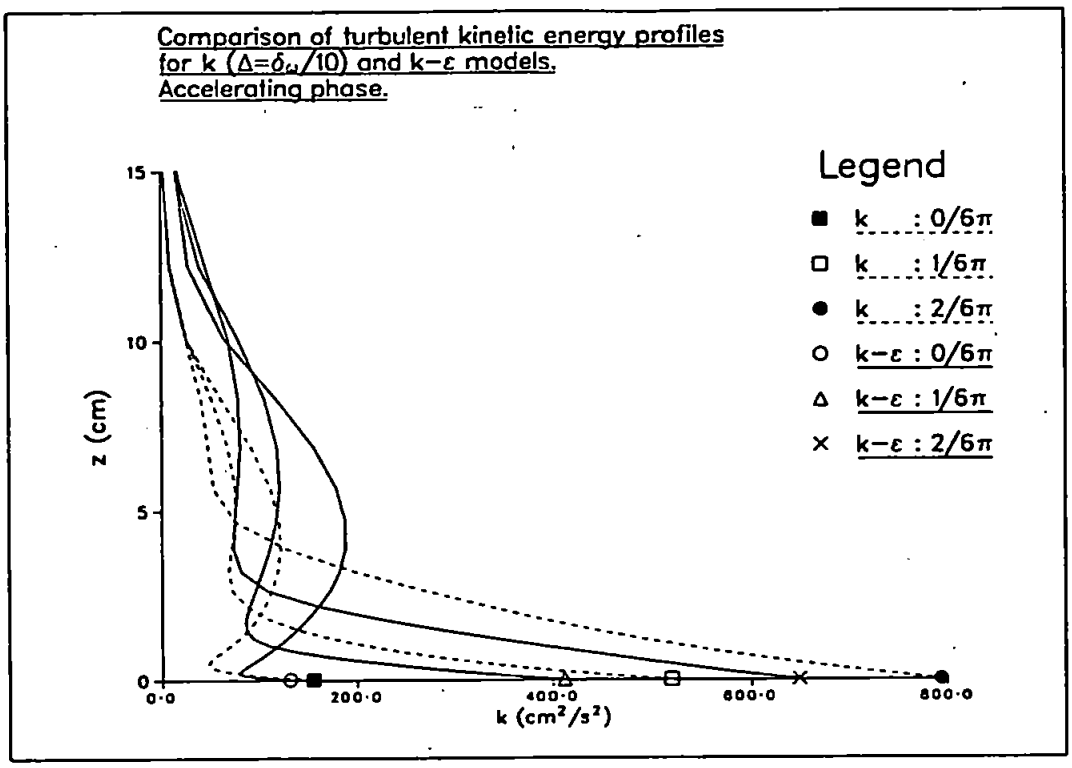

Figure 4.32a:

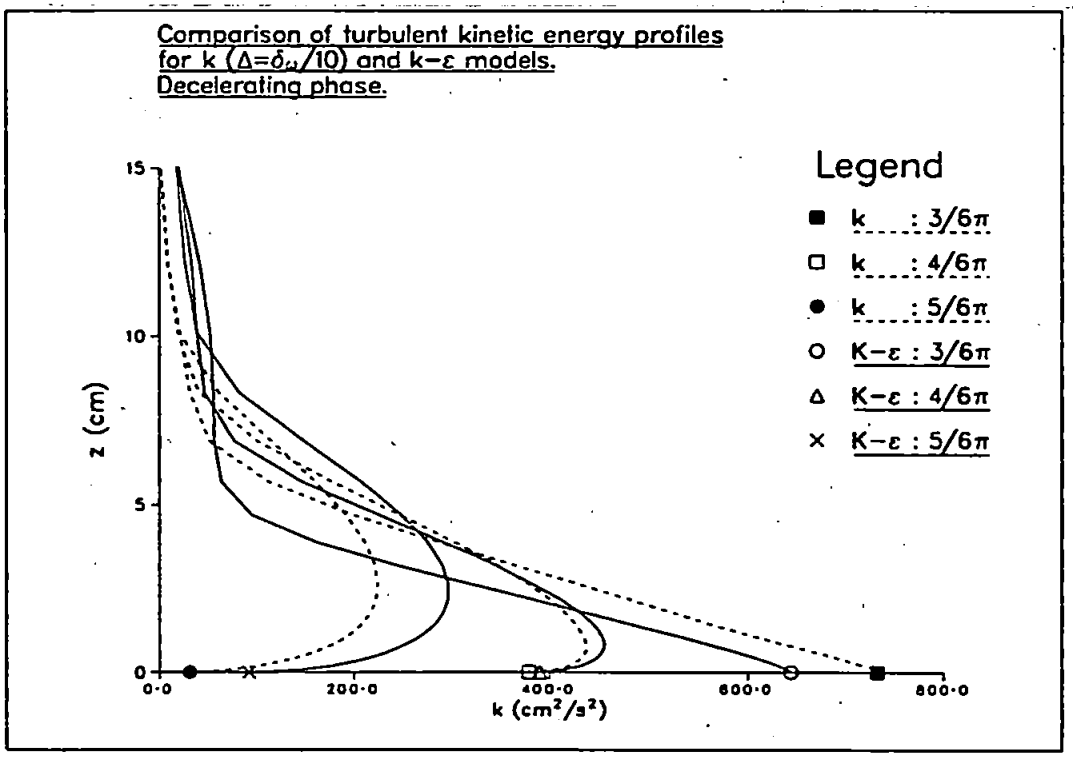

Figure 4.32b:

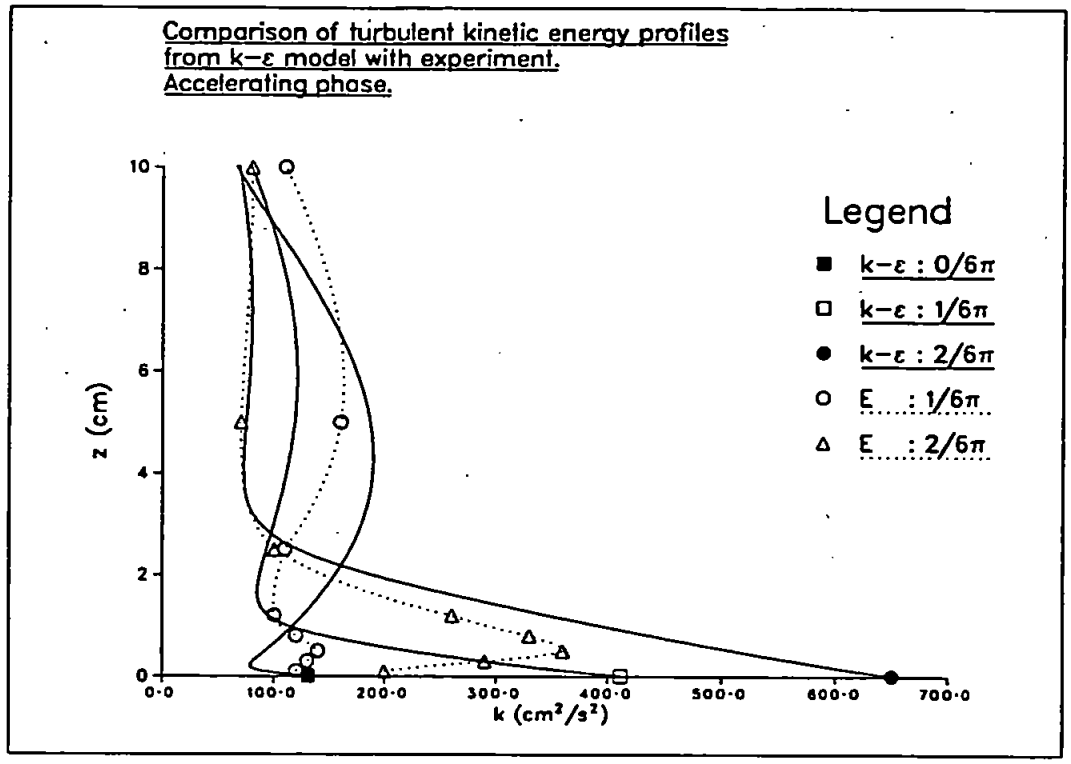

Figure 4.33a:

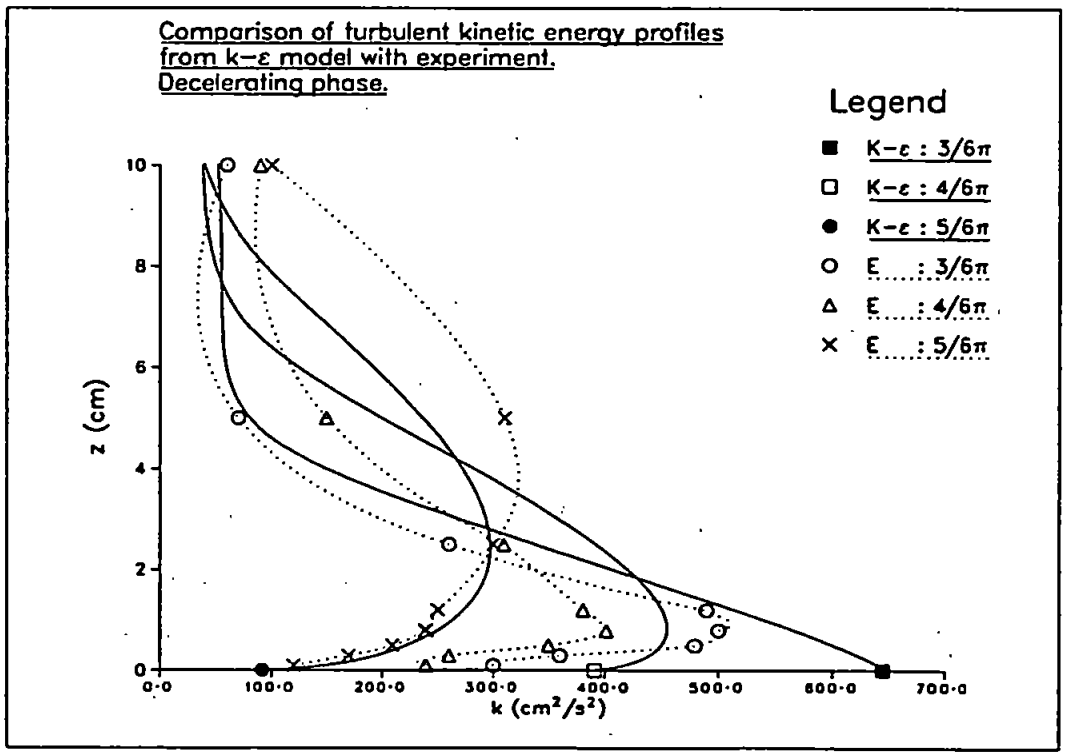

Figure 4.33b:

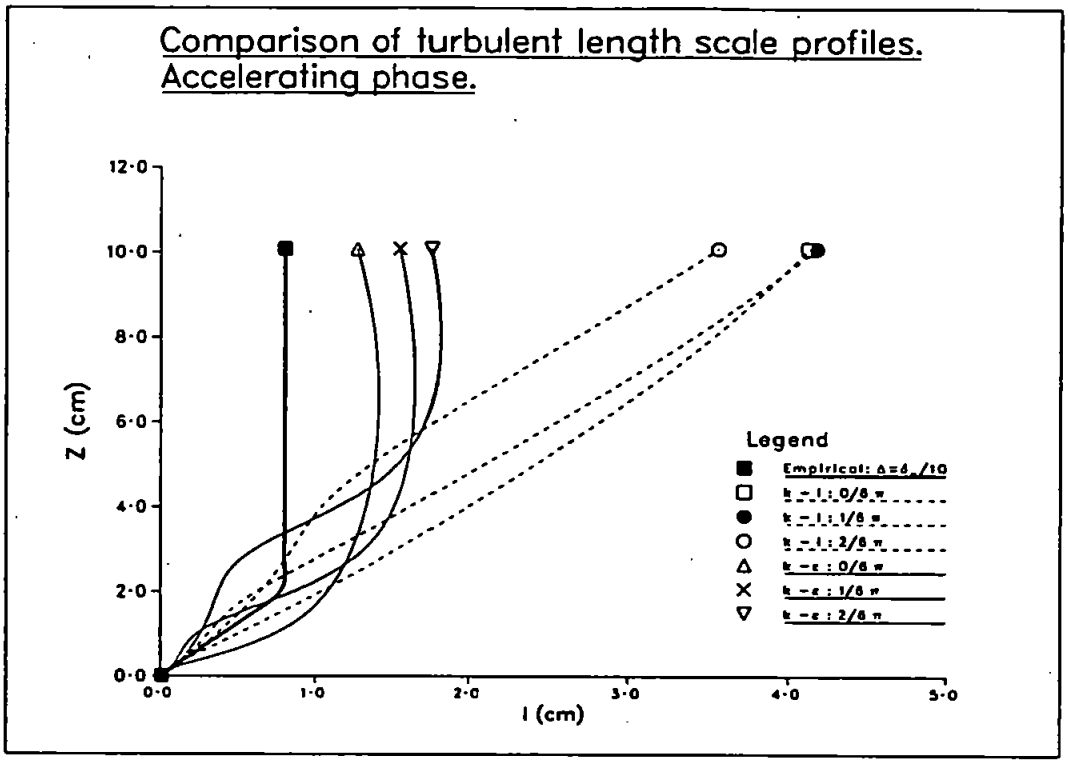

Figure 4.34a:

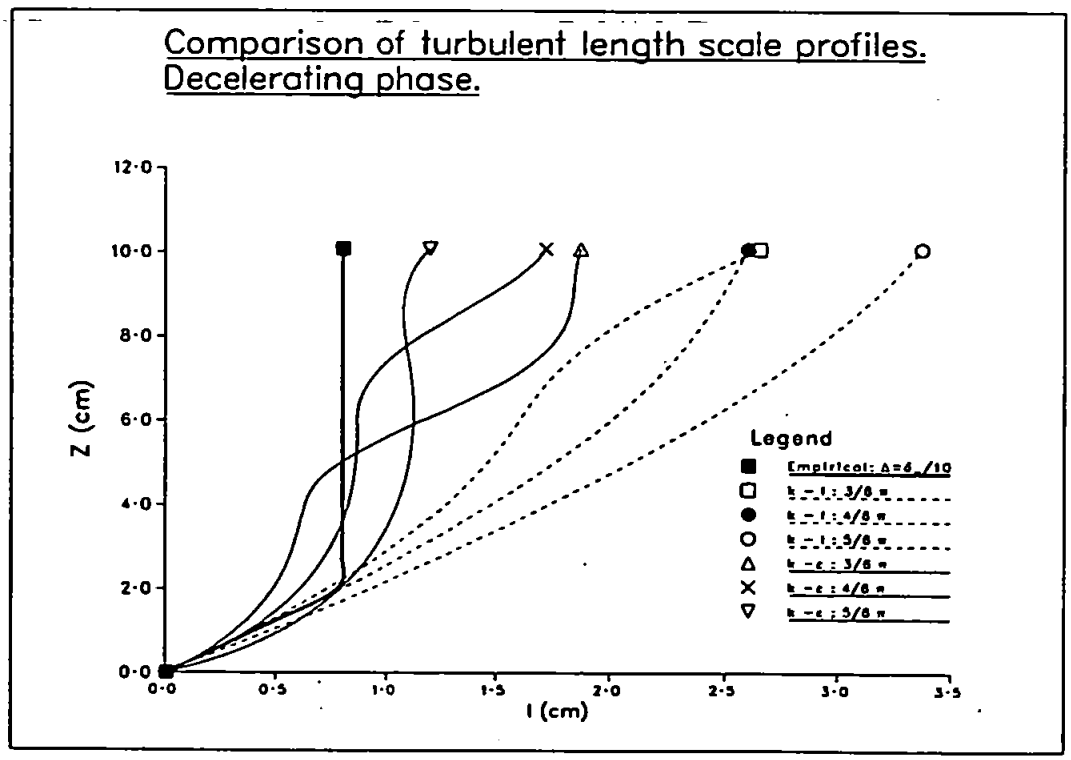

Figure 4.34b:

Summary of results for velocity profiles

In table 4.10 we give the overall root mean square error between the model predictions and the experimental points obtained by considering both accelerating and decelerating phases.

Model	RMS error (cm/s) $\Delta = \infty$	$\Delta = \delta_\omega/10$	$\Delta = \delta_\omega/20$
Linear	10.8	7.5	7.2
Mixing length	8.7	8.0	8.9
k	8.5	7.8	8.8
$k-l$	8.0		
$k-\varepsilon$	4.1		

Table 4.10: Overall rms error between experimental points and model predictions for mean velocity profiles.

From consideration of this, and the results presented in graphical form, the following conclusions are drawn with respect to the mean velocity profiles.

1. The $k-\varepsilon$ model gives significantly better predictions (roughly a factor of two improvement over the other models) for the velocity profiles and requires no "tuning" of parameters.

2. The performance of the more simple turbulence models, as measured by rms deviations from the experimental values, shows none to be clearly superior.

3. No significant difference was found between the predictions of the k and mixing length models. In addition, the $k-l$ model was found to give results very close to the k model with $\Delta = \infty$.

4. If the length scale is to be specified empirically via (4.1), then for the linear model choosing $\Delta = \delta_\omega/20$ appears to give the best result, while for the mixing length and k models, $\Delta = \delta_\omega/10$ seems better.

5. The use of a value of z_0 appropriate for a steady boundary layer flow appears to be justified by the generally good agreement between theory and experiment in the oscillatory case.

Summary of results for friction velocity

We turn now to the model predictions for the friction velocity. Table 4.11 gives the root mean square error between the calculated values of u_* and the experimental

points of Sumer et al. (1987). The experimental values were determined by fitting logarithmic velocity profiles to the experimentally measured velocity curves.

If the length scale is specified empirically, the best result for the mixing length and k models is with $\Delta = \infty$, and for the linear model it is with $\Delta = \delta_\omega/20$. However, the linear model result with $\Delta = \infty$ is only marginally worse than the $\Delta = \delta_\omega/20$ result, and we have chosen to use the former value of Δ for all the curves shown in figure 4.35 that require an empirical specification of length scale.

Model		RMS error (cms/s) Accelerating	Decelerating	Total
Linear	$\Delta = \infty$	1.3	1.3	1.3
Linear	$\Delta = \delta_\omega/10$	1.7	1.3	1.5
Linear	$\Delta = \delta_\omega/20$	1.5	0.7	1.2
Mixing length	$\Delta = \infty$	0.9	0.5	0.5
Mixing length	$\Delta = \delta_\omega/10$	1.3	0.5	1.0
Mixing length	$\Delta = \delta_\omega/20$	1.2	1.1	1.2
k	$\Delta = \infty$	0.66	0.4	0.6
k	$\Delta = \delta_\omega/10$	1.1	0.5	0.9
k	$\Delta = \delta_\omega/20$	1.1	1.1	1.1
$k - l$		0.4	0.4	0.4
$k - \varepsilon$		0.6	0.8	0.7

Table 4.11: RMS error between experimental points and model predictions for friction velocity.

The following conclusions can be drawn from an examination of figure 4.35 and table 4.11.

1. None of the models are able to reproduce the detailed features of the (slightly odd looking) experimental points with their two maxima. It may be that these points are peculiar to this set of data and in any future work it would be valuable to compare the predictions with a second set of data.[6]

2. The model predictions are in reasonable agreement with each other and with the experimental points with regard to the phase, but there are large differences in the magnitude.

3. The linear model gives a good prediction for the magnitude of the maximum friction velocity, although the phase at which this occurs is wrong. The model with the smallest rms error is the $k - l$ model.

[6] Sumer et al. use a second method, based on integrating the experimental curves over the boundary layer, to get the friction velocity. This gives a smooth curve with a single maximum which may provide a better comparison for the model results.

It is interesting to note that, although the mixing length k and $k-l$ models give almost identical predictions for the velocity profiles (see figures 4.28a and 4.28b), they give rise to distinct curves for the friction velocity.

Plotted in figure 4.36 is the friction velocity curve calculated assuming an explicit logarithmic law, and applying boundary conditions (3.35) and (3.38) above z_0. Clearly, with the current set of turbulence constants and specification of the roughness length, this quantity is severely underpredicted compared to the experimental measurements at the beginning of the wave cycle.

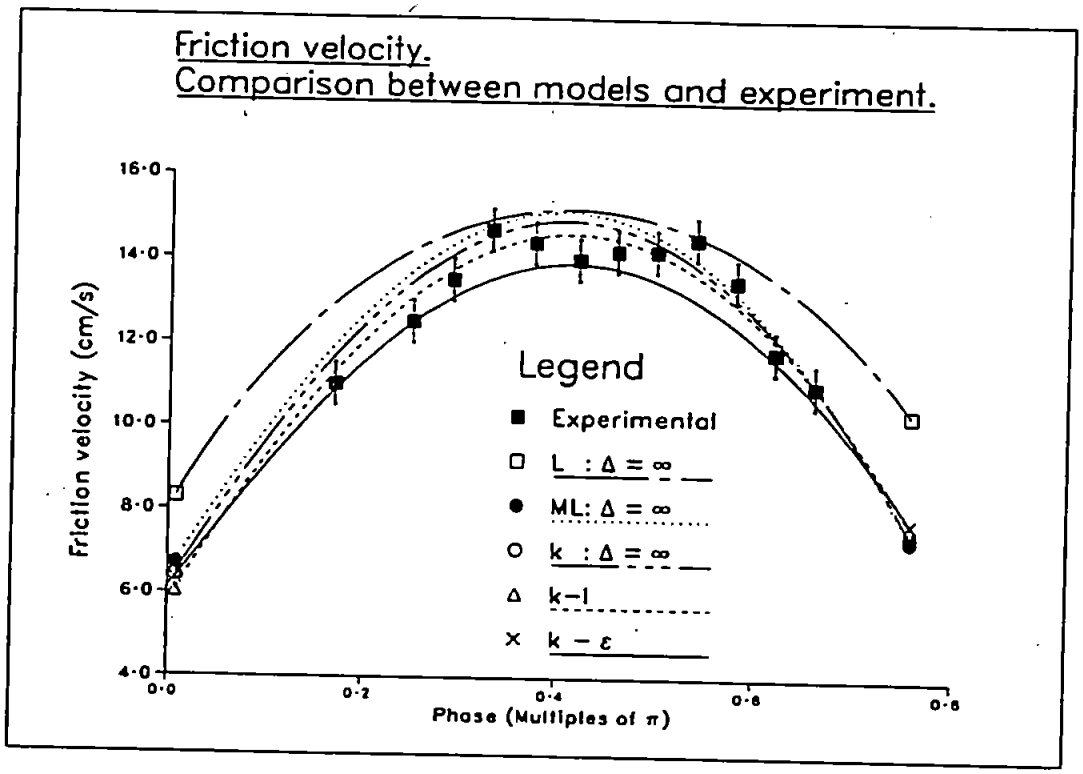

Figure 4.35:

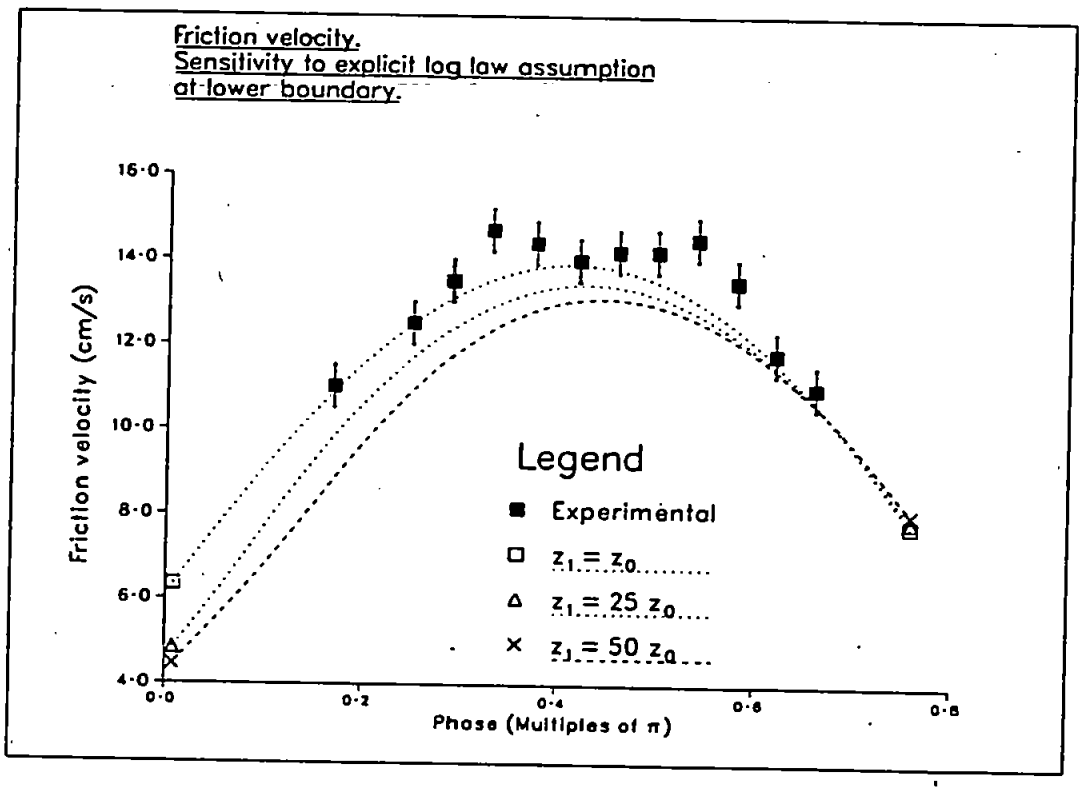

Figure 4.36:

4.2.2 Comparison of sediment predictions between turbulence models

The predictions of the various turbulence models are now compared with each other, and with the experimental data of Staub et al. (1983). Concentrations are generally normalised with the reference concentration c_0, except when compared with experimental data when they take 'actual' values which are volume fractions and so also dimensionless. The free stream velocity is taken as $V_\infty \cos \omega t$.

Sediment parameters are set to the values described at the beginning of Section 4.1.2.

It should be mentioned that the results that Staub et al. present are primarily an illustration of the use of a device to measure particle concentrations in sediment laden oscillatory flow, and do not constitute a rigorous experimental investigation of such flows. Surprisingly, there appears to be virtually no reported investigations of suspended sediment profiles over flat beds in oscillatory flow (Sleath, personal communication). In contrast, the case of suspended sediment over rippled beds has received extensive experimental investigation. For flat beds the only other work that appears to consider suspended sediment is Horikawa et al. (1982). However the emphasis here is on the sediment movement in the bed load region, with only a few suspended sediment profiles presented. A possible explanation for the apparent neglect, compared to the rippled bed case, is that for flat beds the transport is assumed be dominated by bedload, rather than the suspended load.

Linear model

Figures 4.37a and 4.37b show the effect of Δ on the concentration phase ϕ and amplitude c_a. For each value of Δ the value of v_{*m} was re-calculated as described in the description of the linear model in Section 4.2.1. For example, with $\Delta = \delta_\omega/10$ a value of $v_{*m} = 0.063$ was obtained implying a maximum bed stress of approximately 4 N/m^2.

k model

The effect on c_{amp} and ϕ of changing Δ in the k model are shown in figures 4.38a and 4.38b. Values of Δ were those calculated for the linear model above. Also shown are the $k - l$ model results for these quantities.

Concentration amplitudes (figure 4.38a) show the expected trend, with higher sediment concentrations associated with larger values of Δ, and hence diffusivity,

away from the bed. Note, the $k-l$ profile is close to the k model result for $\Delta = \infty$.

The effect of the change in Δ on the concentration phase is shown clearly in figure 4.38b. An increase in the rate of change of ϕ_c with height is apparent in the region where the length scale becomes constant. For this quantity, the curve from the $k-l$ model is indistinguishable from that of the k model with $\Delta = \infty$.

$k-\varepsilon$ model

We first compare the $k-\varepsilon$ predictions with those obtained from the k model. Figures 4.39a and 4.39b show that, for the k model, the curve with $\Delta = \delta_\omega/10$ is the closest to the $k-\varepsilon$ result. It is this value of Δ that will be used in the subsequent comparisons for the linear and mixing length, as well as k, models.

Figure 4.40a shows c_{amp} as calculated by the linear, mixing length, k and $k-\varepsilon$ models. We note first that the mixing length and k models give almost identical curves, and that these are broadly in agreement with the $k-\varepsilon$ result, while the linear model predicts significantly greater concentrations. This last result can be explained as being a consequence of the eddy diffusivity in the linear model which does not decay with height, as with the other models. All the models show an approximately linear dependence of $\log c_{amp}$ with z, implying an exponential decay of c_{amp} with height.

The variation of ϕ with height for the same set of models is shown in figure 4.40b. For this quantity the curves belonging to the mixing length and k models are not identical, and diverge as we move away from the bed. This is likely to be a result of the effect of the transport terms that are neglected in the mixing length formulation. A comparison of the k and $k-\varepsilon$ model curves reveals a distinct difference in the rate of change of ϕ with height in the lower part of the boundary layer. The variation of ϕ given by the linear model is clearly at odds with the other curves. Part of the reason is apparent from figure 4.42 where the variation in concentration over the wave cycle is plotted at a given height (note the concentration is not normalised). Where-as the k and $k-\varepsilon$ models show a rise to a peak followed by a more gentle decline, the linear model shows the opposite trend, with a gradual increase followed by a rapid drop. This behaviour is a consequence of the time independent eddy diffusivity of the linear model. Once the bed load reaches saturation, the concentration near the bed will steadily increase toward a steady state value until the bed stress causes a fall in the value of c specified at the bottom. Thus the peak value of concentration at the bed occurs near the end of a half-cycle, and as this effect diffuses upward we would expect to obtain the curve shown in the figure 4.42. In contrast the eddy diffusivity

in the k and $k-\varepsilon$ models will decrease near the bed once the peak bed stress has been reached, so that the upward flux of concentration will decrease even if the bed concentration remains fixed[7].

Looking in more detail at the differences between the k and $k-\varepsilon$ model predictions, it is interesting to examine the eddy diffusivity curves shown in figures 4.41a and 4.41b. It is apparent that although the profiles are broadly similar in shape, the eddy diffusivity associated with the $k-\varepsilon$ model reaches its maximum value further from the bed than that associated with the k model. In addition, the eddy diffusivity derived from the $k-\varepsilon$ model shows a slower decay with height, so that even at 10 cms from the bed it is typically 25% of its peak value. This behaviour is reflected in the concentrations predicted by the two models in figure 4.40a. Near the bed the k model concentrations are higher, while higher up the situation reverses.

Even though the curves from the two models show the same general features, it is surprising, comparing the eddy viscosity profiles for each model at a given time, how disparate the two are. The fact that the concentration profiles are comparable indicates that the concentration is determined by general features of the eddy diffusivity only.

[7] In fact the results of Section 4.1.2, where the sensitivity of the solution to the bottom boundary was investigated, shows for all models apart from the linear one, that the variation over the wave cycle of the bottom boundary condition is largely irrelevant for the flow parameters used here.

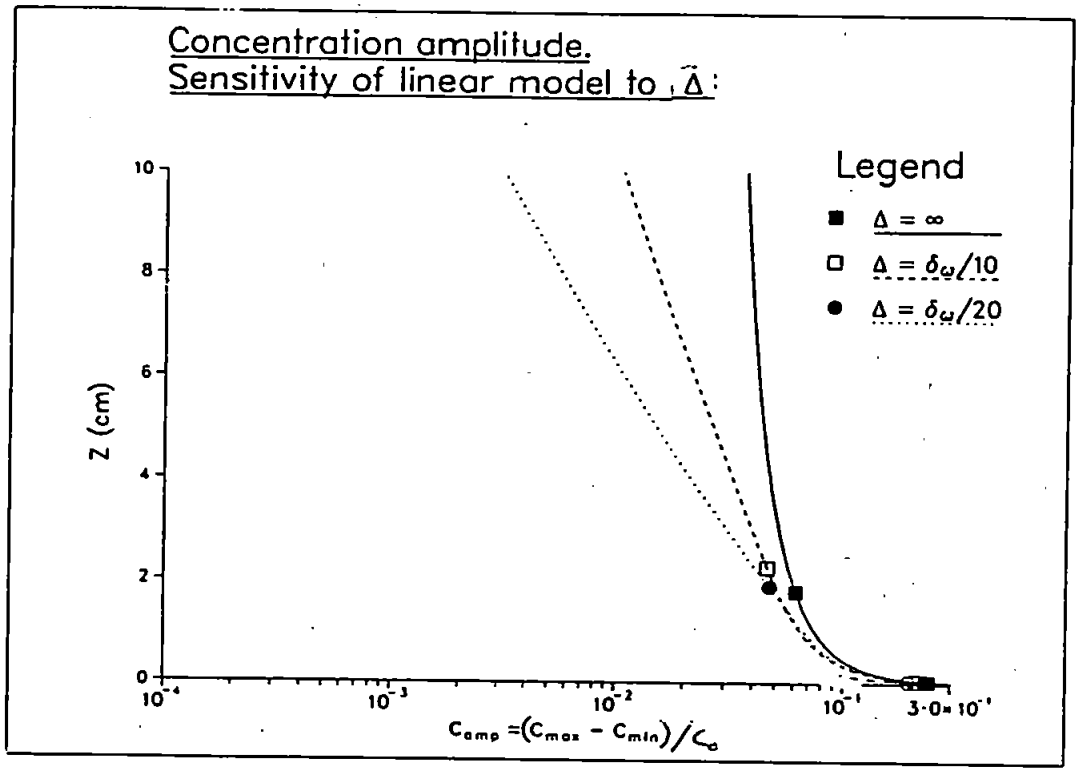

Figure 4.37a:

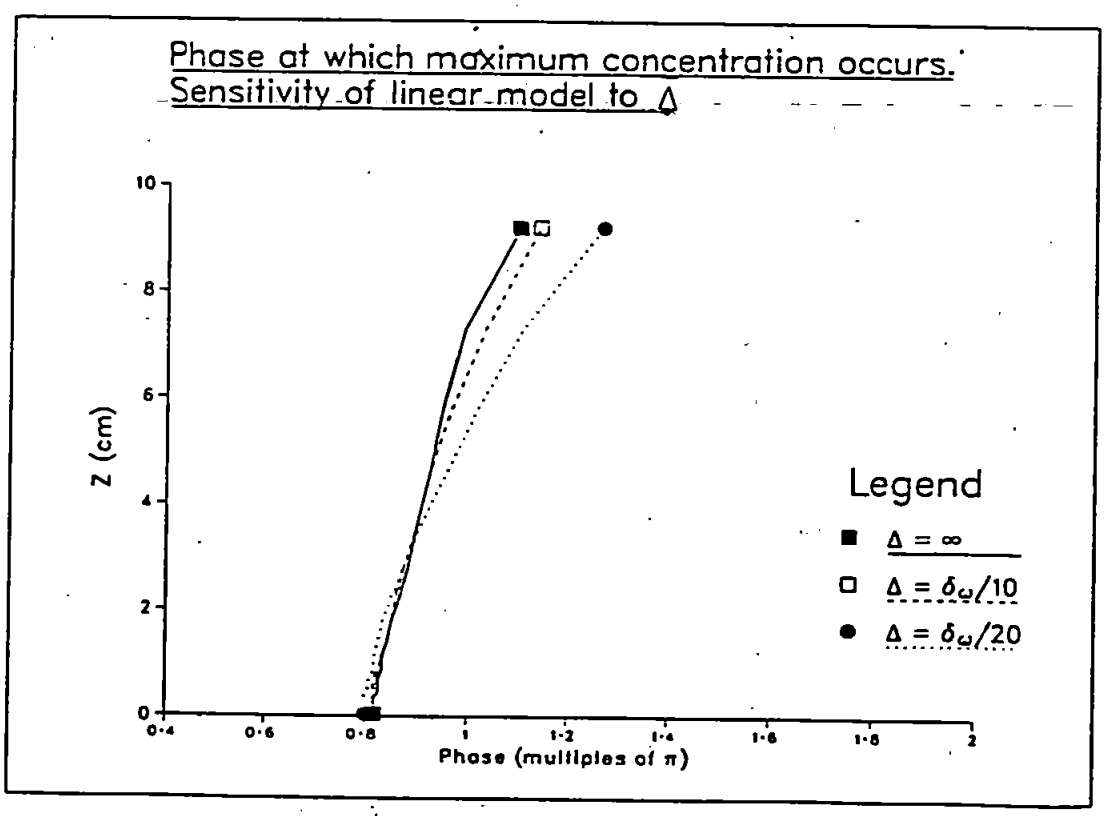

Figure 4.37b:

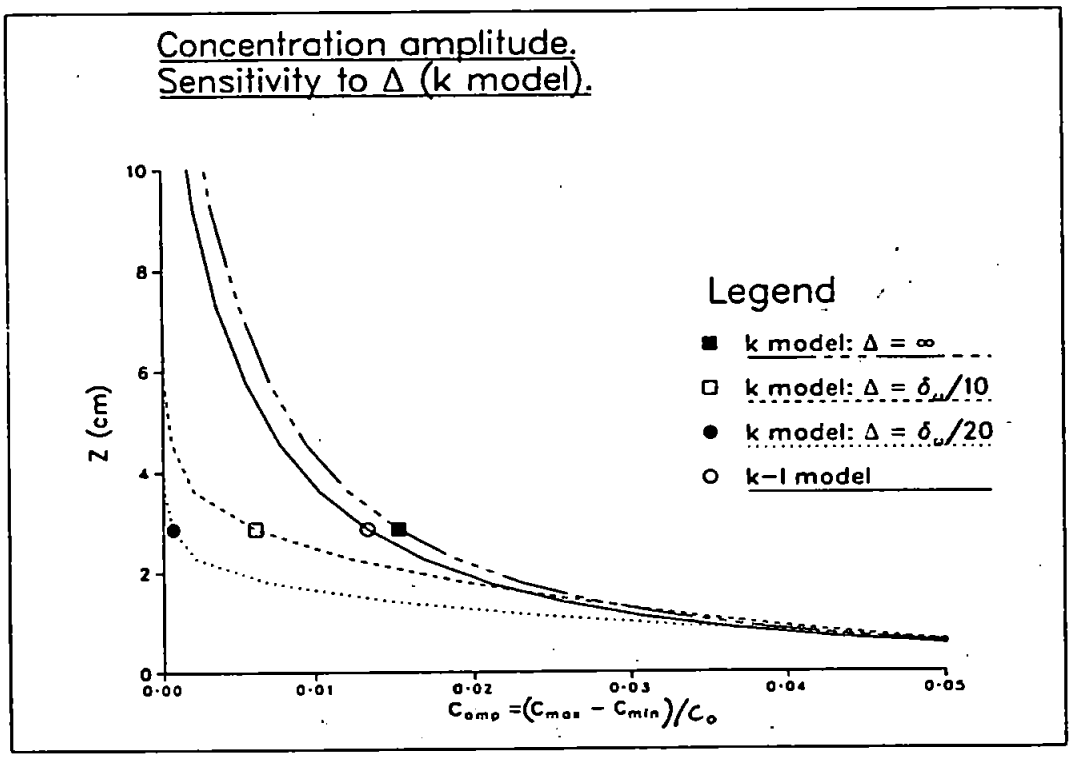

Figure 4.38a:

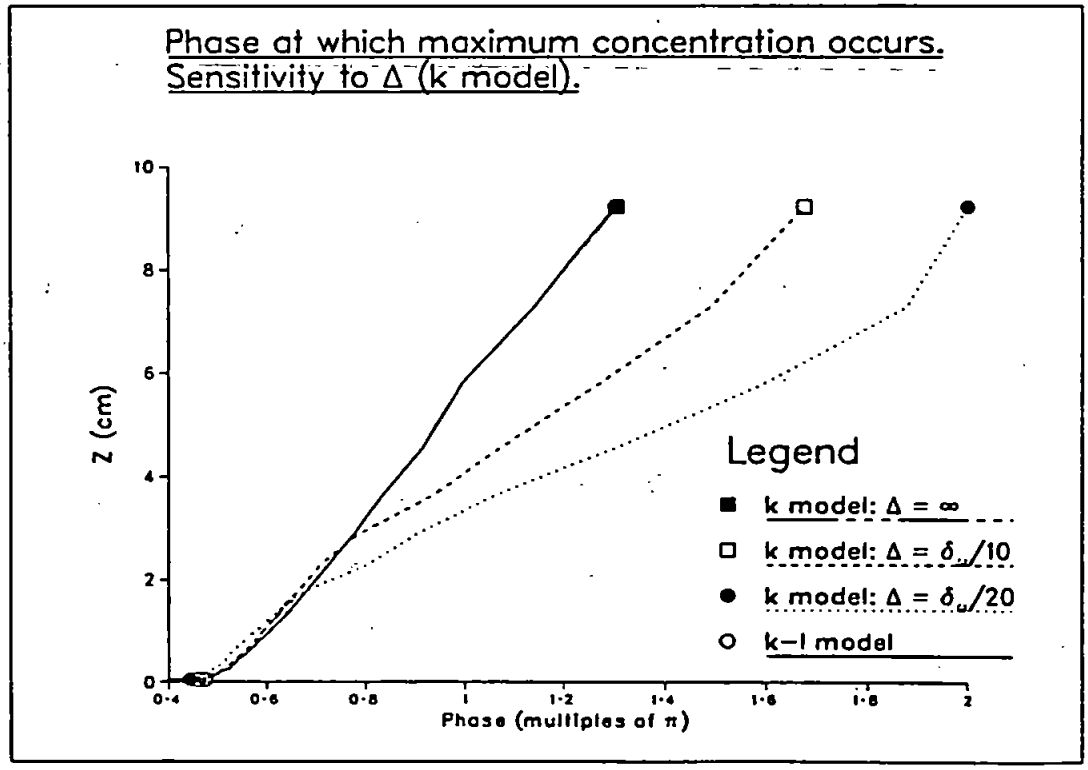

Figure 4.38b:

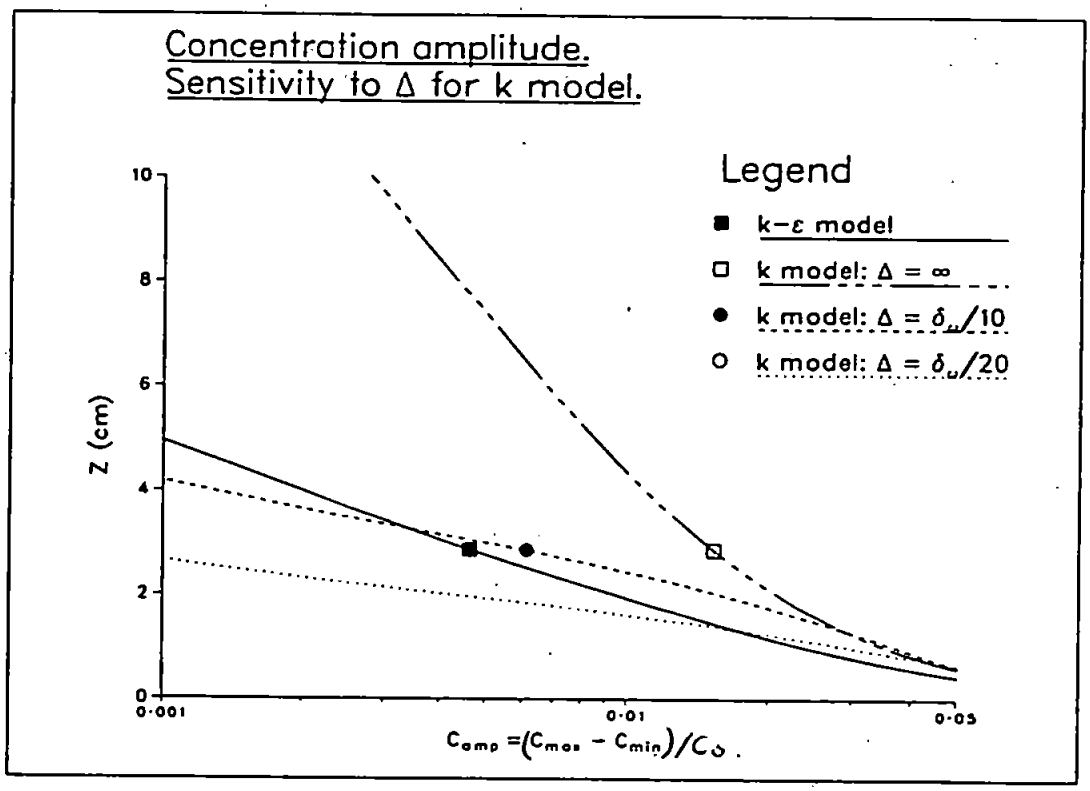

Figure 4.39a:

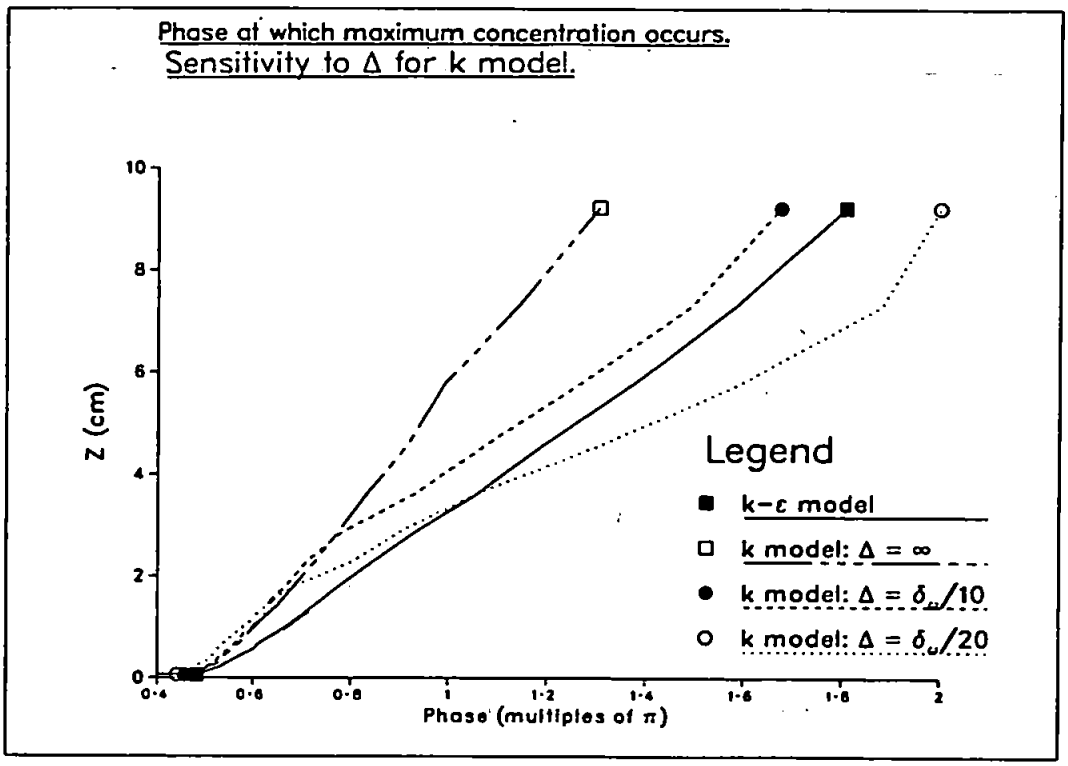

Figure 4.39b:

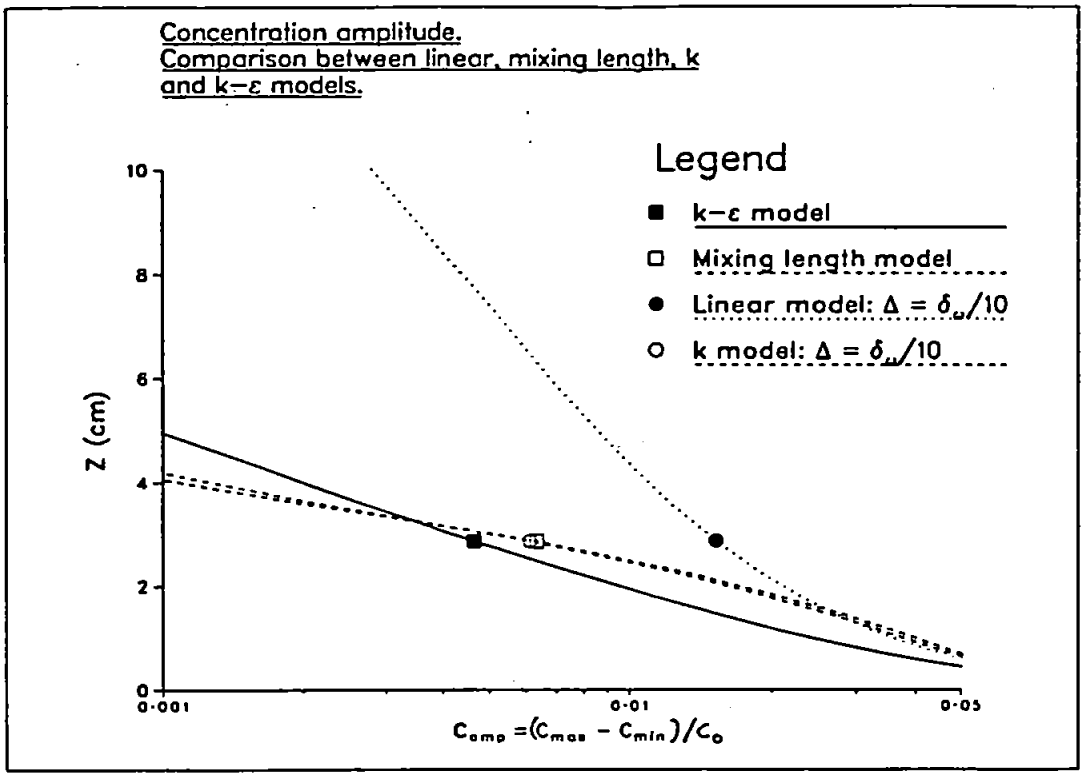

Figure 4.40a:

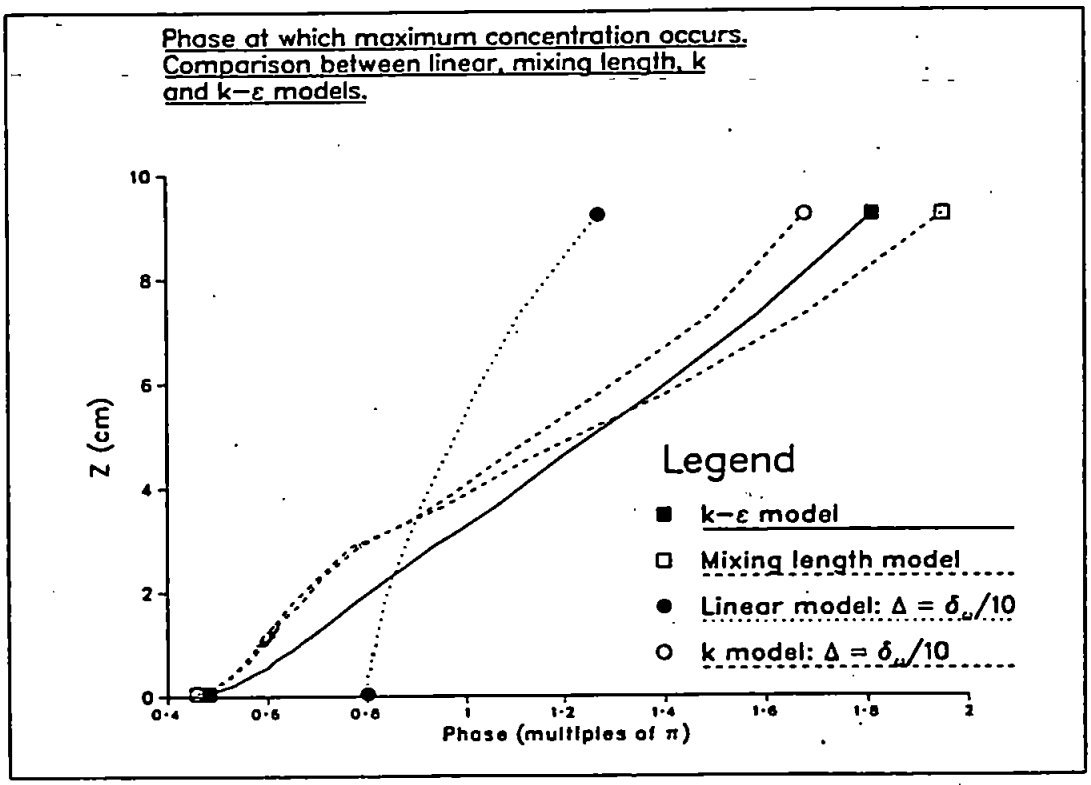

Figure 4.40b:

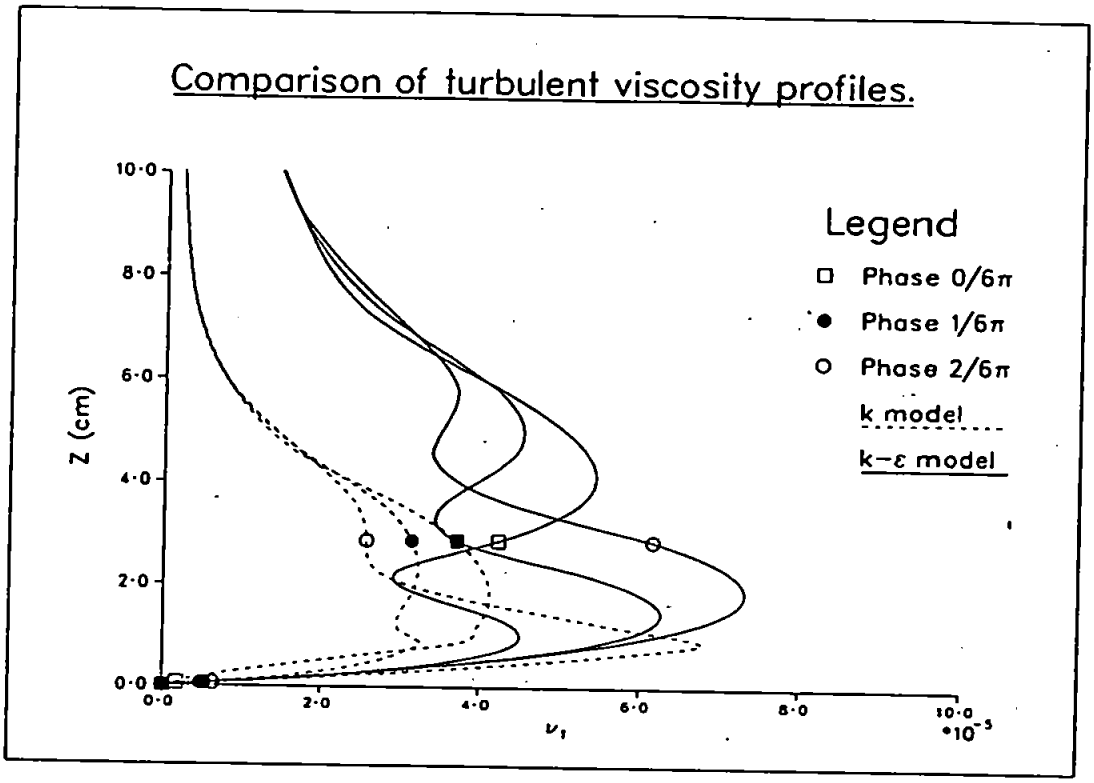

Figure 4.41a:

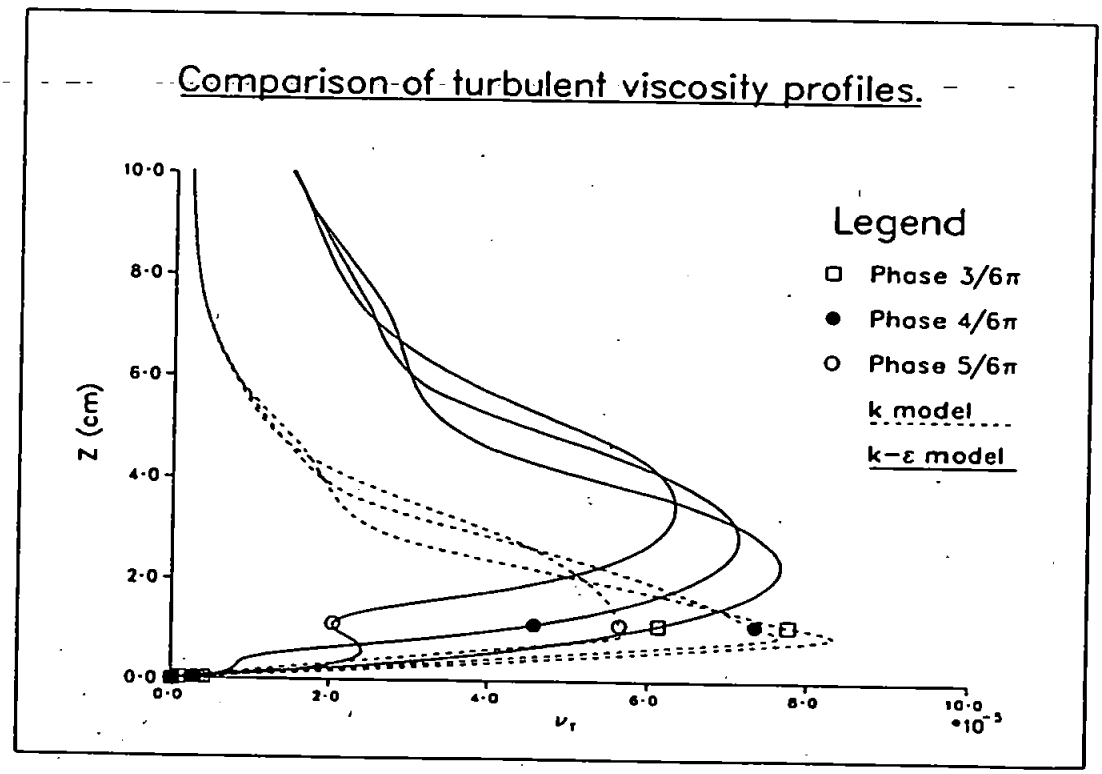

Figure 4.41b:

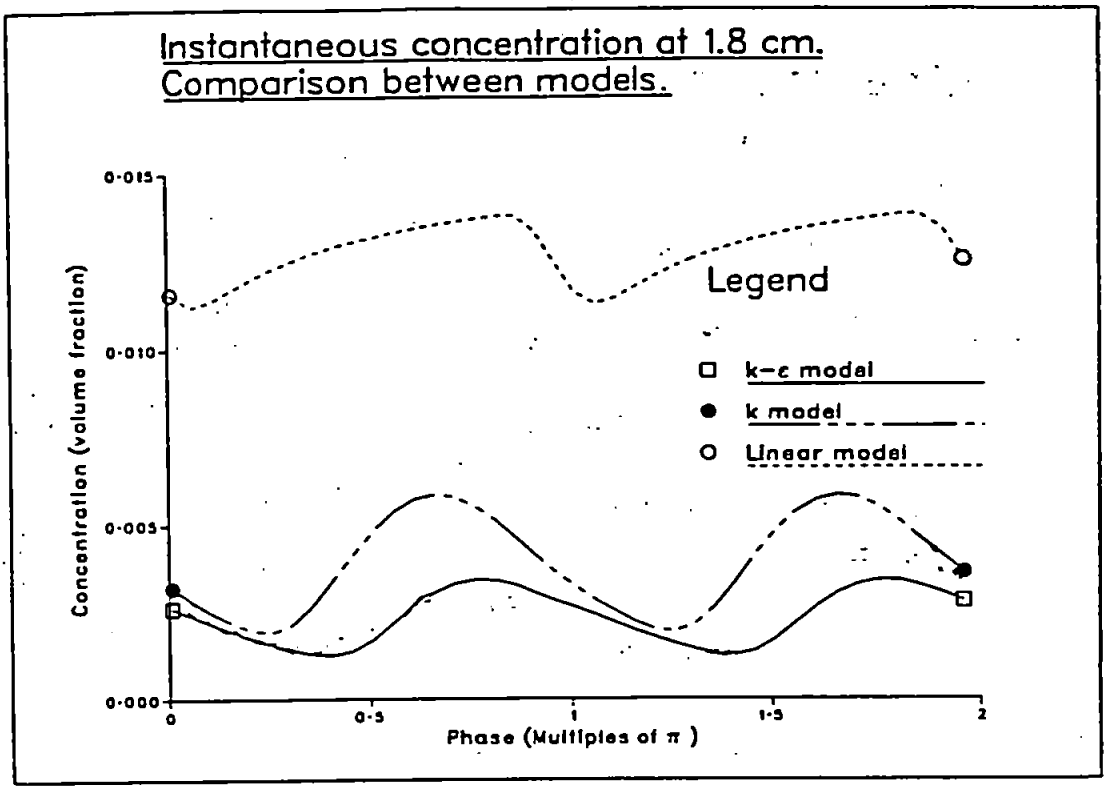

Figure 4.42:

Comparison with experiment

The experimental data of Staub et al. (1983) is presented by the authors as

1. the average concentration over the wave cycle, C, measured at different heights within a range of 1–3 cms above bed, and
2. the variation over a wave cycle of instantaneous concentration measured at a fixed height of 1.8cm.

Figure 4.43a shows a comparison of the average concentration with predictions for three representative models. The large scatter in the data is due to variations in the relative orientation of the suction tube with respect to the direction of the mean flow, and is indicative of the preliminary nature of the experimental results presented. Taking $c_0 = 0.3$ (volume fraction), as used in Hagatun & Eidsvik (1986), the $k-\varepsilon$ model appears to be in best agreement with the experimental data, while the linear model prediction is clearly not consistent with the data. Since however the reference concentration is to some extent adjustable, it should be valid to change c_0

to try and obtain a "best fit" for each model[8]. The logarithmic plot, figure 4.43b, is revealing in this instance as it shows that the lines representing the k and $k-\varepsilon$ models are roughly parallel so that multiplication by a constant will indeed bring the curves to approximately coincide. The linear curve, having a markedly different gradient, cannot be brought into agreement this way. Figure 4.44 shows the expected result, that the k model can be brought into better agreement with the data and the $k-\varepsilon$ model while the linear model cannot. We mention that it is not valid to simply multiply the $c_0 = 0.3$ solution by an appropriate factor to obtain these last curves since, for the $k-\varepsilon$ and k models, the sediment has an effect on the solution via the buoyancy terms which depend on the actual value of the concentration.

Predictions by the $k-\varepsilon$ model of the variation of concentration at a fixed height are shown, along with experimental measurements, in figure 4.46a. We note that the experimental values in the second half of the wave cycle are *not* the same as in the first half as the assumption of symmetrical oscillatory flow requires. A possible explanation for the larger peak concentration in the second half-cycle is that the experimental free stream velocity is greater, for some reason, in one direction. We should therefore take care in comparing in detail the theoretical and experimental curves. It is interesting however, that the experimental points show the same rise to a peak value followed by a more gentle decrease that is apparent in the numerical prediction. The $k-\varepsilon$ model curve also shows a very reasonable agreement in magnitude and phase with the experimental points. A more convincing test would be simultaneous agreement with concentrations measured at another height. Unfortunately, time variations of concentration at a single height only are presented in the published results of Staub et al. (1983).

In figure 4.46b we show, in addition to the experimental values and the $k-\varepsilon$ predictions, the variation given by the linear and k models ($\Delta = \delta_\omega/10$) at 1.8 cms. A reference concentration of 0.3 was used in all cases. The phase and overall shape of the k curve is similar to the experimental values and, although not shown, the two can be brought into good agreement if c_0 is set to 0.2. Clearly the linear model result is not in accord with the shape of the experimental curve, even if it could be scaled to roughly the correct magnitude. As mentioned in Section 4.1.2, the time variation of concentration in the linear model is heavily influenced by the form proposed for the variation in bottom concentration with bed stress.

[8] Although a value of $c_0 \approx 0.3$ has some legitimacy, since this was the value determined experimentally by Engelund & Fredsœ(1976) when developing the bed load model on which Hagatun & Eidsvik (1986) and hence our bottom boundary condition is based.

Finally, the effect on the mean concentration of disregarding the buoyancy terms in the $k-\varepsilon$ model is shown in conjunction with the experimental results for C in figure 4.45. The inclusion of buoyancy terms appears to improve the fit to experiment. Neglect of the Richardson number (R_f) correction in equation (3.22), as in Hagatun & Eidsvik (1986), leads to a very much smaller buoyancy effects.

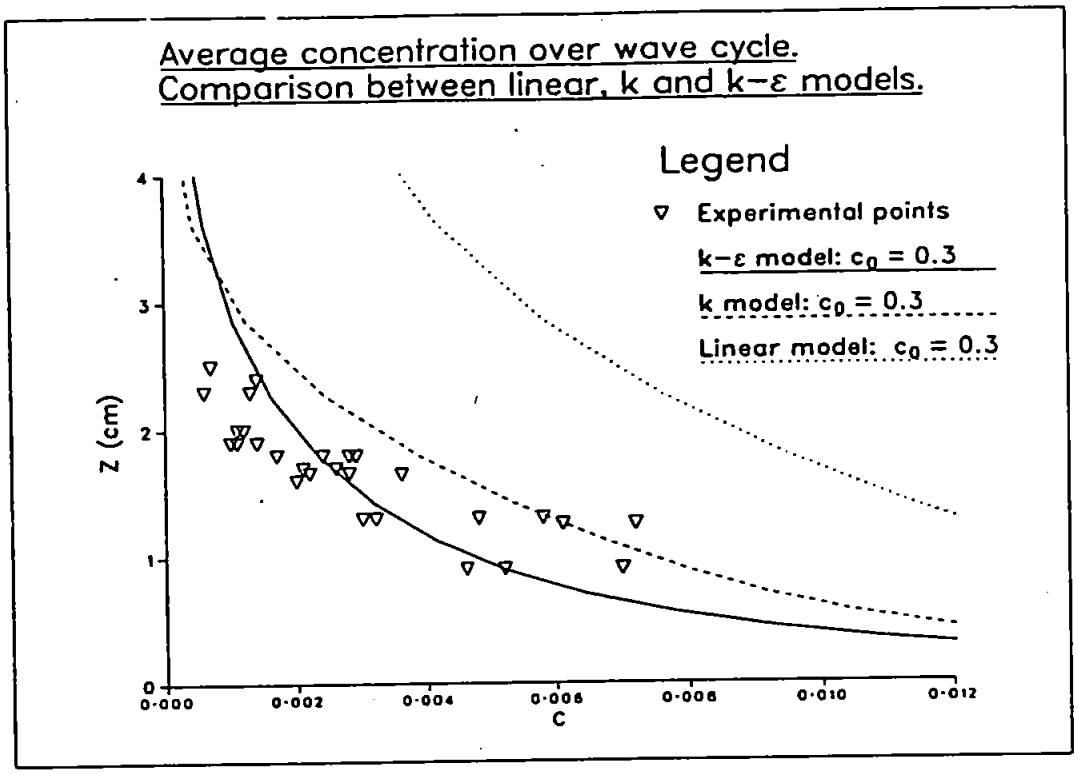

Figure 4.43a:

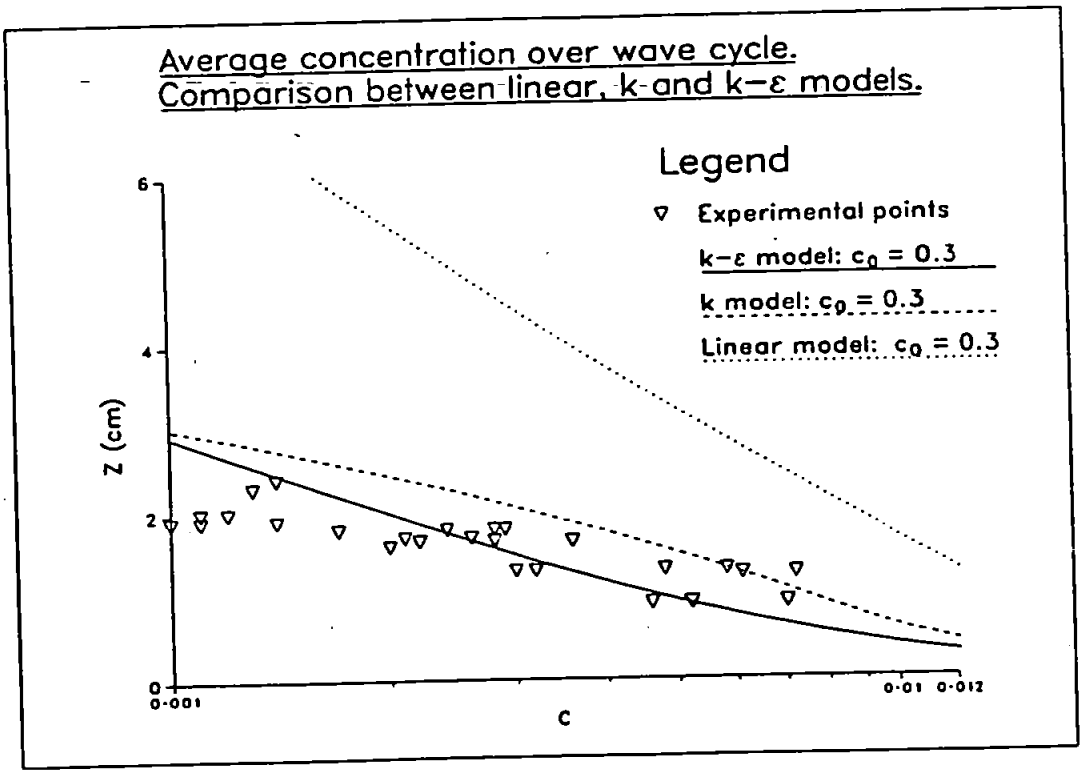

Figure 4.43b:

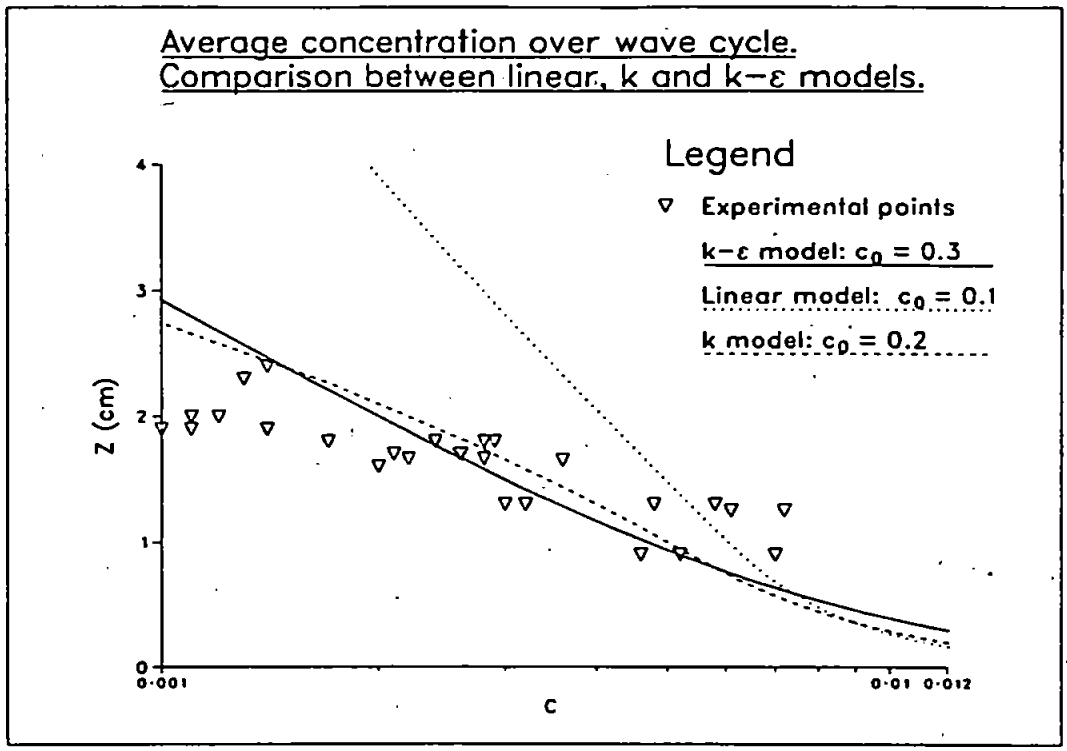

Figure 4.44:

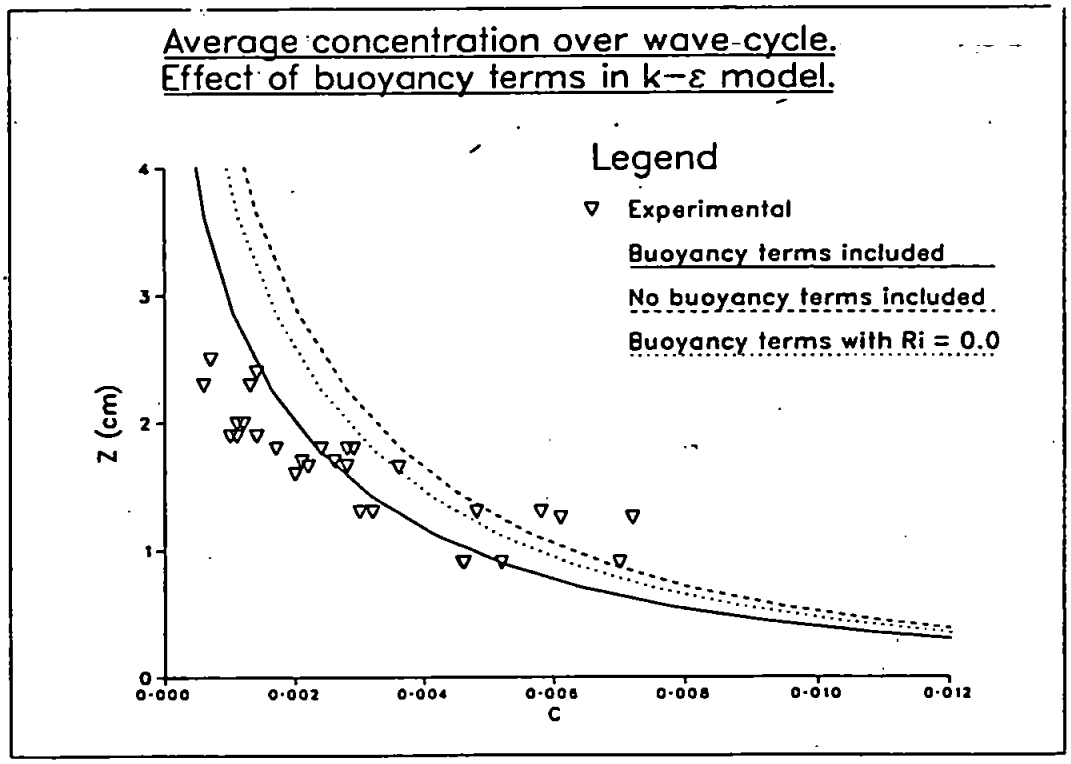

Figure 4.45:

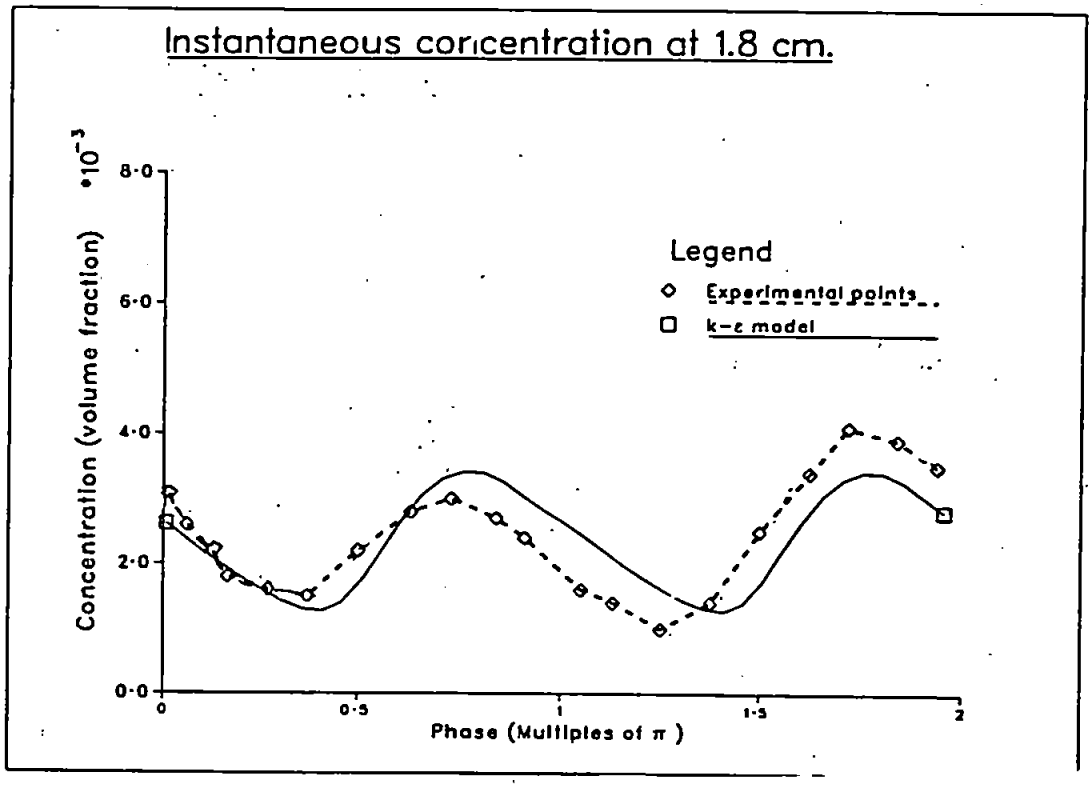

Figure 4.46a:

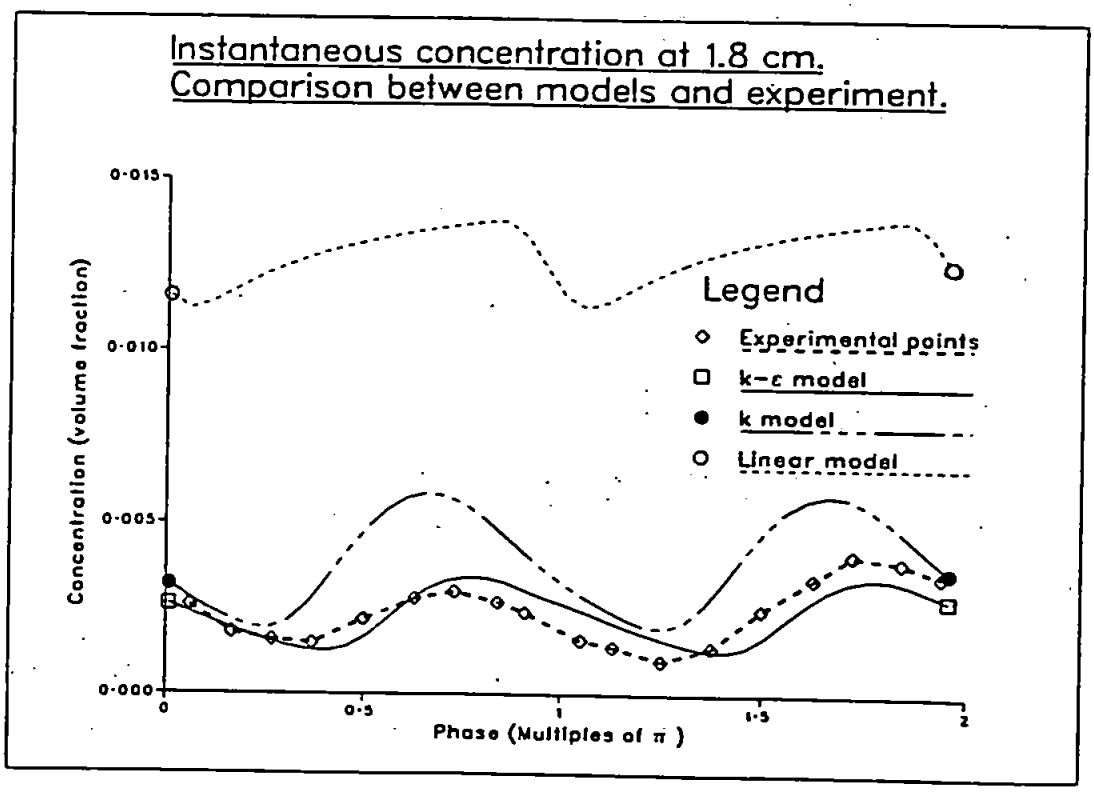

Figure 4.46b:

CPU resources

Figure 4.12 shows the number of CPU seconds per cycle required on a Prime 6350 (peak performance 11 mips) by each turbulence model, with 48 grid points and 240 time steps per cycle. Convergence criteria are as described at the beginning of Chapter 4. The numerical scheme was fully implicit, with θ set equal to one. Parameter are set to reproduce the experiments of Sumer et al. (1987). No sediment concentrations were calculated.

The anomalous result for the mixing length model arises from convergence difficulties encountered as the flow reverses and appears to be a consequence of the vanishing of the velocity gradient, and hence eddy viscosity, at the bed. The problem can be ameliorated by adding a small constant to the eddy viscosity. To completely suppress the oscillations, it is necessary to add a value at least ten times the laminar viscosity and this was found to affect the solution. With the simple numerical scheme employed, this behaviour of the mixing length model is a considerable drawback to its use.

Notable is the longer run time required by the $k-\varepsilon$ model; a consequence of the increased number of iterations required to obtain convergence as well as the greater computation required to solve the extra equation. Also as noted before, the derivative boundary condition on the turbulent kinetic energy leads to a greater number of iterations being required than for the 'stress' condition.

Model	Additional equations	CPU/cycle (secs)	CPU/time step (secs)	Iterations (mode)
Linear	0	3	0.013	0
Mixing length	0	39	0.163	17
k	1	20	0.083	6
$k-l$	1	20	0.083	6
$k-\varepsilon$	2	50	0.208	8
$k-\varepsilon$ †	2	73	0.304	12

Table 4.12: CPU resources and average number of iterations for each model. The number of iterations is the modal value over the wave cycle.

† $\dfrac{\partial k}{\partial z} = 0$ at $z_1 = z_0$.

4.3 Conclusions

First we attempt to interpret the results concerning differences between the model predictions during the accelerating and decelerating stage of the wave cycle. The following observations are of relevance.

1. An examination of the rms error for the mixing length and k models —tables 4.6 and 4.8 — shows that a different value of Δ is required to best fit the data during the accelerating and decelerating phases

2. The explicit assumption of a logarithmic law (3.33) is shown in figure 4.7 to yield a value for the friction velocity that becomes nearer to that obtained without this assumption as the wave cycle proceeds. However we must be careful in that we are making a comparison between two model predictions and not between model predictions and experiment.

3. The $k - \epsilon$ turbulent kinetic energy profiles shown in figures 4.33a and 4.33b give markedly better agreement with experimental values near the bed during the decelerating phase compared to the accelerating phase.

These points indicate that assumptions based on steady boundary layers become more valid as the wave cycle proceeds, a result that intuitively seems reasonable. This implies that it is not whether the flow is accelerating or decelerating, but simply the duration since the previous flow reversal [9] that is important. Improved predictions for the turbulent kinetic energy near the beginning of the cycle is clearly a desirable goal. It seems likely that the poor predictions are due to the flow not being in a fully developed turbulent state, as assumed by the turbulence models. Although we have not presented the results here, a preliminary test using a turbulence model with empirical corrections to account for low Reynolds number effects (Jones & Launder 1972) did not significantly improve the model predictions. A more sophisticated approach, perhaps involving transition between a laminar and turbulent regime, might be necessary.

We also remark upon an important difference between the two equations which describe the behaviour of horizontal momentum and concentration. This is the occurrence of an externally imposed pressure gradient in the momentum equation, which will dominate the balance as the effects of turbulence decrease away from the bed. This helps to explain the relative insensitivity of the velocity field to turbulence

[9] More exactly, the vanishing of the bed stress which occurs just before reversal.

model and the effects of stratification as compared to the concentration field. As a consequence, the accurate modelling of turbulence seems to be relatively unimportant for predicting velocity profiles while for the concentration it plays a significant role. However, at present the uncertainties associated with the bottom boundary condition for sediment transport problems (ie specifying c_0 and z_0) make the use of relatively sophisticated turbulence models difficult to justify.

Finally, we summarize the main conclusions of this chapter.

1. The solution is independent of the choice of the two bottom boundary conditions tried for k at $z_1 = z_0$. However the effect of applying boundary conditions at $z_1 > z_0$ and assuming an explicit logarithmic law has a considerable effect on the solution. A comparison between figures 4.6 and 4.35 indicates that the bed stress is considerably under-estimated near the beginning of the wave cycle if an assumed logarithmic law is used.

2. Where the Shields number exceeds the 'saturation' value for the majority of the wave cycle, the exact form of the bottom concentration variation with Shields number is not important. The specification of the reference concentration, which effectively scales the value of the predicted concentrations throughout the boundary layer, is however crucial.

3. Buoyancy effects are found to have a significant effect in decreasing the amount of sediment in suspension, but to have negligible effect on the mean velocity profiles.

4. If the length scale is to specified explicitly using (4.1), then the best choice for the value of Δ to fit the experimental data for all the quantities considered is not clear. For the linear model, $\Delta = \delta_\omega/20$ gives the best fit for both the mean velocity profiles and the friction velocity. Thus this value, originally proposed by Kajiura (1968), would appear to be best. For the mixing length and k models, the value of Δ required to give the best fit to the mean velocity profile changes as the wave cycle proceeds. During the accelerating stage $\Delta = \infty$ is superior, while for the decelerating stage $\Delta = \delta_\omega/20$ is best. However the best overall fit is with $\Delta = \delta_\omega/10$. As this is also the value of Δ for which the k model best predicts the concentration data, it seems a good choice for this particular model. As indicated by figure 4.20, this value is very close to the value given by (4.3) which can be determined without recourse to calculating δ_ω from the linear model. On the other hand, bed stresses are better predicted with $\Delta = \infty$ (see table 4.11) for the mixing length and k models.

5. The $k-\varepsilon$ model gives clearly superior predictions for the velocity profiles, although all models are in reasonable agreement with the data. The conclusions regarding the prediction of bottom stress, which in practice is probably of greater importance are equivocal. Figure 4.35 and table 4.11 show that for this particular data, the $k-l$ model gives the best fit.

6. The sediment concentrations are predicted well by the $k-\varepsilon$ model with a value of $c_0 = 0.3$. However equally good predictions can be obtained with the k model if c_0 is altered and, given the uncertainties associated with the values of c_0 and z_0, it is not really possible to justify the use of one model above another. The experimental data does seem to show clearly the inadequacy of the linear model, with length scale given by (3.29), for suspended sediment predictions in a wave boundary layer. It is likely that considerable improvement could be achieved in predicting the *average* concentration with this model, if the length scale value were specified to decrease with height instead of remaining fixed at a constant value. For predicting variations in concentration *within* a wave cycle, the results obtained with the linear model are more heavily dependant on the exact form chosen for variation in reference concentration with Shields number than is the case with the other models.

7. In terms of CPU resource the $k-\varepsilon$ model was found to be significantly more expensive than the simpler models. Even so, because only about six wave cycles were needed to achieve an oscillatory solution, run times were of the order of five minutes.

Chapter 5

Numerical Calculations with Particle Inertia Effects

We now present the results of taking into account the effects of particle inertia in the particle momentum equation. Before this, a further discussion of the bottom boundary condition on the concentration is required.

The results in Chapter 4 for the concentration profiles were obtained applying the bottom boundary for c at z_0, well below the top of the bed load region, and in fact within the bed itself. However, expressions for the vertical particle flux, both the the standard one (3.18), and that including particle inertia (3.17), were derived on the basis of low concentrations and the assumption that only gravitational and hydrodynamic forces act on the particles. These assumptions are not valid in the bed load region where particle concentrations are high and where forces arising from particle collisions will be important. When the standard expression for the particle flux is used the results from Chapter 4 show that reasonable agreement with experiment is found, despite the use of (3.18) in the region very near the bed where it cannot be completely valid. This may come about by the use of a bottom boundary condition which can be 'calibrated' via c_0 to ensure agreement with experiment.

A problem arises when the vertical volume flux (3.17) includes the terms associated with particle inertia. The model for the pressure-concentration correlation (2.58) contains a term proportional to ϵ/k and this ratio is found to increase rapidly as the bed is approached. Thus, a substantial effect due to this term is found to result, but in a region that we cannot expect to model. In the bed load region this is due to neglect of particle collisions as mentioned. Further, because of the logarithmic compression the first ten or so grid points are even below the level of the sand grains on

the bed and clearly variations in model concentration at these length scales have no physical meaning. To avoid misleading results when the inertia terms are included, it is clearly important to use the expression for the particle flux (3.17) only where has some validity, that is, above the bed load region. When calculating the inertia effects we therefore specified the concentration at the top of the bed load region and solved for the particle flux in the region of suspended load only. An unfortunate consequence of this is that the effect of the inertia terms is sensitive to where the boundary between bed load and suspended load is taken. However there is no accepted criteria to decide where the boundary occurs. This emphasises the need for a consistent theory that can model the complete two-phase boundary layer, including both bed load and suspended load regions. Although equations (2.8) to (2.10) may form a basis on which to do this no such theory exists at the moment, although the paper by Kobayashi & Seo (1985) is an attempt along these lines.

For steady flows at least, a number of workers have suggested formulae giving the bed load thickness. Einstein (1950) takes the top of the bed load at $2d$. Most authors have taken it to be greater than this; typically two to three roughness heights from the bed. Kobayashi & Seo (1985) allows the bed load height to vary with Shield number, although it is not stated where the expression used originates from. In our calculations the bottom of the suspended load region is taken at $z_b = 2.5d$, close to the value suggested by Einstein . Clearly this is a somewhat arbitrary choice but seems reasonable for preliminary calculations given the lack of specific and well accepted values the literature. An indication of the sensitivity of the concentration profiles to the value of z_b is given later.

Having decided where to specify the concentration when including the particle inertia, we now have to determine the value of that concentration. This was done by calculating concentrations without particle inertia, using the bottom boundary condition (3.41) applied at z_0, and simply using the value predicted by this calculation at z_b. Differences between the concentrations obtained with and without particle inertia can the be attributed solely to the effect of the inertia terms in the suspended load region.

A further complication that arises when the inertia terms are included in the vertical volume flux is that $\bar{c}$ occurs to second order. When (3.17) is substituted into (3.19) a third order differential equation is obtained. This has two consequences: another boundary condition is required, and modifications to the numerical scheme need to be made. It possible to assess the contribution of the second order term by calculating the particle flux predicted by (3.17) using the concentrations derived from

the solution without inertia (this assumes implicitly that the inertia terms represent small corrections to the "inertia less" solution). Comparison of the magnitude of the second order term with the total flux showed the former to be negligible, and hence the term is discarded. This then leaves (3.17) in a form that can very easily be incorporated into the numerical scheme already described in Section 3.2. The advection diffusion equation for the concentration, (3.63), is solved with modified advection and diffusion coefficients which, after non-dimensionalising, take the form:

$$w_I^* = w_0^*(1-\bar{c}) + \tau^*(1-\rho^{-1})\frac{2}{3}\frac{\partial k^*}{\partial z^*}, \tag{5.1}$$

$$\kappa_I^* = \kappa_T^* \left\{ 1 + \tau^* \left[(1-\rho^{-1})\frac{\varepsilon^*}{k^*}\alpha_1 + q^* \right] - \left[-\rho + (\rho-1)\alpha_3 2R\frac{k^*}{\varepsilon^*}\left(\frac{\partial \bar{c}}{\partial z^*}\right)^2 \right] \right\}, \tag{5.2}$$

where

$$q^* = -w_0^*(1+\rho^{-1}C_{vm})(f_1\frac{\partial}{\partial z^*} < c'^2 > -w_0^* f_2),$$

$$< c'^2 > = 2R\frac{k^*}{\varepsilon^*}\kappa_T^*\left(\frac{\partial \bar{c}}{\partial z^*}\right)^2,$$

$$\alpha_i = a_i + a_i' f_c.$$

The vertical particle volume flux is then

$$\bar{c}\bar{u}_2 = -\bar{c}w_I^* - \kappa_I^*\frac{\partial \bar{c}}{\partial z^*};$$

so that

$$\frac{\partial \bar{c}}{\partial t^*} - \frac{\partial}{\partial z^*}(\bar{c}w_I^*) - \frac{\partial}{\partial z^*}(\kappa_I^*\frac{\partial \bar{c}}{\partial z^*}) = 0.$$

We term (5.1) and (5.2) the 'advective' and 'diffusive' contributions to the vertical volume flux respectively.

For numerical solution, the transformation from z to ζ defined by (3.52) is performed on the above expressions.

Values of the turbulence constants appearing in the equations are listed in table 5.1.

Constant	a_1	a_1'	a_2	a_2'	a_3	a_3'	R
Value	3.0	0.5	0.33	0.0	0.11	0.0	0.8

Table 5.1: Value of turbulence constants occuring in inertia terms.

5.1 Vertical particle flux

All the calculations presented here use values of the flow parameters corresponding to the experimental setup of Staub et al. (1983) — see table 4.3. Values of d, z_0, c_0 and w_0 are as described in Section 4.1.2. For particles of radius 0.06mm, the value of τ^* was determined to be 0.0013.

First we examine the magnitude of the inertia effects by plotting the vertical particle volume flux, $\bar{c}\bar{u}_2$, with and without the inertia terms included. Figures 5.1 to 5.6 compare, for the same concentration fields, the fluxes together with the advective and diffusive contributions that comprise them. We can conclude that:

1. the inertia terms always lead to an enhancement of the particle volume flux; this is most apparent as the free-stream velocity nears its maximum;

2. this enhancement appears to be due mainly to an increase in the diffusive contribution;

3. the effects of the inertia terms are negligible above about 0.5 cm (roughly 25 roughness lengths from the bed).

The effect on the concentration profiles is shown in figures 5.7a and 5.7b. As we might expect, the enhanced particle flux gives rise to an increase in the concentration; this is apparent at all phases of the wave cycle. The effect of the inertia terms appears to be quite small for this particle size. Also shown in the same figures is the sensitivity to the height above the bed, z_b, at which the suspended load region is assumed to begin. It can be seen that the solution is not unduly sensitive to the value of this parameter.

In figures 5.8 and 5.9, concentration profiles obtained with and without inertia terms are compared with the experimental data of Staub et al. (1983). Neither value of z_b shown in figure 5.9 yields a curve which is inconsistent with the experimental points.

We now examine the effect of increasing the particle radius by a factor of two, from 0.06mm to 0.12mm. This leads to an increase in τ^* from 0.0013 to 0.0053 and an increase in the fall velocity from 0.010m/s to 0.029m/s. Other flow parameters are kept the same, except the roughness length which is modified assuming the bed to be composed of uniform sand of radius 0.12mm. This is found to lead to a boundary layer of transitional type, neither hydrodynamically smooth or rough, with z_0 equal to be 2.0×10^{-3} cm. The reference concentration at z_0 was taken to be $c_0 = 0.3$ (volume fraction). Figures 5.10a and 5.10b show that the concentration amplitude

for the larger particle size to be significantly greater when particle inertia is taken into account, although little effect is seen on the concentration phase. On the logarithmic plot of the concentration amplitude, the effect of the inertia terms is to shift the line upward, indicating that the effect of including these terms can be regarded as being equivalent to scaling the solution by a constant. The inertia effects could thus be incorporated into the specification of the reference concentration. It is also of interest to note the dependence of buoyancy effects on the particle size, also shown in figures 5.10a and 5.10b. Although the these effects are quite significant for the smaller particle size, they are seen to be negligible for the larger particles. The explanation for this lies in the value of the concentration predicted for the larger particle size. This is seen to be at least an order of magnitude less than for the finer sediment particles, leading to the buoyant production term being negligible in the $k-\varepsilon$ equations.

Reduced form for the inertia terms

Of the large number of terms included in (3.17), most are found to be negligible. Figure 5.11 indicates that only two of the terms associated with particle inertia play any role in modifying the concentration profiles:

1. the gradient of turbulent kinetic energy which models the derivative of $< v_2'^2 >$ arising from vertical component of the mean pressure gradient (3.9); this affects the advection part of the concentration equation;

2. the Π_1 term in the model for the fluctuating pressure correlation $< p'\nabla c' >$; this modifies the diffusion part of the equation.

Although we have not illustrated the result here, it was found that the wall correction factor also had a relatively minor influence on the solution. An attempt to further simplify the equations by neglecting the modification to the advective contribution entirely, as an examination of figures 5.1 to 5.6 suggests might be justified, leads to figure 5.12. Clearly, the neglect of this term is not valid if we wish to include the inertia effects. It is therefore concluded (tentatively) that the complex form of (3.17) can be replaced, for boundary layers at least, by the following modifications to the advection and diffusion coefficients

$$
\begin{aligned}
w_I &= w_0(1-\bar{c}) + \frac{1}{\gamma}\Delta\rho\frac{2}{3}\frac{\partial k}{\partial z}, \\
\kappa_I &= \kappa_T[1 + \frac{1}{\gamma}a_1\Delta\rho\frac{\epsilon}{k}].
\end{aligned}
$$

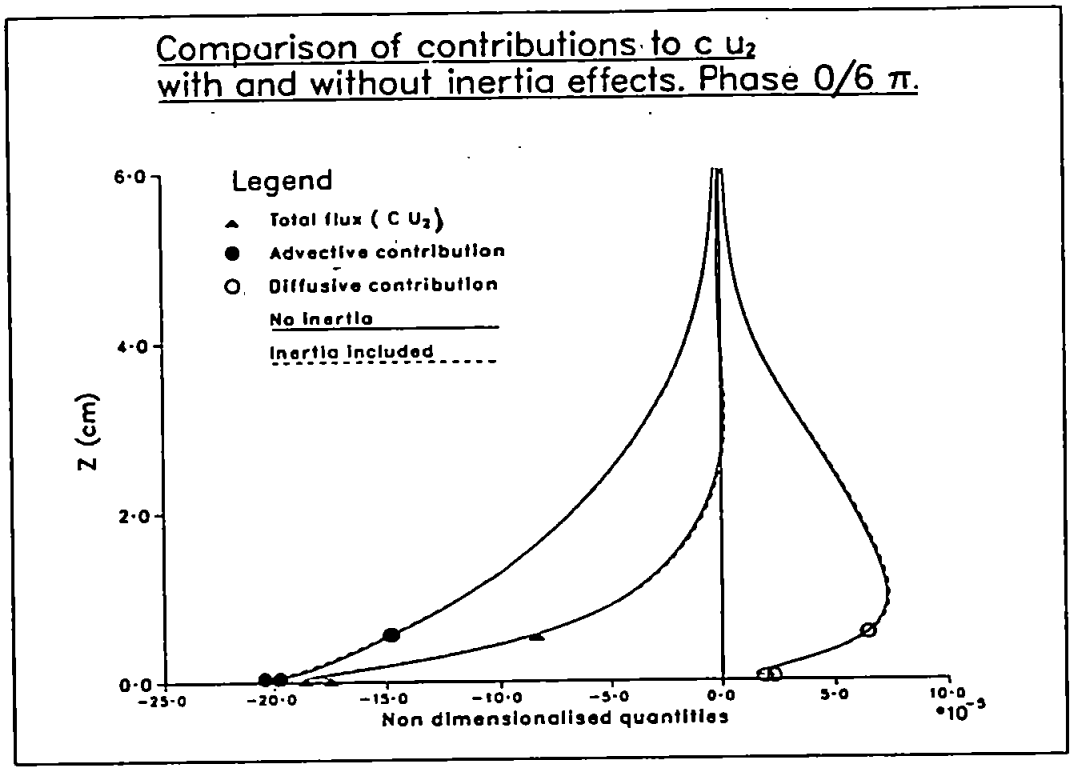

Figure 5.1:

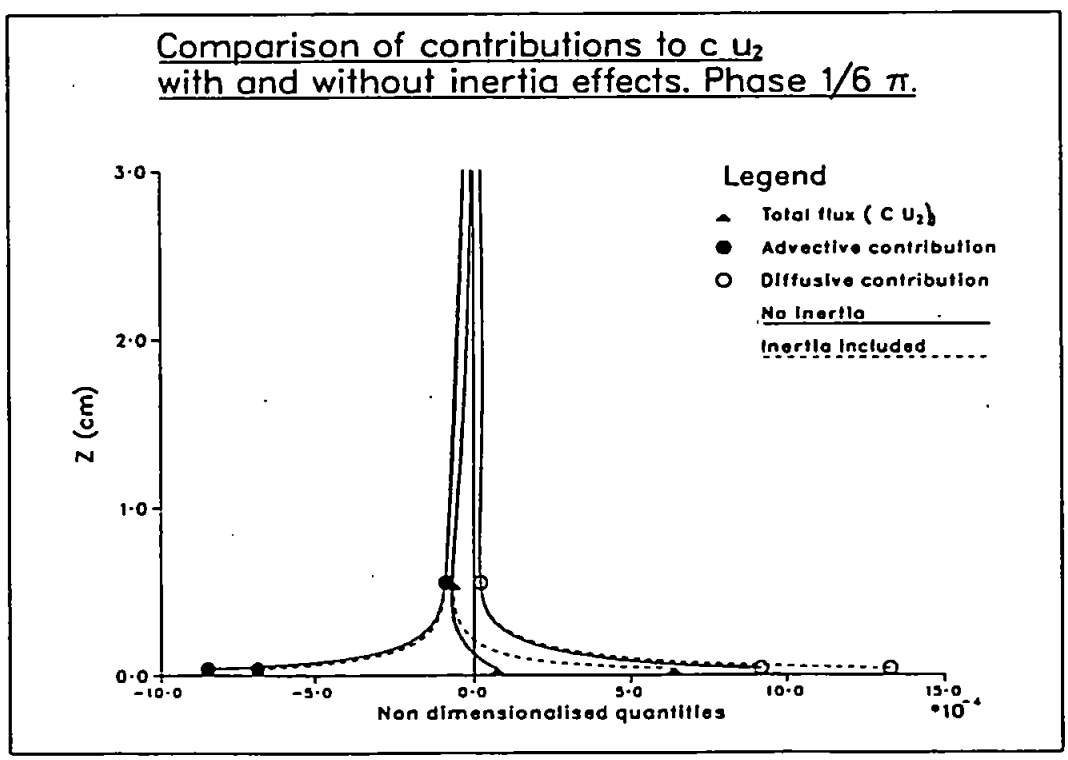

Figure 5.2:

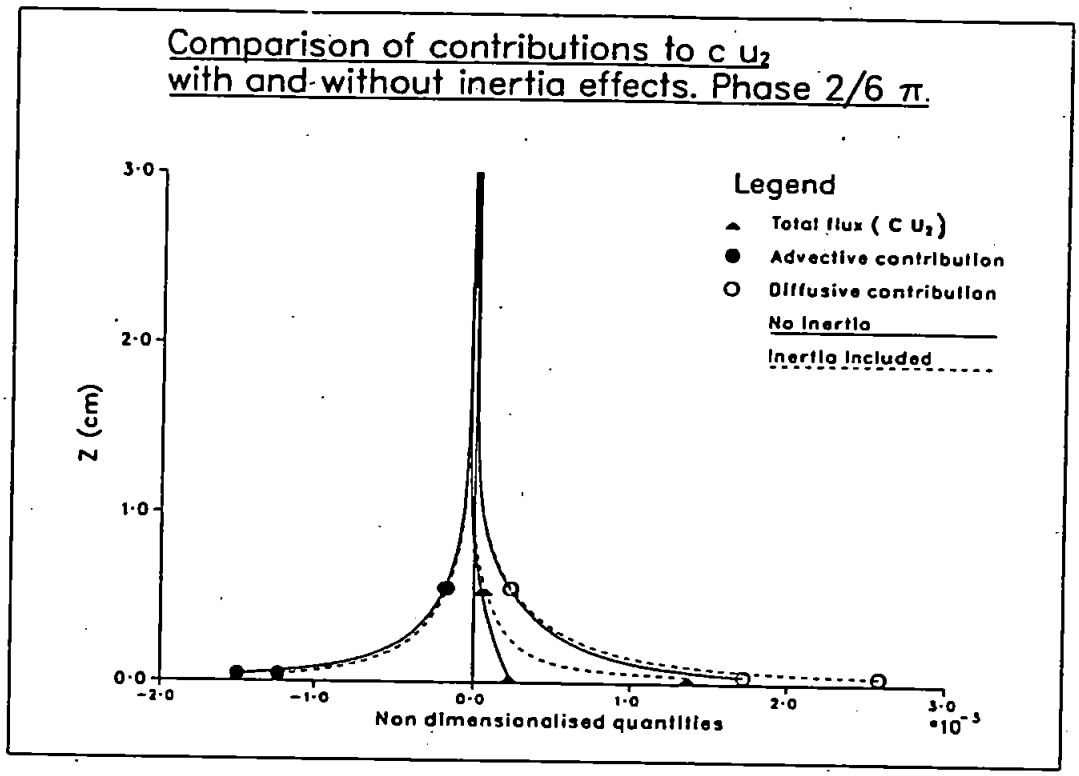

Figure 5.3:

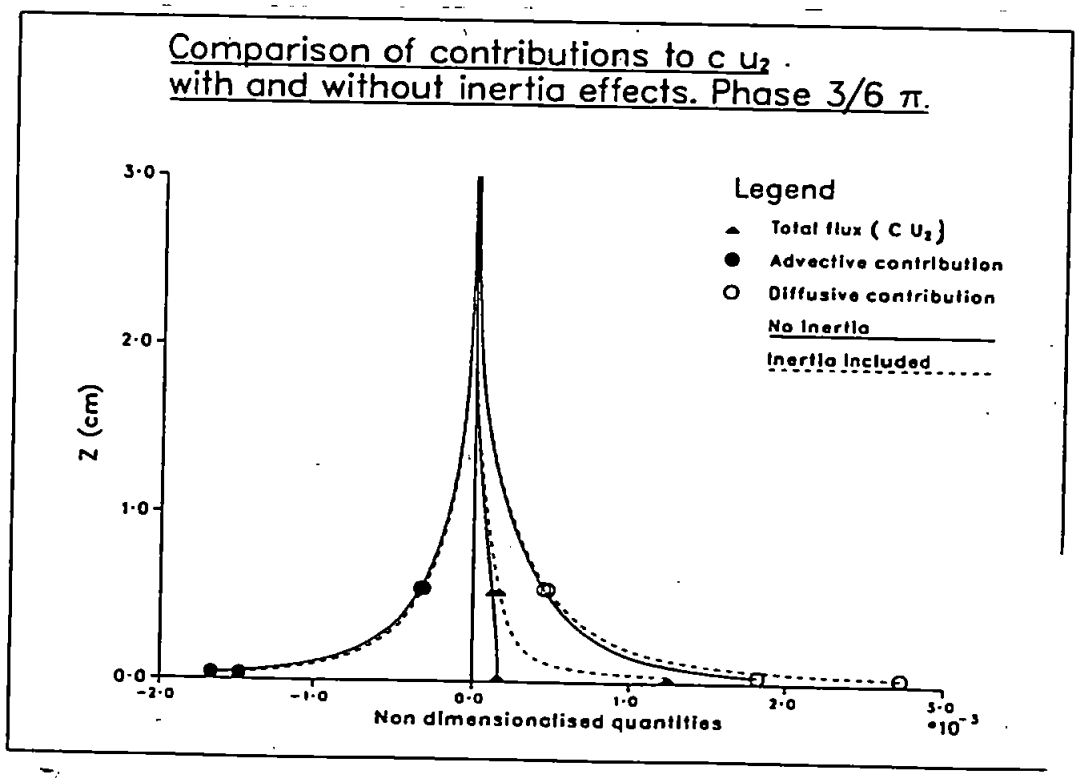

Figure 5.4:

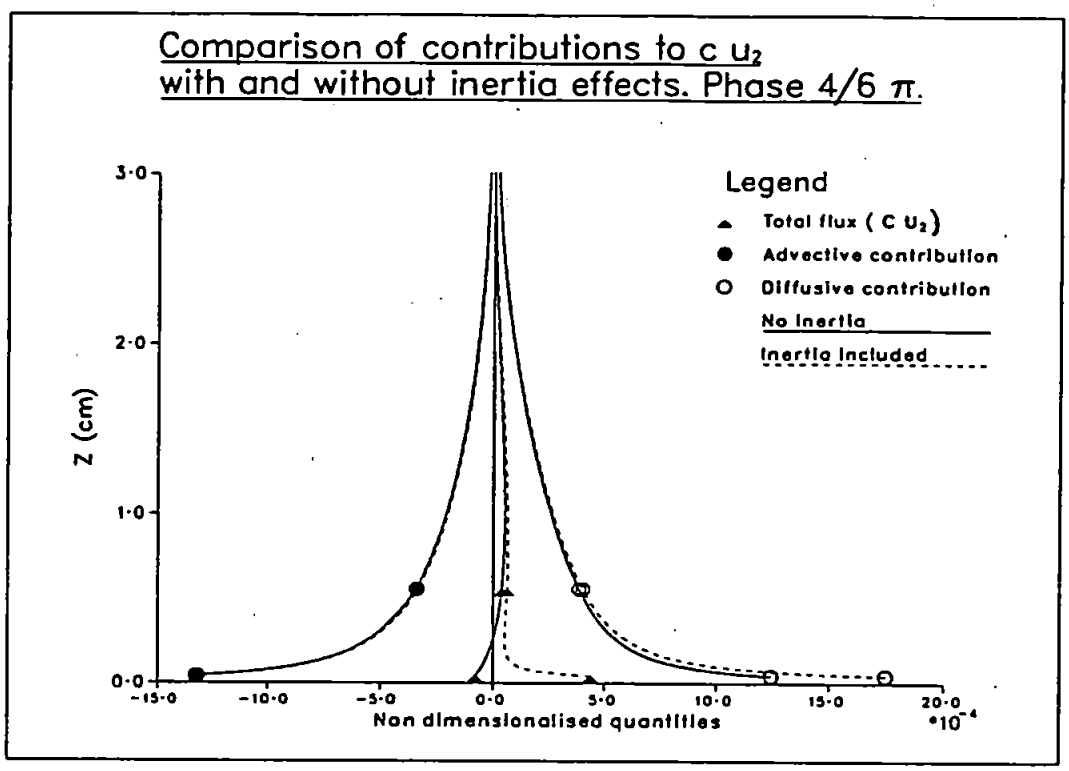

Figure 5.5:

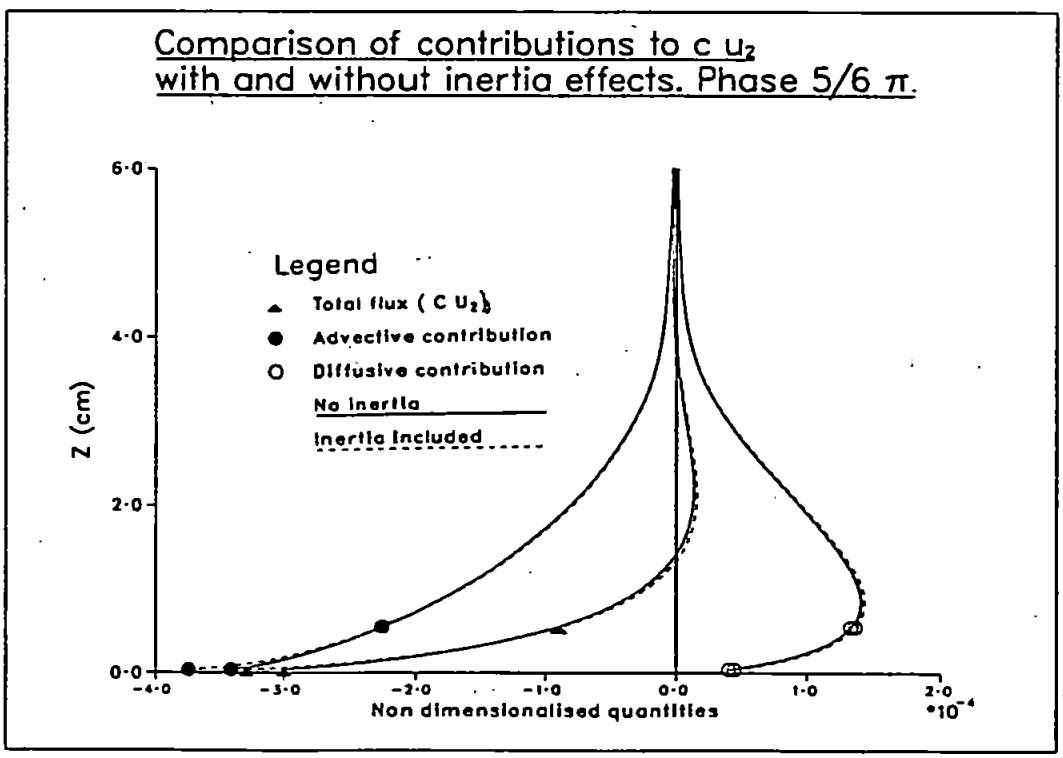

Figure 5.6:

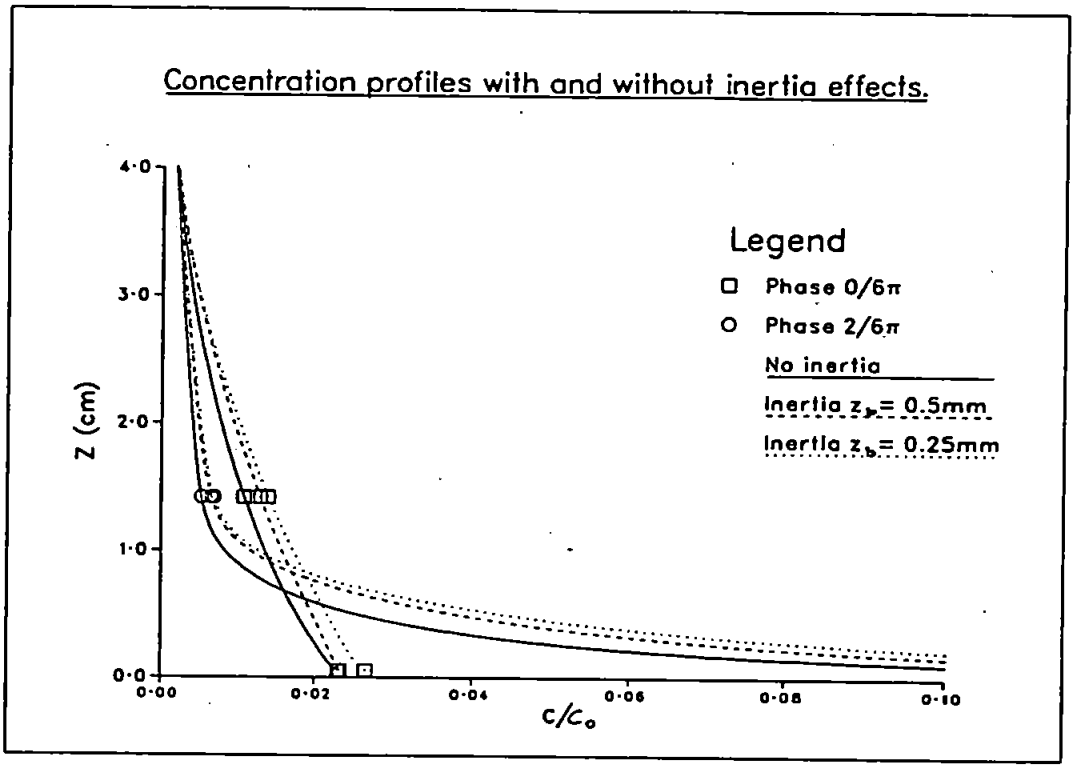

Figure 5.7a:

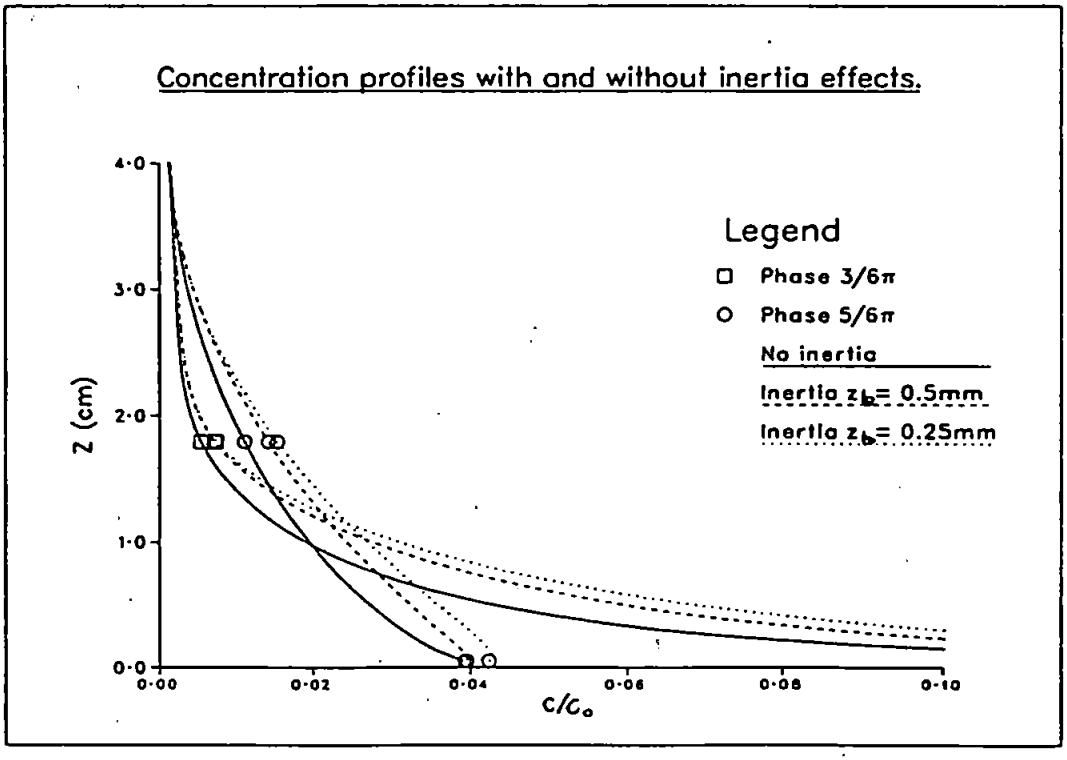

Figure 5.7b:

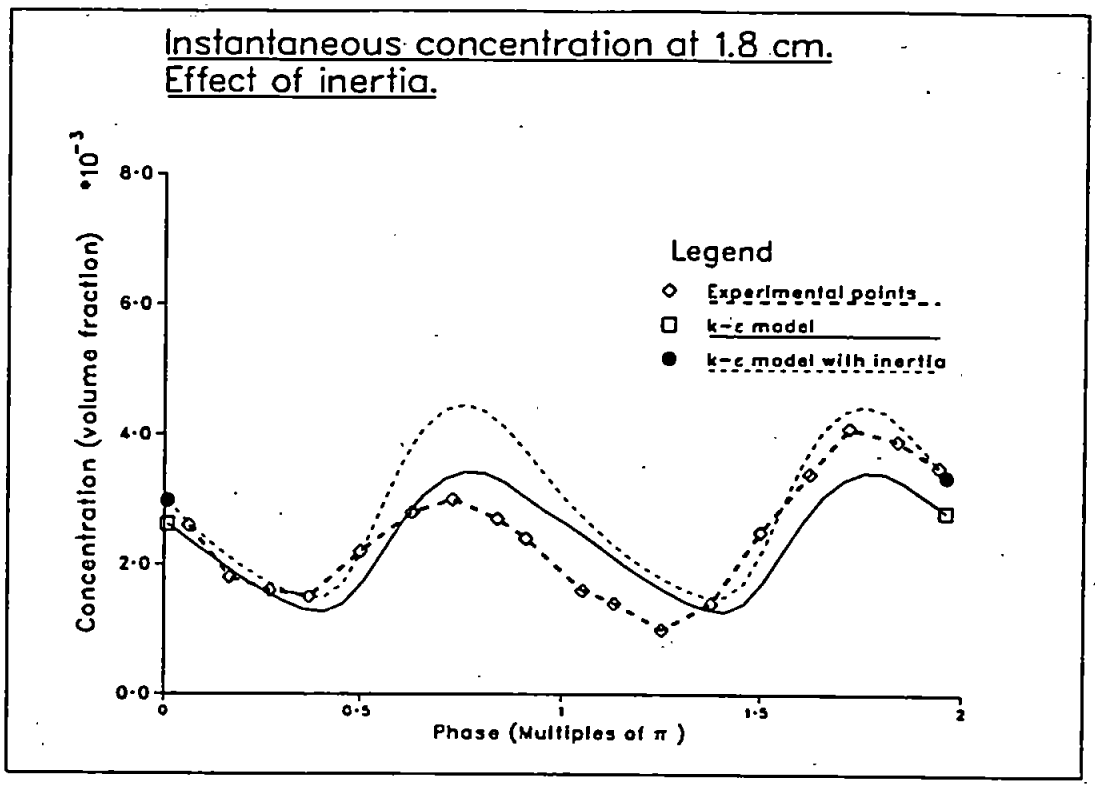

Figure 5.8:

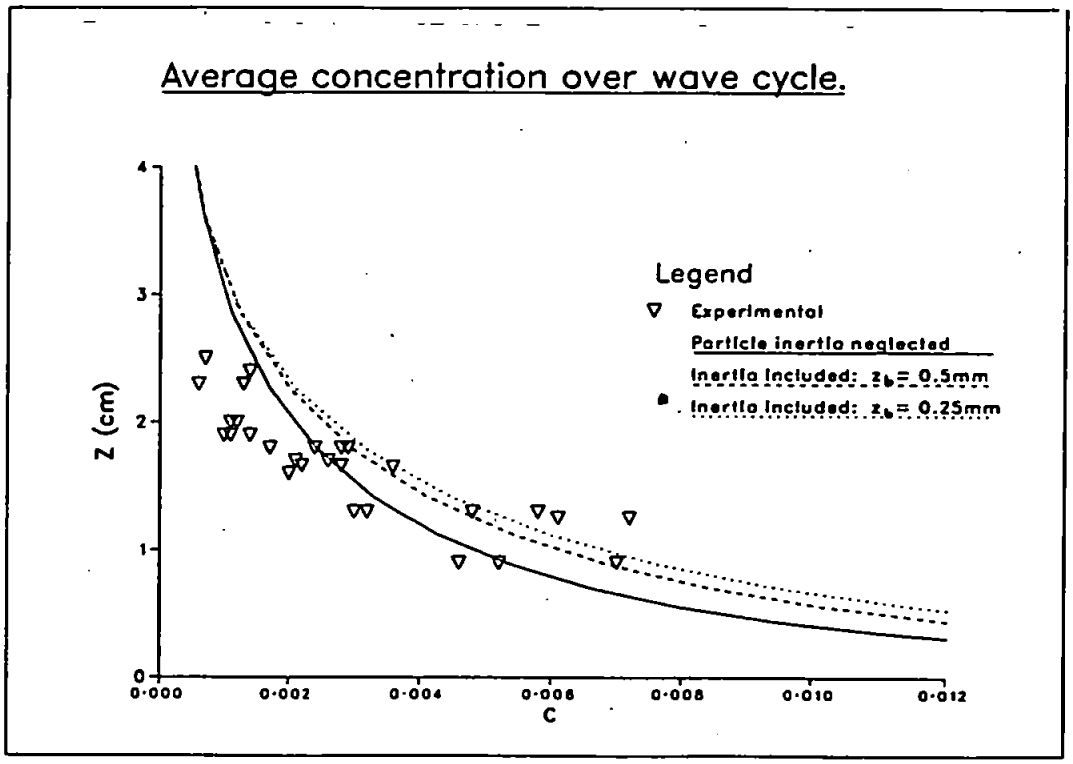

Figure 5.9:

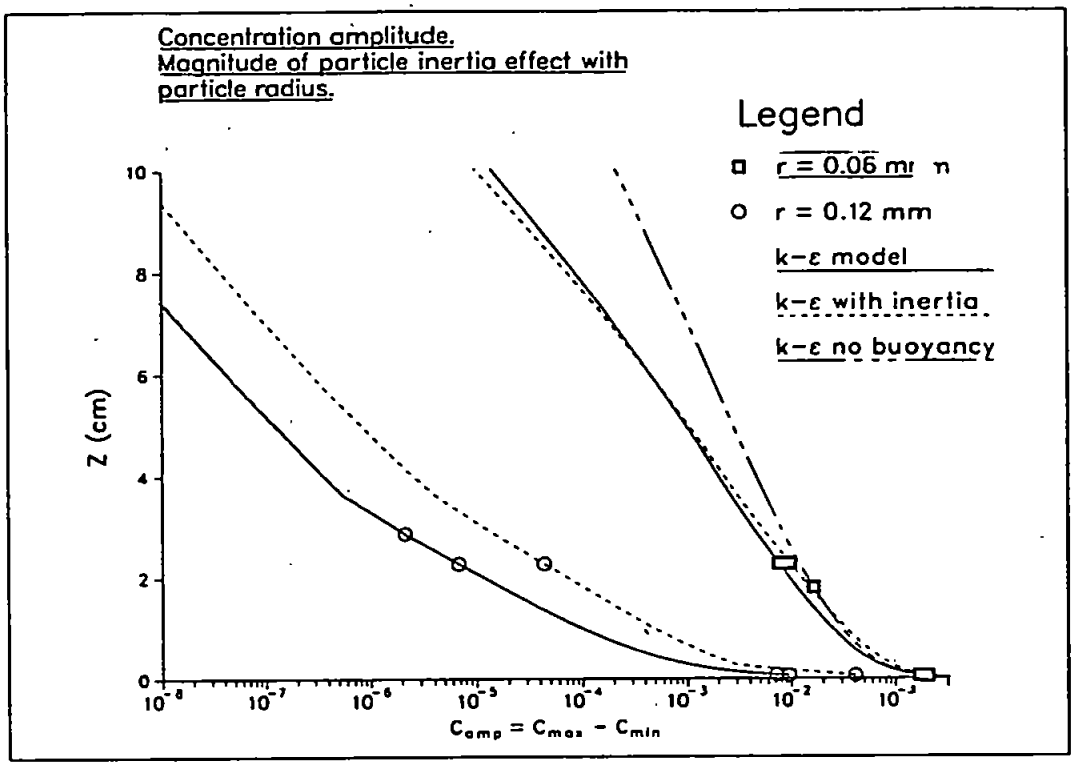

Figure 5.10a:

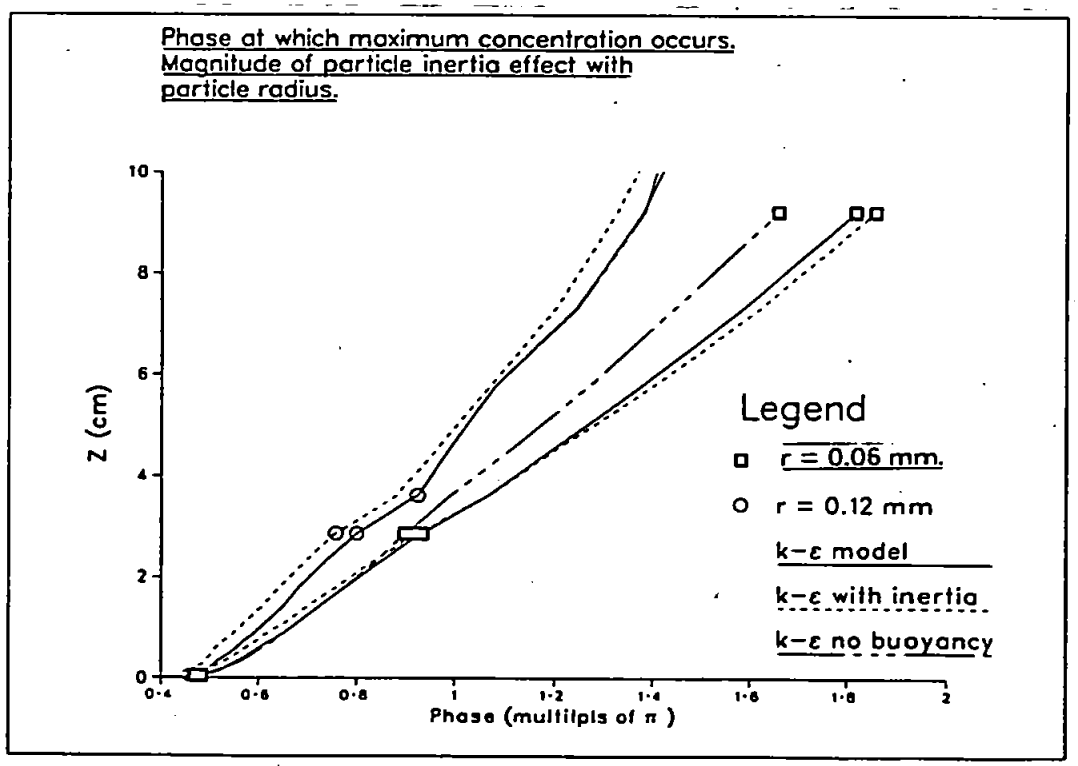

Figure 5.10b:

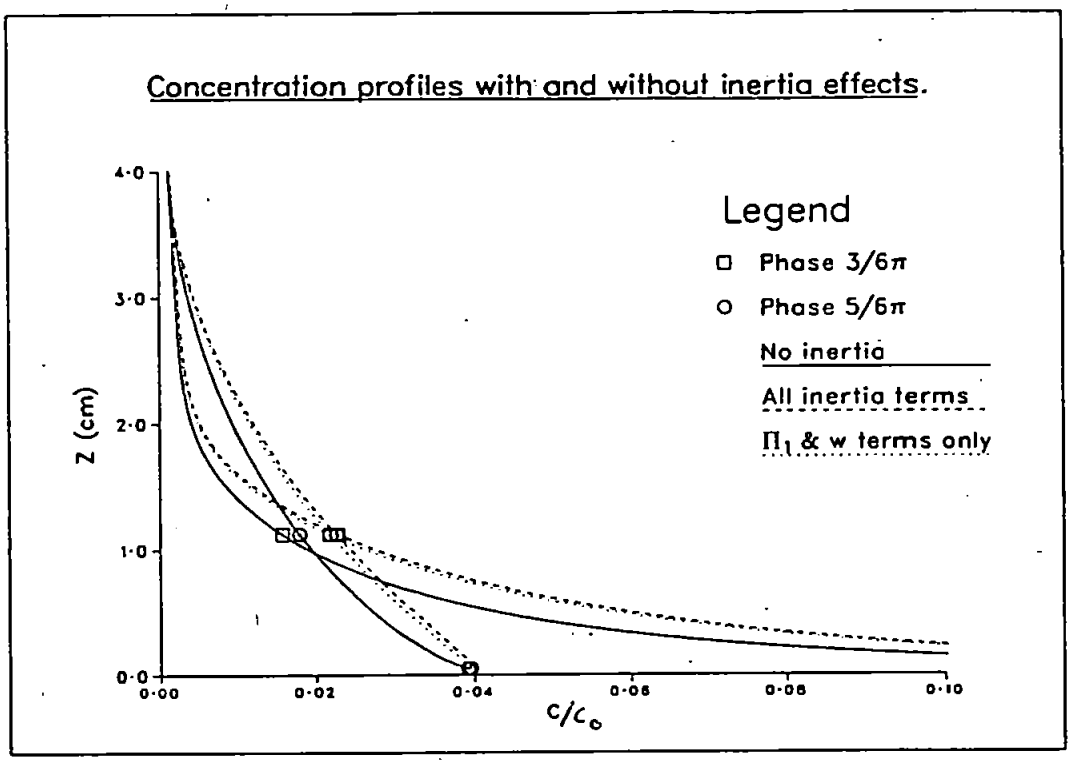

Figure 5.11:

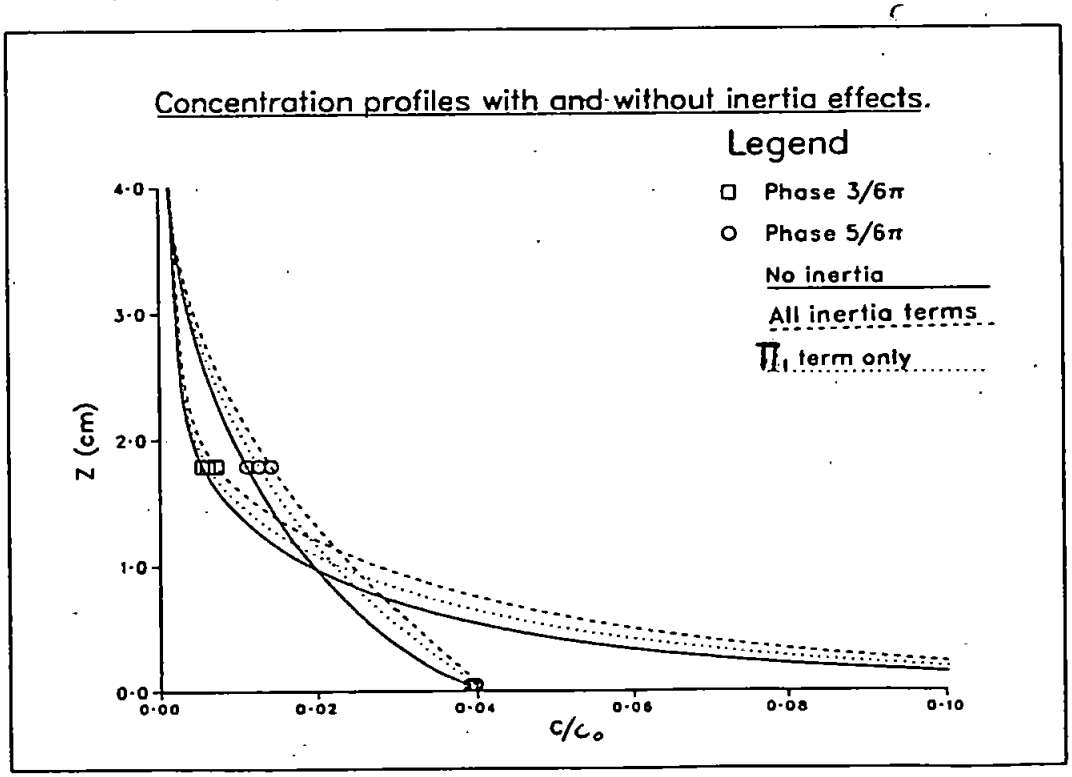

Figure 5.12:

5.2 Horizontal particle velocity

For convenience we reproduce here in non-dimensional form, equation (3.15), the horizontal particle momentum balance derived in Section 3.1:

$$\bar{c}\bar{u}_1^* = \bar{c}\bar{v}_1^* + \tau^* \left\{ \bar{c}(1-\rho^{-1})\frac{\partial P_\infty^*}{\partial x^*} + \left[\bar{c}w_0^* + (a_2 + a_2' f_c)(1-\rho^{-1})\kappa_T^* \frac{\partial \bar{c}}{\partial z^*} \right] \frac{\partial \bar{v}_1}{\partial z^*} \right\}. \tag{5.3}$$

Recall that $\bar{u}_1$ is the average velocity defined in terms of the horizontal particle flux, that is, $\bar{u}_1 = < cu_1 > /\bar{c}$. This is not the same as the direct average of the velocity defined as $< u_1 >$. Also note that with the formulation of added mass adopted, no added mass contribution appears in the above expression. The form of (5.3) is convenient in that it gives $\bar{u}_1$ explicitly in terms of quantities that are already available.

In the following figures, all quantities derived from (5.3) are shown for the supposed region of suspended load, i.e. for z greater than z_b.

First we show the non-dimensional velocity difference, $\bar{v}_1 - \bar{u}_1$, for two particle sizes. Figures 5.13a and 5.13b show profiles at different stages of the wave cycle for particles with radii of 0.06mm and 0.12mm respectively. The flow parameters have been kept identical for both particle sizes, and are those given in table 4.3 corresponding to the experiments of Staub et al. (1983). Both sets of curves show similar behaviour. It is apparent that the predicted velocity difference is always very small, even for the larger particles. During the second half of the wave cycle, during which the flow reverses, the profiles are simply the negative of those shown here. This can be anticipated from the form of (5.3). Both the pressure and velocity gradient satisfy $f(t + T/2) = -f(t)$, where T is the wave period. The coefficient multiplying the velocity gradient, which depends on the concentration field, will remain the same from one half-period to the next, once a periodic state has been achieved.

An examination of the predicted magnitude of the pressure gradient and the velocity gradient terms indicates that in the region of high shear near the bed the latter term dominates. Further away, the velocity gradient diminishes and the velocity difference is determined by the (depth independent) pressure term. This is clearly reflected in the form of the profiles for the velocity difference where a region of rapid change near the bed gives way to a velocity difference that is nearly constant with depth further away.

We now attempt to give a physical interpretation of the mechanisms involved in the behaviour described above. Away from the near-bed region, the horizontal

pressure gradient term gives rise to the (expected) result, that the heavier sediment particles lag the fluid. This leads to a positive velocity difference when the flow is accelerating and a negative one when it is decelerating. This relation is predicted to break down near the bed as a consequence of the term involving the velocity gradient. Examination of this term shows that the contribution involving the fall velocity comes from the systematic difference in acceleration given by (2.59), which itself is a consequence of (2.19). Physically this represents advection of momentum downward and so, when the velocity gradient is positive, can lead to an increase in the value of $\bar{v}_1$ sufficient to make $\bar{v}_1 - \bar{u}_1$ negative. When the velocity gradient is negative, the effect is the reverse and can be sufficient to make $\bar{u}_1$ more negative than $\bar{v}_1$ so that $\bar{v}_1 - \bar{u}_1$ becomes positive. This mechanism does not depend directly on the presence of turbulence and so should occur in suitable non-turbulent flows as well.

Some insight can be obtained by calculating the amplitude and phase of $\bar{v}_1$ and $\bar{u}_1$ as a function of z. We assume that

$$\begin{aligned} \bar{v}_1 &= a_v \cos(t^* - \phi_v) + v_{res}, \\ \bar{u}_1 &= a_u \cos(t^* - \phi_u) + u_{res}, \end{aligned}$$

where v_{res} and u_{res} are residual terms accounting for the numerical errors and higher harmonics that may be present. Higher order harmonics were found to be present in the velocity fields generated by the $k-\varepsilon$ model. The 3rd and 5th order harmonics were approximately 5% and 0.5% respectively of the principal. Amplitudes and phases for the principal fluid velocity harmonic can be found by evaluating

$$\begin{aligned} a(z) &= \frac{2}{T}\int_{t_0}^{t_0+T} \bar{v}_1(z,t)\cos t\, dt, \\ b(z) &= \frac{2}{T}\int_{t_0}^{t_0+T} \bar{v}_1(z,t)\sin t\, dt, \end{aligned}$$

where t_0 is some arbitrary start time, and setting

$$a_v = \sqrt{a^2 + b^2}, \qquad v = \arctan b/a.$$

If an exactly analogous procedure is carried out for $\bar{u}_1$, then the amplitude ratio $a_u/a_v - 1$ and the phase difference $\phi_u - \phi_v$ can be formed. These quantities are plotted in figures 5.14a and 5.14b for the two different particle sizes. Also shown is the effect of neglecting the term involving the concentration gradient in (5.3) — this

is accomplished by setting $a_2 = 0$.

As expected, both the amplitude ratio and the phase difference show a greater effect from the larger particle size. The only noticeable qualitative difference is the appearance of a maximum in the phase difference for the larger particle size. This behaviour was in fact present in the curve for the smaller particle size, but appeared very close to the bed (below z_b) and so was not plotted in figure 5.14b.

We now discuss the effect of neglecting the term involving the concentration gradient. This term comes from the Π_2 component of the model for the pressure-concentration correlation. Its exact physical interpretation is not immediately apparent. However, the following argument suggests that its effect will be small compared to the contribution from $\bar{c}w_0^*$. In form, the term multiplying the velocity gradient is the same as the vertical particle flux (3.23), except that the diffusive contribution is multiplied by $a_2(1-\rho^{-1})$. This constant evaluates to about 0.16. An examination of figures 5.1 to 5.6 shows that at best the diffusive contribution to the vertical particle flux balances the advective contribution; otherwise it is smaller. Since in (5.3) the factor multiplying the concentration gradient is much less than one, we expect overall the $\bar{c}w_0^*$ term will always be larger. This is verified in figures 5.14a and 5.14b where the broken curves show the result of setting $a_2 = 0$. As can be seen, the term affects the results only slightly, tending on the whole to decrease the difference between the fluid and particle velocities. It is interesting to note that, if the concentration gradient term is neglected, one obtains

$$\bar{c}\bar{u}_1 = \bar{c}\bar{v}_1 + \frac{1}{\gamma}\left[\bar{c}(1-\rho^{-1})\frac{\partial P_\infty}{\partial x} + \bar{c}w_0\,\frac{\partial v_1}{\partial z}\right].$$

This is the relation that would be obtained from (2.60) by dividing through by c and applying the turbulent average to obtain an equation for the 'true' (i.e. not concentration weighted) horizontal particle velocity.

At present no experimental measurements appear to be available to ~~to~~ validate the numerical predictions obtained using (5.3). Some measurements of sediment particle velocities have been made in the *bed load* region for oscillatory flow by Horikawa et al. (1982). Unfortunately, these are not relevant to the suspended load region.

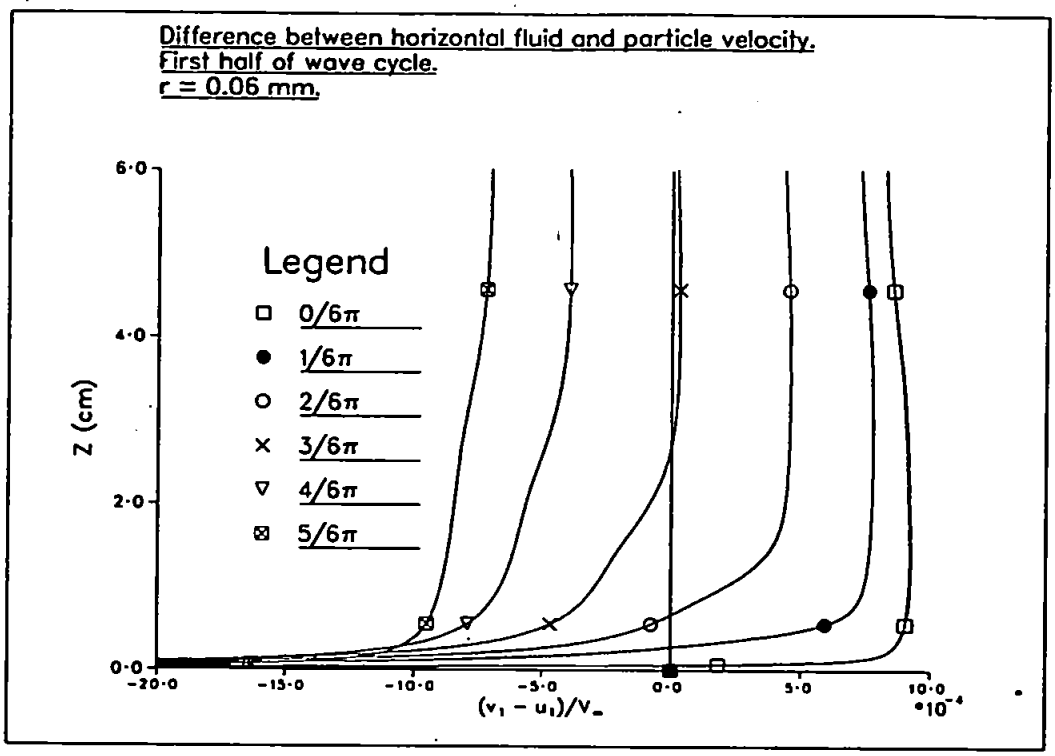

Figure 5.13a:

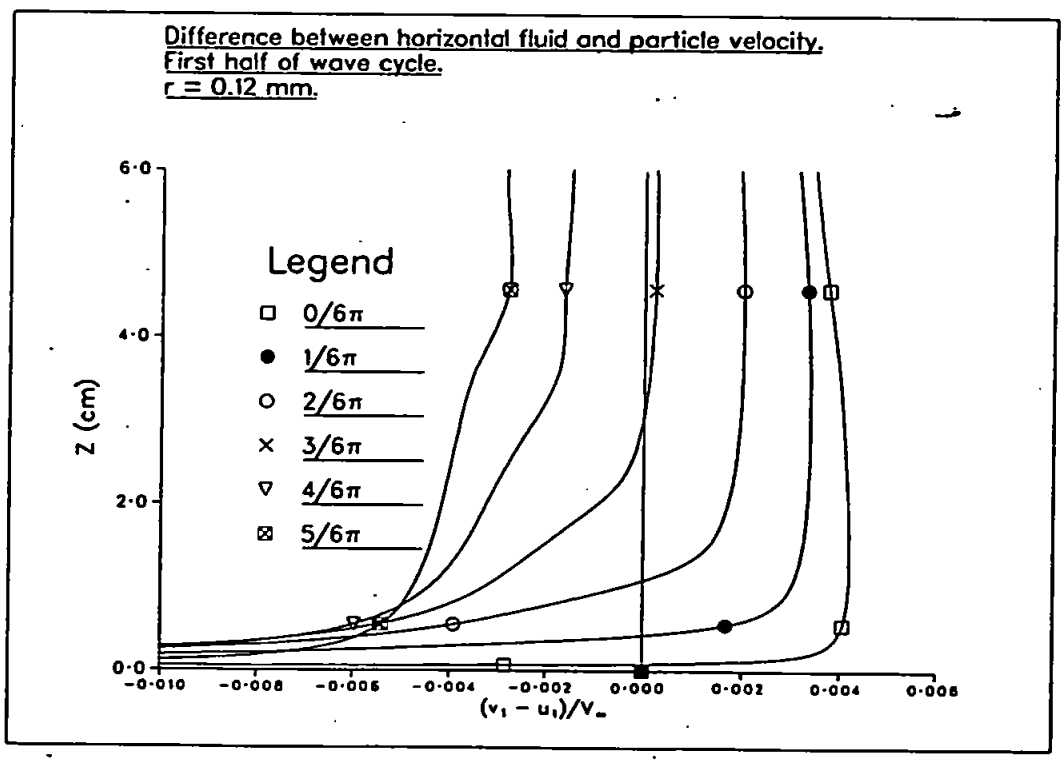

Figure 5.13b:

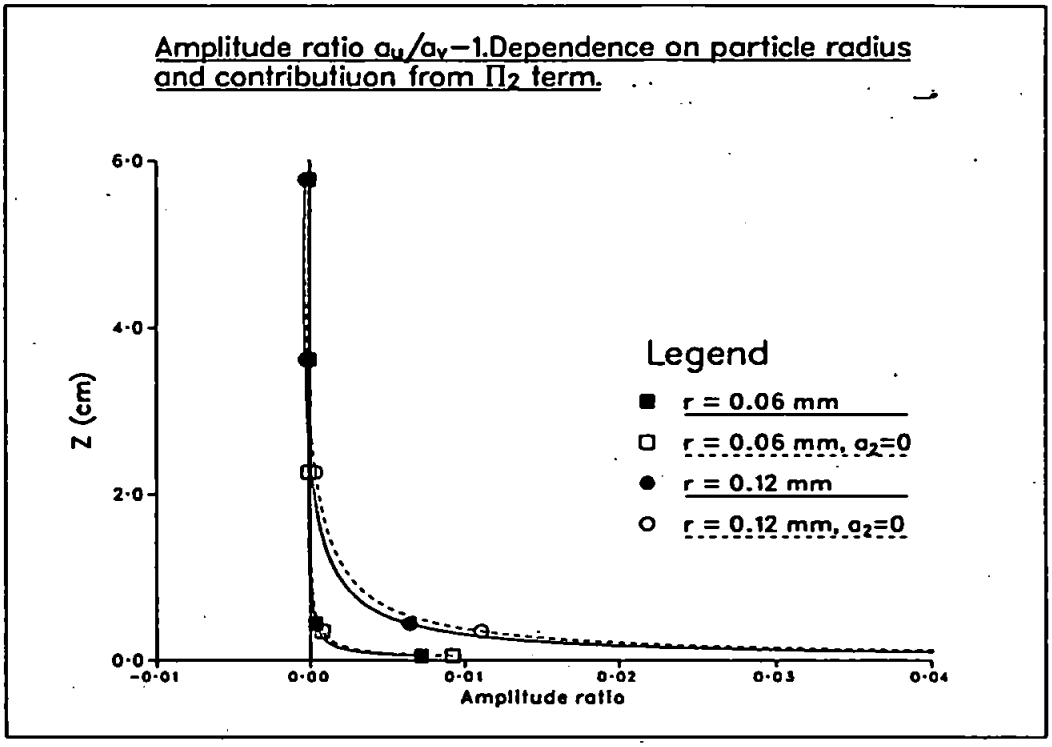

Figure 5.14a:

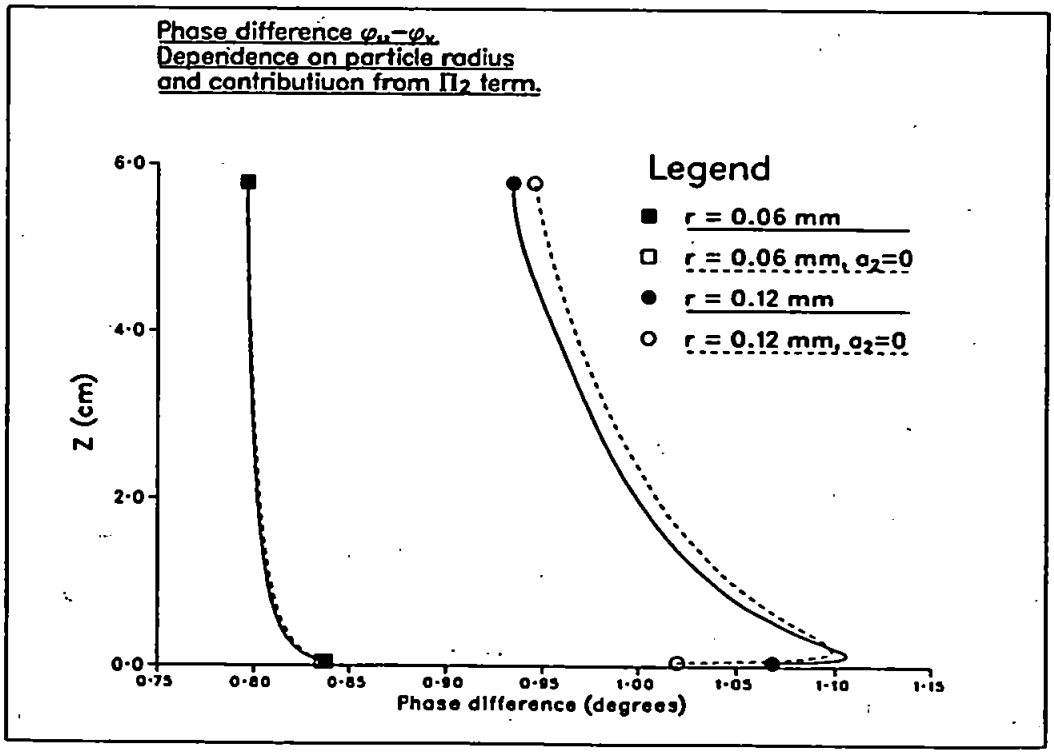

Figure 5.14b:

5.3 Discussion and Summary

As regards the effect of particle inertia on the vertical diffusivity, it is clear that some uncertainties exist. The important term appears to to be the Π_1 part of the pressure-concentration correlation, and there is the question of the the suitability of the expression used to model this term. For a (steady) atmospheric boundary layer, where temperature rather than concentration is the scalar, the general behaviour of the model expression (2.58) agrees with experimental measurements (Gibson & Launder 1978). The performance of the model in the unsteady flow, very close to the boundary, where we have applied it is unknown and would probably be extremely difficult to determine experimentally.

If we accept that the form of the expression for Π_1 is adequate, a second difficulty is the poor prediction of k, and therefore probably ε/k, by the present $k-\varepsilon$ model at the early stages of the wave cycle (c.f. figure 4.33a). It is apparent that we can hope for qualitative predictions only for the effect of the inertia terms as a consequence of this.

Even if the modelling of the pressure-correlation gives qualitatively correct behaviour, then a final problem is the rapid increase in the magnitude of ε/k as the bed is approached. As discussed at the beginning of the chapter, this makes the predictions sensitive to the point at which the inertia terms are "switched on".

Finally, we note that although we have accounted for the effects of inertia in the equations of motion for the particle phase, the inertia also has an effect on the turbulent particle flux $< c'v' >$. This can be accounted for by including inertia terms in the equation for the turbulent particle flux, as in Shih & Lumley (1986). These authors carry out a numerical calculation of particle dispersion for a steady, free-shear mixing layer which highlights the importance of the so-called "crossing trajectory" effect. This arises not from the particle inertia, but from the particle fall velocity which leads to an additional term in the equation for the turbulent particle flux. The effect of this term is to decrease the correlation between c' and v_2'. For the case considered by Shih & Lumley , the magnitude of the effect was found to be significant and greater than that of particle inertia.

Because of the difficulties and limitations mentioned above, the results of this chapter need to be regarded as preliminary in nature. However two conclusions seem justified by the results presented.

1. The effect of the particle inertia, when included in the particle momentum equation has the effect of enhancing the vertical particle flux. This can be

inferred quite generally from equation (5.2), assuming that the ϵ/k term, which comes from Π_1, is the dominant term;

2. Two regimes are apparent in the curves for the difference in horizontal velocity between fluid and particles. Away from the bed, the horizontal pressure gradient term determines this difference, leading to $\bar{v}_1 - \bar{u}_1$ being positive when the flow is accelerating and negative when it is decelerating. Near the bed the sign of $\bar{v}_1 - \bar{u}_1$ is determined by the sign of the mean velocity gradient via a term representing the vertical advection of particle momentum due to the particle fall velocity.

Chapter 6

Conclusions

Two aspects of the modelling of sediment transport processes have been considered; the relative merits and capabilities of various levels of turbulence closure in describing oscillatory boundary layer flows, and the use of continuum mixture theory to provide a base for the development of a satisfactory description of suspended sediment transport. We here draw some final conclusions regarding these two areas in the light of the results presented in the previous chapters, and then discuss possible extensions and further work.

The results obtained for mean velocity profiles using the two-equation $k-\varepsilon$ model recommend its use, particularly if good quantitative agreement with experiment is sought. For the equally important task of predicting bed stress the conclusions are more equivocal, partly because the experimental data appeared less reliable for this quantity, although again the $k-\varepsilon$ model gives good results. When we consider the modelling of suspended sediment, it is clear that the uncertainties in specifying the reference concentration and the appropriate roughness length make the use of relatively sophisticated turbulence closures less easy to justify. Simple linear models, in which the eddy viscosity is prescribed and constant over a wave cycle, are particularly dependant on the form of the bottom boundary condition since this is the only means by which a time variation enters into the solution. This would appear to make them less suitable, compared to other models, for the investigation of time dependant effects in wave boundary layers.

Stratification due to the presence of suspended sediment is predicted to have some effect on concentration profiles, although virtually none on the mean velocity. An advantage in using the $k-\varepsilon$ model is that buoyancy effects have been included in the formulation of the model by workers in other fields and tested against experimental

measurements. The direct verification of some of these results for the case of an oscillatory boundary layer would however be desirable. Uncertainties associated with the reference concentration might be avoided by using experimentally determined values of concentration taken very near the bed as model boundary conditions.

Turning now to a consideration of the other main topic presented in this work, we note that a number of problems exist concerning the foundations of the two-phase flow equations. Although recent work by Geurst (1986) represents a significant advance, the underlying justification of the equations is not perhaps as secure as one would like. Despite this, the use of mixture theory as a basis for formulating the fundamental relations governing sediment transport processes seems to offer considerable promise. Although appearing to yield complicated expressions, this is mainly true only if the effects of particle inertia are to be included. For many sediment types the neglect of inertia appears to be well-justified and, in the limit of dilute particle concentrations, the equations yield standard expressions for the particle volume flux. In addition, neglect of particle inertia and the assumption of low concentration, leads to fluid momentum, turbulent kinetic energy and dissipation rate equations which are again standard, the effects of suspended sediment giving rise to buoyancy type terms. This justifies the use of conventional turbulence closures for describing two-phase flows of the sort encountered in the modelling of suspended sediment. Thus the conventional approach is seen to emerge as a well-founded approximation to a more complete theory, as opposed to being derived in a manner that contains within it a number of implicit assumptions (essentially embodied in the result (2.19)).

Important as this is from a theoretical standpoint, the relative complexity of the mixture theory formulation is likely to limit its use in practice to situations where more simple approaches fail. Two situations suggest themselves as examples of this. One such situation, and the one we have begun to address in this thesis, is where the particle inertia begins to have an effect on the diffusivity; indications are that this may be important for particles of diameter greater than 0.25 mm. The other situation is where the assumption of dilute concentrations is no longer valid, as for example in the bed load region. This case will require, in addition, a consideration of forces due to particle interactions (collisions) and which will have to be modelled. The equations derived from mixture theory should provide the correct framework in which to introduce such models.

Moving on now to a consideration of further work, we discuss first the modelling of turbulent boundary layers then work concerned with continuum mixture theory.

In the context of marine hydrodynamics and sediment transport, the use of tur-

bulence closure schemes needs to be applied to the important area of wave-current interaction. Even more so than for the wave only case, successful quantitative agreement with experimental measurements is most likely to come from the use of relatively sophisticated turbulence models. The empirical specification of a turbulent length scale is not obvious in a situation where two distinct flow regimes are being superimposed and turbulence models which have the ability to do without such information have clear advantages over those that do. Given the well documented success of the $k-\epsilon$ model in other contexts, it is likely to prove a useful tool in the prediction of wave-current interaction effects.

Several aspects of the work on mixture theory require further investigation and improvement; in addition a number of extensions can be considered. Incorporation of further terms into the two-phase flow equations to describe additional forces known to act on particles is a possibility, although this would further complicate the equations. Various lift forces for example are postulated to be important close to the bed. A better approximation for the turbulent average of the non-linear drag law is desirable as the form we use does not account for $O(\tau^*)$ effects. An investigation of steady, fully developed turbulent flows, rather than the oscillatory flows considered here, would be an obvious step for considering the effects of particle inertia. Apart from simplifying the equations, a more important advantage in studying such flows is the greater confidence that can be placed in the models for turbulent quantities. In particular, the pressure-scalar correlation (2.58) and the turbulent kinetic energy equation. To account properly for inertia it is also necessary to consider the scalar flux equation for $< c'v' >$, since this too is affected by particle inertia (see Shih & Lumley 1986). In addition this would allow the importance of the crossing trajectory effect (Lottey et al. 1983) to be investigated in the context of the transport of suspended sediment.

References

Anderson T.B. & Jackson R. (1967), *Ind. Engng. Chem. Fund*,**6**, 527-539.

Anderson T.B. & Jackson R. (1968), *Ind. Engng. Chem. Fund*,**7**, 12–21.

Arai M. (1980), *Nucl. Sci. Eng.* ,74, 77–83.

Aukrust M. & Brevik I. (1985), *ASCE J. Waterway, Port, Coastal & Ocean Eng.* **111(3)**, 525–541.

Baer M.R., Benner R.J., Gross R.J. & Nunziato J.W. (1983), *Jour. Appl. Mech.*,**38**, 1–7.

Bakker W.T. (1974), *Proceedings 14th Coastal Eng. Conference*, Coppenhagen,**2**, 1129–1148

Bagnold R. A. (1966), *U.S. Geological Survey, Professional Paper*,**422-I**, U.S. Dep't of the Interior, U.S. Gov't printing office, Washington D.C.

Barenblatt G. I. (1953), *Zhurnal Prikladnoi Matematiki i Mechanik*, **17 (3)**, 262–265.

Batchelor G.K. (1967) *Introduction to Fluid Dynamics*, Cambridge University Press.

Bedford A. & Drumheller D.S. (1978), *Arch.Rational.Mech.Anal.*, **68**, 37–51.

Bedford A. & Drumheller D.S.(1983), *Int. J. Engng. Sci.*, **21 (8)**, 863–960.

Bedford A. & Ingram J.D. (1983), *Jour. Appl. Mech.*,**38**, 1–7.

Bogardi J. (1974), *Sediment Transport in Alluvial Streams*, Academiai Kiadu, Budapest, Hungary.

Bradshaw P., Cebeci T. & Whitelaw J. H. (1981),*Engineering Calculation Methods for Turbulent Flow*, Academic Press.

Brevik I. (1981), *Journal of the Waterway Port Coastal & Ocean Division ASCE*, 107, WW3, 175–188.

Capriz G. & Giovine P. (1987), *Arch.Rational.Mech.Anal.*, 115–122.

Carley J. F. & Al-Taweel A. M. (1971), *Chem. Eng. Progr. Symp.* Ser. No. 116, 67, (114).

Clifte R., Grace J.R. & Weber M.E. (1978), *Bubbles Drops and Particles*, Academic Press.

Dekeyser I. & Launder B. E. (1983), *Turbulent Shear Flows* 4, Springer-Verlag, Berlin.

Delhaye J. M. (1977), *Two-Phase Flows and Heat Transfer*, Ed S. Kakac & F. Mayinger, Vol 1, Hemisphere, Washington D.C.

De Vantier B.A. & Larock B.E. (1983), *Jour. of Hydraulic Eng.*, 109, (12), 38–44.

Drew D.A. (1971), *Studies Appl. Math*,L(2).

Drew D.A. (1975), *Jour. of Applied Mechanics*, 42, 38–44.

Drew D.A. (1976), *Jour. of Applied Mechanics*, 98(4), 543–547.

Drew D.A. & Lahey R.T. (1987), *Int.Jour.Multiphase Flow*, 13(4), 113–121.

Drew D.A. & Segal L.A.,(1971), *Studies Appl. Math.*,L(2), 205-231.

Dyer K. R. (1986), *Coastal and Estuarine Sediment Dynamics*, John Wiley & Sons.

Einstein H. A. (1950), *Soil Cons. Serv. U.S. Dept. Agric. Tech. Bull*,1026.

Engelund F.A. & Hansen E. (1967), A monograph on sediment transport in alluvial streams, *Tek. Forlag*, Copenhagen.

Engelund F.A. & Fredsœ J. (1976), *Nordic Hydrology*, 7, 293–306.

Ericksen J.L.& Truesdell C. (1958), *Arch. Rat. Mech. Anal.*,1, 296–323.

Eringin A. C. (1964), *Int. Jour.Engineering.Sci.*, 2,pp 205–217.

Eringin A.C. (1974), *Polar and Nonlocal Theories of Continua and Applications*, Bogazici University publications, Bebak, Istanbul, Turkey.

Geurst J.A. (1985), *Physica*, **129A**, 233–261.

Geurst J.A. (1985), *Philips J. Res.*, **40**, 352–374.

Geurst J.A. & Vreenagoor A.J.N. (1988), *J. Applied. Math. Physics (ZAMP)*, **39**, 376–386.

Gibson M.M. & Launder B.E. (1978), *J. Fluid Mech.*, **86**, 491–511.

Givler R.C. (1987), *Int. J. Multiphase Flow*, **13**, 717–722.

Goodman M.A. & Cowin S.C. (1976), *ZAMM*,**56**, 281–286.

Gray W. G. (1975), *Chem. Eng. Sci.* **30**, 229–233.

Gray W.G. & Lee P.G. (1977), *Int. J. Multiphase Flow*, **3**, 333–340.

Hagatun K. & Eidsvik K.J. (1986), *J.Geophysical Res.*, **91, C11**, 13045–13055.

Harlow F.H. & Amsden A.A. (1975), *Jour. Comp. Phys.*, **17**, 19–52.

Hill C.D. & Bedford A. (1979), *Phys. Fluids*, **22**, 1252–1254.

Hinze J.O. (1959), *Turbulence*, McGraw–Hill.

Hinze J. O. (1962), *Appl. Sci. Res.*, **A11**, 33–46.

Holm D.H.& Kupershmidt B.A. (1986), *Int. J. Multiphase Flow*, **12**, 681–697.

Horikawa K., Watanabe A. & Katori S. (1982), *Proceedings 18th Coastal Eng. Conference*, Cape Town.

Ishii M. (1975), *Thermo-Fluid Dynamic Theory of Two Phase Flow*, Eyrolles, Paris.

Johns B. (1975), *J. Geophysical Res.*,**80**, 5109–5012.

Johns B. (1977), *J. Physical Oceanography*, **7** , 13045–13055.

Jones W. P. & Launder B. E. (1972), *Int. J. Heat Mass Transfer*, **15**, 301–318.

Jonsson I. (1980), *Ocean Eng.*, **7**, 109–152.

Justesen P. (1988), *Coastal Engineering*, **12**, 257–284.

Kajiura K. (1968), *Bulletin of the Earthquake Res. Inst.*, **46**, Tokyo, Japan, 75–123.

King H. L., Davies A. G. & Soulsby R. L. (1985), *Report No* **196**, Proudman Oceanograhic Lab. Bidston, UK.

Kobayashi N. & Seo S. N. (1985), *Jour. Hydraulic Eng.*, **111**, (6), 903–921, (1985).

Landau C. F. & Lifshitz E. M. (1987), *Fluid Mechanics*, 2nd Ed, *Course of Theoretical Physics*, Vol 6: *Fluid Mechanics*, Pergamon Press.

Launder B. E. & Spalding D. B. (1972), *Mathematical Models of Turbulence*, Academic Press. /

Lottey J.M., Lumley J.L. & Shih T.H. (1983), *Atmospheric Dispersion of Heavy Gases and Small Particles*, IUTAM Symposium, Delft, (ed G. Ooms & H. Tennekes), Springer, pp 25–38.

Madsen O.S. & Grant W.D. (1983), *Proceedings 15th Coastal Eng. Conference*, vol **II**, 1093–1112, American Society of Civil Engineers, New York.

McTigue D.F. (1981), *Journal of the Hydraulics Division ASCE* **107, HY6**, 659–673.

Murray J. D. (1965), *J. Fluid. Mech.*,**21**, 465–493.

Needham D.J. & Merkin J.H. (1983), *J. Fluid. Mech.*, **21**, 465–493.

Nunziato J.W. & Cowin S.C. (1979), *Arch. Rational Mech. Anal.*, **72**, 175–210.

Nagano Y. & Tagawa M. (1988) *J. Fluid Mech.*, **196**, 157–185.

Nielson P. (1979), *Series Paper 20*, Inst. of Hydrodyn.and Hydraul.Eng., Tech. Univ. of Denmark, Lynby.

Nigmatulin R.I. (1979), *Int. J. Multiphase Flow*, **5**, 353–385.

Panton R. (1968), *J. Fluid Mech.* , **31**, 273–303.

Passman S.L., Nunziato J.W. & Walsh E.K. (1983), *Rational Thermodynamics*, (ed. C. Trusdell), Springer, New York.

Pourahmadi F. & Humphrey J. A. C. (1983), *Physio-Chemical Hydrodynamics*, **4**, 191–219.

Prosperetti P. & Jones A.V. (1984), *Int. J. Multiphase Flow*, **10(4)**, 425–440.

Prosperetti P. & Jones A.V. (1985), *Int. J. Multiphase Flow*, **11(2)**, 133–148.

Proudman J. (1916), *Proc. R. Soc. Lond.*, **A92**, 408–424.

Ramshaw J.D. & Trapp J.A. (1978), *Nucl. Sci. Eng.*, **66**, 93–102.

Raudkivi A. J. (1967), *Loose Boundary Hydraulics*, Pergamon Press.

Rodi W. (1980), *Turbulence Models and Their Application in Hydraulics*, International Association for Hydraulic Research, Delft.

Schlichting H. (1968), *Boundary-layer Theory*, McGraw Hill.

Sheng Y.P. (1982), *Conference Applying Research to Hydraulic Practice*,ASCE, Jackson,MS, 106–119.

Shih T. & Lumley J.H. (1986), *J.Fluid.Mech.*, **163**, 349–363.

Slattery J.C. (1967), *AICheE J.*, **13**, 1066–1071.

Sleath J. F. A. (1984), *Sea Bed Mechanics*, John Wiley & Sons.

Smith G. D. (1978), *Numerical Solution of Partial Differential Equations: Finite Difference Methods*, Clarendon Press, Oxford.

Smith J. D. (1977), *The Sea*, Vol 6, John Wiley & Sons.

Soo S. L. (1967), *Fluid Dynamics of Multiphase Systems*, Blaisdell, Waltham, Massachusetts.

Soo S.L., Sha W.T. & Chao B.T. (1978), *Int. J. Multiphase Flow*, **4**, 219–223.

Soulsby R.L. & Eidsvik K.J. (1988), *J.Geophysical Res.*, **91, C11**, 13045–13055.

Staub C., Svendsen I.A. & Jonsson I.G. (1983), *Prog. Rep. 58*, 41–49, Inst. of Hydrodyn.and Hydraul.Eng., Tech. Univ. of Denmark, Lynby.

Stuhmiller J.H. (1977), *Int. J. Multiphase Flow*, 3, 551–560.

Stewart H.B. & Wendroff B. (1984), *J. Comp. Phys.*, 56, 363–409.

Sumer B.M., Jensen B. L. & Fredsø J (1987), *Advances in Turbulence*, Springer Velag, Berlin, pp 556–567.

Trapp J.A. (1986), *Int. J. Multiphase Flow*, 12, 263–276.

Travis J.H., Harlow F.H. & Amsden A.A., (1976), *J. Nucl. Sci. Eng.*, 61, 1–10.

Truesdell C. (1957), *Rencl. Accad. Line*, Series 8, Vol 22, 33–166.

Turner D.M., (1987), *Central Electricity Research Laboratories*,Report TPRD/L/3101/R87,UK

Wang H. & Liang S.S. (1975), *J. Geophysical Res.*, 80, 3488–3494.

Whitaker S. (1969), *Ind. Eng. Chem.* 61, 14–28.

Wilson K.C. (1989), *Coastal Eng.* 12(4), 371–381.

VanRijn S. Y. (1981), Proc A.S.C.E. *J.Hydraulic. Eng.*, 108(HY18), 1213–1218.

Voinov O.V. & Petrov A.G. (1977), *Prikl. Math. Mech*, 41, 368–369.

Appendix A

Proof of the Averaging Theorem for a Simple Case

Here we give an informal proof of the result (1.5) for the special case of a rectangle in $\mathcal{R}^2$. Referring to figure A, the set of points comprising the averaging volume are:

$$\Omega(x,y) = \{(x',y') \mid x - L/2 \leq x' \leq x + L/2,\ y - M/2 \leq y' \leq y + M/2\}$$

and this is partitioned into two subsets C_1 and C_2 as in section 1.2. Again we have

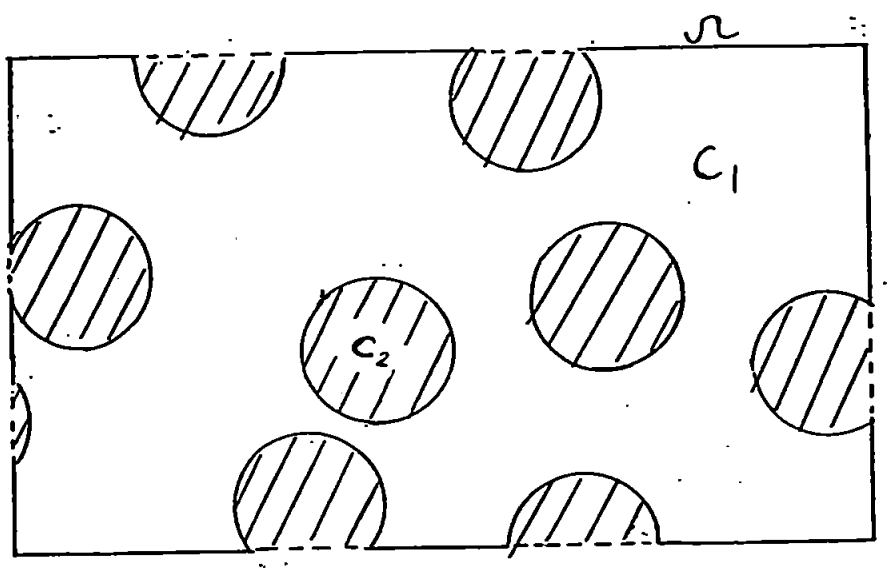

Figure A.1: Rectangular averaging "volume".

the following relations between the boundaries

$$\begin{aligned} \mathcal{I}_k &= \partial\Omega \cap C_k, \\ \mathcal{I} &= (\partial C_1 \cap \partial C_2) \cap \Omega. \end{aligned}$$

If $\hat{f} = f_1 i + f_2 j$ is any function defined on C_k we wish to show

$$\int_{I_k} \hat{f}.n_k \, ds = \nabla . \int_{C_k \cap \Omega} \hat{f} \, dV$$

Let I_k^t, I_k^b, I_k^l and I_k^r to be the subsets of I_k along the top, bottom, left and right sides of Ω respectively. Along these sides the unit outward normals take the simple forms j , $-j$, $-i$ and i , so that

$$\int_{I_k} \hat{f}.n_k \, ds = \int_{I_k^t} f_2 \, ds - \int_{I_k^b} f_2 \, ds + \int_{I_k^r} f_1 \, ds - \int_{I_k^l} f_1 \, ds. \qquad \text{(A.1)}$$

We define $\hat{f}^*$ as being equal to $\hat{f}$ on C_1 and zero elsewhere. Assuming $\hat{f}$ is continuous, this implies that $\hat{f}^*$ is piece-wise continuous and therefore integrable. Thus we can write (A.1) as

$$\begin{aligned} &\int_{I_k} \hat{f}.n_k \, ds \\ &= \int_{x-L/2}^{x+L/2} f_2^*(x', y + M/2) \, dx' - \int_{x-L/2}^{x+L/2} f_2^*(x', y - M/2) \, dx' \\ &\quad + \int_{y-M/2}^{y+M/2} f_1^*(x + L/2, y') \, dy' - \int_{y-M/2}^{y+M/2} f_1^*(x - L/2, y') \, dy' \\ &= \int_{x-L/2}^{x+L/2} [f_2^*(x', y + M/2) - f_2^*(x', y - M/2)] \, dx' \\ &\quad + \int_{y-M/2}^{y+M/2} [f_1^*(x + L/2, y') - f_1^*(x - L/2, y')] \, dy'. \end{aligned}$$

Now

$$\frac{\partial}{\partial \xi} \int_{\xi+a}^{\xi+b} g(z, \xi') \, d\xi' = g(z, \xi + b) - g(z, \xi + a),$$

so that

$$\begin{aligned} &\int_{x-L/2}^{x+L/2} [f_2^*(x', y + M/2) - f_2^*(x', y - M/2)] \, dx' + \int_{y-M/2}^{y+M/2} [f_1^*(x + L/2, y') - f_1^*(x - L/2, y')] \, dy' \\ &= \int_{x-L/2}^{x+L/2} \left[\frac{\partial}{\partial y} \int_{y-M/2}^{y+M/2} f_2^* \, dy' \right] dx' + \int_{y-M/2}^{y+M/2} \left[\frac{\partial}{\partial x} \int_{x-L/2}^{x+L/2} f_1^* \, dx' \right] dy' \end{aligned}$$

$$= \frac{\partial}{\partial y}\int\int f_2^*(x',y')\,dx'\,dy' + \frac{\partial}{\partial x}\int\int f_1^*(x',y')\,dy'\,dx'.$$

Since $\hat{f}^*$ is zero outside C_k we can write

$$\begin{aligned}\frac{\partial}{\partial y}\int\int_\Omega f_2^*(x',y')\,dx'\,dy' + \frac{\partial}{\partial x}\int\int_\Omega f_1^*(x',y')\,dy'\,dx' \\ &= \frac{\partial}{\partial y}\int_{C_k\cap\Omega} f_2\,dV + \frac{\partial}{\partial x}\int_{C_k\cap\Omega} f_1\,dV \\ &= \nabla.\int_{C_k\cap\Omega}\hat{f}\,dV.\end{aligned}$$

Appendix B

Equations for a Mixture Regarded as a Single Continuum

Here we show that a momentum equation for the fluid, essentially identical to (2.27) obtained in Section 2.2.3, can be derived from a slightly different viewpoint. This entails treating the combined fluid particle mixture as a single 'fluid', an approach that has been discussed by Ishii (1975) for example and used in modelling flow containing suspended sediment by De Vantier & Larock (1983). Assuming low particle concentrations, the effect of the particles can be treated as being a small perturbation on the state of single-phase fluid flow. The momentum equation that is derived is analogous to that obtained with the Boussinesq approximation in variable density flows. In the following we neglect the viscosity.

Equations for the combined fluid particle mixture can be found by adding together (2.1), (2.2) and (2.3), (2.4) to give, after some manipulation,

$$\frac{\partial \rho_m}{\partial t} + \nabla.(\rho_m v_m) = 0, \tag{B.1}$$

$$\rho_m \frac{Dv_m}{Dt} = \rho_m g - \nabla p_h - d. \tag{B.2}$$

Here

$$\frac{D}{Dt} = \frac{\partial}{\partial t} + v_m.\nabla,$$

$$\rho_m = \rho_p c + \rho_f (1-c) = \rho_f + \Delta\rho c,$$

$$v_m = [\rho_p c u + \rho_f (1-c) v]/\rho_m$$

and

$$d = \nabla.[\rho_f \rho_p c(1-c)(v-u) \otimes (v-u)/\rho_m].$$

These equations, together with (2.1) and a constitutive relation for $v-u$, yield a complete set of equations which in principal can be solved for ρ_m, c, v_m and p_h.[1] Assuming ρ_f and ρ_p to be constant, (B.1) can be written

$$\nabla.v_m = O(c).$$

For the case $c \ll 1$, the mixture density will be effectively ρ_f and so the hydrostatic pressure gradient is $\rho_f g$. Putting

$$\nabla p_h = \nabla p + \rho_f g$$

(B.2) can be written

$$\rho_m \frac{Dv_m}{Dt} = \Delta\rho c g - \nabla p - d.$$

By analogy with the Boussinesq approximation we neglect all terms of $O(c)$ except those multiplied by g. Since $\rho_m^{-1} = \rho_f^{-1} + O(c)$ and $v_m = v + O(c)$ this gives

$$\frac{Dv}{Dt} = \frac{\rho_m - \rho_f}{\rho_f} g - \frac{1}{\rho_f}\nabla p - \frac{d}{\rho_f}.$$

The following scaling analysis shows that d/ρ_f is negligible if the particle concentration is small. For the horizontal component of momentum, d/ρ_f is compared to the advection term $v_m.\nabla v_m$. The ratio is found to be $O(c)$, assuming that v and u can be scaled with the same velocity. Thus d/ρ_f can be neglected in this case.

For the vertical component of momentum, d/ρ_f is compared with $(\rho_m - \rho_f)g/\rho_f$. In the vertical, the difference $v_2 - u_2$ is of the order of the fall velocity w_0. The ratio of d/ρ_f to the comparison term is found to be of the order w_0^2/gl_z, where l_z is a characteristic length for the vertical gradient of velocity and concentration. With $wo = 5 \times 10^{-2}$ m/s, this ratio becomes order $10^{-4}/l_z$, requiring $l_z \sim 1$ mm for d/ρ_f to be of any significance. As discussed in Section 2.2.4, the only region where such steep gradients might occur is very near the bed. Thus we can, with justification, write the momentum equation for the mixture, in regions away from extreme vertical

[1] If the constitutive relation for the velocity difference is diffusive then the so-called 'diffusion' model for two-phase flow (Ishii 1975) is obtained.

gradients, as

$$\frac{Dv_m}{Dt} = \frac{\rho_m - \rho_f}{\rho_f} g - \frac{1}{\rho_f} \nabla p. \tag{B.3}$$

This is exactly the same as (2.27) which was derived from the fluid momentum equation (2.26) assuming the velocity difference between the fluid phase and particle phase was equal to w_0.